UNIVERSITY OF HERTFORDSHIRE

MSc BY RESEARCH DEGREE THESIS

# PRECISION PHOTOMETRY AT THE UNIVERSITY OF HERTFORDSHIRE'S BAYFORDBURY OBSERVATORY


*Author:*
Peter John BECK

*Supervised by:*
Dr Mark GALLAWAY
Dr Phillip LUCAS

Centre for Astrophysics Research
School of Physics, Astronomy and Mathematics
University of Hertfordshire


*Submitted to the University of Hertfordshire in partial fulfilment of the requirements of the degree of Master of Science*

November 2017

THIS PAGE INTENTIONALLY LEFT BLANK

**Abstract**

This thesis presents work conducted at the University of Hertfordshire's Observatory at Bayfordbury Hertfordshire to develop a model to predict the photometric precision of their 40cm aperture telescopes whilst observing a wide range of targets.

A model was formulated with suitable equations to predict the expected precision with a specified target by using only their catalogue magnitude, the selected exposure time and anticipated value of air mass. Significant effort was made to quantify the parameters for a particular telescope working in V band with 2x2 binning. The model's equations were predicted to be valid from magnitude 5 to magnitude 16.5 and for an air mass of up to 3.0.

The predicted results have typically been within 2 mmag of the measured values obtained from light curves, albeit there are a number of mismatches that may in part be due to poor observing conditions.

As part of the validation exercise, the technique was used to identify which predicted exoplanet transits would be satisfactorily captured by a telescope at the Bayfordbury Observatory, and to optimise the exposure time. Of the achieved observations with images correctly taken during a predicted transit (apart from one very faint target in adverse weather conditions), 12 satisfactory transits were captured and are presented in this thesis.

## Declaration

I declare that no part of this work is being submitted concurrently for another award of the University or any other awarding body or institution. This thesis contains a substantial body of work that has not previously been submitted successfully for an award of the University or any other awarding body or institution. Except where indicated otherwise in the submission, the submission is my own work and has not been submitted successfully for any award.

Peter J Beck
November 2017

# CONTENTS

# FIGURES

## TABLES

# 1 INTRODUCTION

## 1.1 Basic Concepts

Photometry is the technique of measuring the brightness of astronomical objects (Cooper *et al.* 2004). Precision photometry is a crucial requirement for many astronomical observations, in particular in the search for exoplanets (Hartman *et al.* 2005).

Scientific quality Charge Coupled Devices (CCDs) operating in optical wavelengths are routinely used for astronomical purposes. A CCD camera has a large silicon chip with many thousands of CCDs that are arranged in a matrix to form an imaging detector. These matrix elements are called pixels and the photons collected by the telescope are focussed on these pixels to capture an image. Each pixel has a well that accumulates electrons that have been excited to the conductive band by the absorbed incident photons, and as a result the pixels progressively acquire electrical charge. After a suitable exposure time, the electrical charges on the pixels are progressively read and digitised to generate a frame of data called a raw image. The raw images are then calibrated and stored in a form[1] suitable for analysis. CCD cameras used for astronomical purposes are usually cooled to minimise the thermal noise on the measurements. For example the Super Wide Angle Search for Planets (SuperWASP) project had the cameras operating at -75°C (Pollacco *et al.* 2006).

Software is used to identify the target star in an image and in turn measure the brightness of the target star (the measurement of energy (flux) is initially in units of counts and then converted to units of magnitude[2]). A plot (called a light curve) is then produced of the measured brightness over time from a sequence of images. For example, the transit of an exo-planet in front of a host star can be observed as a short duration (typically two or three hours) dip in the light curve, although exoplanet detections with shallow light curve dimmings may require processing by sophisticated software (Collier Cameron *et al.* 2007).

These light curves are also called time series photometry, where photometry is the measurement of the amount of energy received from an object over a set time period and at a specified wavelength band. For scientific work, it is essential that the noise on the light curve is kept as low as possible for precision photometric readings. It is common practice to improve the precision by grouping together several measurements in a short time window to give a single value (this process is referred to as time "binning").

Quantum Efficiency (QE) is a measure of how efficiently photons are detected by the observing device. In the case of a CCD, the QE at a specified wavelength is the proportion of photons that are detected (electrons raised to the conductive band). A CCD camera is far more efficient than human eyesight as its QE is better by a factor of approximately 100. Furthermore, a CCD camera has a much wider operating wavelength band (typically in the range 350nm to 1,100nm compared to 450nm to 650nm for a human eye) (Howell 2006). High QE is important as the higher the Signal to Noise Ratio (SNR) the greater the precision, and the exposure time will be shorter to achieve the same count and in turn improve cadence.

---

[1] The files are structured to meet the requirements of the Flexible Image Transport System (FITS) format NASA., 21.9.2016, that is the standard format used for astronomy images and is the format required by most image processing software.

[2] Magnitude is defined by Pogson's equation where:-
magnitude=-2.5log10(flux/zero point flux).
By definition, an increase in flux by a factor of 100 reduces the magnitude by 5.

Calibration of raw images entails using a set of master calibration files to:-

(a) Remove bias (the output from each pixel with a zero second exposure).
(b) Remove dark current (the bias due to thermal noise that increases with time).
(c) Flat field an image to compensate for the different QE of each pixel and the variation in the illumination across the image field of a chip due to optical conditions in the telescope and fore-optics (eg from dust particles and vignetting) such that all uniformly illuminated functional pixels generate the same value after flat fielding (Budding & Demircan 2007).

It is standard practice to introduce filters to restrict the measurements to photon wavelengths within a specified bandwidth. For example, the Johnson Cousins photometric system has filters called U (ultraviolet), B (blue), V (visible ie green to yellow), R (red) and I (near infra-red) (Cooper et al. 2004). However, this system has limitations in having some wide overlapping bandwidths; consequently other systems such as Sloan filters are also employed, as illustrated in Figure 1 (Bessell 2005).

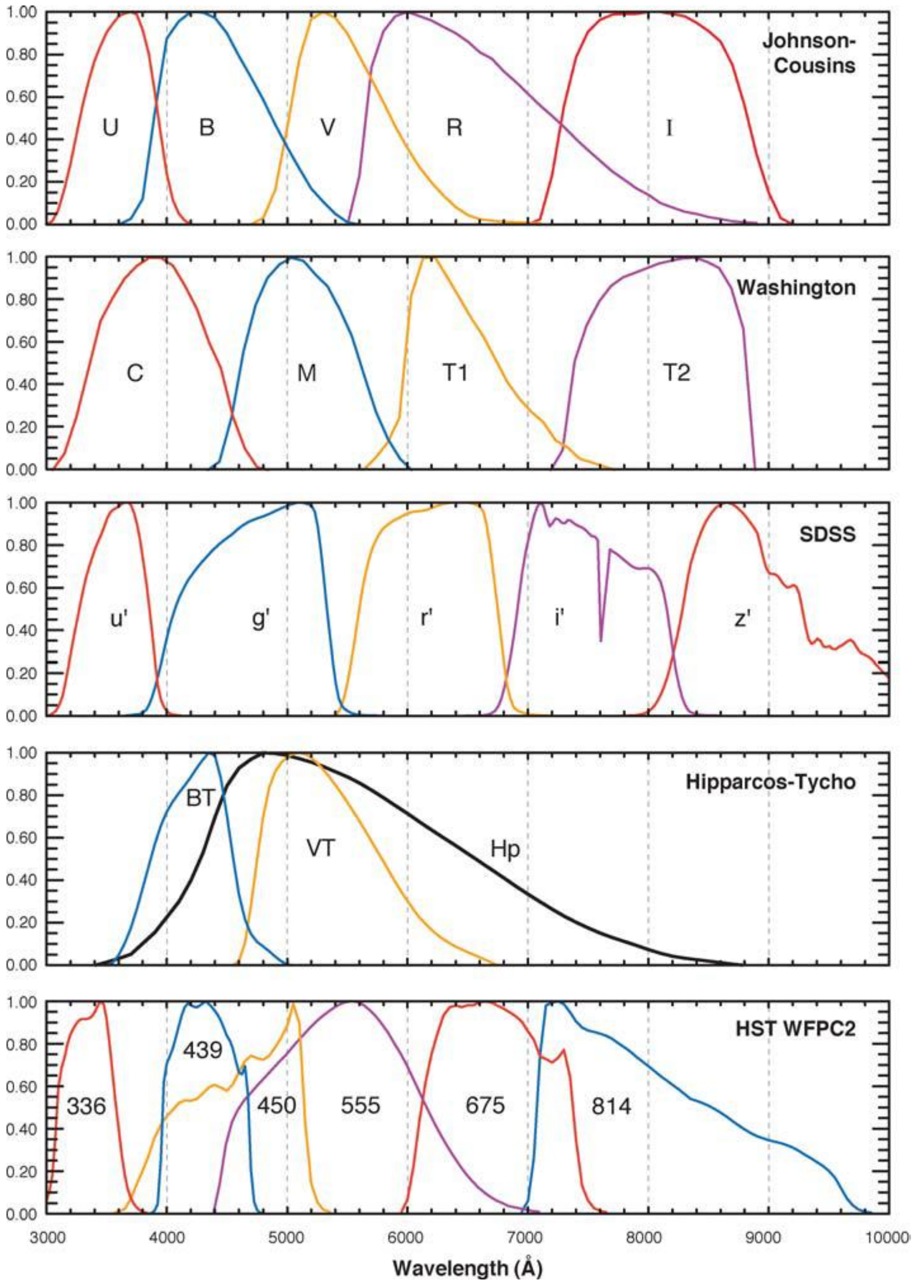


**Figure 1 Illustration of Band Passes with Different Types of Filter**

Some filters (such as an $H_\alpha$ filter) have pass bands chosen to isolate specific spectral line features. Most telescopes can use only one filter at a time to observe a target, however there are specialist telescopes that can simultaneously observe a target with more than one filter. For example, a recent study requiring simultaneous multi-band observations (Ducci 2016) used the Rapid Eye Mount (REM) telescope (that uses plate dichroic splitting) to simultaneously observe with Sloan g, r, i and z filters.

The earth's atmosphere attenuates light. The greater the distance that the light travels through the atmosphere (represented by a term called "air mass") the greater the attenuation. At high values of air mass, there can be significantly more attenuation of blue light rather than red light – consequently the sun at dawn and dusk will appear to be redder than during the day. The same principal applies to observation with stars. The light from a predominantly red star will have significantly less attenuation at high air mass compared to that with a predominantly blue star.

A similar effect occurs with a star's image (a stellar disc) as its brightness reduces and reddens towards the outer edge that is called a limb. Limb darkening is caused by fewer photons escaping the stellar atmosphere at the edges of the limb (compared to those travelling radially outwards from the centre of the disc) because they have a relatively greater optical depth (for a given physical depth) to travel through the stellar atmosphere. Since the temperature reduces as the physical depth reduces then the light from a limb will have a lower radiative spectrum flux density and be more biased to the red end of the spectrum. Consequently the light curves for a transiting planet are more rectangular in shape for red light, whereas the transit floor for violet light can appear to be rounded for the entire transit (Haswell 2010).

Whilst images can be obtained by manually operating a telescope, the observation process can be automated by using robotically controlled telescopes. The user specifies key information such as which telescope and camera combination to use, the target star, the type of filter to select, and the number and duration of the exposures. If the observing conditions are suitable, the chosen robotically controlled telescope will make the required observations at the most appropriate time of night. The user can then access the image files from the telescope's computer at a convenient time afterwards.

Cadence is the rate at which images are taken and needs to be carefully chosen. A high cadence corresponds to a relatively short exposure time and consequently a faint star will have a low SNR as the pixels will capture less target signal compared to the overhead noise. Conversely the pixels capturing a bright target star's photons will saturate with the long exposure times that come with too low a cadence. Most measurement errors can be treated as Poisson and consequently the law of quadrature applies – the error is factored by $1/\sqrt{N}$ where N is the number of images in the same time bin.

Pixel binning is where the electron counts from several adjacent pixels are merged to form a single value. It is introduced to reduce noise, but at the expense of reduced resolution. The most common pixel binning options are 2x2, 3x3 and 4x4 for 4, 9 and 16 adjacent pixels respectively. Hardware pixel binning also reduces the full frame download time (compared to not doing any pixel binning) giving a slightly higher sampling cadence.

Scintillation noise is caused by pockets of hot and cold air bending the incident light from a star by different amounts (since the refractive index of light changes with air density) and consequently introduces distortions to the image (Ryan & Sandler

1998). Scintillation is also referred to as atmospheric air turbulence since the air is continually moving and consequently noise will be introduced as the distortions vary with time. One of the main benefits of observing from a high altitude site is that scintillation noise is much lower than at sea level. The measured noise on a signal due to scintillation is significantly reduced as the exposure time is increased, and smaller with larger diameter telescope apertures. In addition to introducing noise on the received light (flux) from a star, scintillation also increases the size of a star's disc on an image and as a result reduces the resolution of the image.

The angle subtended by a star to an observer is very small due to the enormous distances involved and the relatively small star diameter. So nominally a star viewed from a telescope in space should appear to be point like. However the light from a star passing through a telescope produces a diffraction pattern, with the central bright spot being referred to as an Airy disc (Carrol B.W. 2007). The arbitrary resolution test to differentiate between two sources is called the Rayleigh criterion that defines the minimum subtended angle ($\theta_{min}$) for resolution as:-

$$\theta_{min} = 1.22\frac{\lambda}{D} \qquad (1)$$

Where $\lambda$ is the wavelength of the light and D is the telescope aperture diameter.

Consequently a plot of measured signal strength over an image will appear as a collection of 'hills' with each 'hill' having the approximate shape of a bivariate normal distribution, as illustrated by the aperture slice of star WASP-52 that is presented as Figure 2.

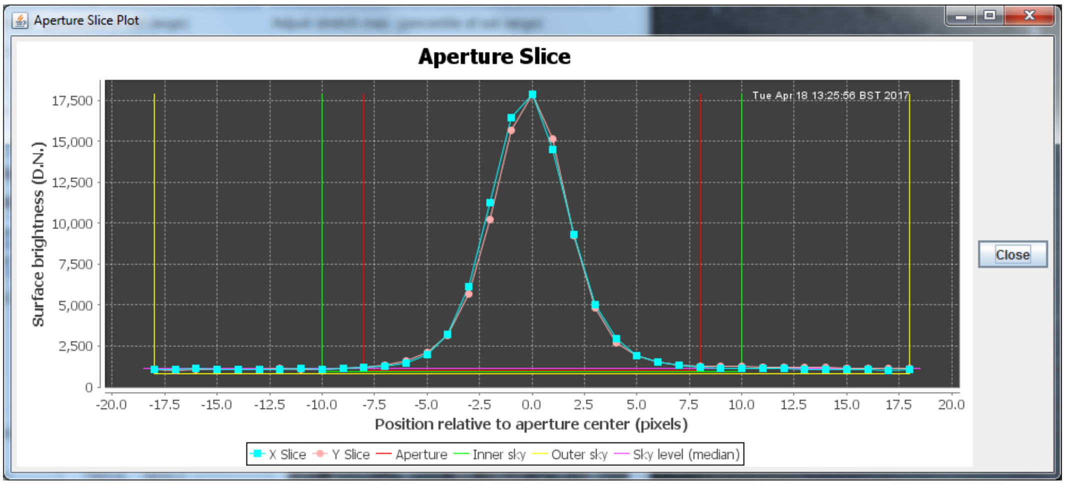


**Figure 2 Horizontal and Vertical Aperture Slices of WASP-52 in Image 27090**

All of the stars observed in an image will have the same diffraction pattern, but will have different brightness levels/ peak amplitudes. Bright stars may appear to be larger than less bright stars because the outer edges of their diffraction patterns are more visible. The diffraction patterns with the Hubble Space Telescope results in the image of a star being ≈0.1" across, as opposed to a width of ≈1" with a ground based telescope since that image is also distorted by atmospheric turbulence (Cooper et al. 2004). The observed distribution of flux over the group of pixels making up a stellar image is often approximated by an empirical Point Spread Function (PSF) (Budding & Demircan 2007), where "seeing" is the main cause of ground based PSFs being much broader than diffraction limited PSFs. The telescope is said to be diffraction-limited if there are no aberrations or any atmospheric turbulence present to broaden the PSF (Cooper et al. 2004). In addition the flux profile from ground based telescopes may be stretched as a result of small tracking errors. Techniques such as lucky imaging and Adaptive Optics (AO) try to minimise the worst effects of atmospheric turbulence in an endeavour to obtaining diffraction-limited images.

One of the highest precision ground based measurements is claimed to have achieved 14μmag precision (Kurtz 2005), although this entailed the use of a “Whole Earth Telescope” and a large number of observations.

## 1.2 Technical Background

### 1.2.1 Photometry

The study of variable stars was the initial major driver for precision photometry (Baptista *et al.* 1995, Dmitrienko 1994). However, following the seminal first detection of an exoplanet by photometric means (Charbonneau *et al.* 2000, Henry *et al.* 2000), the search and characterisation of exoplanets has become a major focus of interest for precision photometry (Pollacco et al. 2006), (Collier Cameron et al. 2007), (Haswell 2010), (de Mooij & Jayawardhana 2013).

Photometry was previously conducted with photographic emulsions and flux measurement devices known as Photo Multiplier Tubes (PMTs). However Charge Coupled Devices (CCDs) in cameras have effectively superseded them, since relatively inexpensive CCD cameras are capable of taking images with a high SNR, high bandpass and better QE (*Howell* 2006). However, PMTs are still used in special applications such as those requiring continuous brightness measurements (Kozhevnikov 2012). Recently more use has been made of CMOS technology in astronomical observations in the Near Infra Red (NIR) part of the spectrum (Kannawadi 2016). Recent innovations indicate that CCD cameras may become available with a high QE in the UV frequency range (Hamden *et al.* 2016).

Each pixel in a CCD camera progressively accumulates a charge as it registers incident photons whilst an exposure is taken. At the end of an exposure a clocking process progressively transports the charge on each pixel across the chip. Poor Charge Transport Efficiency (CTE) will result in charges trailing behind their original charge with a potential loss of measured flux for all stars. However, modern CCD devices now have a very high CTE compared to earlier CCDs and consequently the losses are relatively low. The charge on each pixel is sequentially read and an Analogue to Digital Conversion (ADC) factor is applied to generate a digital value (and consequently losing some resolution by quantisation); this ADC factor is dependent on the pixel electron well capacity and the maximum digital value used by the software. In the common case of a 16 bit camera the maximum value= $2^{16}$-1 = 65,535 unsigned Analogue to Digital Units (ADUs). One key CCD photometry limitation with bright stars is how large a charge a pixel well can hold and still provide linear performance (Castellano *et al.* 2004). Since even the latest CCD chips still have a similar typical maximum low noise well depth of 100,000$e^-$, then the previously used techniques to overcome this limitation are still relevant.

‘Backside’ illuminated CCDs (thinned CCDs illuminated from behind) are considered to be superior to ‘frontside’ CCDs (the photons have to travel through the surface gate structures before being absorbed by the silicon) as they are less affected by intra-pixel variations than front sided-illuminated devices (Buffington *et al.* 1991). The relative QE of a back sided CCD greatly exceeds that of a front sided CCD and has a better short wavelength light detection response (*Howell* 2006).

If the maximum charge on a CCD is exceeded, then a phenomenon known as bleeding (also known as blooming) occurs that can result in a complete column of pixels in the image saturating. One way of avoiding bleeding is to use antiblooming CCDs (Neely A.W. 1993). These CCDs have antiblooming gates inbuilt into the CCD so that saturated pixels have their excess charge 'drained off' without compromising adjacent pixels. However, antiblooming CCDs will have a lower QE (than non anti-blooming CCDs) as they lose a significant percentage of their active pixel area because of the extra circuitry (*Howell* 2006). Consequently an anti-blooming CCD has the benefit of avoiding charge leakage down a column when a well capacity is exceeded, but it comes at the expense of a reduced well capacity and more non-linearity with a high pixel charge (Castellano et al. 2004). The reduced well capacity is a disadvantage since deep wells are required to achieve a large dynamic range, in particular if there is a significant difference in brightness between the target star and the available check stars (Castellano et al. 2004).

Astronomers have used a wide range of different standard CCD cameras for approximately 20 years. Many of the early CCD chips had limitations such as long read-out times (Castellano et al. 2004, Southworth *et al.* 2009) and had noise levels of up to 50 times greater than current chips (*Howell* 2006).

There are numerous factors that have a bearing on how a CCD camera is best employed, in particular:-

(a) The selection of the exposure time for the target to optimise the precision whilst keeping within the pixel linearity range. This decision is complicated if there is a need to take relatively frequent images to observe variable signals such as those during an exoplanet transit.
(b) Read noise that is essentially a fixed error on each pixel.
(c) The chosen CCD operating temperature. The lower the temperature the lower the level of dark current. However, too low a temperature might result in temperature instability over the observing period (in particular on a warm summer's night) and consequently introduce a different dark current to that calibrated for. Furthermore, continuously operating a cooler could result in electrical noise affecting the measurements.
(d) Full frame download time (CCD read out time).This was particularly applicable with early CCD cameras where the read out time could be relatively high compared to the exposure time with bright stars. For example, Castellano (Castellano et al. 2004) had a CCD camera that took 13s to read a frame of data with an exposure time of 2s, that combined with other overheads resulted in a total elapsed time of 36s per 2s exposure. Even today, scientific cameras are on the market that also have a read out time of 13s, such as with the SBIG STX-16803 (SBIG; 7.10.2016).
(e) The choice of filter type and its QE versus wavelength for the target.
(f) The selected level of pixel binning. Eibe (Eibe *et al.* 2012) states that "considering the requirements for signal to noise ratio (S/N), exposure times and spatial sampling of the stellar profile for the seeing that is typically achieved at the observing site, the response of the CCD was found to be optimal if binned 2x2." In addition binning improves the SNR for very dim diffuse objects, since there is only one read out noise error with each bin (SBIG 2003). The disadvantage of binning is that the spatial resolution is reduced.

(g) Deciding whether sufficient information can be obtained from capturing only a partial frame of data and consequently reduce the download time.

In addition the object needs to be adequately sampled to centre and shape the PSF of a star. As a guide to having a high enough sample, a sampling parameter (r) is used that is defined by (Howell 1996):-

$$r = \frac{FWHM}{p} \quad (2)$$

Where p is the pixel size (arc seconds) and FWHM is the Full Width Half Maximum (arc seconds) i.e. the width of a cross section through the centre of a star's image where the pixel count exceeds half the peak pixel count.

A value of r<1.5 is considered to be under sampled and lower values will result in increasingly larger errors (*Howell* 2006).

Filters are often used with a camera to select particular wavelength pass bands (Dmitrienko 1994) (see Figure 1). The standard UBV system used with a PMT is known as the Johnson system (Johnson & Morgan 1953, Budding & Demircan 2007)]. This system was extended to UBVRI to create the Johnson-Cousins system (Cousins 1974, Warner 2006). The introduction of CCD cameras required a different set of filters called Bessel filters for the production of equivalent results as from a PMT (Bessell 1990). The Sloan Digital Sky Survey (SDSS) defined an alternative photometric system for use with large area CCD cameras. The SDSS filters (ugriz) define five pass bands that do not overlap[3] (Fukugita *et al.* 1996). There are however other standards such Gaia, Hipparcos and Tycho, consequently a matched transformation is required so that results derived from different photometric systems can be compared (Jordi *et al.* 2010, Bessell 2000, Davenport *et al.* 2006, Jordi *et al.* 2006).

Dravins et al (Dravins D. 1997) noted a colour dependence to scintillation, showing that observations in red light are less adversely affected than blue light and therefore limiting the bandpass is highly desirable. Everett and Howell (Everett & Howell 2001) judged that a V filter to be the best compromise between CCD QE and observing in redder bands for which variable night-sky emission lines would add to the noise. However, the consequences of differential atmospheric extinction can be considered to be small with differential photometry as the contribution is only due to the colour differences between the target and comparison stars (Eibe *et al.* 2011).

The key calibration processes for data taken by a CCD camera (Snellen 2008), (Cooper et al. 2004), (Gallaway 2016):-

(a) Compensate for Faulty Pixels.
(b) Bias frame subtraction.
(c) Dark frame current removal.
(d) Flat field correction.

Faulty pixels arise from shortcomings in their manufacture and usually have fixed numerical values varying from very high values (hot pixels) to very low values (cold

[3] The Johnson-Cousins standard has a large overlap of the red pass band with the V and I pass bands. The appropriate master calibration frame needs to be selected for the chosen filter when calibration is conducted.

pixels). Research grade CCD chips are CCD chips selected with low numbers of faulty pixels present. The measurements from correctly functioning pixels might also be compromised by a cosmic ray and should be treated as for faulty pixels.

Compensation can be performed by replacing an erroneous value by the average of the pixel counts of adjacent pixels, or by just masking them out. No compensation is made for other extraneous error sources such as cosmic rays and overflying aircraft captured in an image (a particular problem at the Bayfordbury Observatory) – these corruptions need to be identified by careful examination of the images.

A suitable combination of bias and dark current master frames are subtracted from a light frame as part of the calibration process. Bias frames are produced with a zero second exposure time[4]; a bias is applied to each pixel value to prevent the digital value from going negative since the word used for storing the number does not have a sign bit. (*Howell* 2006). The dark frame (dark current) is obtained by taking images with the camera shutter closed for selected 'exposure' times. The dark current could be scaled by the exposure time as this background electronic signal increases linearly with time and is often insignificant for many visible-light CCDs (Cooper et al. 2004). However, it is preferable to generate a tailor made set of master dark frames that map to the chosen light exposure time, selected CCD operating temperature and pixel binning option[5] to simplify the calibration process and reduce the scope for interpolation errors.

Flat fielding is the process to correct for different pixel sensitivity to light with the selected filter. It also compensates for other shortcomings such as dust in the optical path and for the vignetting of the field of view (Budding & Demircan 2007).

It is usual to take multiple flat fields to improve the quality of the master flat field; with typically 5 to 10 calibrations per filter. For example, 120 flat field calibrations were taken over 5 days of an observing run (Everett & Howell 2001). Flat fields need to be made with a uniformly illuminated field (either as dome flats with a diffuse background, or as sky flats with a cloudless twilight sky). Each flat field taken needs to have filled the CCD wells (close to 50% full) to ensure a high SNR ratio. Dome flats are made inside an observatory by taking images of a diffusely illuminated white board (Budding & Demircan 2007). Ideally a master flat is generated by taking the median values from corresponding pixels in a series of flat fields that have been debiased and had the dark current subtracted. The master flat field is then normalised and subsequently divided into each image so that each pixel will nominally give the same count with the same illumination. It has been shown that the sensitivity variation across a CCD is independent of time (Balona *et al.* 1995). However, some contributors to flat field variation across a CCD frame may be temporary in nature and hence nightly flat fielding is common practice (Budding & Demircan 2007).

Photometric calibration uncertainties were considered to be the dominant source of systematic errors in the Pan-STARRS survey (Scolinic 2014) where the telescope is

[4] Each telescope used at the Bayfordbury Observatory has a master set of 2x2, 3x3 and 4x4 pixel binning bias frames produced at the CCD operating temperature of -20°C.

[5] Each telescope used at the Bayfordbury Observatory has a master set of 2x2, 3x3 and 4x4 pixel binning dark frames produced at the CCD operating temperature of -20°C, for each of the fixed range of exposure times available to a user. The appropriate master dark frame is selected when calibration is conducted.

located at high altitude with limited atmospheric turbulence. However, atmospheric extinction and scintillation can be one of the largest sources of error in photometric observations (Balona et al. 1995), (Gilliland & Brown 1992), (Hartman et al. 2005), (Ryan & Sandler 1998).

Absolute (all sky) photometry calibrates a local photometric system to a standard or reference system, by conducting detailed comparisons with the magnitude and colour values of standard stars (Budding & Demircan 2007)]. The major disadvantage of conducting absolute photometry, apart from having more steps than differential photometry (see below), is that it requires very good (transparent and stable/ constant) sky conditions, and furthermore these "photometric nights" rarely occur at most observatories. In addition, the required standard star frames may be unique to a given observing site and time of year (*Pecker* 1970).

Differential photometry is where one calculates the difference between a target's magnitude and that of a comparison star (or the average of several comparison stars) (Cooper et al. 2004); it provides the most accurate method of measuring small variations in magnitudes (*Warner* 2006). One of the key benefits of differential photometry is that it can be conducted on nights of lesser quality (Budding & Demircan 2007). The basic implementation of Pogson's equation to calculate the differential magnitude (Budding & Demircan 2007) is:-

$$\Delta m' = -2.5 log\left(\frac{object - sky}{comparison - sky}\right) \qquad (3)$$

Where *object*, *comparison* and *sky* are the respective counts for the target, reference star and sky background.

Differential photometry obtains magnitudes of a target star relative to a non-variable reference star of known magnitude. A field of standard Landolt stars (Landolt 1992) can be observed with Johnson UBVRI filters in conjunction with the observations of the survey fields to calibrate the magnitudes in each filter (Everett & Howell 2001). The key benefit of differential photometry is that the unsteadiness of the Earth's atmosphere (seeing) and extinction will apply equally to all stars in the Field Of View (FOV). It is usual that differential photometry against a reliable reference star is also conducted with several check stars. The light curves for the check stars should not vary with time if the processing is correctly conducted (eg using the correct aperture sizes), the check stars are of similar magnitude to the reference star and the observing conditions and measurements are of good quality.

A check star should be:-

(a) in close proximity to the target star to reduce the effects of differential atmospheric extinction and noise from atmospheric scintillation, to reduce differences in the stellar point spread functions due to optical aberrations, and to minimise spatial variations in obscuring clouds (Everett & Howell 2001).

(b) a similar colour as the target star (Ryan & Sandler 1998). A high air mass will result in light from blue stars being attenuated more than the light from red stars, and in turn artificially bias the differential photometry measurements taken at high air mass. Since observations of exo-planet transits last for a long time then it is likely that some readings will be taken at high air mass.

(c) of similar magnitude as the target star such that all CCD pixel measurements have high ADU counts but remain within the linearity range. Under estimation of errors can occur by using brighter check stars as they will have a higher SNR and hence a lower estimate of error (Koppelman 2010).

Software is usually used to automate the process of establishing the magnitudes of the target and check stars relative to the supplied magnitude of the reference star. Any unreliable check stars identified (with magnitudes having a relatively high standard deviation) are discarded. If the light curves for check stars vary during the observing session, it may be because they are variable stars, there has been an anomalous event or some non-uniform obscuration in an image has occurred. The changes in the mean magnitude of a bright ensemble of check stars can be used to correct the instrumental magnitudes of each star to produce a precise differential light curve for each star (Everett & Howell 2001); the sifted ensemble star light curves was found to have a typical standard deviation from their means of 2 milli magnitude with a target with V magnitude of 14 with a 0.9m telescope (Everett & Howell 2001).

The importance of having a high ADU count for **both** the target and reference star is illustrated using the following equation (Cooper et al. 2004) to give an approximate estimate of the magnitude error ($\delta m$) given a flux (F) with an uncertainty of $\delta_F$:-

$$\delta m = 2.5log_{10}(1 + \frac{\delta_F}{F}) \quad (4)$$

Assuming that the flux uncertainty of $\sqrt{F}$ dominates gives:-

$$\delta m = 2.5log_{10}(1 + \frac{1}{\sqrt{F}}) \quad (5)$$

Thus if one star has a flux count of 10,000 then the instrument magnitude error is ~0.01. If a star has a low flux reading of 1,000 then the error is ~0.03.

Consequently an ADU reading of 50,000 corresponds to a magnitude error of ~0.005, i.e. 5 milli magnitude.

Aperture photometry places an aperture around the target in the image to measure the combined target and implicitly sky flux as well. A concentric annulus (or another aperture) is then placed over a relatively nearby clear area in the image to measure the sky background flux; a software package is usually used to calculate the target flux (Cooper et al. 2004). The number of pixels in the sky annulus should be relatively large (a factor of 3) compared to the number in the source aperture (*Howell* 2006). There should not be any extraneous bright sources (such as stars or galaxies) in the sky annulus used to derive the background sky magnitude as this will artificially reduce the measured target magnitude. An alternative is to use profile fitting using a Point Spread Function (PSF) obtained from nearby bright stars to establish the PSF for the target, and in turn establish its photon count. Profile fitting is more appropriate if there is severe blending (*Howell* 2006) where other stars are also present in an aperture.

PSF photometry is chosen with very crowded fields (where it becomes difficult to conduct aperture photometry) such as obtaining light curves for main belt asteroids (Szabo 2016), (Pal 2012). However, Gilliland reported that PSF could not be relied upon as it varied across the CCD chip and also with time (Bramich 2008, Gilliland *et al.* 1991, Warner 2006). PSF on the target star's image shape can be conducted by either profile fitting or by using an algorithm (Naylor 1998). In large extragalactic surveys it is necessary to automate the extraction of source data in astronomic images or Schmidt plates due to the large number of targets, as it would be far too time consuming to process manually (Bertin & Arnouts 1996, Maddox *et al.* 1990, Irwin 1985). It has been found that aperture photometry gives better precision than PSF photometry for the brightest stars, but PSF photometry gives better precision with fainter stars due to the presence of higher sky flux through an unweighted aperture (Hartman et al. 2005).

Relative photometry is where the known magnitude of the comparison star is added to the target star's differential magnitude (Cooper et al. 2004). Difference image photometry, also known as or Difference Image Analysis (DIA) or image subtraction (Tomaney A.B. 1996), is a useful variation of differential photometry for measuring large amplitude changes in a crowded field (*Howell* 2006) and in these circumstances superior to profile fitting photometry (Bramich 2008).

One feature of observing exoplanets and binary stars is that their orbital time is often precisely known (Conroy *et al.* 2013, Samolyk 2013, Gursoytrak *et al.* 2013); consequently greater precision can be achieved by obtaining data from multiple observations and then temporal bin the data into small bins of similar phase angle. This process is referred to as "folding". Assuming Poisson noise, folding reduces the error in a bin by $1/\sqrt{N}$, where N is the number of samples in a given bin (Castellano et al. 2004).

Telescopes are often described by their "focal ratio" or "F value" (Jenkins 1957), (Carrol B.W. 2007) where F=f/D, where f is the focal length of the objective lens and D is the aperture diameter. The speed of an optical system is 'faster' the higher the illuminance (J) – this is defined as the amount of light energy per second focussed on a unit area of the resolved image. From geometry it can be shown that

$$J \propto \frac{1}{F^2} \qquad (6)$$

Thus the greater the focal length of the telescope, the greater the F number and in turn the lower the illuminance. Conversely, reducing the value of f, gives a smaller the value of F and in turn the greater the value of J. Thus a focal reducer (reducing the value of f) will increase the illuminance on a CCD chip, however the magnification ($M=(f_{objective}/f_{eyepiece})$) will also be reduced. A reduced magnification means that observed size of a star's image will become smaller on the CCD chip (with the star's image still receiving the same number of incident photons as it would have done without a focal reducer). Consequently the exposure time with a focal reducer needs to be shorter (to obtain the same number of electrons in a given pixel well as would have been obtained without a focal reducer) and can also lead to 'under sampling' of an image (ie insufficient pixels representing a star to accurately describe its profile) (Castellano et al. 2004). A reduced magnification ($M=(\theta_{eyepiece}/\theta_{objective})$) with a fixed eyepiece angle means that the objective angle is larger – ie there is a larger Field Of View (FOV) and potentially increases the number of suitable check stars in the FOV (Castellano et al. 2004), or is more suitable for applications studying faint extended objects (Afanasiev 2005). However, a focal-reducing imager can be prone to internal reflections which may slightly increase the noise levels (Southworth *et al.* 2013) and furthermore any additional optical component will reduce efficiency.

The 'plate scale' (P) of an image defines the angle subtended at a pixel and is usually quoted in units of arcsecs per pixel (Howell 2006). Thus with a focal length

(f) in units of mm, a CCD pixel size (μ) in units of microns, 206,265 for the conversion from radians to arcseconds and 1000 for the conversion factor between millimetres and microns gives:-

$$P = \frac{206265*\mu}{1000*f} \quad (7)$$

### 1.2.2 Pixel Binning

There are two types of pixel binning that may be available with a CCD camera – off-chip binning and on-chip binning.

SBIG consider that off-chip binning to be useful when a non-anti-blooming CCD chip is installed. When this option has been selected, it causes any binning to be performed after the CCD chip has been read and greatly reduces blooming. (SBIG 12.10.2016). In other words off-chip binning is a cosmetic process to avoid large vertical streaks in an over exposed image by averaging high pixel counts with adjacent low pixel counts and has no relevance with precision photometry.

The precise method how on-chip binning is conducted is unclear in many publications and needs to be carefully interpreted for the particular CCD chip used by the camera. The documentation provided by the camera supplier may not include crucial information on the operation of the appropriate CCD chip and consequently the manufacturer's documentation should be consulted. For example, many CCD cameras use the Kodak "KAF" series of CCD sensors and the maximum pixel well depth quoted for the SBIG KAF-6303E by the SBIG camera manufacturer (SBIG 2003) is 100,000e-. However, the CCD chip manufacturer explains that when conducting 2x2 pixel binning (KODAK 1999), two rows in the CCD chip are added to a horizontal register that has a CCD charge capacity of 200,000 to 240,000e- (KODAK 1999), the first two pixels in the horizontal register are then added to the output diffusion node (for reading) that has a CCD charge capacity of 220,000 to 240,000e-. In other words, the average maximum charge on all 4 pixels with 2x2 pixel binning is 220,000/4= 54,000e- and NOT 100,000e- as implied by the camera manufacturer. Paradoxically, Howell (Howell 2006) states that "Generally, the output register pixels can hold five to ten times the charge of a single active pixel", so in such circumstances there would not be a risk of saturation as a result of 2x2 binning.

### 1.2.3 Milli Magnitude Photometry With Small Telescopes (<1m)

Milli magnitude photometric precision can be achieved with 'small' telescopes, where 'small' refers to telescopes that typically have an aperture size of 20cm, but can be as large as 1m, (Alton 2013), (Balona et al. 1995), (Licchelli 2007), (López-Morales 2006), (Pollacco et al. 2006).

Three milli magnitude photometric precision (Castellano et al. 2004) was achieved with a small aperture telescope (0.2m) Meade LX200 and a consumer grade CCD camera (chip size 765x510 pixels of 9 microns size). This equipment was used to observe the transits of HD 209458b (V=7.63mag) and OGLE-TR-56 (V=16.56mag).

Tracking, auto-guiding (or both) is required otherwise the stellar images will drift across the CCD giving uniformly poor measurements.

The scintillation error with a small telescope and a bright target (Castellano et al. 2004) is shown to be the dominant source of error. Had the telescope's aperture been D=0.4m (instead of 0.2m) then from inspection of equation (8) the scintillation noise would have been reduced by a factor of $2^{-2/3}$=0.63 (also see Figure 3).

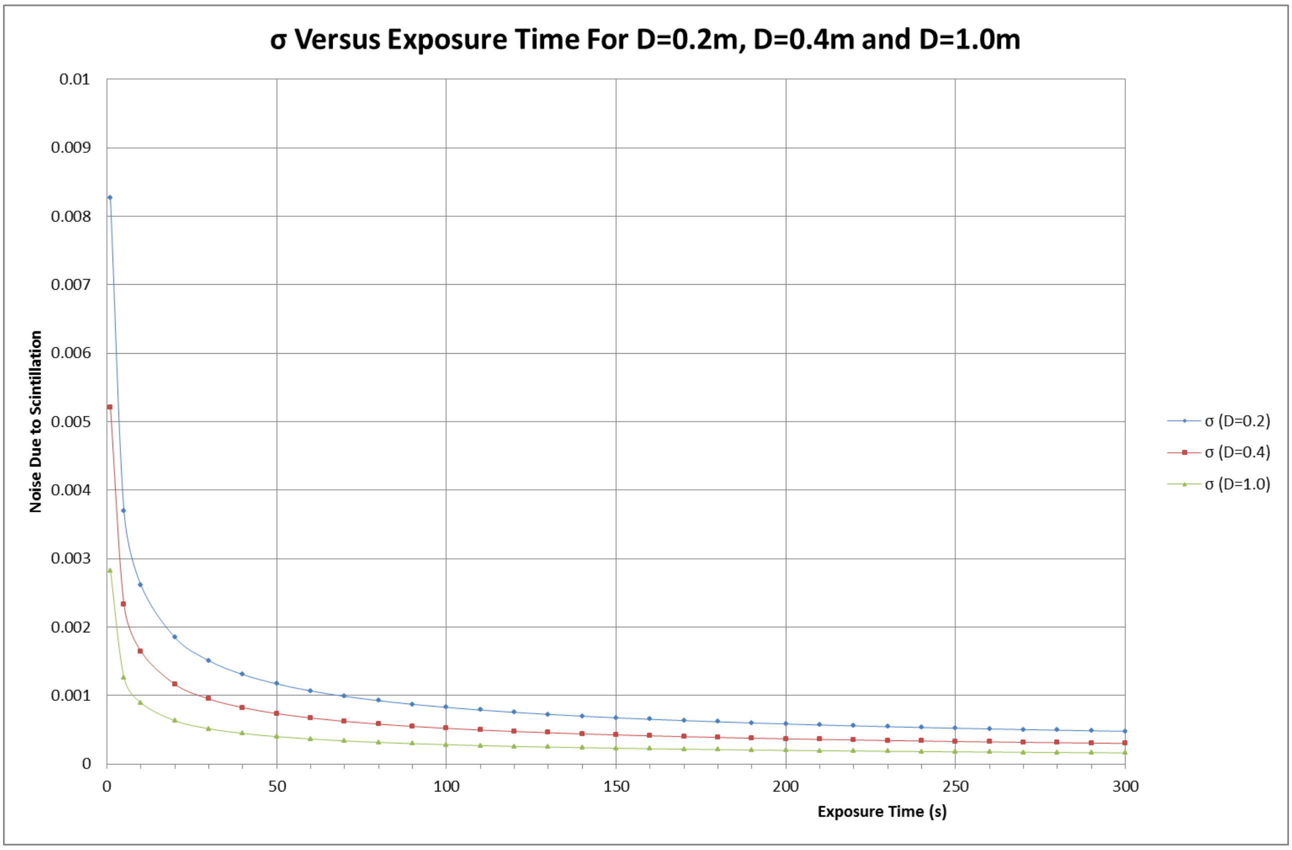


**Figure 3 Predicted Scintillation Noise Levels With Different Exposure Times and Aperture Sizes**

Differential photometry is well suited to detect transits, ideally with similar colour[6] stars and small values of air mass, enabling a 1m telescope to achieve as low as 0.8 milli magnitude accuracy (Castellano et al. 2004). However, there is a potential problem if there are too few bright comparison stars in the CCD FOV as several similar check stars are needed to minimise the differential photometry noise.

Castellano (Castellano et al. 2004) also states that there are four sources of random noise:-

(a) Poisson noise from the target and comparison stars.
(b) Noise introduced by calibrations.
(c) Noise from atmospheric scintillation: atmospheric scintillation was considered to be a major noise source with bright stars (ie short exposure times were required).
(d) CCD read noise: amateur quality CCDs typically have a read noise of 15$e^-$ Root Mean Square (RMS) whereas scientific CCDs typically have a read noise of 1 to 2 $e^-$ RMS.

Licchelli (Licchelli 2007) estimated that the scintillation noise at 30° elevation was 0.01 magnitude. Also that the different air mass extinction with an air mass of 1.8

[6] Similar colour stars mean that the second order colour difference dependent extinction corrections are relatively small compared to a photometric transit depth.

between HD 209458 and its comparison star (HD 209346) due to a 12’ angular offset[7] was estimated to be 0.003 magnitude.

Sky background becomes more important with fainter targets and is ideally the dominant contribution. On the best quality nights, and with instrumentation with low noise, the background sky noise represents the final limiting for accurate measurement of weak astronomical sources – ‘sky limited’ detection (Budding & Demircan 2007).

Milli magnitude-precision (0.0008-0.0010 magnitude) photometry of bright stars (V<9.0 magnitude) with a 1m telescope and a standard CCD is reported by López-Morales (López-Morales 2006); with 0.0015 magnitude precision being achieved for observations of over 6 hours. It is stated that “The photometric precision of this setup is only limited by scintillation.” There are a number of features of this paper that would not apply with a more modern CCD camera:-

(a) The major limitations of this study were the shortest achievable CCD exposure time of 5s and a 1x1 unbinned read-out time of 128s.
(b) The star was too bright for a 5s exposure. The aperture was reduced to shrink the collecting area from $0.589m^2$ to $0.146m^2$ to overcome this problem – negating the full benefit of a 1m telescope and the reduction in scintillation with a larger diameter aperture.

Although one suggestion to avoid saturation is to use a neutral density filter (López-Morales 2006), there is a danger that the neutral density filter will have poor photometric characteristics and provide inconsistent attenuation of the signal received by the CCD. However a neutral density filter with a Bessel R filter (requiring two filter wheels) has been used to obtain unsaturated focussed images for the study of a planetary transit using 1.2m and 1.93m telescopes (Moutou *et al.* 2009) with a V=9 magnitude target and with an Root Mean Square (RMS) error of between 0.0023 and 0.003 magnitude from a relatively low number of frames.

### 1.2.4 Ground Based Detection of Transits of Extrasolar Giant Planets

The exoplanet transit of the relatively bright star HD 209458 (V=7.63 magnitude) has been used by many astronomers (Castellano et al. 2004) as the reference for their studies. The results can be quite varied, but have progressively improved over time. The online catalogue of exoplanets (Zolotukhin 20.10.2016) defines the characteristics of this planet and also provides a long list of relevant papers, alternatively a MIT derived catalogue (Hanno Rein 5.9.2016) can be consulted instead. The predicted exoplanet transits times can be derived from the orbital period and the Julian time of a particular eclipse, however this information is readily available online as via an Exoplanet Transit Database (Czech 5.9.2016).

Martioli and Jablonski (Martioli & Jablonski 2007) describe observing HD 209458 with a 0.28m aperture telescope and an SBIG ST7E CCD camera. The light curves had RMS errors compatible with the depth of the transit (2%). They identified the following improvements that they could make:-

(a) To use a larger unvignetted field-of-view to obtain more comparison stars.
(b) To use auto-guiding to keep the target in the same area of the detector.

[7] The implication of this is that the check stars should be equally distributed about the target star so that the differential extinction due to different air masses should tend to cancel out.

(c) To use a red band pass filter to minimise the effects of differential extinction and differential refraction.
(d) To select comparison stars as close in spectral type (G0V) to HD 209458 as possible.

Everett and Howell (Everett & Howell 2001) describe how to conduct high precision, wide field, time sampled stellar UBVRI photometry that is suitable for the discovery of exoplanets using a 0.9m telescope. It claims 2.0 milli magnitude precision with V~14 magnitude and 1.9 milli magnitude precision after binning with the brightest stars. The camera had eight CCD chips, each with 4096x2048 pixels[2], linearity of 0.1% for a well depth of up to 70,000 electrons. The CCD FOV was relatively small as its linear plate scale of 0".43 pixel$^{-1}$ translates to a relatively large FOV of 59'x59'. The UBVRI[8] filters were used to estimate the spectral type and luminosity class of each star.

A number of wide field surveys have been conducted using small telescopes, and in particular the SuperWASP survey (Pollacco et al. 2006) has been very productive in obtaining light curves that after analysis (Collier Cameron et al. 2007) have yielded many candidate exo-planets. This survey was conducted after first establishing how many transiting planets that the survey was likely to find (Haswell 2010). The Multi-Site All Sky Camera (MASCARA) project (MASCARA 2017) aims to identify the brightest transiting planet systems in the sky. A smaller scale study with a particularly small aperture (4cm) camera by the Kilodegree Extremely Little Telescope (KELT) survey has successfully identified a number of exoplanets transiting bright stars (Soutter 2015): consequently transits by exoplanets identified by the KELT survey are likely to be good targets to observe.

In deciding whether it is worthwhile attempting to observe a known transit the following points need to be considered:-

(a) The times that a transit occurs must be correspond to the times that the target is actually observable (i.e. dark enough for observing, and the star is observable with the chosen telescope) to establish if the full transit can be recorded. The observations must include sufficient coverage of the "before" and "after" transit periods to have enough points to give the required precision. However, this requirement can be relaxed by binning of observations from other occurrences of the same transit.
(b) The target magnitude will determine the minimum exposure time. Knowing the transit duration will give the number of images taken during the transit and in turn the expected precision.
(c) The Root of the Sum of Squares (RSS) of the predicted errors of the "in" and "out" of transit magnitudes must be significantly smaller than the specified depth of transit.
(d) Minimise the background sky noise by choosing transits that occur with a favourable phase of the moon and with target stars with a line of sight well away from that of the moon.
(e) The weather forecast needs to indicate an extended period of clear observations.
(f) The number of times that the target star will be observable during an observing campaign.

[8] U=Ultra-violet, B=blue, V=photovisual, R=red and I=infrared (*Norton* 2004, *Warner* 2006).

(g) The precision of the measurements will depend on the air mass throughout the observing period and also on the suitability of the available check stars.
(h) The target star might be a variable star. This might not be a problem if the variability is relatively insignificant compared to the change in magnitude with a transit. For example, although WASP-33 has a pulsation period of 69min its variability is only 0.001m (Herrero) which is far smaller than the transit depth of 0.0151m (Czech 5.9.2016).

The light curves for a transiting exo-planet are complicated by factors such as:-

(a) Limb darkening. An analytical approach is presented by Mandel and Algol (Mandel 2002) to fit a theoretical algorithm to a light curve.
(b) Impact parameter: a planet does not necessarily traverse the centre of the star as viewed by the observer. Impact parameter is a measure of the way the exoplanet has transited in front of the star and is defined as the shortest distance from the centre of the star's disc to the locus of the planet (Haswell 2010).
(c) The four contact points during a transit. The first contact is when the limb of the planet makes first contact with the star and, the second contact is when the entire disc of the planet is observed to be just within the stellar disc. The third and fourth contacts are the equivalent points as the exoplanet completes its transit (Haswell 2010). In other words the extinction due to the transit will be partial for the period between first and second contacts and also for the period between third and fourth contacts.
(d) The inferred exoplanet's radius can be larger than the actual radius due to attenuation through the atmosphere on the exoplanet (Tinetti 2014). In particular, the inferred radius can be larger at certain specific wavelengths corresponding to absorption lines for components in the atmosphere. For example, the inferred radius of exoplanet HD 209458b in Lyman α[9] (transition from the ground state of neutral hydrogen) is approximately $4R_J$ (radius of Jupiter) whereas the actual value is approximately only $1.4R_J$ (Vidal-Madjar 2002), (Haswell 2010).

### 1.2.5 Defocussing Photometry

Defocussing the telescope has been used to obtain precision photometry (Ferrero *et al.* 2010, Southworth et al. 2013), (de Mooij 2009). The preceding Southworth paper (Southworth et al. 2009) explains that heavy defocussing was employed with several minutes of exposure time to disperse the large number of photons over many pixels. Special attention needs to be taken to tune the defocussing in order to work only in the linear regime of the CCD (Mancini 2015). It is claimed that this approach reduced the problems due to scintillation and atmospheric effects until they became irrelevant and that the flat fielding errors were reduced by several orders of magnitude compared to focussed observations. The main objective being to maximise the S/N per unit of time (Southworth et al. 2009).

Too strong a defocus can increase the noise as the larger aperture increases the contribution from the sky-background to the total flux in the aperture and in turn

[9] Lyman α absorption corresponds to a wavelength of 1216Å (corresponding to an electron transiting from the n=1 to n=2 orbits). It does NOT correspond to the centre frequency of 6563Å for an $H_\alpha$ filter (corresponding to a Balmer α transition between the n=3 and n=2 orbits). Furthermore, the Lyman α frequency is NOT detectable by standard CCD chips.

reduce the SNR (de Mooij & Jayawardhana 2013); however this effect is relatively small in a scintillation dominated regime (eg with bright stars and short exposure times).

A bigger problem is that the accurate removal of background flux becomes more important as the relative contribution of the background (especially in the infra-red region) to the total flux increases (de Mooij & Jayawardhana 2013). This problem can be compounded by any residual sky background gradient and hot pixels[10].

A defocussed star takes longer to fill its pixel bins to their non-linearity level than a focussed star as it occupies more pixels on a CCD chip, and consequently has a longer exposure time and lower noise due to scintillation (Dravins *et al.* 1998, Young *et al.* 1992). The scintillation noise is given by:-

$$\sigma_{scint} = 0.004 D^{-\frac{2}{3}} X^{\frac{7}{4}} e^{-\frac{h}{H}} (2t_{exp})^{-0.5} \quad (8)$$

Where:-

$\sigma_{scint}$ is the normalised standard deviation (-).

D is the telescope aperture (m).

X is the air mass (-).

H is the altitude of the telescope (m).

H=8000 (m) is the scale height of the atmosphere.

$t_{exp}$ is the exposure time (s).

The sensitivity of scintillation error with telescope aperture size (using the above equation) is illustrated in Figure 3 Where aperture sizes of 0.2m, 0.4m and 1.0m have been considered. This Figure clearly demonstrates that scintillation error is significantly reduced by having a longer exposure time and a larger aperture size.

A large defocus was used by Licchelli, (Licchelli 2007) to extend the exposure time from 1s to 7s for HD 209458 (V=7.65 magnitude) to limit the noise due to scintillation and to achieve 3-4 milli magnitude precision with a 0.2m aperture reflector telescope and a commercial CCD camera.

Under normal circumstances, telescopes at the Bayfordbury Observatory will always remain focussed throughout an observing session. Disengaging the auto-focus would be undesirable as the telescope would be unusable for subsequent users on the same night. Furthermore, disengaging the auto-focus would not give full control of the amount of defocussing and potentially result in problems in producing the light curves as the optimum target aperture size will vary during an observing session. Consequently an intentional defocus would be the preferred solution with a dedicated overnight session. It should be noted that defocussing is only of use where the target is very bright and would normally require a relatively short exposure time (i.e. there would potentially be a benefit from having a lower scintillation error as a result of having a longer exposure time plus a higher target count). However the need to conduct defocussing in the first place is limited since many of the potential exoplanet targets have relatively faint host stars that already require several minutes of exposure time before any pixel in a target aperture

[10] The area used to estimate the sky background of a strongly defocussed image could inadvertently include faint stars that have been rendered invisible by the defocussing.

reaches its linearity limit. Alternatively, there is also the option to jitter the target (emulating an orthogonal transfer CCD) during an observation to provide a broadly equivalent effect.

### 1.2.6 Non Exoplanet Differential Photometry Studies

Arellano Ferro (Arellano Ferro *et al.* 2013) conducted CCD differential photometry with targets in a crowded central region of a cluster. This paper describes how the photometric precision for targets in crowded fields was typically of the order of 10 milli magnitude with one telescope (2.0m aperture) and 1-5 milli magnitude with the other telescope (1.54m aperture).

An improved method of differential photometry using auxiliary stars (stars outside of the main observing image) has been presented by (Fernández Fernández *et al.* 2012) to generate a light curve that is smoother than those obtained by more conventional methods by the use of many non-variable auxiliary stars when there are very few comparison stars available in the FOV.

### 1.2.7 Robotic Observations

The introduction of Automatic Precision Telescopes (APT) was assessed to speed up extinction observations by an order of magnitude, permitted much faster chopping between program and extinction stars (Young et al. 1992).

Robotically controlled observations are being conducted at several observatories such as:-

(a) Cala Alta Observatory, Almeira, Spain, 50cm aperture (Eibe et al. 2012).
(b) Mauna Loa Observatory (Hawaii), 8.5cm aperture (Guyon *et al.* 2011).
(c) SuperWASP, Observatorio del Roque de los Muchachos on the island of La Palma in the Canary Islands, and at the Sutherland Station of the South African Astronomical Observatory, 20cm aperture (Pollacco et al. 2006).
(d) Bradford robotic telescope, Mount Tiede, Tenerife, 1.6cm to 36.5cm (Seal Braun & Baruch 2009).
(e) TRAPPIST, ESO La Silla Observatory, Chile, 0.6m aperture (Jehin *et al.* 2011).
(f) Watcher, Boyden Observatory, S Africa, 40cm aperture (Ferrero et al. 2010).
(g) Bayfordbury Observatory, 5 telescopes with 40cm aperture (Bayfordbury-Observatory 5.9.2016).
(h) Oversky Observatory, La Palma, Canary Islands, 35cm aperture (Vanhuysse *et al.* 2011).
(i) PIRATE, La Palma, Canary Islands, 42.5cm aperture (Holmes *et al.* 2011).
(j) BlueEye600 robotic observatory, Ondrejov, Czech Republic, 60cm aperture (Durech *et al.* 2017).
(k) DEMONEX, Winer Observatory, Sonoita, Arizona, USA, 50cm aperture (Villanueva *et al.* 2017).
(l) Isaac Newton Telescope, La Palma, Canary Islands, 254cm aperture (Thompson *et al.* 2016).
(m) COATLI, Observatorio Astronomico Nacional, Sierra San Pedro Martir, Mexico, 50cm aperture (Watson *et al.* 2016, Snodgrass *et al.* 2016).
(n) Liverpool Telescope, La Palma, Canary Islands, 200cm aperture (Steele 2004).
(o) STELLAR, Teide Observatory, Tenerife, Canary Islands, 80cm and 120cm aperture (Strassmeier *et al.* 2004).
(p) LCOGT, global network, nine apertures on 1.0m and two apertures of 200cm (Brown *et al.* 2013).

(q) LSGT, Siding Spring Observatory, Australia, 43cm aperture (Im *et al.* 2015).
(r) pt5m, William Herschel Observatory, Roque de los Muchachos, Observatory, La Palma, 50cm aperture (Hardy *et al.* 2015).

Eibe considered that robotic photometric observations may be of higher quality than manual observations due to the repetitive nature of the process (Eibe et al. 2011).

Vanhuysse demonstrated detection of an exoplanet with a remotely controlled observatory equipped with a small (35mm aperture) telescope. The precision of the equipment was assessed as 4 milli magnitude precision during the transit of HAT-P-8b (V=10.17) (Vanhuysse et al. 2011).

### 1.2.8 Non-Uniform Atmospheric Attenuation

Although differential photometry is considered to be suited to degraded observing conditions, observations at low altitude observatories (such as at Bayfordbury) are particularly subject to attenuation due to cirrus cloud, haze, mist, fog, dust, etc. Consequently there is the possibility that non-uniform attenuation could occur across an image and consequently the reference, check and target stars could all experience different time changing attenuations. Since the variation in observed magnitudes could be significant across an image under adverse conditions, it could result in the light curves for check stars having variable star characteristics. This feature might be more of a problem with 'fast' telescopes as they have a wider field of view (than an 'equivalent' 'slow' telescope with the same aperture size) and consequently the selected comparison stars could be much further away in angle from the target and hence more likely to have a different level of cirrus cloud cover.

There is a source of photometric uncertainty due to the variations in the colours of the calibration stars. This source of noise is considered to be negligible (as confirmed by the calibration measurements and final results).

### 1.2.9 Calculating Total Noise

One method of calculating the total noise is given in Southworth (Southworth et al. 2009):-

$$\sigma_{total} = \sqrt{\sigma_{target}^2 + \sigma_{sky}^2 + \sigma_{ron}^2 + \sigma_{flat}^2 + \sigma_{scint}^2} \qquad (9)$$

Where $\sigma_{target}$ is the noise on the target,

$\sigma_{sky}$ is the noise from the sky.

$\sigma_{ron}$ is the read out noise

$\sigma_{flat}$ is the flat field noise

This equation does not include the error due to thermal drift noise in the CCD as it was very low for the equipment used by Southworth. Likewise no allowance is made for cirrus noise, however this is less likely to have been a problem for the results presented in the Southworth paper as they were produced at the La Silla Observatory that is located at an altitude of 2,400m (La_Silla 5.9.2016).

Measurements with the non-variable stars should give a low standard deviation, with Southworth (Southworth et al. 2009) suggesting that the noise from differential photometry due to the measurement of the magnitude of the comparison star can be ignored if one uses many comparison stars.

Note: There are more rigorous methods such as given by Kjeldsen and Frandsen (Kjeldsen & Frandsen 1992) and Hartman (Hartman et al. 2005).

### 1.2.10 Estimation of Photometric Accuracy

The accuracy of the photometry depends on both the noise and the seeing. Koppelmann (Koppelman 2010) combines these sources of error to give a representative measurement of accuracy:-

$$\Delta M = \sqrt{\sigma^2_{Ref-Cavc} + \left(\frac{1}{SNR}\right)^2} \qquad (10)$$

Where $\sigma_{Ref-Cavc}$ is the standard deviation on the difference between the reference star magnitude and the average magnitudes of the check stars. SNR is the signal to noise ratio that can be directly measured on the target star; ideally a measurement of SNR should be taken of the target star in each image, and any images that have a particularly poor SNR should be discarded. Ideally there should be several standard stars (Cooper et al. 2004) of known magnitude close to the target such that they undergo similar seeing.

A detailed analysis of the sources of error is presented by Kjeldsen and Frandsen (Kjeldsen & Frandsen 1992), which in turn calls up the oft cited Gilliland (Gilliland et al. 1991) for CCD calibration techniques. Alternatively, PSF fitting can be used to minimise error, but should not be used if the PSF varies significantly across a CCD frame.

### 1.2.11 Lucky Imaging

Lucky Imaging is a process of achieving greater photometric precision by taking very large numbers of short exposure images, selecting only the best images (when the air turbulence is lower than at other times) and then merge these images to form a composite image (Faedi *et al.* 2013), (Baldwin *et al.* 2001), (Fried 1978), (Law *et al.* 2006), (Mackay 2013). Lucky images can be produced irrespective of the science target (Law *et al.* 2009). Automatic selection of the best images using the Strehl ratio (the peak value of a PSF divided by the theoretical diffraction-limited value) as a selection criterion has been used at the Palomar Observatory (Law 2007, Law et al. 2006, Mahajan 1982, Janssen *et al.* 2006).

There can be a high discard rate of images, although there are techniques to improve on the percentage of images that can be used (Mackay 2013). The lucky imaging technique has been used to obtain almost diffraction limited resolution for observing exoplanet transits. In the case of Bergfors, only the best 5% to 10% of the images were presented (Bergfors *et al.* 2013, Faedi et al. 2013).

The theoretical probability of obtaining a short exposure image is given by Fried (Fried 1978) as:-

$$Probability \approx 5.6e^{\left[-0.15579({D}/{r_0})^2\right]} \qquad (11)$$

For ${D}/{r_0} \geq 3.5$, where D is the aperture diameter and $r_0$ is the coherent length of the distorted wave front (also called the turbulence-limited coherence factor). The conclusion from this work is that careful choice of the aperture diameter and selecting the best images from several hundred exposures will produce images that are significantly better than ordinary turbulence limited images (Fried 1978).

However, since a large number of images will be discarded, especially at low level sites that will have significant atmospheric turbulence (such as the Bayfordbury Observatory), it is considered unlikely that lucky imaging will provide enough images, especially with faint targets (requiring long exposure times) to adequately capture events such as exo-planet transits.

Standard camera shutters take a finite time to move and for very short exposure times the relatively slow shutter speed can result in shadows on an image as there is significantly more exposure at the centre of an image compared to that received at the sides of an image. Consequently specialist cameras such as the Cambridge LuckyCam (Law et al. 2006) have been used for lucky imaging observations such as those conducted by Faedi (Faedi et al. 2013) to minimise the uneven illumination due to shutter speed.

One way to increase cadence is to reduce the frame size used to record an image. This means that there are fewer pixels to down load, a reduced download time and consequently higher frame rates.

Lucky imaging will improve the PSF of a star making it narrower and with a higher peak value. As a result there will be fewer pixels capturing the image and consequently reduces the maximum exposure time. Although this is an undesirable feature for most differential photometry, it is important in crowded fields to avoid blending of the target (and reference stars).

### 1.2.12 Adaptive Optics

The angular width of the principal diffraction image (radians) has previously been defined as:-

$$\theta_{min} = 1.22\frac{\lambda}{D} \quad (1)$$

Where:-

λ is the wavelength (m).

D is the aperture width (m).

θ is defined as the optimum angular resolution that can be achieved by a system; this diffraction limit constrains the size of the smallest optical image. Unfortunately this performance is not normally achieved with a conventional telescope due to turbulence in the earth's atmosphere. (Zeilik & Gregory 1998) causing twinkling, quiver and spreading (Tyson 1998). However, technological developments mean that ground based telescopes at many observatories can now achieve the diffraction limit as a result of introducing adaptive optics to compensate for a turbulent refractive atmosphere (Davies & Kasper 2012). In the case of the 5m telescope at the Palomar Observatory (Law et al. 2009), a combination of Lucky Imaging and adaptive optics achieved the diffraction limit of 35mas at the FWHM with light at 750nm.

Commercial manufacturers are now producing relatively simple adaptive optics systems for smaller telescopes. For example, SBIG claim that their adaptive optics system has achieved a reduction of the FWHM from 3.1” to 2.2” and an increase in brightness of approximately 30% (SBIG 5.9.2016).

AO are now considered to be sufficiently good that they can be used in the search for exoplanets by direct imaging (Yamamoto *et al.* 2013, Wahhaj *et al.* 2013, Rameau *et al.* 2013).

## 1.3 Study Aims

The primary study aims are to:-

(a) Create a validated model of equations that quantify the predicted photometric precision of images taken with a specific telescope, camera and filter configuration at the University of Hertfordshire's robotically controlled telescopes located at the Bayfordbury Observatory in Hertfordshire.

(b) Demonstrate that the predicted precision can be achieved by satisfactorily capturing transits with known transit depths.

Thus following an observing session (or with historical images), one could derive an estimated measurement error with any image. This process allows one to weight results, in particular, weighting data obtained on different nights for repeating events such as exoplanet transits. Although merging results from different telescopes has previously not been advocated because the measurement errors would be different (Young et al. 1992), by knowing the precision with each measurement opens the possibility of combining results from other nearby telescopes.

Other low altitude observatories could potentially also predict the precision of their images using the techniques adopted in this study.

The secondary study aims are to:-

(a) Provide a tool to calculate predicted precision so that one can quickly decide if one can reliably observe an event such as the transit of the exoplanet for star WASP-33. This tool would also enable a user to investigate the optimal value of exposure time and cadence.

(b) Establish a more reliable calculation for the recommended target exposure time for use at the Bayfordbury Observatory.

# 2 METHOD

Chapter 1 has outlined the background to conducting precision photometry. This Chapter identifies the method followed to achieve the stated project objectives. The approach taken has been to:-

(a) Define the generic model of equations to calculate the SD of measurements taken with any telescope and camera combination (Section 2.1). These equations relate the predicted precision of ground based photometric measurements, without specifying any telescope/ camera specific characteristics. These equations not only define the predicted noise in an observation, but also provide predictions on the measured target flux. In the case of achieved precision where images and measurements are available, a subset of the equations can be used but with numerical measurements used instead of their equivalent predicted values.

(b) Specify how the parameters in the generic equations defined in Section 2.1 are to be quantified for a specific telescope and camera combination (Section 2.2).

(c) Identify how observational data is to be generated, processed and used to measure the achieved degree of validation of equations defined in Section 2.1 (Sections 2.3 and 2.4).

Standard Deviation (SD) has the conventional definition of:-

$$\sigma^2 = \frac{1}{(n-1)}\sum_{i=1}^{n}(x_i - \mu)^2$$

Where:-

n is the number of values of x,

$x_i$ is the ith value of x and

$\mu$ is the mean value of x given by:-

$$\mu = \frac{1}{n}\sum_{i=1}^{n} x_i$$

## 2.1 Definition of Generic Model of Equations for Any Telescope and Camera

### 2.1.1 Generic Equations

The observed total standard deviation for a target (or reference star) in units of photons (or ADU) is a combination of intrinsic calibration noise and the noise on a science frame, and is given by:-

$$\sigma_{total} = \sqrt{\sigma_{bias}^2 + \sigma_{dark}^2 + \sigma_{flat}^2 + I_{rms}^2 + \sigma_{sky}^2 + \sigma_{target}^2} \qquad (2.1.1.1)$$

$\sigma_{bias}$ is the bias noise defined by equation (2.2.2.1).

$\sigma_{dark}$ is the dark current noise defined by equation (2.2.3.1)

$\sigma_{flat}$ is the flat field noise defined by equation (2.2.4.4).

$I_{rms}$ is scintillation noise defined by equation (2.2.5.2).

$\sigma_{sky}$ is sky noise defined by equation (2.2.6.2).

$\sigma_{target}$ is the target noise defined by equation (2.2.7.1).

The predicted total count in the target aperture from all sources is given by:-

$$N_{total} = N_{bias} + N_{dark} + N_{sky} + N_{target} \qquad (2.1.1.2)$$

$N_{bias}$ is the bias count defined by equation (2.2.2.2).

$N_{dark}$ is the dark current count defined by equation (2.2.3.2).

$N_{sky}$ is the sky count defined by equation (2.2.6.4).

$N_{target}$ is the target count defined by equation (2.2.7.2) for a measured count or equation (2.2.7.5) for a predicted count.

## 2.2 Method of Deriving Parameters for Equations for a Specific Telescope and Camera

### 2.2.1 General Considerations

The calibrations have been conducted for:-

(a) 2x2 pixel binning.

(b) V filter (where applicable).

The calculations of the SD of the calibration noise was conducted using a specially written Python program to establish the noise on each PIXEL (as opposed to a value for the whole frame). The SD of each pixel was derived from the corresponding pixel counts on a series of images; the overall SD is simply the average of all the individual pixel SDs. A 5 sigma clipping process was applied first to avoid an excessively high SD being introduced by the presence of 'warm' and 'cold' pixels.

The choice of telescope and cameras was restricted to the equipment in the list provided in Appendix A. The use of nominally identical telescope and camera configurations (such as those for the CKT and JHT telescopes) offers the prospect of relatively straight forward read-across and the potential of merging results. The choice was further restricted to equipment that was both functional and available to this project.

The observing campaign endeavoured to be kept reasonably short (although weather restrictions and equipment failures extended the campaign for longer than originally intended), not just to limit the scope for the equipment noise changing over this period, but also because the observatory undergoes regular equipment upgrades and consequently the equipment being used might be changed to a different standard that in turn would require another set of error measurements/ calculations.

Although flat fielding is applied to the images, there can still be a variation in the measured pixel count across an image. This feature is undesirable as not only will different relative magnitudes arise depending on which star is chosen as the reference star, but if the tracking drifts off, then different pixels will be accumulating ADU counts for both the target and reference stars from different locations on the CCD chip: nominally identical readings will consequently differ slightly and introduce an additional noise component. It was decided that a uniformly illuminated calibrated image should have lines drawn horizontally, vertically and diagonally to form a ‘Union Jack’ set of cross-sections and to establish the variation along these lines to see if there was a potential problem (see Section 3.1).

### 2.2.2 Bias Noise and Count

The bias noise and count are constants for a given CCD temperature. The required CCD operating temperature used at the Bayfordbury Observatory is -20°C. They were determined from an analysis of a series of bias images, as outlined in Section 2.2.1.

$$\sigma_{bias} = \text{Constant} \tag{2.2.2.1}$$

$$\mathrm{N_{bias}} = \text{Constant} \tag{2.2.2.2}$$

### 2.2.3 Dark Current Noise and Count

The dark current noise and count are constants and were taken at the CCD operating temperature of -20°C for each of the 2x2, 3x3 and 4x4 hardware pixel binning options. Since the dark current noise and count are both proportional to $t_{exp}$, several dark current images were taken for each value of $t_{exp}$. The dark current and bias for each value of $t_{exp}$ were then determined as outlined in Section 2.2.1.

$$\sigma_{dark} = \dot{\sigma}_{dark} t_{exp} \tag{2.2.3.1}$$

$$N_{dark} = \dot{N}_{dark} t_{exp} \tag{2.2.3.2}$$

### 2.2.4 Flat Field Noise and Count

Dome flats were taken at the CCD operating temperature of -20°C for each of the 2x2, 3x3 and 4x4 hardware pixel binning options. For this study, the dome flat field images were taken with pixel ADU counts close to the linearity limit (see Section 3.3.2) with the bias and dark frames subtracted. The overall pixel calibration SD for each binning option was then calculated using the method outlined in Section 2.2.1. Since the total measured calibration SD ($\sigma_{cal}$) includes both flat field ($\sigma_{flat}$), bias ($\sigma_{bias}$) and dark frame noise ($\sigma_{dark}$), then:-

$$\sigma_{cal} = \sqrt{\sigma_{bias}^2 + \sigma_{dark}^2 + \sigma_{flat}^2} \tag{2.2.4.1}$$

Re-arranging to isolate $\sigma_{flat}$ gives:-

$$\therefore \sigma_{\mathrm{flat}} = \sqrt{\sigma_{\mathrm{cal}}^2 - \sigma_{bias}^2 - \sigma_{dark}^2} \tag{2.2.4.2}$$

Where $\sigma_{bias}$ and $\sigma_{dark}$ have been calculated in equations (2.2.2.1) and (2.2.3.1). It was assumed that $\sigma_{\mathrm{flat}}$ is independent of $t_{exp}$, but directly proportional to the target count. The next step was to establish a value for $\sigma_{flat}$ for an ADU count of 1 (ie $N_{target} = 1$ derived from an ADU count of $(N_{target})_{flat}$ for the flat field measurement) to give the flat field noise for $N_{target} = 1$:-

$$(\sigma_{flat})_{N_{target}=1} = \sigma_{flat}/(N_{target})_{flat} \quad (2.2.4.3)$$

Thus the general case for the flat field noise with any ADU count ($N_{target}$) is:-

$$\sigma_{flat} = (\sigma_{flat})_{N_{target}=1} N_{target} \quad (2.2.4.4)$$

Flat field does not introduce a net change in flux as it is a noise.

### 2.2.5 Scintillation Noise and Count

From equation (8) the standard scintillation noise equation for $N_{target} = 1$ is:-

$$\sigma_{scint} = 0.004 D^{-\frac{2}{3}} X^{\frac{7}{4}} e^{-\frac{h}{H}} (2t_{exp})^{-0.5} \quad (2.2.5.1)$$

Thus the general case for the scintillation noise with any ADU count ($N_{target}$) is:-

$$I_{rms} = N_{target} \sigma_{scint} \quad (2.2.5.2)$$

Scintillation does not introduce a net change in flux as it is a noise.

### 2.2.6 Sky Noise

Let $\sigma'_{sky}$ be the background noise taken with a region of sky essentially devoid of bright stars. (ie $\sigma^2_{target}$=0). Rewriting equation (2.1.1.1) with equation (2.2.4.1) with $\sigma_{target} = 0$ and setting $\sigma_{total} = \sigma'_{sky}$ gives:-

$$\sigma'_{sky} = \sqrt{\sigma^2_{cal} + (I_{rms})^2_{sky} + \sigma^2_{sky}} \quad (2.2.6.1)$$

$$\therefore \sigma_{sky} = \sqrt{\sigma'^2_{sky} - \sigma^2_{cal} - (I_{rms})^2_{sky}} \quad (2.2.6.2)$$

Where $\sigma_{cal}$ is given by equation (2.2.4.1) and $(I_{rms})_{sky}$ is generated using a revised version of equation (2.2.5.2):-

$$(I_{rms})_{sky} = N_{sky} * \sigma_{scint} \quad (2.2.6.3)$$

where $\sigma_{scint}$ is given by equation (2.2.5.1) and $N_{sky}$ is the count from the sky that is assumed to increase linearly with exposure time:-

$$N_{sky} = constant * t_{exp} \quad (2.2.6.4)$$

It is common practice to define sky noise at different levels depending on how bright the sky is on a particular observing night. For example, Southworth (Southworth et al. 2009) identifies different sky conditions as “dark”, “grey” and “bright”. In the case of predicting the expected precision, it will be necessary to identify the predicted sky conditions and use sky noise data appropriate for those conditions. Conversely, if an image has already been taken, then an estimate of the sky conditions is required to give appropriate values of sky noise[11].

[11] Potentially a bespoke calculation of sky noise could be made with an image by making a measurement of the sky noise in that image.

### 2.2.7 Target Noise and Count

The standard assumption is made that the target signal has Poisson characteristics and consequently the target noise is given by:-

$$\sigma_{target} = \sqrt{N_{target}} \qquad (2.2.7.1)$$

Where $N_{target}$ is either the measured value in the case of existing images:-

$$N_{target} = [(\mathrm{N_{target}})_{\mathrm{t=t_{exp},X=X}}]_{\mathrm{measured}} \qquad (2.2.7.2)$$

which corresponds to an average count per second of:-

$$[(\mathrm{N_{target}})_{\mathrm{t=1s,t_{exp},X=X}}]_{\mathrm{measured}} = \frac{1}{t_{exp}}[(\mathrm{N_{target}})_{\mathrm{t=t_{exp},X=X}}]_{\mathrm{measured}} \qquad (2.2.7.3)$$

Or alternatively $N_{target}$ is a predicted value when planning an observation:-

$$N_{target} = [(\mathrm{N_{target}})_{\mathrm{t=t_{exp},X=X}}]_{\mathrm{predicted}} \qquad (2.2.7.4)$$

Where the predicted count after an exposure of $\mathrm{t_{exp}}$ is simply:-

$$[(\mathrm{N_{target}})_{\mathrm{t=t_{exp},X=X}}]_{\mathrm{predicted}} = \mathrm{t_{exp}}[(\mathrm{N_{target}})_{\mathrm{t=1s,X=X}}]_{\mathrm{predicted}} \qquad (2.2.7.5)$$

Where $[(\mathrm{N_{target}})_{\mathrm{t=1s,X=X}}]_{\mathrm{predicted}}$ is derived for a particular telescope and camera combination in equation (2.2.8.8).

### 2.2.8 Conversion of Catalogue Magnitude to Instrument Magnitude

A large number of images were examined covering a wide range of catalogue magnitudes with the objective of establishing:-

(a) An accurate slope of a line fitted to a plot of instrument magnitude (m’) versus catalogue magnitude (m).
(b) The range of magnitudes that the equations (shown below) were valid.

However, since all measurements of m’ have been taken with different values of air mass and exposure times, it was necessary to first scale for $t_{exp}$ to give a common exposure time of 1.0s (Howell 2006) ($m'_{t=1s,X=X}$) and to then compensate the instrument magnitudes for an air mass of 1.0 to generate $m'_{t=1s,X=1.0}$. To compensate for air mass (X), it is assumed that m’ changes linearly with X, and since m is a constant, then the following relationship applies (Cooper et al. 2004):-

$$m'_{t=1s,X=X} - m = \epsilon X + \zeta \qquad (2.2.8.1)$$

Where $\zeta$ is the zero-point offset (depends on the value of $t_{exp}$) and $\epsilon$ is the extinction coefficient that is independent of $t_{exp}$. The analysis by Pereyra (Pereyra *et al.* 2017) with a CCD camera similar to those used at Bayfordbury Observatory indicates that linearity would be expected for up to 90% of well capacity.

A plot of $m'_{t=1s,X=X}$ versus X was then produced and a best fit line fitted to the data points to give the slope ($\epsilon$) and its attendant bias ($\zeta$). A general expression giving $m'_{t=1s,X=1.0}$ was generated by re-expressing equation (2.2.8.1) to give:-

$$m'_{t=1s,X=1.0} - m = \epsilon 1.0 + \zeta \qquad (2.2.8.2)$$

and then equation (2.2.8.1) was subtracted from equation (2.2.8.2) to give:-

$$m'_{t=1s,X=1.0} - m'_{t=1s,X=X} = \epsilon(1.0 - X) \qquad (2.2.8.3)$$

$$\therefore m'_{t=1s,X=1.0} = m'_{t=1s,X=X} + \epsilon(1.0 - X) \qquad (2.2.8.4)$$

The predicted instrumentation magnitude for a star that has a catalogue magnitude of m (that is observed with an air mass of 1.0 and a 1s exposure) is defined by the best straight line fit of a plot of observed magnitude versus catalogue magnitude:-

$$[m'_{t=1s,X=1.0}]_{predicted} = gradient * m + Bias \qquad (2.2.8.5)$$

Where 'gradient' and 'bias' can be extracted from a plot of $m'_{t=1s,X=1.0}$ versus m.

Derived values for $m'_{t=1s,X=1.0}$ were established in Section 3.2.6 from a mixture of archived Bayfordbury images and from some specially generated images where there were too few archived images over the magnitude range of interest. A plot of $m'_{t=1s,X=1.0}$ versus m was then produced and a best line fitted to the data points to give a slope of <u>measured</u> m' versus m and its attendant bias.

The derived equation then underwent a verification exercise by inputting the observation conditions for the same images to generate corresponding <u>predicted</u> values for instrument magnitude ($[m'_{t=t_{exp},X=X}]_{predicted}$). The difference between the predicted and measured values of m' needed to be small and it also provided a measure of the accuracy of the plot. The equation was then subjected to a validation exercise using an independent set of data – the obtained difference between the predicted and achieved values of m' was required to be similar to that obtained in the verification exercise to give confidence in the validity of the approach and to establish the range of catalogue magnitudes that the equations are valid.

The derivation of a predicted instrument magnitude for $t = t_{exp}$ and $X = X$ ($[m'_{t=t_{exp},X=X}]_{predicted}$) has been achieved by the following method. For a proposed observation, the predicted instrument magnitude for a given catalogue magnitude (m) can be established from equation (2.2.8.5). To compensate the predicted value for $[m'_{t=1s,X=1.0}]_{predicted}$ for X, one can re-express equation (2.2.8.3) to predict $m'_{t=1s,X=X}$:-

$$[m'_{t=1s,X=X}]_{predicted} = [m'_{t=1s,X=1.0}]_{predicted} - \epsilon(1.0 - X) \qquad (2.2.8.6)$$

Having obtained a predicted value for $m'_{t=1s,X=X}$, one can then calculate the corresponding predicted value for $(N_{target})_{t=1s,X=1.0}$. Since Pogsen's equation gives:-

$$m'_{t=1s,X=X} = -2.5log_{10}[(N_{target})_{t=1s,X=X}] \qquad (2.2.8.7)$$

Then re-expressing equation (2.2.8.7) gives:-

$$[(N_{target})_{t=1s,X=X}]_{predicted} = 10^{-[m'_{t=1s,X=X}]_{predicted}/2.5} \qquad (2.2.8.8)$$

$[(N_{target})_{t=1s,X=X}]_{predicted}$ is an important term as it can be used to derive the peak count in a pixel and in turn the maximum exposure time to keep the measured counts within the linearity limit for the CCD chip (see Section 3.3.2).

The highest achievable value for $N_{target}$ corresponds to an air mass of X=1.0 and is a more rigorous condition for predicting the peak count in a pixel. Re-stating equation (2.2.8.8) for X=1.0 gives:-

$$[(N_{target})_{t=1s,X=1.0}]_{predicted} = 10^{-[m'_{t=1s,X=1.0}]_{predicted}/2.5} \qquad (2.2.8.9)$$

The predicted count for any other time is obtained by factoring the predicted count for t=1s by $t_{exp}$.

$$\therefore [(N_{target})_{t=t_{exp},X=X}]_{predicted} = t_{exp}[(N_{target})_{t=1s,X=X}]_{predicted} \qquad (2.2.7.4)$$

Thus the predicted instrument magnitude is at $t = t_{exp}$ and X=X is given by:-

$$[m'_{t=t_{exp},X=X}]_{predicted} = -2.5log_{10}\{[(N_{target})_{t=t_{exp},X=X}]_{predicted} \qquad (2.2.8.10)$$

By definition, the measured instrument magnitude is:-

$$[m'_{t=t_{exp},X=X}]_{measured} = -2.5log_{10}[(N_{target})_{t=t_{exp},X=X}]_{measured} \qquad (2.2.8.11)$$

The difference ($\Delta m'$) between the predicted and measured values of m' at $t = t_{exp}$ and X=X is simply:-

$$\Delta m' = [m'_{t=t_{exp},X=X}]_{predicted} - [m'_{t=t_{exp},X=X}]_{measured} \qquad (2.2.8.12)$$

## 2.3 Method of Calculating Achieved Photometric Precision

### 2.3.1 Strategy to Assess Predicted Precision Against Achieved Precision

Sufficiently large numbers of observations were required to validate the formulation over a large range of target magnitudes, exposure time and air mass. Consequently the following information was required:-

(a) A list of a limited number of non-variable targets that are observable at Bayfordbury Observatory for substantial periods of time that cover a sufficiently wide spread of magnitudes to validate the formulation over the predicted range of magnitude validity (Section 2.3.2).
(b) A list of targets that are suitable to observe on any given day (Section 2.3.3).
(c) The recommended exposure times for observing each selected target (Section 2.3.4).

The images obtained from an observing session need to be processed to generate results that can be used to demonstrate compliance with the project objectives (Sections 2.3.5 and 2.3.6).

The formulation given in Section 2.2 to calculate precision for a given set of observing conditions needed to be validated using a credible set of tests to demonstrate that the project objectives have been met. The three general test conditions are:-

(a) Observing a non-variable star over a prolonged observing period. The measured noise can then be compared against the predicted noise (Section 3.4.1).
(b) Observing transits with a known transit depth. The predicted precision for a known transit should indicate whether the transit could be reliably detected and the subsequent observations should confirm that such transits have indeed

been captured. In the case of exo-planets, a secondary measure of precision is to use a transit fitting program with the measured data to derive the measured depth of transit. This depth can then be compared with the corresponding reference value for the depth of transit to give a measure of the achieved precision Section 3.4.2.

(c) Observing variable star UX UMa to demonstrate that the predicted precision can be used to define the tolerance bars for the light curves of variable stars (Section 3.4.3).

### 2.3.2 Identify Suitable Targets for Validation of Equations

Suitable targets covering a wide range of magnitudes were required to validate the equations. The following considerations were made to select targets that were considered to be the most useful in confirming the predicted precision of the equations:-

(a) Although the instrument magnitude can be predicted for a large range of target catalogue magnitudes, the target choice needed to be restricted to a magnitude range where reliable measurements can be made. For instance, a very low target magnitude required a very long exposure time to obtain a meaningful flux measurement. The general guide being to not exceed an exposure time exceeding 10 to 15 minutes in order that reliable tracking could be achieved.
(b) Exo-planet transits were identified where there is a known change in magnitude.
(c) All targets were non-variable, or have a variability that is significantly lower than the depth of a transit.
(d) The targets were ideally observable for a significant period of time over much of the year so that measurements could be more readily taken and provide the opportunity to fold results into a composite set of results.
(e) The target star should have suitable check stars in close proximity (see Section 1.2.1).
(f) The Declination angle should ideally be not be too low since a low an angle will:-
    (i) Risk being too low for the telescopes to mechanically slew to observe the target (the limits are defined in the Bayfordbury Observatory web site (Bayfordbury-Observatory 5.9.2016)).
    (ii) Result in an undesirably high air mass on the observations.

### 2.3.3 Identify Targets to Observe When Observing Conditions are Predicted to be Favourable

The observation campaign needed to be planned with the following guidelines:-

(a) Consult the BBC weather web site (BBC 6.10.2017) to establish the predicted cloud cover over the following few days. Identify any nights that were predicted to provide a prolonged period of clear skies that were needed to obtain images of a full transit.
(b) Avoid nights when there was a high moon phase angle and the moon would be in close proximity to the target.
(c) Establish the predicted exo-planet transits on the proposed observing night using the web site of the Czech Astronomy Society (Czech 5.9.2016).
(d) Dismiss unsuitable transits using the following criteria as a starting point:-
    (i) Stars with a Declination angle below the lowest value that the chosen telescope could achieve.

(ii) Any exoplanets with transit depth of less than 0.005 magnitude so that the transit can be clearly identified.

(iii) Any exoplanets whose transit begins/ ends outside of the hours of observing at the Bayfordbury web site.

(iv) Any transits that start or end outside of the period that the target star is observable from the chosen telescope.

A simple sketch on graph paper showing the timings for items (iii) and (iv) simplifies the process of not only identifying the transits that can potentially be fully observed, but also to define the duration of the observations with each target if more than one transit is to be observed on the same night with the same telescope.

### 2.3.4 Decide on the Exposure Time

The exposure time needed to be carefully chosen with the following issues considered:-

(a) The maximum exposure times for the target and its associated stars used for differential photometry were chosen to avoid exceeding the linearity limit of the CCD chip.

(b) To not exceed 15 minutes as higher values might result in the telescopes having tracking difficulties.

(c) An optimised value needed to be selected to give a high enough cadence yet still give sufficient precision. Better precision comes with longer exposure times (to minimise scintillation noise) but a higher cadence provides more images in the same available time such that the transit can be clearly identified from the light curve.

(d) Avoid serious blooming problems by using a non anti-blooming CCD camera.

### 2.3.5 Obtaining Images to Generate Light Curves and Derive an Estimate of Achieved Precision

Large numbers of images requiring several hours of observing time were required to provide a sufficient number of images to measure the achieved precision over a wide range of target magnitudes to:-

(a) demonstrate that the predicted precision would be achieved in practice,

(b) encompass a sufficiently large number of targets and

(c) provide a large number of points for a transit fitting program to be able to generate a good curve to fit to the observed transit.

The images could be obtained either by manually controlling the telescopes, or by submitting robotically controlled jobs as described by Appendix B. Although operating the telescopes manually is fairly straightforward for a limited number of images, the need for several hours of contiguous observations throughout a night with tightly specified time windows was found to be more suitable for robotically controlled observing.

### 2.3.6 Checking Images

Images taken after (or preferably during) an observing session, and their associated FITS headers, needed to be checked for faults that might impact on the precision of the analysis. These issues include:-

(a) The telescope was so far mis-aligned that it could not be 'plate solved' by the processing software as it could relate the image to what should be observed in that image.
(b) Aircraft tracks through the image.
(c) The image was badly out of focus (the stars had the appearance of ring doughnuts).
(d) Badly overexposed stars (with a non anti-blooming CCD camera) causing vertical lines in the vicinity of the stars being used for photometry purposes.
(e) Cirrus cloud.
(f) Proximity and phase of the moon from the target star.
(g) Icing on the CCD chip during periods of warm weather.
(h) The CCD temperature, as recorded in the FITS header (CCD-TEMP) to an image needed to be inspected for compliance with the intended operating temperature (SET-TEMP). For example, the CCD could have been either set at the wrong temperature or the cooling was not requested. In periods of warm weather when the ambient temperature was high, the CCD temperature could drift if the CCD camera cooling system is unable to stabilise at the required temperature (see Figure 6 in Section 3.4.2) for an example of such a failure).
(i) Maximum air mass achieved: any images with an air mass greater than 2.0 might have questionable accuracy.
(j) Conduct aperture slices through the target, reference and all check stars to verify that the peak values have not saturated, and more importantly have not exceeded the CCD linearity limit.

### 2.3.7 Method of Processing of Results

**Faulty Pixels**

The high quality CCD chips used meant that there should have been very few faulty pixels and as a consequence it was unlikely, considering the relatively small size of the target aperture and sky annulus that they would interfere with photometric measurements. The derivation of the SD values, in the calibration files identified very few deficient pixels and consequently they were not considered to be a problem. A faulty hot pixel could have been identified by using one of the software processing package (such as Maxim DL) to graphically display the values in selected areas of the image.

**Differential Photometry**

Differential photometry was used with an aperture over the target star and an surrounding annulus to establish the background sky brightness[12]. The size of the aperture is a compromise between including all the light from the star and including excessive noise (Cooper et al. 2004). The convention adopted is to identify an aperture size with a radius in pixels of 3*FWHM. The annulus needs to have radii that encompass an area of at least 3 times that of the target aperture to give a good statistical determination of the background level (Howell 2006). Differential photometry could only be conducted with valid data files; for instance the software

[12]Unless special circumstances prevail such as when there was blending or an aircraft track passes through the sky annulus: in such circumstances an aperture was placed in a nearby region of sky and used instead.

package Maxim DL™ (CyanogenImaging 2016) would not calculate photometry for an image that has not been plate solved[13].

A suitable reference star of known magnitude and several check stars were identified to the software processing package in order that a tabular set of magnitude data could be produced and in turn a set of light curves. The light curves were inspected to ensure that the light curves for the check stars were reasonably horizontal. A limited magnitude range plot then needed to be produced for the target star to reveal the detailed transit. Any apparently 'rogue' points needed to be investigated (see Section 2.3.6).

The data was initially assigned a Julian Date (JD) time that needs to be converted to either the time from the start of observations or some other reference time such as the scheduled start of transit. The time base needed to be converted to hours and fractions of hours and the start and end of transit needed to be represented in the composite plot.

The observed differential magnitude of target ($\Delta m$) was calculated by a data processing package and added to the reference star magnitude ($m_{REF}$) to give a relative magnitude of the target star:-

$$m = m_{REF} + \Delta m \qquad (2.3.7.1)$$

The standard deviation on the relative magnitude of the target star is consequently a function of the error on the magnitude measurement noise of both the target ($\sigma_{\text{total}}$) and reference star ($\sigma_{REF}$). The all-inclusive SD (assuming small magnitude errors) for the difference between the target approximates to:-

$$\sigma_{all} = \sqrt{\sigma_{\text{total}}^2 + \sigma_{REF}^2} \qquad (2.3.7.2)$$

If N reference stars were to be used then the standard deviation (using the law of quadrature) on the composite reference magnitude is:-

$$\sigma_{REF} = \frac{\sqrt{\sigma_{REF1}^2 + \sigma_{REF2}^2 + \cdots + \sigma_{REFN}^2}}{N} \qquad (2.3.7.3)$$

Let $\sigma_{REF1} = \sigma_{REF2} \ldots = \sigma_{REFN}$

$$\therefore \sigma_{REF} = \frac{\sqrt{\sigma_{REF1}^2 + \sigma_{REF1}^2 + \cdots + \sigma_{REF1}^2}}{N} \qquad (2.3.7.4)$$

$$\therefore \sigma_{REF} = \frac{\sigma_{REF1}}{\sqrt{N}} \qquad (2.3.7.5)$$

In other words the precision will improve with additional reference stars, provided that the errors on individual reference stars are not excessively large. For example, if there are two stars with the first reference star having an SD of $\sigma_{REF1}$ and the second reference star with a high standard deviation of (say) $\sigma_{REF2} = 4\sigma_{REF1}$ is used, then the revised error with two reference stars $\sigma_{REF}$=$\sqrt{(\sigma_{REF1}^2 + 4^2\sigma_{REF1}^2)}/2$ $\approx 2\sigma_{REF1}$. This means that taking another reference star with a high noise can significantly increase the overall noise. However, since the value of the noise with

[13] An image that has not been plate solved has a slightly smaller file size than an image that has been plate solved.

each reference star is known, it should be possible to calculate whether using a particular star would be useful as a reference star.

**Data Folding**

Although multiple transits of the same exo-planet (or UX UMa: see Table 6) could have been data folded and time binned, it has not been conducted for a number of reasons. The main one being that it was judged that significant effort might be required to conduct data folding correctly and would not add significantly to the project. Potential technical issues identified with data folding were:-

(a) It might have been necessary to compensate for different systematic biases when over plotting complementary sets of observations. Consequently the mean measured magnitude whilst the exoplanet is out of transit might need to be worked out for each set of observations and the light curve shifted accordingly.
(b) There is a danger with long exposure times (eg 10 minutes) that the time window might straddle the start or end of a transit and distort the shape of the transit.
(c) The data folding that was conducted with UX UMa found that the orbital period would noticeable vary and as a consequence the transit needed to be aligned by hand. The varying orbital time with UX UMa is a known feature (Kjurkchieva & Marchev 1994) that can also apply with exo-planet transits.

**Curve Fitting**

Curve fitting using the tool provided by the web site for the Czech Astronomy Society (Czech 5.9.2016) was conducted to obtain a matched curve for each transit – and a measured transit depth and duration established by this tool that could then be compared to the supplied reference data.

## 2.4 Method of Assessing Photometric Precision

### 2.4.1 Software Tools

A number of commercially available and free issue software packages (such as APT™, DSL™ and Maxim DL™) were used with the appropriate equations to analyse images to produce a table of data for input into a Microsoft EXCEL©™ spread sheet (or a user written program) to calculate the SD (see Appendix D). The predicted SD was calculated using a Microsoft EXCEL©™ spread sheet (or a user written program).

### 2.4.2 Calculating Measured Standard Deviation

The achieved precision for a series of existing images was calculated by an analysis of individual images with the equations given in Section 2.2 tailored for the particular telescope (see Section 3.3.1)[14]. Alternatively, the SD was also directly calculated from the light curve (whilst a target was not in transit).

---

[14] It can be quite labour intensive to extract all of the data for the equations, especially with large numbers of images. However, since the dominant reason for a variation in the measured precision is the air mass (X), then it is assumed that it is sufficient to analyse a small number of images in detail to indicate how the precision varies across the light curve.

### 2.4.3 Calculating Predicted Standard Deviation

The predicted precision for the anticipated observing conditions was calculated using the equations given in Chapter 2 tailored for the particular telescope (see Section 3.3.2) to predict the standard deviation.

### 2.4.4 Compare the Predicted and Achieved Values of Standard Deviation

The predicted and observed values of standard deviation were compared in an EXCEL™ spread sheet. The differences were plotted against target magnitude. Any 'rogue' values identified by this process were investigated to establish whether there was:-

(a) A problem with that particular set of observations, or
(b) a calculation error, or
(c) a weakness in the formulation, or
(d) significantly different observing conditions to that assumed.

# 3 RESULTS

Chapter 2 has defined the generic model and its equations for any combination of telescope and camera. This Chapter provides results for a specific telescope, camera and filter configuration operating at the Bayfordbury Observatory. The approach taken has been to:-

(a) Verify that a calibrated uniformly illuminated image has a very small gradient in ADU values across the image. (Section 3.1).
(b) Derive the parameters for the equations derived in Section 2.1 for a specific telescope, camera and filter combination at Bayfordbury Observatory (Section 3.2).
(c) Populate the generic equations with the telescope, camera and filter specific data and sequentially order such that the achieved/ predicted precision can be calculated in a spread sheet (Section 0).
(d) Present the results of observations taken (Section 3.4).
(e) Compare the predicted precision from the equations with the achieved precision from the observations (Section 3.5).

The location of soft copies of images used for this analysis is defined in Appendix C and proprietary software packages used identified in Appendix D.

## 3.1 'Union Jack' Analysis

The purpose of this exercise was to demonstrate that light images had been accurately calibrated by the dome flats. i.e. to prove that a light images of the sky have uniform brightness after calibration using the dome flats. Poor quality differential photometry might arise if there was a significant slope in brightness across a calibrated image.

Several sets of 10 images with few stars present were taken in quick succession to provide a set of calibrated images. i.e. The images had bias, dark and flat field calibrations applied and the next phase was to 'remove' the presence of stars in order to measure the variation in the measured sky over a complete image. This has been achieved by a purpose written Python program to apply sigma clipping with multiple passes to successively remove the return from the stars and 'rogue' points.

For each set of 10 image files, each of the 10 image files was successively processed to remove the stars by applying multi pass sigma clipping. Initially only $+\sigma$ clipping was conducted to remove the stars, however one diagonal was found to have a dead pixel and consequently gave a zero output, so $\pm\sigma$ clipping has been conducted. Another factor was that applying only $+\sigma$ clipping meant that the updated $\sigma$ value for use in the next pass did not change very quickly: this was because there were still some large low value pixels (eg dead pixels) distorting the SD calculation.

All 10 of the sigma clipped files were then processed to generate a single image holding composite pixel values for the mean and a further single image with the composite median values. For information, a composite array was also produced for the SD values. These arrays were subsequently used to generate 3 files in FITs format for plotting.

The next phase of the processing was to ‘cut’ two diagonal lines and two lines to form a cross over the image comprising median values. A linear array was formed for each line and plots of median counts versus column number were generated.

A Python linear regression module was then applied to each cut to give a best fit linear line. The gradient gives a measure of the flat field slope. In addition, calculations have been conducted to work out the “variation” of the plot compared to the linear line to obtain a measure of how good a straight line fit is to the plots. The variation was calculated using the best fit line ($y=mx_i + c$) to calculate a measure of the divergence of the values on a cut from the best fit line. Using the convention adopted shown by Norton (Cooper et al. 2004) where “i” is the column number for a pixel along a cut and ($x_i$,$y_i$) are the values of the “i”th data point in a cut, and N is the number of columns:-

$$SD = \left[\frac{\sum(y_i - mx_i - c)^2}{N}\right]^{0.5} \qquad (3.1.1)$$

All data processing was of images taken on the CKT telescope with 2x2 binning and a “V” filter. The following data files were processed:-

(a) Six sets of ten files with 60s images with UX UMa. 3 sets from 6.9.2013 (images in the range 15140 to 15169) and 3 sets from 7.9.2013 (images in the range 15338 to 15367).

(b) 9 sets of 10 files with 60s images for V795 Her. All 9 sets were from 4.9.2013 (images in the range 14859 to 14973).

(c) 9 sets of 10 files with 120s images for V795 Her. All 9 sets were from 5.8.2013 (images in the range 14141 to 14254).

The images were processed by a specially written Python program to calculate these slopes and the SDs about these slopes, with variants tailored for 60s and 120s exposures, for plotting by the Matplotlib routines called up by the Python program. Straight forward directory name changes were required in the program to access the files in the directory allocated for each set of 10 files.

The program can be readily changed to select the number of passes and SDs to apply. In all cases ±σ and 3 passes were selected.

The results presented in Appendix E show the observed variation across a large number of images: the slopes show very small (typically <0.003 ADU counts per pixel in any direction across the chip), so the error resulting from a tracking error shifting the images by several pixels across the chip will be insignificant compared to other sources of error. The SDs about the slopes were typically <5ADU which is considered to be relatively insignificant compared to other errors, and considering the intrinsic uncertainty in these processed images. This also means that the calculated instrument magnitude (m’) derived for different reference stars should not be significantly influenced by any slope that is present across the CCD chip.

## 3.2 Derived Data for a Site Specific Telescope and Camera Configuration

Section 3.2 provides numerical values for the CKT telescope (its configuration and camera are outlined in Appendix A) with a V filter and 2x2 hardware binning. The key characteristics of the CKT telescope are that it is a robotically controlled Meade LX200GPS telescope with an aperture of 406.4mm and a focal length of 4064mm. As indicated by Appendix A, the JHT telescope has an identical configuration to the CKT telescope and consequently read-across of the CKT telescope characteristics can be applied to the operation of the JHT telescope. Occasional use has been made of the RPT telescope that has the same telescope build standard, but has a different camera to that used by the CKT telescope. Consequently any analysis conducted using the CKT telescope data is believed to be only indicative of the expected performance with the RPT telescope.

The approach taken has been to:-

(a) Generate calibration data (Section 3.2.1 to Section 3.2.3).
(b) Define the parameters for the scintillation error (Section 3.2.4).
(c) Calculate a representative formulation for sky noise (Section 3.2.5).
(d) Establish parameters for the catalogue to instrument magnitude equation using images from the Bayfordbury Observatory archives and specially taken images for this project (Section 3.2.6).

### 3.2.1 Bias

The SD and bias values (obtained from an analysis of a series of bias frames) respectively replace the constants in equations (2.2.2.1) and (2.2.2.2) to give:-

$$\sigma_{bias} = 6.37 \qquad (3.2.1.1)$$

$$N_{bias} = 839 \qquad (3.2.1.2)$$

### 3.2.2 Dark Current

The SD and dark current values (obtained from an analysis of a series of dark current frames) respectively replace the constants in equations (2.2.3.1) and (2.2.3.2) to give:-

$$\sigma_{dark} = 0.0028 t_{exp} \qquad (3.2.2.1)$$

$$N_{dark} = 0.0306 t_{exp} \qquad (3.2.2.2)$$

### 3.2.3 Flat Field

The analysis of a series of flat field frames has derived the constant term $(\sigma_{flat})_{N_{target}=1}$ in equation (2.2.4.4):-

$$\sigma_{flat} = (\sigma_{flat})_{N_{target}=1} N_{target} \qquad (2.2.4.4)$$

to give:-

$$\sigma_{flat} = 0.00211 N_{target} \qquad (3.2.3.1)$$

### 3.2.4 Scintillation Error

The standard scintillation equation (2.2.5.1):-

$$\sigma_{scint} = 0.004D^{-\frac{2}{3}}X^{\frac{7}{4}}e^{-\frac{h}{H}}(2t_{exp})^{-0.5} \qquad (2.2.5.1)$$

has the scale height (H), the Bayfordbury Observatory height (h) and telescope aperture diameter (D) substituted by 8000m, 60m and 0.4m respectively to give:-

$$\sigma_{scint} = 0.00731301 * X^{\frac{7}{4}} * \left(2t_{exp}\right)^{-0.5} \qquad (3.2.4.1)$$

The equation for the total scintillation error ($I_{rms}$) is simply equation (2.2.5.2) as the SD scales with target count.

$$\therefore I_{rms} = N_{target}\sigma_{scint} \qquad (2.2.5.2)$$

### 3.2.5 Sky Noise

The SD and bias equations were populated with values obtained from an analysis of areas of sky in several images to give numerical values in equation numbers (2.2.6.2) and (2.2.6.4).

$$\sigma_{sky} = \sqrt{\sigma'^2_{sky} - \sigma^2_{cal} - (I_{rms})^2_{sky}} \qquad (2.2.6.2)$$

$$N_{sky} = constant * t_{exp} \qquad (2.2.6.4)$$

The mean count for the sky in these images was calculated as:-

$$N_{sky} = 3.95t_{exp} \qquad (3.2.5.1)$$

The corresponding SD analysis of the sky data from a series of images gives:-

$$\sigma'_{sky} = 0.078t_{exp} + 6.37 \qquad (3.2.5.2)$$

$$\therefore \sigma'^2_{sky} = 0.006084t^2_{exp} + 0.99372t_{exp} + 6.37^2 \qquad (3.2.5.3)$$

Now $\sigma_{cal}$ is defined by equation (2.2.4.1):-

$$\sigma_{cal} = \sqrt{\sigma^2_{bias} + \sigma^2_{dark} + \sigma^2_{flat}} \qquad (2.2.4.1)$$

Where

$$\sigma_{bias} = 6.37 \qquad (3.2.1.1)$$

$$\sigma_{dark} = 0.0028t_{exp} \qquad (3.2.2.1)$$

Substituting $N_{sky}$ for $N_{target}$ in equation (3.2.3.1)

$$\sigma_{flat} = 0.00211N_{target} \qquad (3.2.3.1)$$

gives:-

$$\sigma_{flat} = 0.00211N_{sky} \qquad (3.2.5.4)$$

Substituting $N_{sky}$ from equation (3.2.5.1) into equation (3.2.5.4) gives:-

$$\therefore \sigma_{flat} = 0.00211 * 3.95t_{exp} = 0.0083345t_{exp} \qquad (3.2.5.5)$$

Substituting $\sigma_{bias}$ from equation (3.2.1.1), $\sigma_{dark}$ from equation (3.2.2.1) and $\sigma_{flat}$ from equation (3.2.5.5) into equation (2.2.4.1) gives:-

$$\therefore \sigma_{cal}^2 = (6.37)^2 + (0.0028t_{exp})^2 + \left(0.0083345t_{exp}\right)^2 \quad (3.2.5.6)$$

$$\therefore \sigma_{cal}^2 = 0.0000773t_{exp}^2 + 6.37^2 \quad (3.2.5.7)$$

Substituting $N_{sky}$ in equation (3.2.5.2)

$$I_{rms} = N_{target}\sigma_{scint} \quad (2.2.5.2)$$

gives:-

$$I_{rms} = N_{sky}\sigma_{scint} \quad (3.2.5.8)$$

The typical value for air mass is in the range 1 to 2. Taking an average value for X=1.5 in equation (3.2.4.1)

$$\sigma_{scint} = 0.00731301 * X^{\frac{7}{4}} * \left(2t_{exp}\right)^{-0.5} \quad (3.2.4.1)$$

gives

$$\sigma_{scint} = 0.014868 * \left(2t_{exp}\right)^{-0.5} \quad (3.2.5.9)$$

Substituting $N_{sky}$ from equation (3.2.5.1) and $\sigma_{scint}$ from equation (3.2.5.9) into equation (3.2.5.8) gives:-

$$I_{rms} = 3.95t_{exp} * 0.014868 * \left(2t_{exp}\right)^{-0.5} \quad (3.2.5.10)$$

$$\therefore I_{rms} = 0.0415274 * t_{exp}{}^{0.5} \quad (3.2.5.11)$$

$$\therefore I_{rms}^2 = 0.0017245t_{exp} \quad (3.2.5.12)$$

Substituting $\sigma_{sky}'^2$ from equation (3.2.5.3), $\sigma_{cal}^2$ from equation (3.2.5.7) and $I_{rms}^2$ from equation (3.2.5.12) into equation (2.2.6.2) gives:-

$$\begin{aligned}\sigma_{sky}^2 = {} & 0.006084t_{exp}^2 - 0.000773t_{exp}^2 \\ & +0.99372t_{exp} - 0.0017245t_{exp} \\ & +6.37^2 - 6.37^2\end{aligned} \quad (3.2.5.13)$$

$$\therefore \sigma_{sky}^2 = 0.0060067t_{exp}^2 + 0.9919955t_{exp} \quad (3.2.5.14)$$

$$\sigma_{sky} = \sqrt{t_{exp}(0.0060067t_{exp} + 0.992)} \quad (3.2.5.15)$$

Note: these values correspond to a relatively low sky noise, as the intention has been to find the limiting precision that could be achieved. Ideally a set of equations corresponding to equation (3.2.5.15) should be generated corresponding to different amounts of sky noise, perhaps as a function of the moon brightness. As stated in Section 2.2.6, measurements of sky noise can potentially be calculated for individual images, although this does require a significant effort.

### 3.2.6 Catalogue to Instrument Magnitude Relationship

Section 2.2.8 outlined the relationship between catalogue and instrument magnitude that is central to calculating a predicted ADU count for a target (and reference star).

Appendix F presents the results of a significant exercise to derive values for the “gradient” and “Bias” in equation (2.2.8.5) from Figure 22 (also shown below for convenience) to give a predicted instrument magnitude (with an air mass of 1.0 and a 1s exposure) for a given catalogue magnitude (m):-

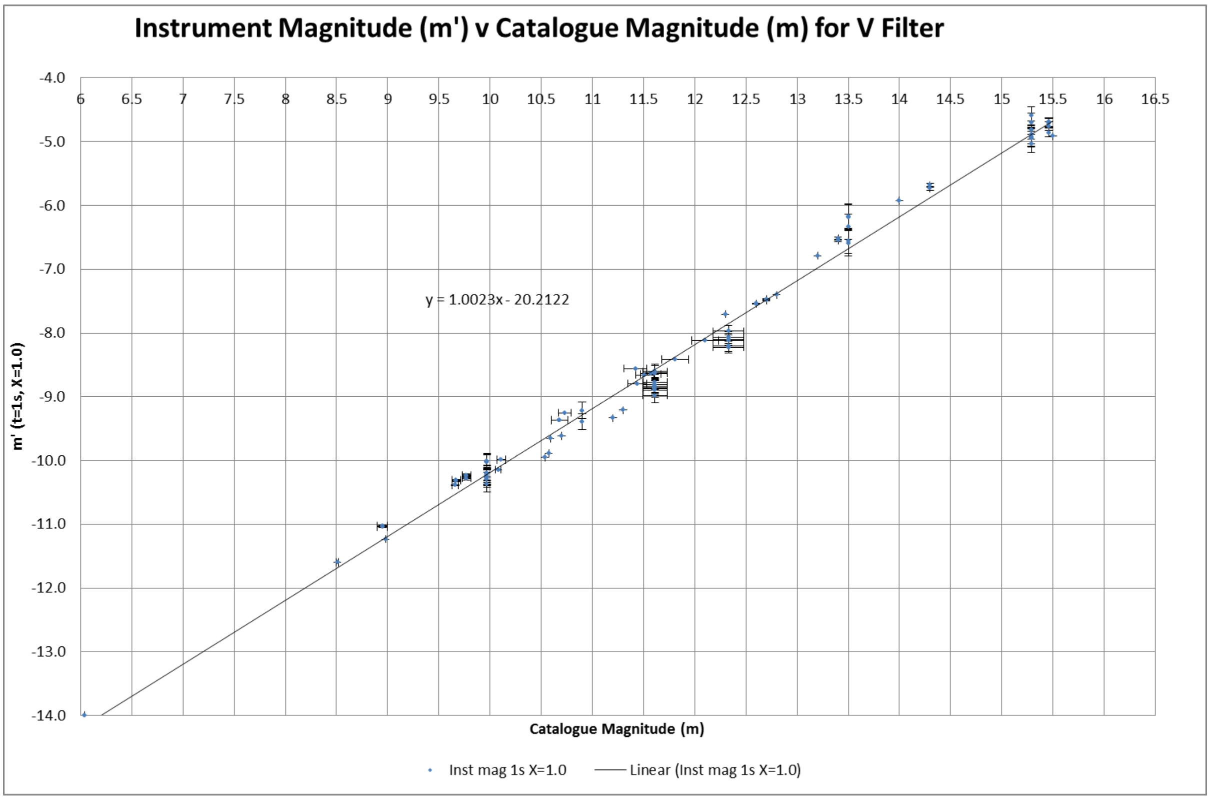


**Figure 22 Plot of Instrument Magnitude ($m'_{t=1s,X=1.0}$) Versus Catalogue Magnitude (m)**

$$[\mathrm{m'}_{\mathrm{t=1s,X=1.0}}]_{\mathrm{predicted}} = 1.0023\mathrm{m} - 20.2122 \qquad (3.2.6.1)$$

These parameters were established using non variable target stars chosen to include extremes of magnitude that could be observed by the Observatory’s telescopes to indicate the range of magnitudes that the equations are valid for.

Appendix F also established a value for ε from the slope in Figure 21 (also shown below for convenience) to compensate instrument magnitude for air mass in equation (2.2.8.6) to give:-

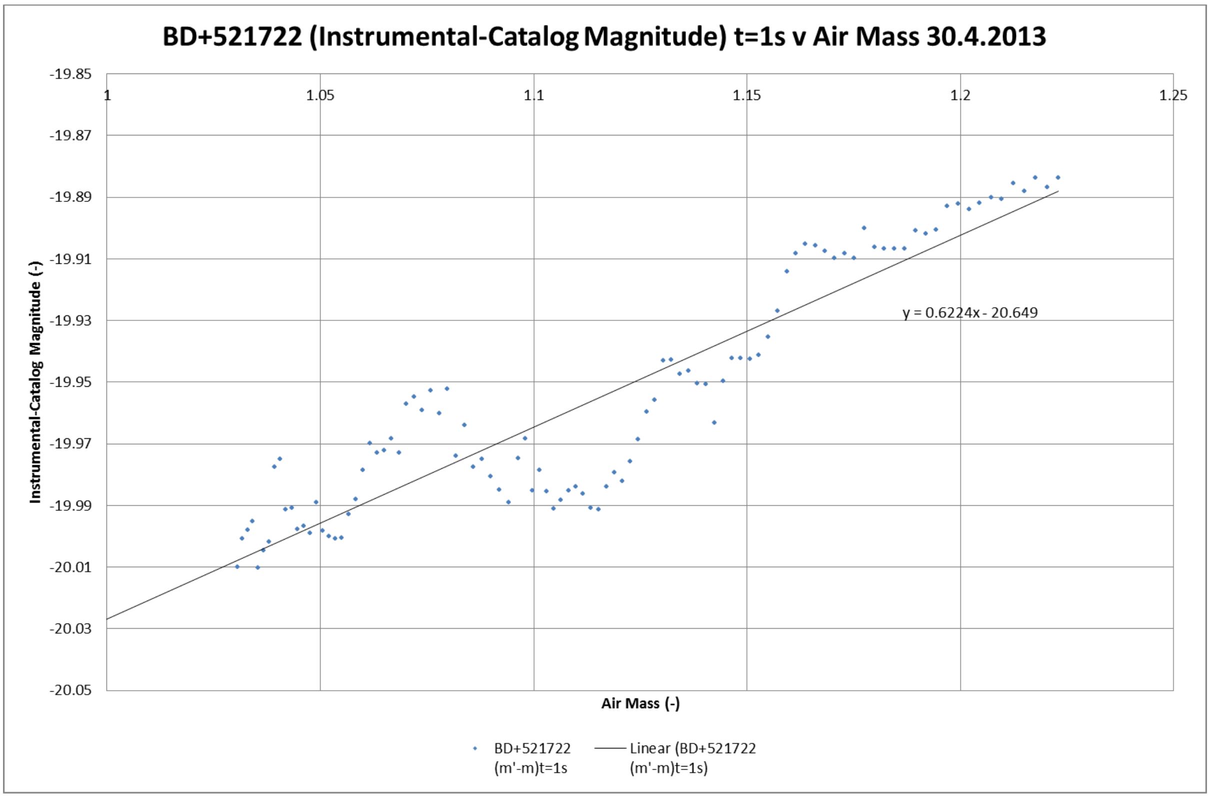


**Figure 21 (m'- m) v Air Mass for BD+52 1722 on 30.4.2013 with a V Filter**

$$[\mathrm{m'}_{\mathrm{t=1s,X=X}}]_{\mathrm{predicted}} = [\mathrm{m'}_{\mathrm{t=1s,X=1.0}}]_{\mathrm{predicted}} - 0.62(1.0 - \mathrm{X}) \qquad (3.2.6.2)$$

Alternatively:-

$$[\mathrm{m'}_{\mathrm{t=1s,X=1.0}}]_{\mathrm{predicted}} = [\mathrm{m'}_{\mathrm{t=1s,X=X}}]_{\mathrm{predicted}} + 0.62(1.0 - \mathrm{X}) \qquad (3.2.6.3)$$

Scaling for t=$t_{exp}$ using equations (2.2.8.8), (2.2.7.4) and (2.2.8.10) gave $[\mathrm{m'}_{\mathrm{t}=t_{exp},\mathrm{X=X}}]_{\mathrm{predicted}}$). Thus measured values of instrument magnitude ($[\mathrm{m'}_{\mathrm{t}=t_{exp},\mathrm{X=X}}]_{\mathrm{measured}}$) from equation (2.2.8.11) could be directly compared with the predicted values of instrument magnitude ($[\mathrm{m'}_{\mathrm{t}=t_{exp},\mathrm{X=X}}]_{\mathrm{predicted}}$). The work not only verified that the populated equations were self-consistent with the source data, but subsequently validated them using a larger pool of additional data covering an even larger range of catalogue magnitudes. The evidence suggested that the equations might be valid for catalogue magnitudes in the range 5 to at least 16.5 when working in V band and using 2x2 hardware binning.

### 3.3 Equations to Calculate Standard Deviation For a Specific Telescope and Camera Configuration

This Section summarises the equations to be used to calculate the predicted or achieved precision[15]:-

(a) Equations for calculating the achieved precision from existing images (Section 3.3.1).

(b) Equations to calculating the predicted precision when observing a target with user defined observing conditions (Section 3.3.2).

#### 3.3.1 Equations for Calculating Achieved Standard Deviation for a Given Image

The following equations have been employed to calculate the achieved SD in existing images using the user defined $t_{exp}$, the achieved air mass (X) and the measured values of $N_{target}$, $(\sigma_{sky})_{target}$, $N_{reference}$ and $(\sigma_{sky})_{reference}$ for the CKT (or JHT) telescope operating with a V filter and 2x2 binning for the target star. The total SD for the target is essentially equation (2.1.1.1).

$$(\sigma_{total})_{target} = \sqrt{\sigma_{bias}^2 + \sigma_{dark}^2 + \sigma_{flat}^2 + (I^2{}_{rms})_{target} + (\sigma_{sky}^2)_{target} + \sigma_{target}^2} \quad (3.3.1.1)$$

$$\sigma_{bias} = 6.37 \quad (3.2.1.1)$$

$$\sigma_{dark} = 0.0028 t_{exp} \quad (3.2.2.1)$$

$$\sigma_{flat} = 0.00211 N_{target} \quad (3.2.3.1)$$

$$(I_{rms})_{target} = N_{target}\sigma_{scint} \quad (2.2.5.2)$$

$$\sigma_{scint} = 0.00731301 * X^{\frac{7}{4}} * \left(2t_{exp}\right)^{-0.5} \quad (3.2.4.1)$$

Where X and $t_{exp}$ are the values given in the FITS header block.

$N_{target}$ is the sky subtracted[16] measured target count i.e. $[(\mathrm{N_{target}})_{t=t_{exp}, X=X}]_{\mathrm{measured}}$ from the calibrated image. The measured values for $N_{target}$ and $(\sigma_{sky})_{target}$ are directly given by a software package such as APT by aperture photometry. It is essential that the user defined radii of the aperture and sky annulus circles are recorded as part of the process.

Since the image is already calibrated and the software package subtracts the sky component in the target aperture ($N_{sky}$), then the software package effectively calculates equation (2.1.1.2) re-expressed as:-

[15] The term “predicted precision” refers to a predicted precision (potentially before any images have been taken) for a given set of observing conditions as calculated by the equations presented in this thesis. Whereas the term “achieved precision” is the achieved precision with an image as calculated by the equations presented in this thesis. “Achieved precision” is potentially of particular use when dealing with light curves from variable stars. However, the term “measured precision” has been reserved for the measured precision in a light curve of a star with a nominally constant magnitude.

[16] The software package (such as APT) calculates the sky count per pixel from a user defined sky annulus. The scaled sky count is subtracted from the target count in a user defined target aperture of nominally 3 FWHM radii.

$$N_{target} = N_{total} - N_{sky} - N_{dark} - N_{bias} \qquad (3.3.1.2)$$

The target SD equation is given by the existing equation:-

$$\sigma_{target} = \sqrt{N_{target}} \qquad (2.2.7.1)$$

Re-expressing equation (4) to convert to units of magnitude (neglecting the sign as one is only interested in the size of the uncertainty) gives:-

$$(\sigma_{total})_{target\ in\ magnitude} = 2.5 * \log\left[1 + \frac{(\sigma_{total})_{target}}{N_{target}}\right] \qquad (3.3.1.3)$$

Including the errors in the reference star, using the same equations but with the subscript of 'reference'. Thus amending equation (3.3.1.1) gives:-

$$(\sigma_{total})_{reference} = \sqrt{\sigma_{bias}^2 + \sigma_{dark}^2 + (\sigma_{flat}^2)_{reference} + (I^2{}_{rms})_{reference} + (\sigma_{sky}^2)_{reference} + \sigma_{reference}^2} \qquad (3.3.1.4)$$

$$\sigma_{bias} = 6.37 \qquad (3.2.1.1)$$

$$\sigma_{dark} = 0.0028 t_{exp} \qquad (3.2.2.1)$$

$$(\sigma_{flat})_{reference} = 0.00211 N_{reference} \qquad (3.3.1.5)$$

$$\sigma_{reference} = \sqrt{N_{reference}} \qquad (3.3.1.6)$$

$$(I_{rms})_{reference} = N_{reference} * \sigma_{scint} \qquad (3.3.1.7)$$

$$\sigma_{scint} = 0.00731301 * X^{\frac{7}{4}} * \left(2t_{exp}\right)^{-0.5} \qquad (3.2.4.1)$$

The measured values for $N_{reference}$ and $(\sigma_{sky})_{reference}$ are directly given by a software package such as APT by aperture photometry. It is essential that the radii of the aperture and sky annulus circles are recorded as part of the process.

Re-expressing equation (3.3.1.3) to convert to units of magnitude for the reference star gives:-

$$(\sigma_{total})_{reference\ in\ magnitude} = 2.5 * \log\left[1 + \frac{(\sigma_{total})_{reference}}{N_{reference}}\right] \qquad (3.3.1.8)$$

Re-expressing equation (2.3.7.2) gives the total error in magnitude:-

$$(\sigma_{total})_{all\ in\ magnitude} = [((\sigma_{total})_{target\ in\ magnitude})^2 + ((\sigma_{total})_{reference\ in\ magnitude})^2]^{0.5} \qquad (3.3.1.10)$$

### 3.3.2 Equations for Calculating the Predicted Standard Deviation for a Given Target

**Equations For Predicting SD for a Target of Magnitude $m_{target}$**

The following equations give the predicted SD for the target star as a function of $t_{exp}$, X and $m_{target}$ for the CKT telescope operating with a V filter and 2x2 binning:-

$$(\sigma_{total})_{target} = \sqrt{\sigma_{bias}^2 + \sigma_{dark}^2 + (\sigma_{flat})_{target}^2 + (I_{rms})_{target}^2 + \sigma_{sky}^2 + \sigma_{target}^2} \quad (3.3.2.1)$$

Where:-

$$\sigma_{bias} = 6.37 \quad (3.2.1.1)$$

$$\sigma_{dark} = 0.0028 t_{exp} \quad (3.2.2.1)$$

$$(\sigma_{flat})_{target} = 0.00211 N_{target} \quad (3.3.2.2)$$

$$(I_{rms})_{target} = N_{target}\sigma_{scint} \quad (3.3.2.3)$$

$$\sigma_{scint} = 0.00731301 * X^{\frac{7}{4}} * \left(2t_{exp}\right)^{-0.5} \quad (3.2.4.1)$$

$$\sigma_{target} = \sqrt{N_{target}} \quad (3.3.2.4)$$

$$\sigma_{sky} = \sqrt{t_{exp}(0.00600763 t_{exp} + 0.992)} \quad (3.2.5.15)$$

and X is the predicted value of air mass at a specific time in a planned observing session. The predicted total count for the target in the target aperture is a re-expression of equation (2.1.1.2):-

$$(N_{total})_{target} = N_{target} + N_{sky} + N_{dark} + N_{bias} \quad (3.3.2.5)$$

where

$$N_{target} = [(\mathrm{N_{target}})_{\mathrm{t=t_{exp},X=X}}]_{\mathrm{predicted}} \quad (3.3.2.6)$$

where $[(\mathrm{N_{target}})_{\mathrm{t=t_{exp},X=X}}]_{\mathrm{predicted}}$ is given by equation (2.2.7.4):-

$$[(\mathrm{N_{target}})_{\mathrm{t=t_{exp},X=X}}]_{\mathrm{predicted}} = \mathrm{t_{exp}}[(\mathrm{N_{target}})_{\mathrm{t=1s,X=X}}]_{\mathrm{predicted}} \quad (2.2.7.4)$$

and $[(\mathrm{N_{target}})_{\mathrm{t=1s,X=X}}]_{\mathrm{predicted}}$ is defined by equation (2.2.8.8):-

$$[(\mathrm{N_{target}})_{\mathrm{t=1s,X=X}}]_{\mathrm{predicted}} = 10^{-[m'_{t=1s,X=X,target}]_{\mathrm{predicted}}/2.5} \quad (2.2.8.8)$$

and $[m'_{t=1s,X=X,target}]_{\mathrm{predicted}}$ is given by equation (3.2.6.1):-

$$[\mathrm{m'_{t=1s,X=X,target}}]_{\mathrm{predicted}} = [\mathrm{m'_{t=1s,X=1.0,target}}]_{\mathrm{predicted}} - 0.62(1.0 - \mathrm{X}) \quad (3.2.6.1)$$

and $[\mathrm{m'_{t=1s,X=1.0,target}}]_{\mathrm{predicted}}$ is given by equation (3.2.6.2):-

$$[\mathrm{m'_{t=1s,X=1.0,target}}]_{\mathrm{predicted}} = 1.0023 m_{target} - 20.2122 \quad (3.2.6.2)$$

and $m_{target}$ is the catalogue magnitude of the target. The equations deriving $N_{sky}$, $N_{dark}$, and $N_{bias}$ are respectively defined by equations (3.2.5.1), (3.2.2.2) and (3.2.1.2).

$N_{sky} = 3.95 t_{exp}$ (3.2.5.1)

$N_{dark} = 0.0306 t_{exp}$ (3.2.2.2)

$N_{bias} = 839$ (3.2.1.2)

Where the selected value of the exposure time ($t_{exp}$) is a user defined input. Appendix G provides guidelines on the choice of the maximum value for $t_{exp}$ to keep the peak target count in a pixel within the linearity range. The key Figure 27 illustrating where linearity is lost is shown below for convenience.

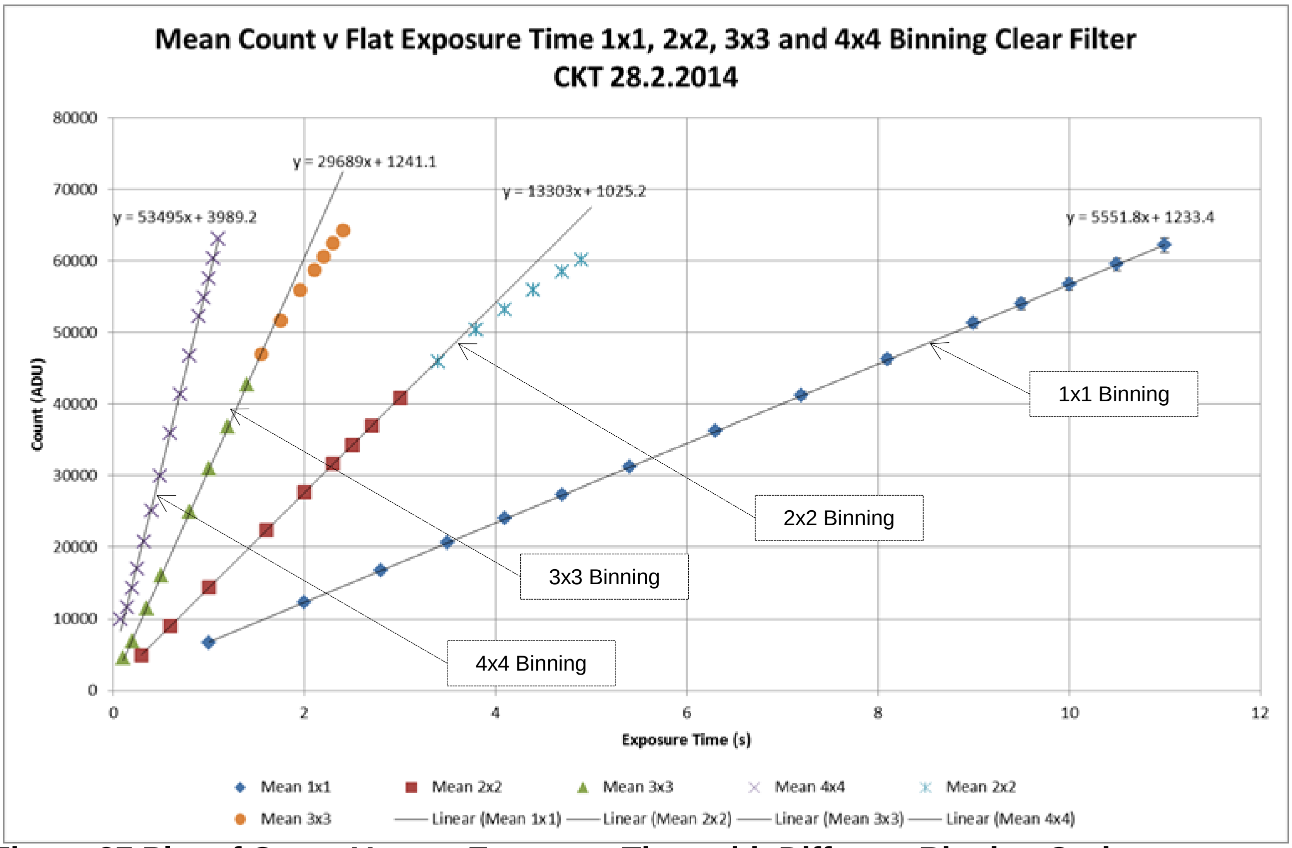


**Figure 27 Plot of Count Versus Exposure Time with Different Binning Options**

The choice of the maximum value for $t_{exp}$ should not be made without considering the stars available (as either reference or check stars with known values of magnitude) that will also be present in the same image as the target star: the corresponding values of maximum value for $t_{exp}$ for these stars should also be considered to ensure that a sufficient number of these stars can be used for the differential photometry. A secondary consideration is to ensure that the sampling rate is sufficiently high enough to obtain a light curve with sufficient resolution to observe, for example, a transit.

**Equations For Predicting SD for a Reference Star of Magnitude $m_{reference}$**

The following equations give the predicted SD for the reference star as a function of $t_{exp}$, X and $m_{reference}$ for the CKT telescope operating with a V filter and 2x2 binning:-

$$(\sigma_{total})_{reference} = \sqrt{\sigma_{bias}^2 + \sigma_{dark}^2 + (\sigma_{flat})_{reference}^2 + (I_{rms})_{reference}^2 + \sigma_{sky}^2 + \sigma_{reference}^2} \quad (3.3.2.11)$$

$$\sigma_{reference} = \sqrt{N_{reference}} \quad (3.3.2.12)$$

Where $\sigma_{sky}$, $\sigma_{bias}$ and $\sigma_{dark}$ are the same values as used for the target and consequently are derived from the same equations.

$$\sigma_{bias} = 6.37 \quad (3.2.1.1)$$

$$\sigma_{dark} = 0.0028 t_{exp} \quad (3.2.2.1)$$

$$(\sigma_{flat})_{reference} = 0.00211 N_{reference} \quad (3.3.2.13)$$

$$(I_{rms})_{reference} = N_{reference}\sigma_{scint} \quad (3.3.2.14)$$

$$\sigma_{scint} = 0.00731301 * X^{\frac{7}{4}} * \left(2t_{exp}\right)^{-0.5} \quad (3.2.4.1)$$

$$\sigma_{sky} = \sqrt{t_{exp}(0.00600763 t_{exp} + 0.992)} \quad (3.2.5.15)$$

Where X is the predicted value of air mass at a specific time in a planned observing session. The predicted total count for the reference star in the aperture is given by restating equation (3.3.2.5) for the reference star:-

$$(N_{total})_{reference} = N_{reference} + N_{sky} + N_{dark} + N_{bias} \quad (3.3.2.15)$$

The following equations are directly equivalent to the ones used for the target, but with ‘target’ replaced by ‘reference’:-

$$N_{reference} = [(\mathrm{N_{reference}})_{\mathrm{t=t_{exp},X=X}}]_{\mathrm{predicted}} \quad (3.3.2.16)$$

$$[(\mathrm{N_{reference}})_{\mathrm{t=t_{exp},X=X}}]_{\mathrm{predicted}} = \mathrm{t_{exp}}[(\mathrm{N_{reference}})_{\mathrm{t=1s,X=X}}]_{\mathrm{predicted}} \quad (3.3.2.17)$$

$$[(\mathrm{N_{reference}})_{\mathrm{t=1s,X=X}}]_{\mathrm{predicted}} = 10^{-[m'_{t=1s,X=X,target}]_{\mathrm{predicted}}/2.5} \quad (3.3.2.18)$$

$$[\mathrm{m'}_{\mathrm{t=1s,X=X,reference}}]_{\mathrm{predicted}} = [\mathrm{m'}_{\mathrm{t=1s,X=1.0,reference}}]_{\mathrm{predicted}} - 0.62(1.0 - \mathrm{X}) \quad (3.3.2.19)$$

$$[\mathrm{m'}_{\mathrm{t=1s,X=1.0,reference}}]_{\mathrm{predicted}} = 1.0023 m_{reference} - 20.2122 \quad (3.3.2.20)$$

Where $N_{sky}$, $N_{dark}$ and $N_{bias}$ are the same values as used for the target and consequently are derived from the same equations. Likewise, the selected value of the exposure time ($t_{exp}$) is a user defined input.

$$N_{sky} = 3.95 t_{exp} \quad (3.2.5.2)$$

$$N_{dark} = 0.0306 t_{exp} \quad (3.2.2.2)$$

$$N_{bias} = 839 \quad (3.2.1.2)$$

**Equations For Predicting Overall SD in units of Magnitude**

The same equations used to predict the magnitude of the overall SD with the target and reference stars are the same as used to calculate the achieved SD:-

The total SD for the target star in units of magnitude is:-

$$(\sigma_{total})_{target\ in\ magnitude} = 2.5 * \log\left[1 + \frac{(\sigma_{total})_{target}}{N_{target}}\right] \quad (3.3.1.3)$$

The total SD for the reference star in units of magnitude is:-

$$(\sigma_{total})_{reference\ in\ magnitude} = 2.5 * \log\left[1 + \frac{(\sigma_{total})_{reference}}{N_{reference}}\right] \quad (3.3.1.8)$$

The SD for both stars in units of magnitude is given by:-

$$(\sigma_{total})_{all\ in\ magnitude} = [((\sigma_{total})_{target\ in\ magnitude})^2 + ((\sigma_{total})_{reference\ in\ magnitude})^2]^{0.5} \quad (3.3.1.10)$$

## 3.4 Observational Data

The majority if not all of the observations presented in this Section were taken robotically. Many attempted observations failed to take all of the requested images for a wide range of reasons, in particular adverse weather conditions: the sky temperature was above the -22°C threshold for observing (used to decide if there is cloud present), equipment failures, dead zones with the JHT telescope, clashes with other users' jobs, etc. Of those robotic observing sessions that produced images, a significant number of the images were compromised and some had to be discarded: the reasons ranged from equipment problems, poor weather conditions (e.g. see Figure 4), inappropriate exposure time, not being plate solved, (ie the Pinpoint software package could not identify the location of the image in the sky from the supplied coordinates and is usually caused by imprecise tracking) etc.

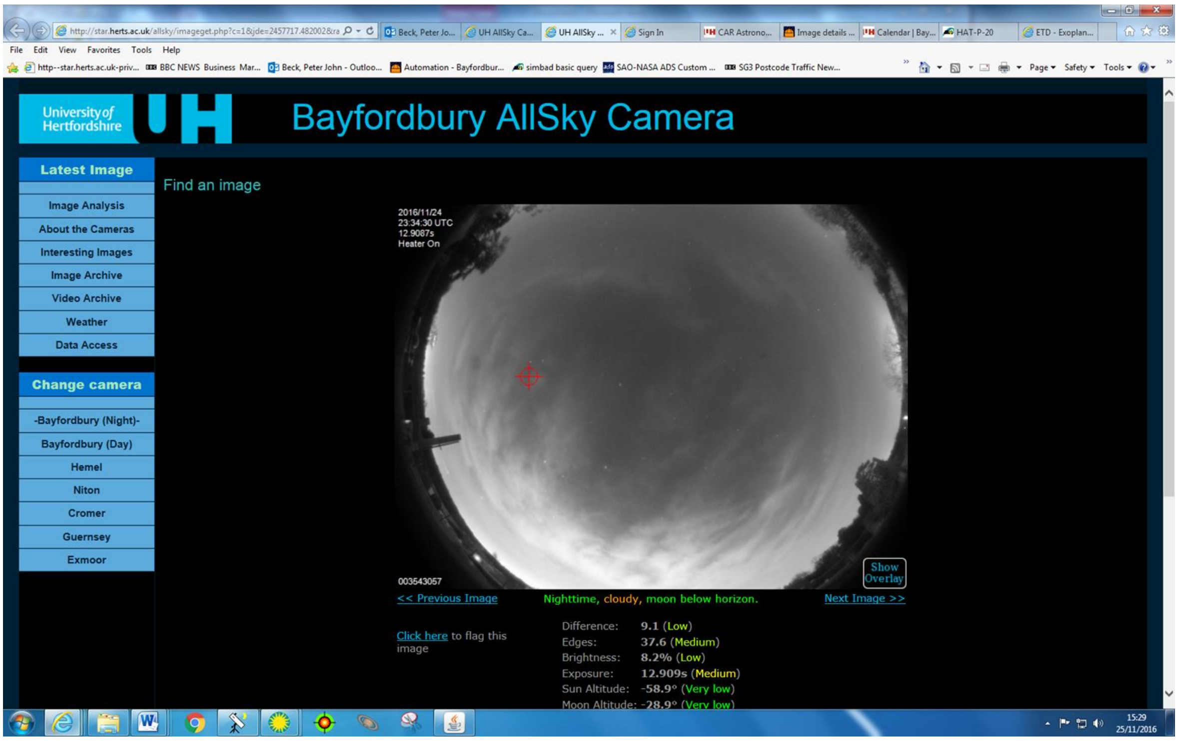


**Figure 4 Example of the Sky Conditions Whilst Observing HAT-P-20 on 24/25.11.2016**

One of the major problems in obtaining suitable data was the long continuous period of observing required to obtain a full exoplanet transit (with a meaningful period of observations both before and after transit) whilst the target was observable and the weather conditions were good enough to permit robotic observations for the entire period. Figure 5 provides an example of where the cloud cover interrupted an observation.

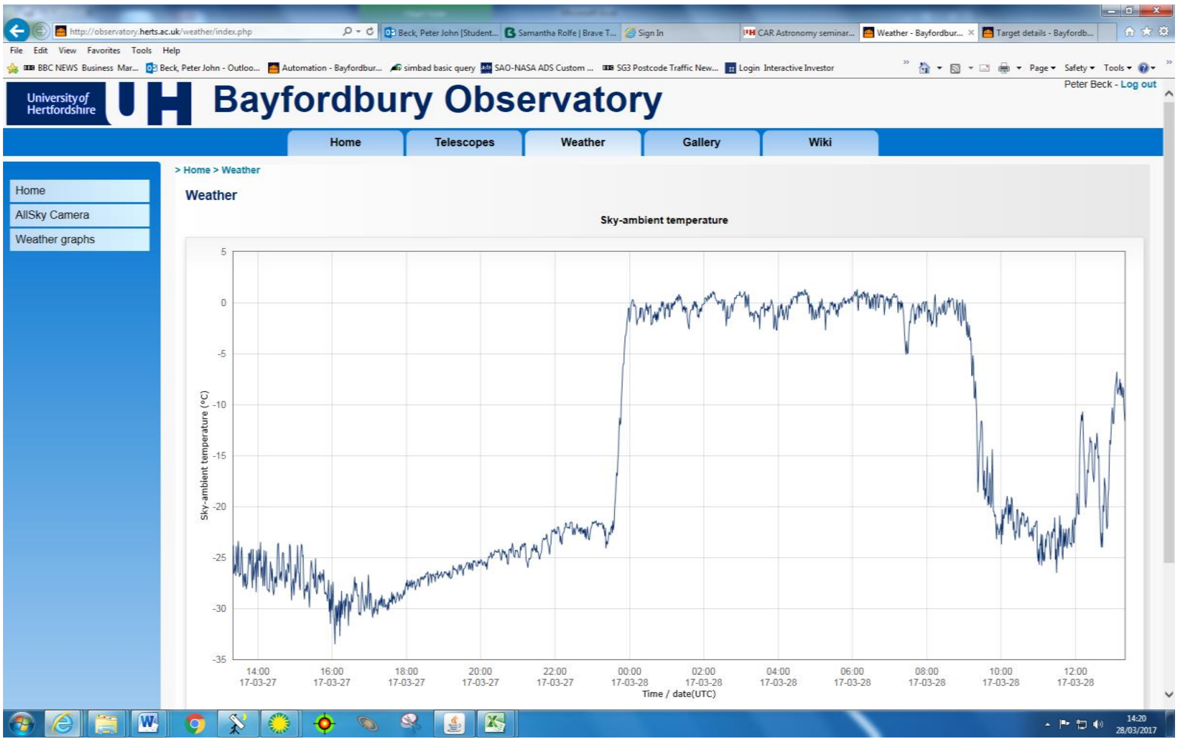


**Figure 5 Example of Increasing Sky Temperature Due to Cloud Conditions Terminating Observations (27/28-3-2017)**

Inevitably some transits were not as complete as required and could include measurements with a high value of air mass, but wherever possible this data has been analysed to make best use of this valuable data. The observations could only come from the telescopes that were both operational and available at the time of the required observations. Consequently preference was given to observations from the CKT, JHT and RPT telescopes in that order (see Appendix A). The JHT telescope has an identical configuration to the CKT telescope and therefore read-across of results can be made. However, as previously discussed in Section 3.2, the RPT telescope has a different camera, albeit of scientific standard, and therefore comparison is more tentative, but the predicted performance would still be expected to be similar to that predicted for the CKT telescope.

### 3.4.1 Observations with a Non Variable Star in the Absence of a Transit

The results presented in Section 3.4.1 not only cover non variable stars without a known or predicted exoplanet transit, but also non variable stars where an extended period of observing has been captured whilst they are not undergoing a transit.

The analysis is presented in two parts:-

(a) Results presented in Table 2 that predict the SD primarily using measured target count obtained from images.

(b) Results presented in Table 4 that predict the SD primarily using target catalogue magnitudes but without any data from images. Consequently this approach is a more challenging exercise as it makes full use of the equations developed in this thesis.

## SD Calculated Using Target Count

Table 2 presents the list of observations with their SDs calculated using an analysis of the images identified by the first column, corresponding to the first, middle and last image of their sequences. The values in the column entitled "Derived SD from Target Counts" have been calculated using the measured target count with the method outlined in Section 3.3.1. An example of the calculations in a spread sheet is presented as Table 1.

| Item | Value | Value | Value | Equation |
|---|---|---|---|---|
| Image | 26560 | 26628 | 26708 | |
| Telescope | CKT | CKT | CKT | |
| Date/Time | 2016-09-13T20:33:58 | 2016-09-13T23:31:49 | 2016-09-14T01:42:53 | |
| Julian Date | 2457645.357 | 2457645.48 | 2457645.571 | |
| Moon | Nighttime, clear, high gibbous moon. | Nighttime, clear, high gibbous moon. | Nighttime, clear, low gibbous moon. | |
| CCD Temperature | -17.36867625 | -19.97710074 | -20.41762135 | |
| x= | 1.288038766 | 1.065788438 | 1.159495248 | |
| texp | 300 | 300 | 300 | |
| σbias | 6.37 | 6.37 | 6.37 | 3.2.1.1 |
| σdark | 0.84 | 0.84 | 0.84 | 3.2.2.1 |
| FWHM (FITS Header) | 2.904665208 | 4.622466612 | 4.33121798 | |
| Aperture Radius (APT/MaximD | **8** | **8** | **8** | |
| Inner Sky Radius (APT/MaximD | **10** | **10** | **10** | |
| Outer Sky Radius (APT/MaximD | **18** | **18** | **18** | |
| **TARGET** | WASP-10/ 1214-0612683 | VASP-10/ 1214-0612683 | VASP-10/ 1214-0612683 | |
| Peak Value (MaximDL) | 34051 | 11276 | 9294 | |
| Spectral Type | K5V | K5V | K5V | |
| m target | 12.71 | 12.71 | 12.71 | |
| σ_sky target from APT | 29.287 | 29 | 21.481 | |
| Ntarget from APT | 285538 | 284847 | 270399 | |
| Sigma flat target | 602.48518 | 601.02717 | 570.54189 | 3.2.3.1 |
| Sigma scint | 0.000464939 | 0.000333768 | 0.000386804 | 3.2.4.1 |
| Irms target | 132.7578132 | 95.07283627 | 104.5914842 | 2.2.5.2 |
| Sigma target | 534.3575582 | 533.7105957 | 519.9990385 | 2.2.7.1 |
| Sigma total target | 816.7313144 | 809.9393717 | 779.3324982 | 3.3.1.1 |
| Sigma target total (Magnitude) | 0.003101125 | 0.003082822 | 0.003124762 | 3.3.1.3 |
| **Reference Star** | 1214-0612756 | 1214-0612756 | 1214-0612756 | |
| m reference | 12.19 | 12.19 | 12.19 | |
| Spectral Type | Not found | Not found | Not found | |
| Nreference from APT | 465308 | 462815 | 442047 | |
| Sigma sky reference from APT | 30.493 | 29.882 | 24.65 | |
| Peak Value from MaximDL | 34097 | 16195 | 15338 | |
| Sigma flat reference | 981.79988 | 976.53965 | 932.71917 | 3.3.1.5 |
| Sigma scint | 0.000464939 | 0.000333768 | 0.000386804 | 3.2.4.1 |
| Irms Reference | 0.9996 | 154.4728739 | 170.9856613 | 3.3.1.7 |
| σReference | 682.134884 | 680.3050786 | 664.8661519 | 3.3.1.6 |
| Sigma total reference (count) | 1195.91434 | 1200.516878 | 1158.402802 | 3.3.1.4 |
| Sigma reference total magnitu | 0.002786932 | 0.002812694 | 0.002841496 | 3.3.1.8 |
| Sigma all (Magnitude) | **0.004169408** | **0.004173133** | **0.004223534** | 3.3.1.10 |
| TRANSFIT FIT EQUATION Ref | 0.0394 | 0.0394 | 0.0394 | N/A |
| TRANSFIT FIT EQUATION Measured | 0.0366 | 0.0366 | 0.0366 | N/A |
| TRANSFIT FIT EQUATION Δmag | **0.0028** | **0.0028** | **0.0028** | N/A |
| SD 3-5hrs | **0.003049377** | **0.003049377** | **0.003049377** | |

**Table 1 Analysis of 3 Images for WASP-10 Taken by CKT Telescope 13/14-9-2016 Using Measured Counts**

The calculations have used image specific values for the following terms:-

(a) The achieved air mass (X) from the FITS header block.
(b) The selected exposure time ($t_{exp}$) from the FITS header block.
(c) The measured target count ($N_{target}$) calculated using APT with the chosen radius for the target star aperture.
(d) The measured sky noise ($(\sigma_{sky})_{target}$) calculated using APT with the chosen sky annulus dimensions for the target star.
(e) The measured reference star count ($N_{reference}$) calculated using APT with the chosen radius for the reference star aperture.
(f) The measured sky noise ($(\sigma_{sky})_{reference}$) calculated using APT with the chosen sky annulus dimensions for the reference star.

The column entitled "Figure Number in Appendix H" identifies the Figures with the corresponding light curves. The column entitled "Measured SD from Plots" is the SD obtained from an Excel spread sheet when there was no transit present. For clarity, the Figures show the 'mean', 'mean + σ' and 'mean – σ' for the period examined, plus the scheduled start and end of transit. NB The SD from the plots may correspond to a relatively short period of time that is significantly displaced in time relative to the time of some of the analysed images. For example, inspection of Figure 62 (for WASP-10 on 13/14.9.2016 and reproduced below for convenience) shows that the first image 26560 was taken 3 hrs before the start of the period used to determine the "Measured SD from Plots", and had a higher air mass (giving a higher predicted SD) than for the period used to derive the SD from the plots.

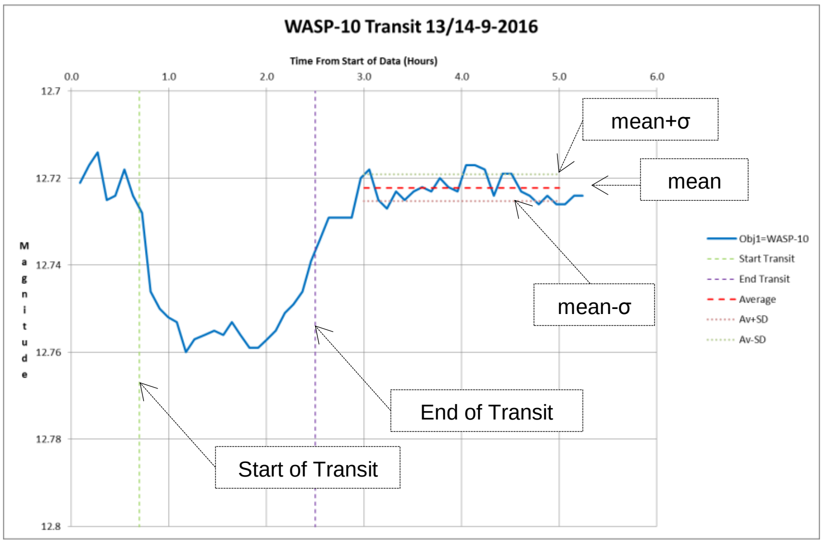


**Figure 62 WASP-10 Transit of 13/14-9-2016 by CKT Telescope**

The results from the RPT telescope have been greyed out as they were generated using equations tailored for the CKT telescope.

| Image Number | Target | Date | V (mag) | Telescope | $t_{exp}$ (s) | No. of Images | Air Mass (-) | Achieved SD from Target Counts (mmag) | Measured SD from Plots (mmag) | Difference (mmag) | Difference (%) | Figure Number in Appendix H |
|---|---|---|---|---|---|---|---|---|---|---|---|---|
| 26560 | WASP-10 | 13/14.9. 2016 | 12.71 | CKT | 300 | 22 (3hr to 5hr) | 1.29 | 4.17 | 3.05 | -1.12 | -37 | Figure 62 |
| 26628 | | | | | | | 1.07 | 4.17 | | -1.12 | -37 | |
| 26708 | | | | | | | 1.16 | 4.22 | | -1.17 | -39 | |
| 26880 | WASP-52 | 23/24.9. 2016 | 12.0 | CKT | 300 | 20 (4hr to 6hr) | 1.78 | 4.32 | 4.45 | 0.12 | 3 | Figure 63 |
| 26931 | | | | | | | 1.40 | 4.18 | | 0.26 | 6 | |
| 26990 | | | | | | | 1.84 | 4.62 | | -0.18 | -4 | |
| 27090 | WASP-52 | 30.9. 2016 | 12.0 | CKT | 300 | 9 (0hr - 1.25hr) | 1.56 | 4.24 | 4.09 | -0.15 | -4 | Figure 64 |
| 27101 | | | | | | | 1.38 | 4.19 | | -0.09 | -2 | |
| 27120 | | | | | | | 1.42 | 4.51 | | -0.41 | -10 | |
| 28265 | WASP-52 | 4.11. 2016 | 12.0 | CKT | 300 | 3 (1.7hr to 1.9hr) | 1.48 | 4.30 | 4.36 | 0.06 | 1 | Figure 65 |
| 28295 | | | | | | | 1.68 | 4.39 | | -0.03 | -1 | |
| 28295 | | | | | | | 2.05 | 4.59 | | -0.23 | -5 | |
| 28473 | WASP-52 | 5.11. 2016 | 12.0 | CKT | 300 | 48 (0hr to 4.4hr) | 1.52 | 4.36 | 3.83 | -0.52 | -14 | Figure 36 (No transit) |
| 28573 | | | | | | | 1.36 | 4.23 | | -0.40 | -10 | |
| 28620 | | | | | | | 1.65 | 4.37 | | -0.54 | -14 | |
| 27955 | HAT-P-20 | 2.11. 2016 | 11.34 | CKT | 180 | 15 (0hr to 0.8hr) | 1.78 | 4.29 | 2.08 | -2.21 | -106 | Figure 66 |
| 28003 | | | | | | | 1.36 | 4.09 | | -2.01 | -97 | |
| 28053 | | | | | | | 1.17 | 4.04 | | -1.96 | -94 | |
| 34128 | COROT-1 | 19/20.1. 2017 | 13.6 | CKT | 300 | 22 2.9hr to 4.9hr | 2.04 | 5.69 | 13.61 | 7.92 | 58 | Figure 67 |
| 34206 | | | | | | | 1.79 | 5.56 | | 8.05 | 59 | |
| 34249 | | | | | | | 3.03 | 12.77 | | 0.83 | 6 | |
| 40969 | HAT-P-4 | 8/9.4 .2017 | 11.12 | CKT | 180 | 19 (4.3hr to 5.4hr) | 1.33 | 4.09 | 2.09 | -2.00 | -96 | Figure 68 |
| 41014 | | | | | | | 1.05 | 3.89 | | -1.80 | -86 | |
| 41058 | | | | | | | 1.10 | 3.96 | | -1.87 | -89 | |
| 39486 | WD 1145 +017 | 25/26.3 .2017 | 17.28 | CKT | 600 | 10 (3.1hr to 4.4hr) | 1.66 | 15.71 | 156.2 | 140.49 | 90 | Figure 69 |
| 39676 | | | | | | | 1.63 | 18.58 | | 137.62 | 88 | |
| 39896 | | | | | | | 2.45 | 27.36 | | 128.84 | 82 | |
| 29685 | HAT-P-20 | 24/25.11. 2016 | 11.34 | JHT | 180 | 40 (4hr to 6.3hr) | 1.54 | 4.38 | 2.79 | -1.59 | -57 | Figure 70 |
| 29734 | | | | | | | 1.14 | 4.07 | | -1.28 | -46 | |
| 29784 | | | | | | | 1.33 | 4.14 | | -1.35 | -49 | |
| 31024 | HAT-P-22 | 28/29.11. 2016 | 9.73 | JHT | 20 | 75 2.8hr to 3.8hr | 1.23 | 6.76 | 7.23 | 0.48 | 7 | Figure 71 |
| 31212 | | | | | | | 1.06 | 7.72 | | -0.49 | -7 | |
| 31383 | | | | | | | 1.00 | 7.63 | | -0.40 | -5 | |
| 27358 | WASP-10 | 17/18.10. 2016 | 12.7 | **RPT** | 300 | 16 (2.4hr to 3.8hr) | 1.07 | 4.10 | 3.18 | -0.92 | -29 | Figure 72 |
| 27387 | | | | | | | 1.23 | 4.22 | | -1.04 | -33 | |
| 27402 | | | | | | | 1.50 | 4.70 | | -1.52 | -48 | |
| 28229 | WASP-52 | 4.11. 2016 | 12.0 | **RPT** | 300 | 23 (0hr to 2.4hr) | 1.40 | 3.98 | 5.32 | 1.34 | 25 | Figure 73 |
| 28258 | | | | | | | 1.43 | 3.94 | | 1.37 | 26 | |
| 28324 | | | | | | | 2.03 | 4.22 | | 1.10 | 21 | |

| Image Number | Target | Date | V (mag) | Telescope | $t_{exp}$ (s) | No. of Images | Air Mass (-) | Achieved SD from Target Counts (mmag) | Measured SD from Plots (mmag) | Difference (mmag) | Difference (%) | Figure Number in Appendix H |
|---|---|---|---|---|---|---|---|---|---|---|---|---|
| 40191 | HAT-P-22 | 27/28.3. 2017 | 9.73 | **RPT** | 60 | 58 (0hr to 1.4hr) | 1.02 | 4.09 | 5.86 | 1.78 | 30 | Figure 74 |
| 40270 | | | | | | | 1.00 | 4.12 | | 1.74 | 30 | |
| 40377 | | | | | | | 1.03 | 4.66 | | 1.20 | 20 | |

**Table 2 Derived and Measured Standard Deviations Using Measured Counts (No Transits Present)**

### SD Calculated Using Target Catalogue Magnitude

Table 4 presents the equivalent results for the same images listed in Table 2 plus the results from a number of check stars, but this time using catalogue magnitudes to predict the SD instead of using target counts from the images. The predicted SD has been calculated using the method and equations given in Section 3.3.2 and an example of the calculations in a spread sheet is presented as Table 3.

The calculations have used values for the following terms:-

(a) Target catalogue magnitude ($m_{target}$).
(b) Reference star catalogue magnitude ($m_{reference}$).
(c) Selected exposure time ($t_{exp}$).
(d) Achieved air mass (X) from the FITS header block.

The column entitled “Figure Number in Appendix H” identifies the Figures with the corresponding light curves. The column entitled “Measured SD from Plots” is the SD obtained from an Excel spread sheet when there was no transit present. For clarity, the Figures show the ‘mean’, ‘mean + SD’ and ‘mean – SD’ for the period examined, plus the scheduled start and end of transit.

| Item | Value | Value | Value | Equation |
|---|---|---|---|---|
| Image | 26560 | 26628 | 26708 | |
| Telescope | CKT | CKT | CKT | |
| Date/Time | 2016-09-13T20:33:58 | 2016-09-13T23:31:49 | 2016-09-14T01:42:53 | |
| Julian Date | 2457645.357 | 2457645.48 | 2457645.571 | |
| Moon | Nighttime, clear, high gibbous moon. | Nighttime, clear, high gibbous moon. | Nighttime, clear, low gibbous moon. | |
| CCD Temperature | -17.36867625 | -19.97710074 | -20.41762135 | |
| x= | 1.288038766 | 1.065788438 | 1.159495248 | |
| texp | 300 | 300 | 300 | |
| σ_sky | 28.9517357 | 28.9517357 | 28.9517357 | 3.2.5.15 |
| σbias | 6.37 | 6.37 | 6.37 | 3.2.1.1 |
| σdark | 0.84 | 0.84 | 0.84 | 3.2.2.1 |
| FWHM (FITS Header) | 2.904665208 | 4.622466612 | 4.33121798 | |
| Aperture Radius (APT/MaximD | **8** | **8** | **8** | |
| Inner Sky Radius (APT/MaximD | **10** | **10** | **10** | |
| Outer Sky Radius (APT/MaximD | **18** | **18** | **18** | |
| **TARGET** | WASP-10/ 1214-0612683 | VASP-10/ 1214-0612683 | 9294 | |
| Peak Value (MaximDL) | 34051 | 11276 | 9294 | |
| Spectral Type | K5V | K5V | K5V | |
| m target | 12.71 | 12.71 | 12.71 | |
| m' t=1, x=1.0 predicted | -7.472967 | -7.472967 | -7.472967 | 3.2.6.2 |
| m't=1,x=x predicted | -7.294382965 | -7.432178168 | -7.374079946 | 3.2.6.1 |
| Ntarget t=1,x=x predicted | 827.4717696 | 939.4448009 | 890.4960115 | 2.2.8.9 |
| Ntarget predicted | 248241.5309 | 281833.4403 | 267148.8034 | 2.2.7.4 |
| Sigma flat target | 523.7896302 | 594.668559 | 563.6839753 | 3.3.2.3 |
| Sigma scint | 0.000464939 | 0.000333768 | 0.000386804 | 3.2.4.1 |
| Irms target | 115.4172221 | 94.06700622 | 103.3342943 | 3.3.2.4 |
| Sigma target | 498.2384277 | 530.8798737 | 516.8643956 | 3.3.2.2 |
| Sigma total target | 732.664813 | 803.2385838 | 772.2990931 | 3.3.2.1 |
| Sigma target total (Magnitude) | 0.003199743 | 0.003089998 | 0.003134221 | 3.3.1.3 |
| **Reference Star** | 1214-0612756 | 1214-0612756 | 1214-0612756 | |
| m reference | 12.19 | 12.19 | 12.19 | |
| Spectral Type | K5V | K5V | K5V | |
| m't=1s,x=1.0,predicted | -7.994163 | -7.994163 | -7.994163 | 3.3.2.20 |
| m't=1,x=x predicted | -7.815578965 | -7.953374168 | -7.895275946 | 3.3.2.19 |
| Nreference t=1,x=x predicted | 1337.3084 | 1518.272295 | 1439.164304 | 3.3.2.18 |
| Nreference predicted | 401192.5325 | 455481.6886 | 431749.2913 | 3.3.2.17 |
| Peak Value from MaximDL | 34097 | 16195 | 15338 | |
| Sigma flat reference | 846.5162437 | 961.0663629 | 910.9910045 | 3.3.2.13 |
| Sigma scint | 0.000464939 | 0.000333768 | 0.000386804 | 3.2.4.1 |
| Irms Reference | 186.5301406 | 152.0252486 | 167.0024637 | 3.3.2.14 |
| σReference | 633.3976102 | 674.893835 | 657.0763207 | 3.3.2.12 |
| Sigma total reference (count) | 1073.990345 | 1184.534256 | 1135.967962 | 3.3.2.11 |
| Sigma reference total magnitu | 0.002902627 | 0.002819921 | 0.00285291 | 3.3.1.8 |
| Sigma all (Magnitude) | **0.004320139** | **0.004183305** | **0.004238211** | 3.3.1.10 |
| TRANSFIT FIT EQUATION Ref | 0.0394 | 0.0394 | 0.0394 | |
| TRANSFIT FIT EQUATION Measured | 0.0366 | 0.0366 | 0.0366 | |
| TRANSFIT FIT EQUATION Δmag | **0.0028** | **0.0028** | **0.0028** | |
| SD 3-5hrs | 0.003049377 | 0.003049377 | 0.003049377 | |

**Table 3 Analysis of 3 Images for WASP-10 Taken by CKT Telescope 13/14-9-2016 To Calculate the Predicted SD Using Catalogue Magnitudes**

| Image Number | Target | Date | V (mag) | Telescope | $t_{exp}$ (s) | No. of Images | Air Mass (-) | Predicted SD from Catalogue Magnitudes (mmag) | Measured SD from Plots (mmag) | Difference (mmag) | Difference (%) | Figure Number in Appendix H |
|---|---|---|---|---|---|---|---|---|---|---|---|---|
| 26560 | WASP-10 | 13/14.9. 2016 | 12.71 | CKT | 300 | 22 (3hr to 5hr) | 1.29 | 4.32 | 3.05 | -1.27 | -42 | Figure 62 |
| 26628 | | | | | | | 1.07 | 4.18 | | -1.13 | -37 | |
| 26708 | | | | | | | 1.16 | 4.24 | | -1.19 | -39 | |
| 26560 | WASP-10 Check Star 1213-0608720 | 13/14.9. 2016 | 12.73 | CKT | 300 | 56 (0hr to 5.2hr) | 1.29 | 4.33 | 2.72 | -1.61 | -59 | Figure 28 |
| 26628 | | | | | | | 1.07 | 4.19 | | -1.47 | -54 | |
| 26708 | | | | | | | 1.16 | 4.25 | | -1.52 | -56 | |
| 26560 | WASP-10 Check Star 1214-0612767 | 13/14.9. 2016 | 12.92 | CKT | 300 | 56 (0hr to 5.2hr) | 1.29 | 4.44 | 3.67 | -0.77 | -21 | Figure 29 |
| 26628 | | | | | | | 1.07 | 4.29 | | -0.62 | -17 | |
| 26708 | | | | | | | 1.16 | 4.35 | | -0.68 | -19 | |
| 26880 | WASP-52 | 23/24.9. 2016 | 12.0 | CKT | 300 | 20 (4hr to 6hr) | 1.78 | 4.41 | 4.45 | 0.03 | 1 | Figure 63 |
| 26931 | | | | | | | 1.40 | 4.14 | | 0.31 | 7 | |
| 26990 | | | | | | | 1.84 | 4.47 | | -0.02 | 0 | |
| 26880 | WASP-52 Check Star TYC 1161-890-1 | 23/24.9. 2016 | 11.84 | CKT | 300 | 60 (0hr to 6.0hr) | 1.78 | 4.36 | 2.72 | -1.64 | -60 | Figure 30 |
| 26931 | | | | | | | 1.40 | 4.10 | | -1.37 | -50 | |
| 26990 | | | | | | | 1.84 | 4.42 | | -1.69 | -62 | |
| 26880 | WASP-52 Check Star TYC 1161-728-1 | 23/24.9. 2016 | 11.42 | CKT | 300 | 60 (0hr to 6.0hr) | 1.78 | 4.26 | 3.19 | -1.06 | -33 | Figure 31 |
| 26931 | | | | | | | 1.40 | 4.01 | | -0.81 | -25 | |
| 26990 | | | | | | | 1.84 | 4.31 | | -1.11 | -35 | |
| 27090 | WASP-52 | 30.9. 2016 | 12.0 | CKT | 300 | 9 (0hr - 1.25hr) | 1.56 | 4.25 | 4.09 | -0.16 | -4 | Figure 64 |
| 27101 | | | | | | | 1.38 | 4.13 | | -0.04 | -1 | |
| 27120 | | | | | | | 1.42 | 4.15 | | -0.06 | -1 | |
| 27090 | WASP-52 Check Star TYC 1161-890-1 | 30.9. 2016 | 11.84 | CKT | 300 | 31 (0hr to 3.3hr) | 1.56 | 4.20 | 3.27 | -0.94 | -29 | Figure 32 |
| 27101 | | | | | | | 1.38 | 4.08 | | -0.82 | -25 | |
| 27120 | | | | | | | 1.42 | 4.11 | | -0.84 | -26 | |
| 27090 | WASP-52 Check Star TYC 1161-728-1 | 30.9. 2016 | 11.42 | CKT | 300 | 31 (0hr to 3.3hr) | 1.56 | 4.11 | 5.21 | 1.10 | +21 | Figure 33 |
| 27101 | | | | | | | 1.38 | 4.00 | | 1.22 | +23 | |
| 27120 | | | | | | | 1.42 | 4.02 | | 1.20 | +23 | |
| 28265 | WASP-52 | 4.11. 2016 | 12.0 | CKT | 300 | 3 (1.7hr to 1.9hr) | 1.48 | 4.19 | 4.36 | 0.17 | 4 | Figure 65 |
| 28295 | | | | | | | 1.68 | 4.33 | | 0.03 | 1 | |
| 28325 | | | | | | | 2.05 | 4.67 | | -0.31 | -7 | |
| 28265 | WASP-52 Check Star TYC 1161-890-1 | 4.11. 2016 | 11.84 | CKT | 300 | 20 (0hr to 1.9hr) | 1.48 | 4.15 | 3.50 | -0.65 | -18 | Figure 34 |
| 28295 | | | | | | | 1.68 | 4.28 | | -0.78 | -22 | |
| 28325 | | | | | | | 2.05 | 4.61 | | -1.11 | -32 | |
| 28265 | WASP-52 Check Star TYC 1161-728-1 | 4.11. 2016 | 11.42 | CKT | 300 | 20 (0hr to 1.9hr) | 1.48 | 4.05 | 3.57 | -0.49 | -14 | Figure 35 |
| 28295 | | | | | | | 1.68 | 4.18 | | -0.61 | -17 | |
| 28325 | | | | | | | 2.05 | 4.49 | | -0.91 | -26 | |
| 28473 | WASP-52 | 5.11. | 12.0 | CKT | 300 | 48 | 1.52 | 4.22 | 3.83 | -0.39 | -10 | Figure 36 |

| Image Number | Target | Date | V (mag) | Telescope | $t_{exp}$ (s) | No. of Images | Air Mass (-) | Predicted SD from Catalogue Magnitudes (mmag) | Measured SD from Plots (mmag) | Difference (mmag) | Difference (%) | Figure Number in Appendix H |
|---|---|---|---|---|---|---|---|---|---|---|---|---|
| 28573 | | 2016 | | | | (0hr to 4.4hr) | 1.36 | 4.12 | | -0.29 | -8 | (No Transit) |
| 28620 | | | | | | | 1.65 | 4.31 | | -0.48 | -13 | |
| 28473 | WASP-52 Check Star TYC 1161-890-1 | 5.11. 2016 | 11.84 | CKT | 300 | 48 (0hr to 4.4hr) | 1.52 | 4.17 | 4.13 | -0.05 | -1 | Figure 37 |
| 28573 | | | | | | | 1.36 | 4.08 | | 0.05 | +1 | |
| 28620 | | | | | | | 1.65 | 4.26 | | -0.14 | -3 | |
| 28473 | WASP-52 Check Star TYC 1161-728-1 | 5.11. 2016 | 11.42 | CKT | 300 | 48 (0hr to 4.4hr) | 1.52 | 4.08 | 6.41 | 2.33 | 36 | Figure 38 |
| 28573 | | | | | | | 1.36 | 3.99 | | 2.43 | 38 | |
| 28620 | | | | | | | 1.65 | 4.16 | | 2.25 | 35 | |
| 27955 | HAT-P-20 | 2.11. 2016 | 11.34 | CKT | 180 | 15 (0hr to 0.8hr) | 1.78 | 4.29 | 2.08 | -2.21 | -106 | Figure 66 |
| 28003 | | | | | | | 1.36 | 4.09 | | -2.01 | -97 | |
| 28053 | | | | | | | 1.17 | 4.04 | | -1.96 | -94 | |
| 27955 | HAT-P-20 Check Star TYC 1914-17-1 | 2.11. 2016 | 11.69 | CKT | 180 | 52 (0 to 3.1 hr) | 1.78 | 4.57 | 4.96 | 0.4 | 8 | Figure 39 |
| 28003 | | | | | | | 1.36 | 4.20 | | 0.76 | 15 | |
| 28053 | | | | | | | 1.17 | 4.07 | | 0.89 | 18 | |
| 34128 | COROT-1 | 19/20.1. 2017 | 13.6 | CKT | 300 | 22 (2.9hr to 4.9hr) | 2.04 | 6.71 | 13.61 | 6.89 | 51 | Figure 67 |
| 34206 | | | | | | | 1.79 | 6.31 | | 7.29 | 54 | |
| 34249 | | | | | | | 3.03 | 8.79 | | 4.82 | 35 | |
| 34128 | COROT-1 Check star COROT-102915842 | 19/20.1. 2017 | 13.517 | CKT | 300 | 48 (0.0hr to 4.9hr) | 2.04 | 6.62 | 9.26 | 2.64 | 28 | Figure 40 |
| 34206 | | | | | | | 1.79 | 6.23 | | 3.03 | 33 | |
| 34249 | | | | | | | 3.03 | 8.66 | | 0.59 | 6 | |
| 34128 | COROT-1 Check star COROT-102881564 | 19/20.1. 2017 | 13.465 | CKT | 300 | 48 (0.0hr to 4.9hr) | 2.04 | 6.57 | 7.58 | 1.02 | 13 | Figure 41 |
| 34206 | | | | | | | 1.79 | 6.18 | | 1.41 | 19 | |
| 34249 | | | | | | | 3.03 | 6.52 | | 1.07 | 14 | |
| 40969 | HAT-P-4 | 8/9.4. 2017 | 11.12 | CKT | 180 | 19 (4.3hr to 5.4hr) | 1.33 | 3.96 | 2.09 | -1.87 | -89 | Figure 68 |
| 41014 | | | | | | | 1.05 | 3.81 | | -1.72 | -82 | |
| 41058 | | | | | | | 1.10 | 3.83 | | -1.74 | -83 | |
| 40969 | HAT-P-4 Check Star BD+36 2594 | 8/9.4. 2017 | 11.55 | CKT | 180 | 90 (0.0hr to 5.4hr) | 1.33 | 4.07 | 3.11 | -0.96 | -31 | Figure 42 |
| 41014 | | | | | | | 1.05 | 3.91 | | -0.80 | -26 | |
| 41058 | | | | | | | 1.10 | 3.93 | | -0.82 | -26 | |
| 40969 | HAT-P-4 Check Star TYC 2569-1501-1 | 8/9.4. 2017 | 11.68 | CKT | 180 | 90 (0.0hr to 5.4hr) | 1.33 | 5.72 | 3.85 | -1.87 | -49 | Figure 43 |
| 41014 | | | | | | | 1.05 | 3.95 | | -0.10 | -3 | |
| 41058 | | | | | | | 1.10 | 3.47 | | 0.38 | 10 | |
| 40969 | HAT-P-4 Check Star TYC 2569-1230-1 | 8/9.4. 2017 | 12.05 | CKT | 180 | 90 (0.0hr to 5.4hr) | 1.33 | 5.75 | 3.94 | -1.81 | -46 | Figure 44 |
| 41014 | | | | | | | 1.05 | 4.08 | | -0.14 | -4 | |
| 41058 | | | | | | | 1.10 | 3.52 | | 0.42 | 11 | |
| 40969 | HAT-P-4 Check Star | 8/9.4. | 12.13 | CKT | 180 | 90 (0.0hr to | 1.33 | 5.76 | 3.65 | -2.11 | -58 | Figure 45 |

| Image Number | Target | Date | V (mag) | Telescope | $t_{exp}$ (s) | No. of Images | Air Mass (-) | Predicted SD from Catalogue Magnitudes (mmag) | Measured SD from Plots (mmag) | Difference (mmag) | Difference (%) | Figure Number in Appendix H |
|---|---|---|---|---|---|---|---|---|---|---|---|---|
| 41014 | TYC 2569-1310-1 | 2017 | | | | 5.4hr) | 1.05 | 4.12 | | -0.47 | -13 | |
| 41058 | | | | | | | 1.10 | 3.53 | | 0.11 | 3 | |
| 39486 | WD 1145 +017 | 25/26.3. 2017 | 17.28 | CKT | 600 | 10 (3.1hr to 4.7hr) | 1.66 | 17.36 | 156.2 | 138.84 | 89 | Figure 69 |
| 39676 | | | | | | | 1.63 | 17.18 | | 139.02 | 89 | |
| 39896 | | | | | | | 2.45 | 23.41 | | 1362.79 | 85 | |
| 39486 | WD 1145 +017 Check Star UCAC4 458-051088 | 25/26.3. 2017 | 11.75 | CKT | 600 | 27 (0.0hr to 4.7hr) | 1.66 | 3.67 | 4.89 | 1.23 | 25 | Figure 46 |
| 39676 | | | | | | | 1.63 | 3.66 | | 1.24 | 25 | |
| 39896 | | | | | | | 2.45 | 4.07 | | 0.82 | 17 | |
| 29685 | HAT-P-20 | 24/25.11. 2016 | 11.34 | JHT | 180 | 40 (4hr to 6.3hr) | 1.54 | 6.62 | 2.79 | -3.83 | -137 | Figure 70 |
| 29734 | | | | | | | 1.14 | 3.96 | | -1.17 | -42 | |
| 29784 | | | | | | | 1.33 | 4.07 | | -1.28 | -46 | |
| 29685 | HAT-P-20 Check Star TYC 1914-17-1 | 24/25.11. 2016 | 11.69 | JHT | 180 | 98 (0ht to 6.3hr) | 1.54 | 4.34 | 10.39 | 6.05 | 58 | Figure 47 |
| 29734 | | | | | | | 1.14 | 4.05 | | 6.33 | 61 | |
| 29784 | | | | | | | 1.33 | 4.18 | | 6.21 | 60 | |
| 29685 | HAT-P-20 Check Star TYC 1910-361-1 | 24/25.11. 2016 | 11.21 | JHT | 180 | 98 (0ht to 6.3hr) | 1.54 | 4.19 | 7.26 | 3.07 | 42 | Figure 48 |
| 29734 | | | | | | | 1.14 | 3.93 | | 3.33 | 46 | |
| 29784 | | | | | | | 1.33 | 4.04 | | 3.22 | 44 | |
| 31024 | HAT-P-22 | 28/29.11. 2016 | 9.73 | JHT | 20 | 75 (2.8hr to 3.8hr) | 1.23 | 6.310 | 7.235 | 0.925 | 12.7 | Figure 71 |
| 31212 | | | | | | | 1.06 | 5.922 | | 1.313 | 18.1 | |
| 31383 | | | | | | | 1.00 | 5.804 | | 1.431 | 19.7 | |
| 31024 | HAT-P-22 Check Star TYC3441-370-1 | 28/29.11. 2016 | 11.59 | JHT | 20 | 281 (0hr to 3.8hr) | 1.23 | 7.73 | 11.73 | 4 | 34 | Figure 49 |
| 31212 | | | | | | | 1.06 | 7.29 | | 4.44 | 38 | |
| 31383 | | | | | | | 1.00 | 7.16 | | 4.57 | 39 | |
| 27358 | WASP-10 | 17/18.10. 2016 | 12.7 | **RPT** | 300 | 16 (2.4 to 3.8hr) | 1.07 | 4.18 | 3.18 | -1.00 | -32 | Figure 72 |
| 27387 | | | | | | | 1.23 | 4.28 | | -1.10 | -35 | |
| 27402 | | | | | | | 1.50 | 4.47 | | -1.29 | -41 | |
| 27358 | WASP-10 Check Star 1213-0608720 | 17/18.10. 2016 | 12.73 | **RPT** | 300 | 45 (0.0 to 4.3hr) | 1.07 | 4.19 | 3.51 | -0.68 | -19 | Figure 50 |
| 27387 | | | | | | | 1.23 | 4.29 | | -0.78 | -22 | |
| 27402 | | | | | | | 1.50 | 4.48 | | -0.97 | -28 | |
| 27358 | WASP-10 Check Star 1214-0612767 | 17/18.10. 2016 | 12.92 | **RPT** | 300 | 45 (0.0 to 4.3hr) | 1.07 | 4.29 | 3.54 | -0.75 | -21 | Figure 51 |
| 27387 | | | | | | | 1.23 | 4.39 | | -0.86 | -24 | |
| 27402 | | | | | | | 1.50 | 4.60 | | -1.06 | -30 | |
| 28229 | WASP-52 | 4.11. 2016 | 12.0 | **RPT** | 300 | 23 (0hr to 2.4hr) | 1.40 | 4.14 | 5.32 | 1.18 | 22 | Figure 73 |
| 28258 | | | | | | | 1.43 | 4.16 | | 1.16 | 22 | |
| 28324 | | | | | | | 2.03 | 4.64 | | 0.67 | 13 | |
| 28229 | WASP-52 Check Star TYC 1161- | 4.11. 2016 | 11.84 | **RPT** | 300 | 46 (0hr to | 1.40 | 4.10 | 3.33 | -0.77 | -23 | Figure 52 |
| 28258 | | | | | | | 1.43 | 4.12 | | -0.79 | -24 | |

| Image Number | Target | Date | V (mag) | Telescope | $t_{exp}$ (s) | No. of Images | Air Mass (-) | Predicted SD from Catalogue Magnitudes (mmag) | Measured SD from Plots (mmag) | Difference (mmag) | Difference (%) | Figure Number in Appendix H |
|---|---|---|---|---|---|---|---|---|---|---|---|---|
| 28324 | 890-1 | | | | | 4.6hr) | 2.03 | 4.59 | | -1.26 | -38 | |
| 28229 | WASP-52 Check Star TYC 1161-728-1 | 4.11. 2016 | 11.42 | **RPT** | 300 | 46 (0hr to 4.6hr) | 1.40 | 4.01 | 7.91 | 3.90 | 49 | Figure 53 |
| 28258 | | | | | | | 1.43 | 4.03 | | 3.88 | 49 | |
| 28324 | | | | | | | 2.03 | 4.47 | | 3.43 | 43 | |
| 40191 | HAT-P-22 | 27/28.3. 2017 | 9.73 | **RPT** | 60 | 58 (0hr to 1.4hr) | 1.02 | 4.29 | 5.86 | 1.57 | 27 | Figure 74 |
| 40270 | | | | | | | 1.00 | 4.27 | | 1.59 | 27 | |
| 40377 | | | | | | | 1.03 | 4.30 | | 1.56 | 27 | |
| 40191 | HAT-P-22 Check Star TYC3441-370-1 | 27/28.3. 2017 | 11.59 | **RPT** | 60 | 104 (0hr to 2.6hr) | 1.02 | 4.92 | 7.23 | 2.31 | 32 | Figure 54 |
| 40270 | | | | | | | 1.00 | 4.91 | | 2.32 | 32 | |
| 40377 | | | | | | | 1.03 | 4.94 | | 2.29 | 32 | |
| 40191 | HAT-P-22 Check Star TYC3441-1256-1 | 27/28.3. 2017 | 10.85 | **RPT** | 60 | 104 (0hr to 2.6hr) | 1.02 | 4.55 | 11.13 | 6.58 | 59 | Figure 55 |
| 40270 | | | | | | | 1.00 | 4.53 | | 6.60 | 59 | |
| 40377 | | | | | | | 1.03 | 4.56 | | 6.57 | 59 | |
| 39997 | GJ436 | 26/27.3. 2017 | 10.613 | **RPT** | 60 | 43 (0hr to 1.0hr) | 1.18 | 4.34 | 2.8 | -1.54 | -55 | Figure 75 |
| 40091 | | | | | | | 1.11 | 4.27 | | -1.47 | -52 | |
| 40170 | | | | | | | 1.14 | 4.30 | | -1.50 | -54 | |
| 39997 | GJ436 Check Star TYC 1984-1928-1 | 26/27.3. 2017 | 11.43 | **RPT** | 60 | 111 (0hr to 3.0hr) | 1.18 | 4.74 | 5.09 | 0.36 | 7 | Figure 57 |
| 40091 | | | | | | | 1.11 | 4.66 | | 0.44 | 9 | |
| 40170 | | | | | | | 1.14 | 4.69 | | 0.40 | 8 | |
| 39997 | GJ436 Check Star TYC1984-1952-1 | 26/27.3. 2017 | 11.27 | **RPT** | 60 | 111 (0hr to 3.0hr) | 1.18 | 4.64 | 6.19 | 1.55 | 25 | Figure 58 |
| 40091 | | | | | | | 1.11 | 4.56 | | 1.63 | 26 | |
| 40170 | | | | | | | 1.14 | 4.59 | | 1.59 | 26 | |
| 39997 | GJ436 Check Star TYC1984-1840-1 | 26/27.3. 2017 | 11.23 | **RPT** | 60 | 111 (0hr to 3.0hr) | 1.18 | 4.61 | 6.7 | 2.09 | 31 | Figure 59 |
| 40091 | | | | | | | 1.11 | 4.54 | | 2.16 | 32 | |
| 40170 | | | | | | | 1.14 | 4.57 | | 2.13 | 32 | |
| 39997 | GJ436 Check Star TYC1984-1884-1 | 26/27.3. 2017 | 10.76 | **RPT** | 60 | 111 (0hr to 3.0hr) | 1.18 | 4.39 | 4.16 | -0.23 | -6 | Figure 60 |
| 40091 | | | | | | | 1.11 | 4.32 | | -0.16 | -4 | |
| 40170 | | | | | | | 1.14 | 4.35 | | -0.19 | -5 | |
| 39997 | GJ436 Check Star TYC 1984-2006-1 | 26/27.3. 2017 | 10.48 | **RPT** | 60 | 111 (0hr to 3.0hr) | 1.18 | 4.29 | 4.00 | -0.30 | -7 | Figure 61 |
| 40091 | | | | | | | 1.11 | 4.22 | | -0.23 | -6 | |
| 40170 | | | | | | | 1.14 | 4.26 | | -0.26 | -6 | |

**Table 4 Predicted and Measured Standard Deviations Using Catalogue Magnitudes (No Transits Present)**

Although obtaining a light curve with good precision for WD 1145+017 was expected to be challenging, the results were found to be less precise than had been predicted. Further investigation established that WD 1145+017 is identified as a variable star and the light curve produced using K2 data (assumed to be very precise) shown as Figure 1 in Gary (Gary *et al.* 2017) shows significant periodic variations between 17.2 and 17.7mag: this is far greater variation than the quoted transit depth of 0.1035mag given by the web site for the Czech Astronomy Society (Czech 5.9.2016). Consequently, in addition to other factors discussed in

Section 4.2, it has been concluded that this target is unsuitable for the purposes of demonstrating the validity of the SD equations and has been discarded from the analysis. However, the light curve for its check star UCAC4 457-051088 (V=11.75mag) is still suitable for analysis.

### 3.4.2 Observations Taken To Capture Exoplanet Transits

The results presented in this Section 3.4.2 cover observations made of known exoplanet transits with non-variable[17] stars. The purpose of this exercise was to demonstrate that the predicted precision obtained using the equations presented in Section 3.3.2 (and reflected by the results presented by Table 4) translates in practice to a capability to observe transits of known transit depth that are larger than the predicted SD. Table 5 presents a list of successful observations that captured ‘scheduled’ exo-planet transits provided by the web site for the Czech Astronomy Society (Czech 5.9.2016). The column entitled “Measured Transit Depth” presents the depth of transit generated from the data by the transit fitting process that is also provided by the web site for the Czech Astronomy Society (Czech 5.9.2016). The selected exposure time was chosen using the methodology outlined in Section 2.3.4 and the spread sheet illustrated by Table 3. The light curves have been presented as Appendix I and the plots of fitted transits obtained after processing have been presented in Appendix J.

| Date | Target | V | Telescope | $t_{exp}$ (s) | Number of Images | Measured Transit Depth (mmag) | Reference Transit Depth (mmag) | Abs Differ-ence (mmag) | Abs Differ-ence (%) | Figure Number in Appendix I | Figure Number in Appendix J |
|---|---|---|---|---|---|---|---|---|---|---|---|
| 13/14.9.2016 | WASP-10 | 12.7 | CKT | 300 | 57 | 36.6 ± 1.3 | 39.4 | 2.8 | 7.1 | Figure 62 | Figure 76 |
| 23/24.9.2016 | WASP-52 | 12.0 | CKT | 300 | 62 | 29.6 ± 1.9 | 29 | 0.6 | 2.1 | Figure 63 | Figure 77 |
| 30.9.2016 | WASP-52 | 12.0 | CKT | 300 | 31 | 38.3 ± 1.8 | 29 | 9.3 | 32.0 | Figure 64 | Figure 78 |
| 4.11.2016 | WASP-52 | 12.0 | CKT | 300 | 21 | 23.2 ± 2.8 | 29 | 5.8 | 20.0 | Figure 65 | Figure 79 |
| 2.11.2016 | HAT-P-20 | 11.34 | CKT | 180 | 52 | 22.7 ± 0.8 | 20.4 | 2.3 | 11.3 | Figure 66 | Figure 80 |
| 19/20.1.2017 | COROT-1 | 13.6 | CKT | 300 | 55 | 33.0 ±5.1 | 24.7 | 8.3 | 33.6 | Figure 67 | Figure 81 |
| 8/9.4.2017 | HAT-P-4* | 11.12 | CKT | 180 | 90 | 13.6* ±0.9 | 7.9 | 5.7 | 72.2 | Figure 68 | Figure 82 |
| 25/26.3.2017 | WD 1145+017 | 17.28 | CKT | 600 | 27 | - | - | - | - | Figure 69 | - |
| 24/25.11.2016 | HAT-P-20 | 11.34 | JHT | 180 | 62 | 21.9 ± 1.0 | 20.4 | 1.5 | 7.4 | Figure 70 | Figure 83 |
| 28/29.11.2016 | HAT-P-22 | 9.73 | JHT | 20 | 281 | 17.2 ± 1.3 | 11.9 | 5.3 | 4.5 | Figure 71 | Figure 84 |
| 17/18.10.2016 | WASP-10 | 12.7 | **RPT** | 300 | 49 | 33.1 ± 1.5 | 39.4 | 6.3 | 16.0 | Figure 72 | Figure 85 |
| 4.11.2016 | WASP-52 | 12.0 | **RPT** | 300 | 46 | 33.9 ± 2.3 | 29 | 4.9 | 16.8 | Figure 73 | Figure 86 |
| 26/27.3.2017 | GJ436 | 10.6 | **RPT** | 60 | 111 | 5.9 ±0.7 | 9.0 | 3.1 | 34.4 | Figure 75 | Figure 87 |

* Incomplete transit captured

**Table 5 List of Observations Made Capturing Full Exoplanet Transits**

[17] Or the variability is considered to be insignificant. For example WASP-10 has a small variability in brightness: Maciejewski (Maciejewski, 2011) has identified a worst case of a 3mmag variation in WASP 10 in a 4 hour period due to sun spots: this change is relatively small compared to the transit depth of 39.4mmag, and might be removed anyway in the trend removal process by the transit fit program (eg see Figure 76).

Figure 76 to Figure 87 present the results from the transit fitting program with Figure 76(a) reproduced below for convenience.

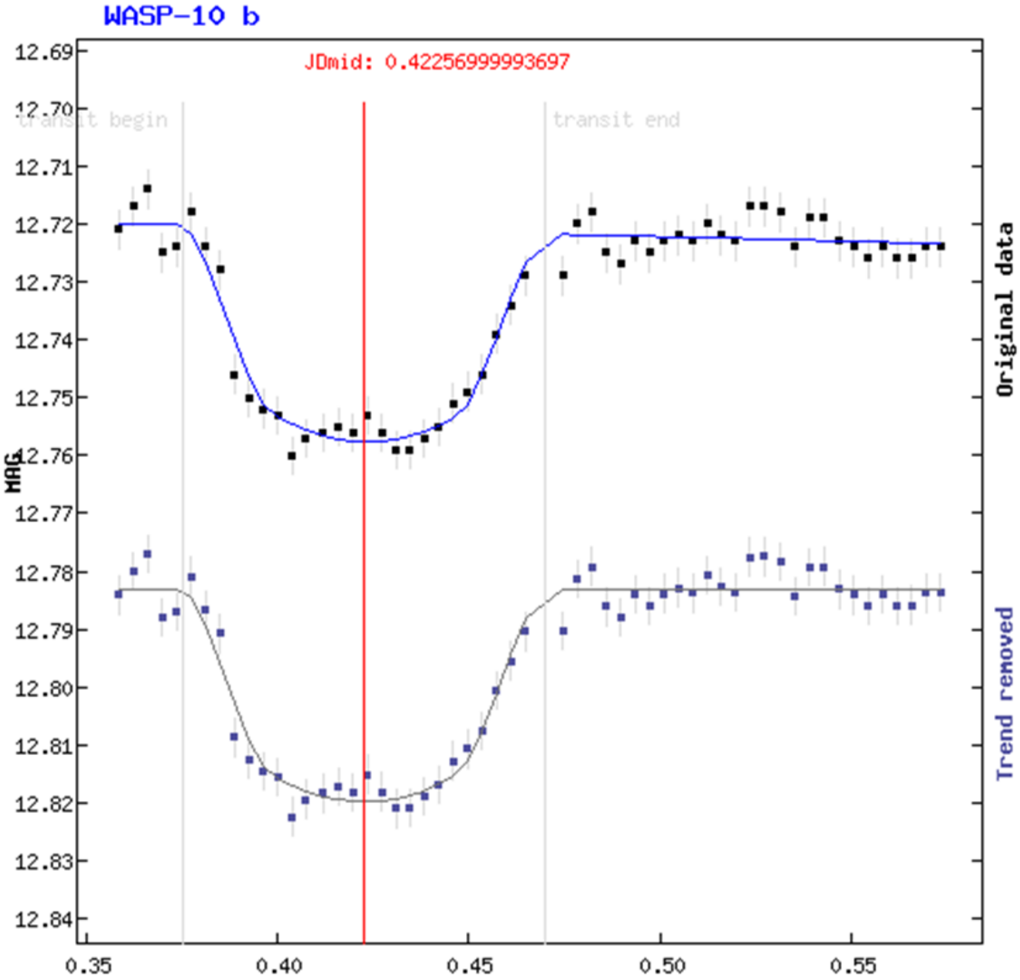


**Figure 76(a) WASP-10 Transit of 13/14-10-2016 With CKT Telescope and Equation Fitting – Fitted Transits**

The plot on the top of Figure 76(a) is an initial fit to the raw data by the transit fitting program. The lower plot shows the corresponding transit curve produced with linear bias removal. The error bars shown in the plots are the SD values extracted from Figure 76(b) (reproduced below for convenience) presents the difference between the fitted curve and the raw data.

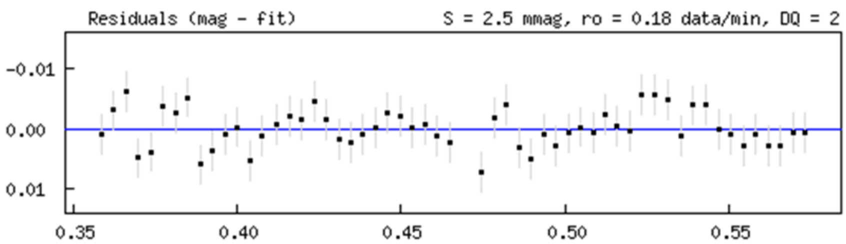


**Figure 76(b) WASP-10 Transit of 13/14-10-2016 With CKT Telescope and Equation Fitting – Residual Differences**

As illustrated by Figure 76(c) (reproduced below for convenience), the set of data on the bottom right corresponds to key parameters obtained from the curve fitting process, in particular the reference depth of transfer that has been included in

Table 5 in the column entitled "Measured Transit Depth (mmag)". The reference transit depth data is from the web site for the Czech Astronomy Society (Czech 5.9.2016), however, it does not quote their uncertainty[18][19].

| | | |
|---|---|---|
| **JD mid**: | 2457645.42257 +/- 0.00067 | |
| **HJD mid**: | 2457645.42733 +/- 0.00067 | (helcor = **0.00476**) |
| **Duration**: | 135.9 +/- 2.9 | minutes |
| **Depth**: | 0.0366 +/- 0.0013 | mag |

**Figure 76(c) WASP-10 Transit of 13/14-10-2016 With CKT Telescope and Equation Fitting – Measured Parameters**

A CCD temperature stability problem was encountered on 13/14-9-2016 (as shown by Figure 6) when the required -20°C camera temperature was not achieved until near to the end of the transit by WASP-10b.

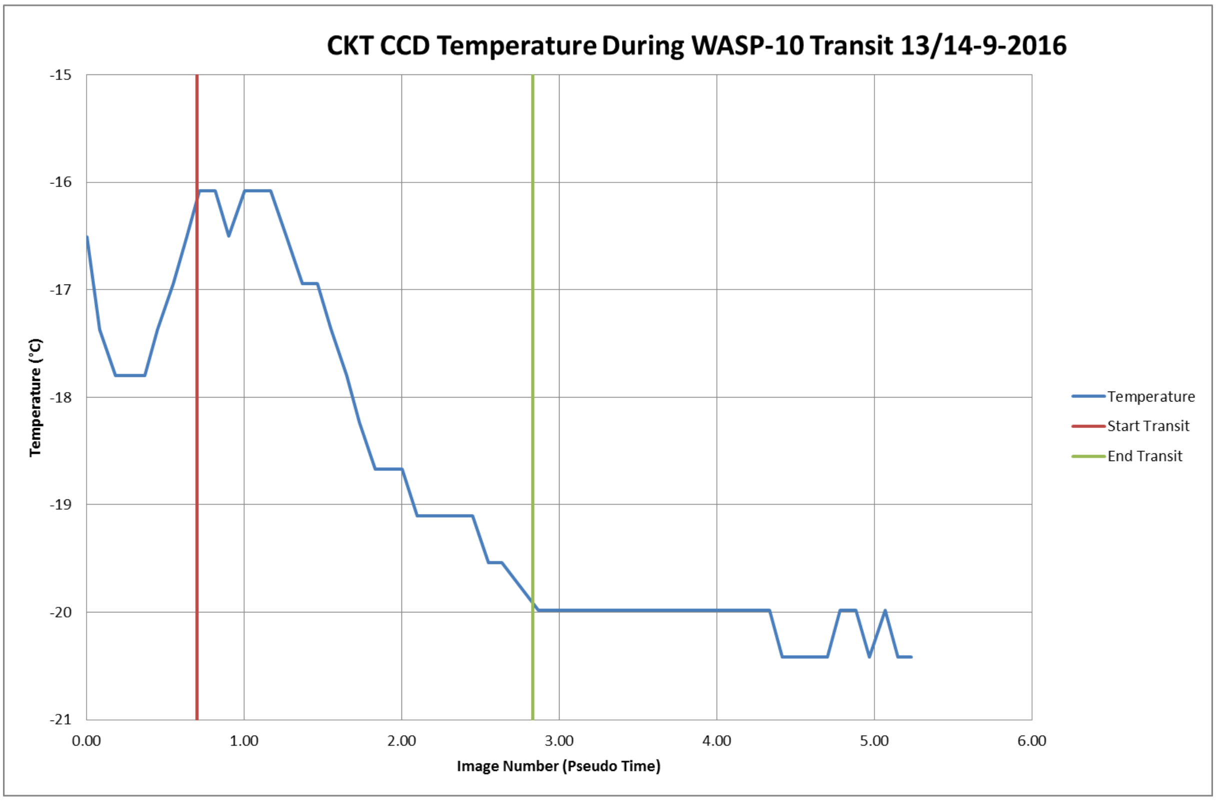


**Figure 6 CCD Temperature Variation on 13/14-9-2016**

[18] In the case of WASP-10: the quoted transit depth of 39.4mmag appears to be slightly high as Christian (Christian, 2009) quotes a transit depth of 33±1 mmag that is broadly consistent with the results presented in Table 5. Furthermore, inspection of the numerous transit depth measurements shown in the plot for WASP-10 on the web site for the Czech Astronomy Society also indicates that a transit depth of 39mmag is slightly too high.

[19] Transit depth is often given by the term $k^2=(R_P/R_*)^2$ where $R_P$ is the planet radius and $R_*$ is the star radius. This is an approximation since using Pogson's equation, converting from $\log_{10}$ to $\log_e$ and then applying a McClaurin expansion gives $\Delta m = 1.087\left[k^2 + \left\{k^4/2\right\} + \cdots\right]$. Since the size of the planets is usually relatively large compared to the size of the host star, the value of the smaller terms in the expansion may not necessarily be insignificant.

The otherwise satisfactory transit for WASP-10 shown as Figure 62 and Figure 76 is thus initially slightly compromised by this temperature variation as the dark current at temperatures higher than -20°C will not be fully compensated by the calibration using standard -20°C master dark current frame.

### 3.4.3 Eclipsing Cataclysmic Variable Star UX UMa

An observing campaign was conducted with eclipsing binary star UX UMa (V=13.26±0.31mag). UX UMa was chosen as a target as it is well documented, has a relatively short orbital period and has a significant depth for its primary transit. The results have been included as it provides further evidence that one can observe events that have a magnitude variation greater than the predicted precision. Furthermore, the predicted precision has been used to define the uncertainty on these measurements: the significant variation in the brightness of UX UMa outside of the eclipse precludes reliable measurement of the SD from the light curve. Table 6 presents a list of observations made of UX UMa taken by the CKT and DAT telescopes (see Appendix A). The column entitled “Start” corresponds to the predicted precision for the first image of the sequence, the column entitled “Mid” corresponds to the predicted precision for the middle image of the sequence and the column entitled “End” corresponds to the predicted precision for the last image of the sequence.

| Date | Telescope | Filter | $t_{exp}$ (s) | Number of Images | Predicted Precision (mmag) | | | SD from Light Curve (mmag) | Observed Transit Depth (mag) | Figure Number in Appendix K |
|---|---|---|---|---|---|---|---|---|---|---|
| | | | | | Start | Mid | End | | | |
| 30.4.2013 | CKT | V | 60 | 100 | 5.8 | 5.8 | 6.1 | 32.5 | 1.16 | Figure 88 |
| 21.6.2013 | DAT | V | 60 | 55 | 5.9 | 6.0 | 6.1 | 19.6 | 1.08 | Figure 89 |
| 18.7.2013 | DAT | V | 60 | 58 | 6.2 | 6.4 | 6.7 | 17.5 | 1.04 | Figure 90 |
| 7.9.2013 | CKT | V | 60 | 30 | 6.7 | 6.9 | 7.1 | 20.7 | 1.01 | Figure 91 |
| 9.9.2013 | CKT | V | 60 | 30 | 6.6 | 6.8 | 7.0 | 18.9 | 0.89 | Figure 92 |
| 27.5.2017 | JHT | V | 60 | 66 | 5.8 | 5.8 | 5.9 | 12.9 | - | Figure 93 |
| 27.5.2017 | RPT | V | 60 | 119 | 5.8 | 5.9 | 6.2 | 16.1 | - | |

**Table 6 List of Observations with Eclipsing Binary Star UX UMa**

The column entitled “Figure Number in Appendix K” references the Figures presented in Appendix K with Figure 88 reproduced below for convenience.

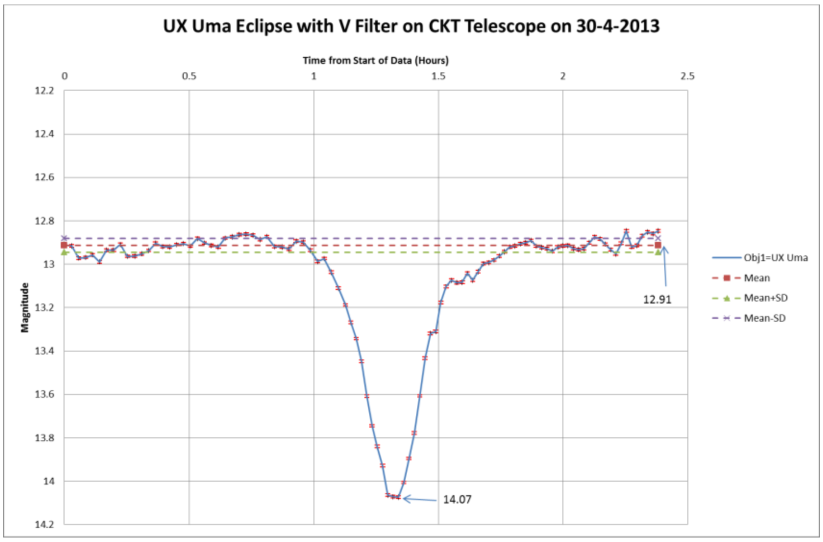


**Figure 88 UX UMa Eclipse with V Filter on CKT Telescope on 30-4-2013**

The tolerance bars in all light curves indicate the predicted precision that has been obtained by interpolating between the corresponding values presented in the column entitled "Predicted Precision". The transit depths are presented in column entitled "Observed Transit Depth" and have been calculated as the difference in magnitude between the mean value and lowest value, as indicated in the respective Figure. The column entitled "SD from Light Curve" is the measured SD from the light curve (whilst there was not a transit) and are represented in the respective Figure as the ±SD lines about the mean value line.

Figure 93 (reproduced below for convenience) presents the light curves from the simultaneous observations by the JHT and RPT telescopes, with a common time base corresponding to the start of data from the JHT telescope. Unfortunately the JHT camera temperature was initially at only -12.7°C, but improved to -15.7°C by the end of the observations. Secondly, there was some saturation of the reference star with the RPT telescope observations that diminished as the value of air mass increased. A shift was applied to the JHT plot corresponding to the mean difference between the two plots in the first 2.3 hours. The main objective of this plot is to demonstrate that large variations in one light curve are also present in the other light curve, and ideally demonstrate that the predicted tolerance values from each light curve overlap.

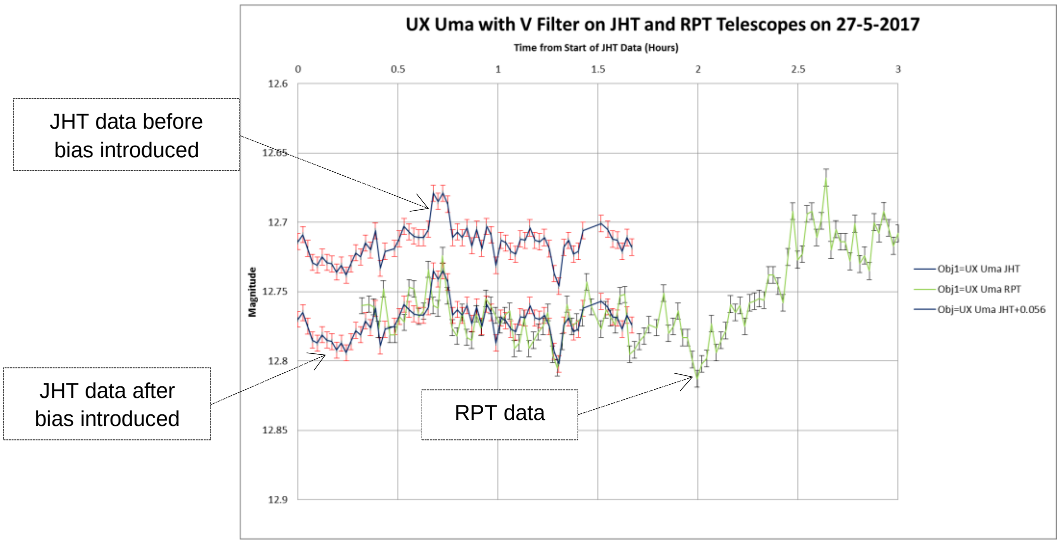


**Figure 93 UX UMa with V Filter on JHT and RPT Telescopes on 27-5-2017**

### 3.5 Comparison of Achieved Versus Predicted Precision

#### 3.5.1 Non Variable Stars Without Transits

Section 3.4.1 compares values of SD from either the measured or predicted values of SD (derived using the formulation presented in Sections 3.3.1 and 3.3.2) against the reference SD values obtained from light curves. These results have been taken over a wide range of observing conditions in terms of cloud cover and phase of moon. This means that the achieved observing performance should be representative for a wide range of observing conditions, as opposed to defining the best possible achievable performance that can be rarely obtained.

**SD Calculated using Target Count**

The results presented in Table 2 and Figure 7 present the SD error obtained for all telescopes for target V magnitudes in the range 9.7mag to 13.6mag. A negative number for the SD error shown in Table 2 and Figure 7 means that the SD derived from target counts is larger (more pessimistic) than the SD derived from the light curve. The results typically show errors of less than 2mmag between the SDs derived from counts from individual images and the respective SD values calculated using an Excel spread sheet from the light curve data. The relatively poor performance with COROT 1 (V=13.6mag) was obtained with observing conditions that were far from ideal, in particular the air mass varied between 1.8 and 3.0.

Inspection of Table 2 and Figure 7 shows that the results for the RPT telescope, even though it uses a different camera to that used by the CKT and JHT telescopes, typically have an error of less than 2mmag.

It is to be noted that the measured SD values for stars with transiting planets have often been obtained for relatively short durations and few data values (especially with high values of exposure time) and is consequently liable to more error than with a longer term reading. Conversely, the measured SD for the companion check stars have been obtained for the full observing periods, however these data may include periods with significantly different values of air mass and consequently different signal to noise ratios and air turbulence.

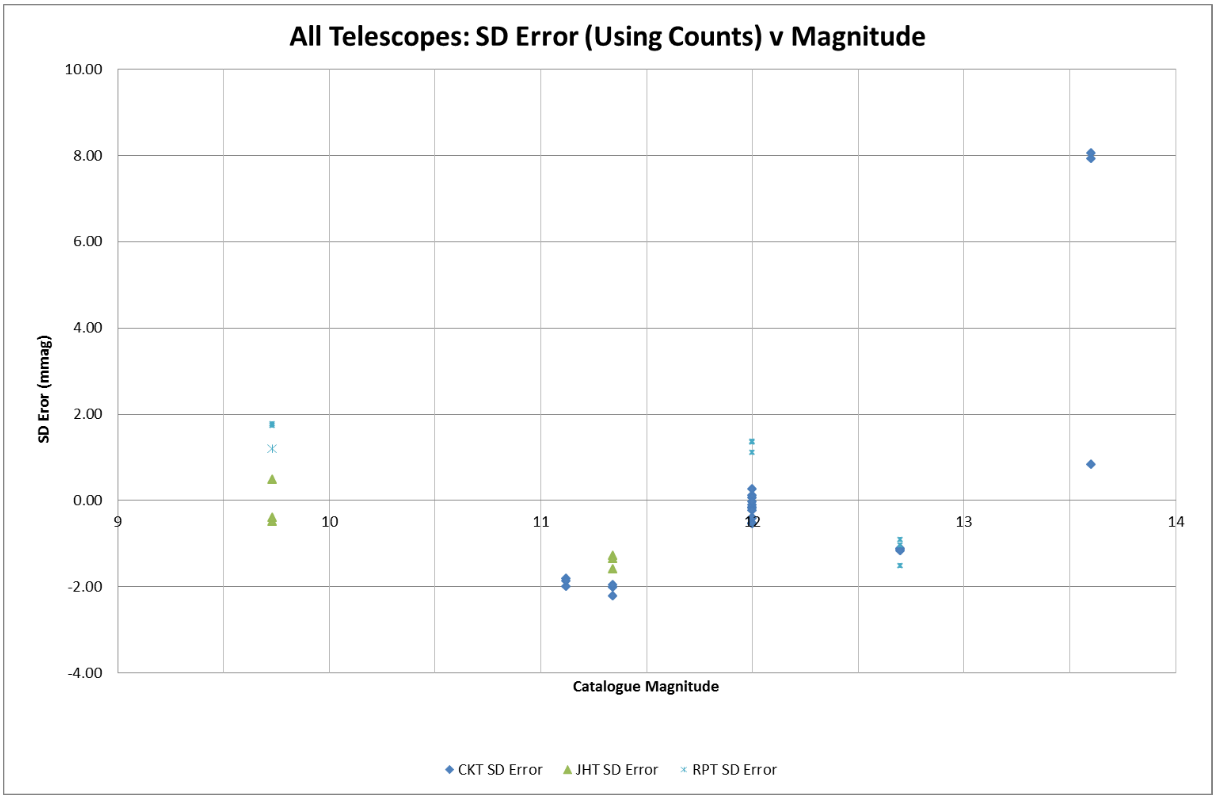


**Figure 7 All Telescopes: SD Error (using Counts) v Magnitude**

Figure 8 presents the same information for the CKT telescope only, but without the results for COROT 1. In all cases the SD error is less than 2mmag. The trend line shows a gradual increase in the SD error from a negative (overestimate of the SD) to a positive (underestimate of the SD) as the catalogue magnitude increases.

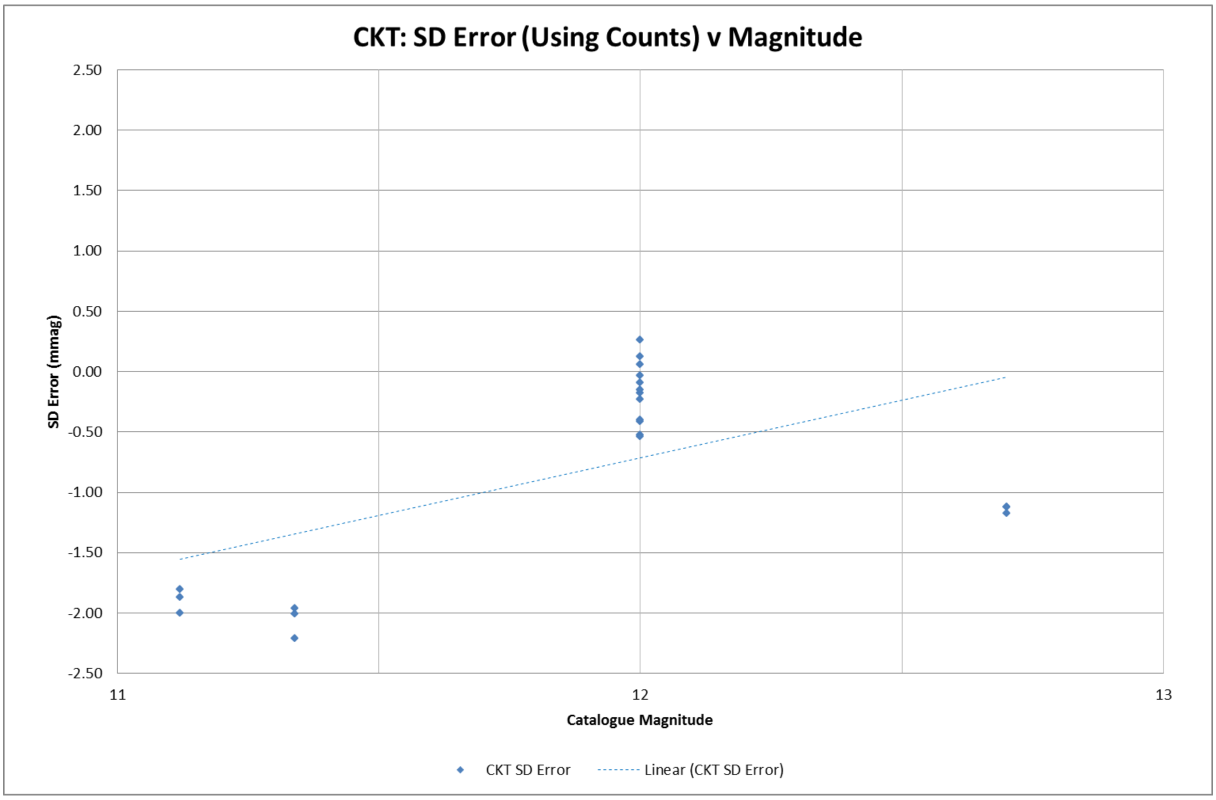


**Figure 8 CKT Telescope: SD Error (using Counts) v Magnitude**

Figure 9 has the same information presented in Figure 8 (and the results from COROT-1) but expressed as an absolute percentage error. This plot does not provide any evidence to suggest that the relative size of the errors increases with catalogue magnitude.

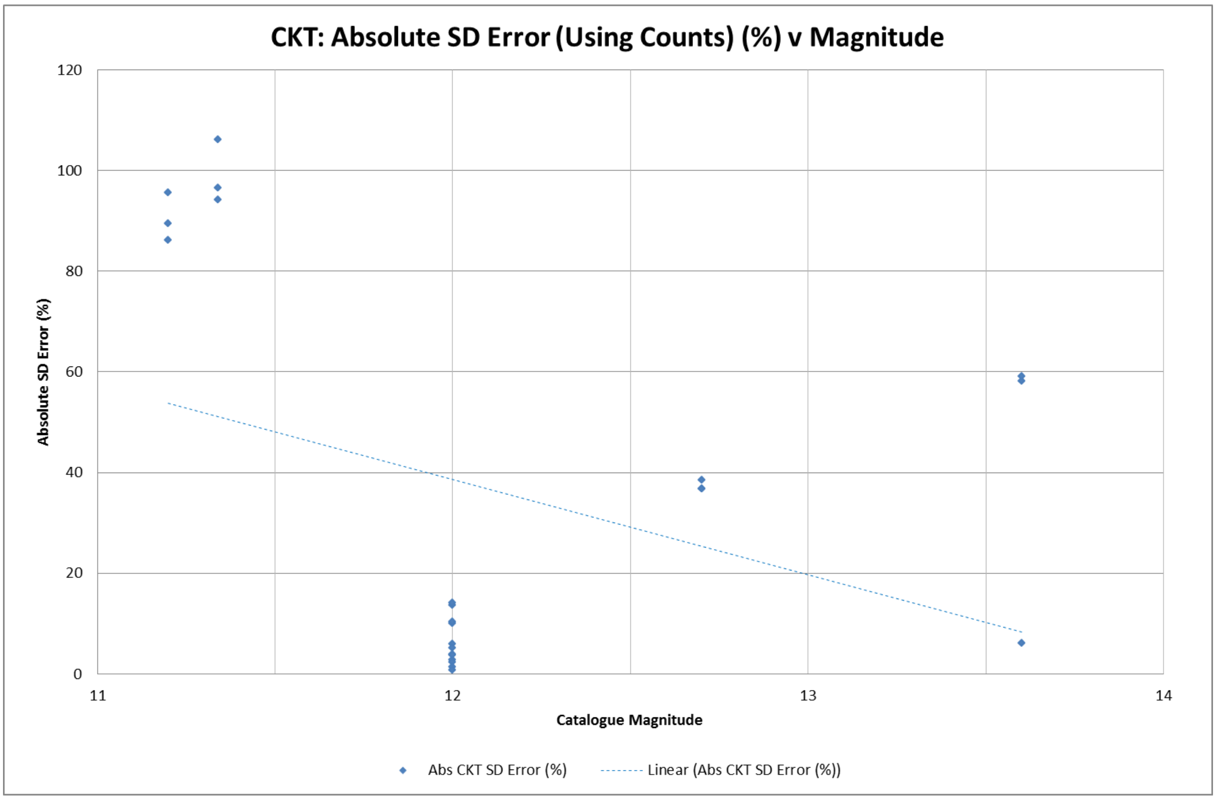


**Figure 9 CKT Telescope: Absolute SD Error (%) (Using Counts) v Magnitude**

Figure 10 presents the absolute SD error plotted against air mass. The trend line does not show a reduction in performance with increase in air mass, although it might be influenced by the single point with an air mass of 3 that may fortuitously have a low SD error.

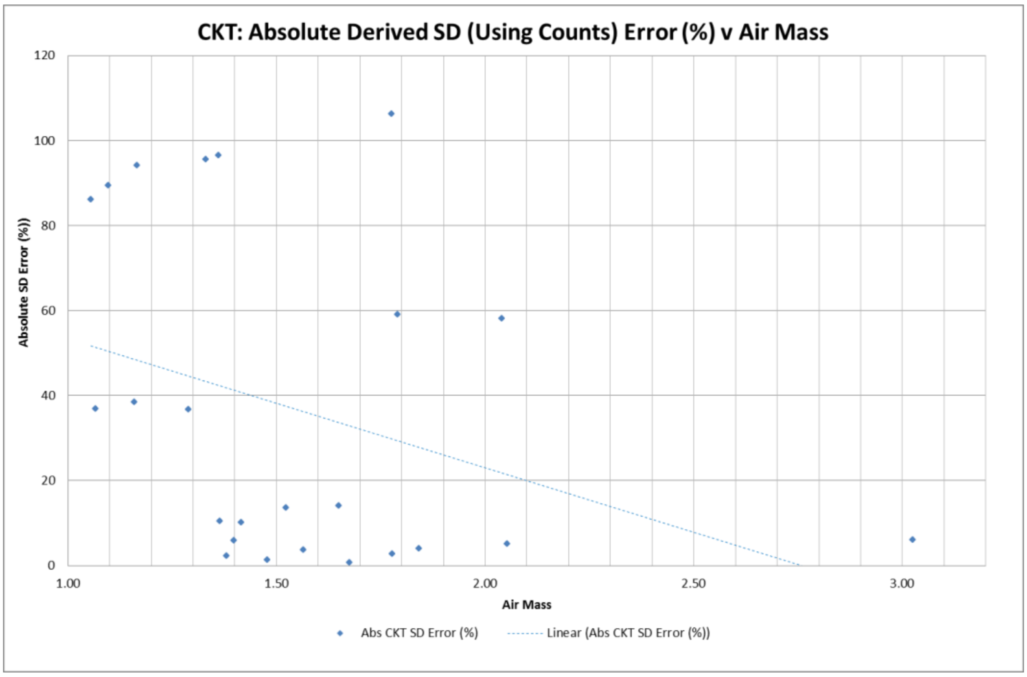


**Figure 10 CKT Telescope: Absolute SD Error (using Counts) (%) v Air Mass**

### SD Calculated Using Target Catalogue Magnitude

It can be observed that Table 4 demonstrates that the SD results obtained solely from the catalogue magnitudes, measured air masses and exposure times show that the predicted SD values are broadly similar to the SD values from the light curve data for all telescopes. There are far more measurements presented in Table 4 than with Table 2, as the analysis presented in Table 2 was primarily to prove the analysis process using a limited number of equations, whereas Table 4 presents results obtained using the full equations and includes many results from check stars to provide additional evidence of the validity of the equations. Although the derived results have been matched to the achieved air mass and selected value for $t_{exp}$, they are still 'predicted' results as no reference has been made to the data in any of the images taken. Furthermore, the equations in an EXCEL spreadsheet (such as illustrated in Table 3) were used **before** any observations were taken in an endeavour to give the best compromise between precision and cadence to capture an exoplanet transit of known duration and transit depth.

Figure 11 presents the error between predicted SD (using magnitudes) and measured SD values from light curves plotted against catalogue magnitude, for measurements taken from Table 4 with all of the telescopes.

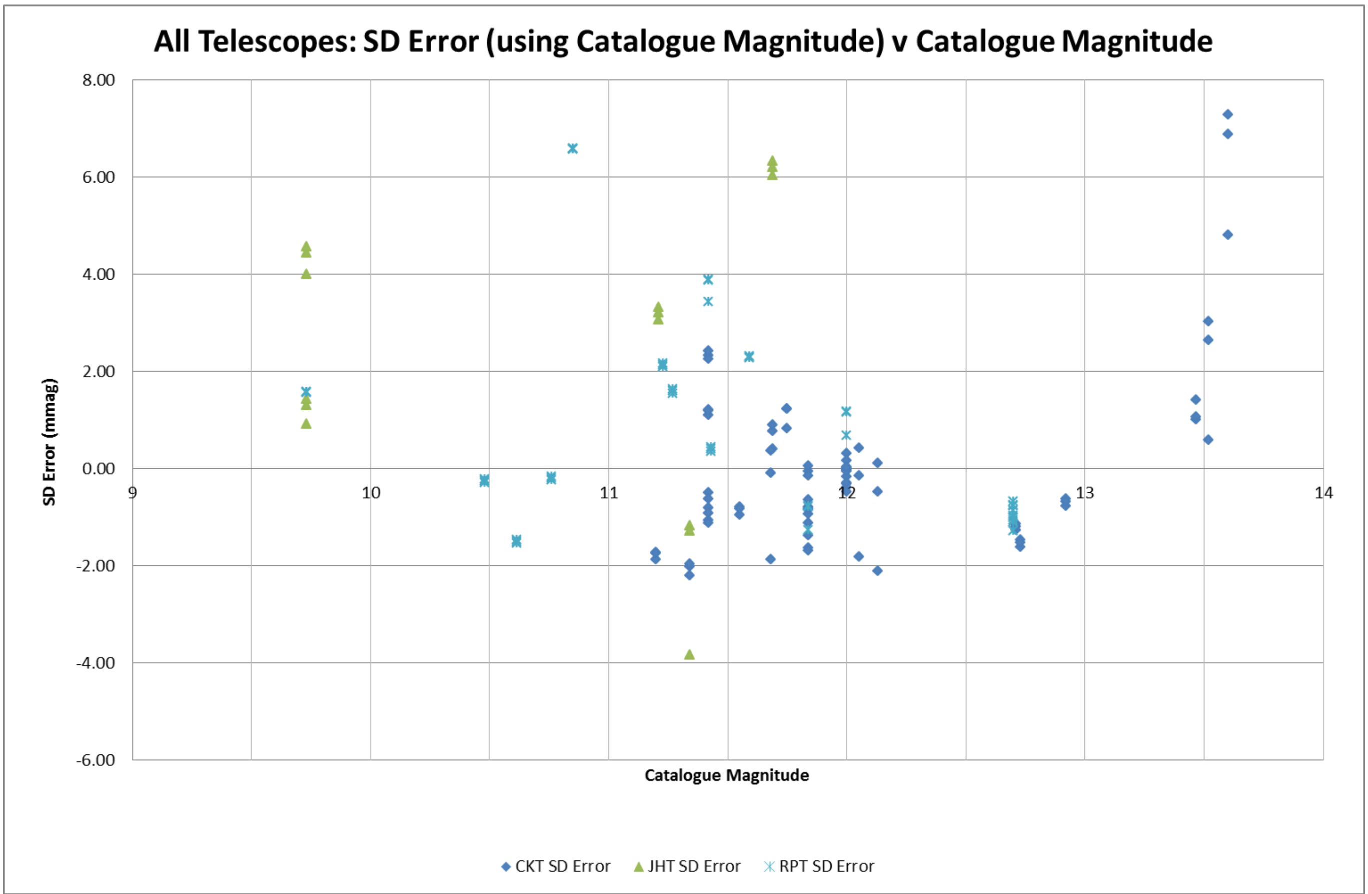


**Figure 11 All Telescopes: SD Error (using Catalogue Magnitude) v Magnitude**

Figure 12 presents data for the CKT telescope only, and shows the difference between the predicted SD using target catalogue magnitude compared to the measured SD values from a designated period in the respective light curves. In many cases the SD error is less than 2mmag. This plot shows that (apart from the results from COROT 1) most of the predicted SD values are larger than the measured SD values from the light curves.

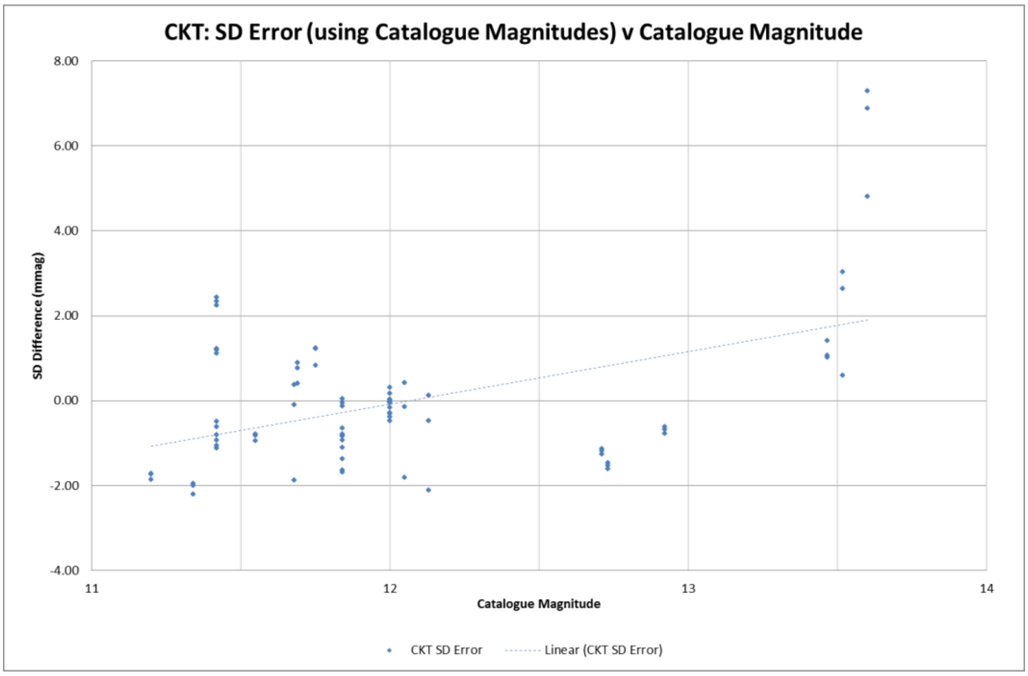


**Figure 12 CKT Telescope: SD Error (using Catalogue Magnitude) v Magnitude**

Figure 13 has the same information presented in Figure 12 but expressed as an absolute percentage error. The trend line implies that there is no obvious increase in SD error with catalogue magnitude for the selected range of target catalogue magnitudes.

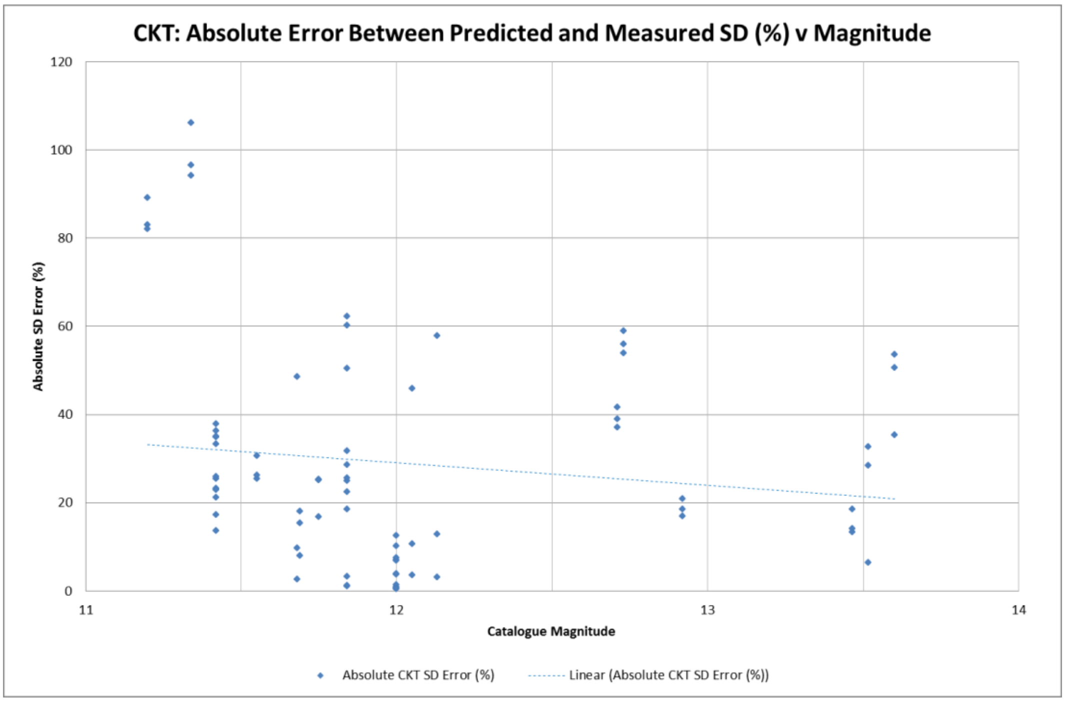


**Figure 13 CKT Telescope: Absolute SD Error (%) v Magnitude**

Figure 14 presents the same SD error but plotted against air mass. From inspection there is no evidence of increasing SD with increasing air mass. This implies that the equation compensation for air mass is proving to provide good compensation for a wide range of values of air mass.

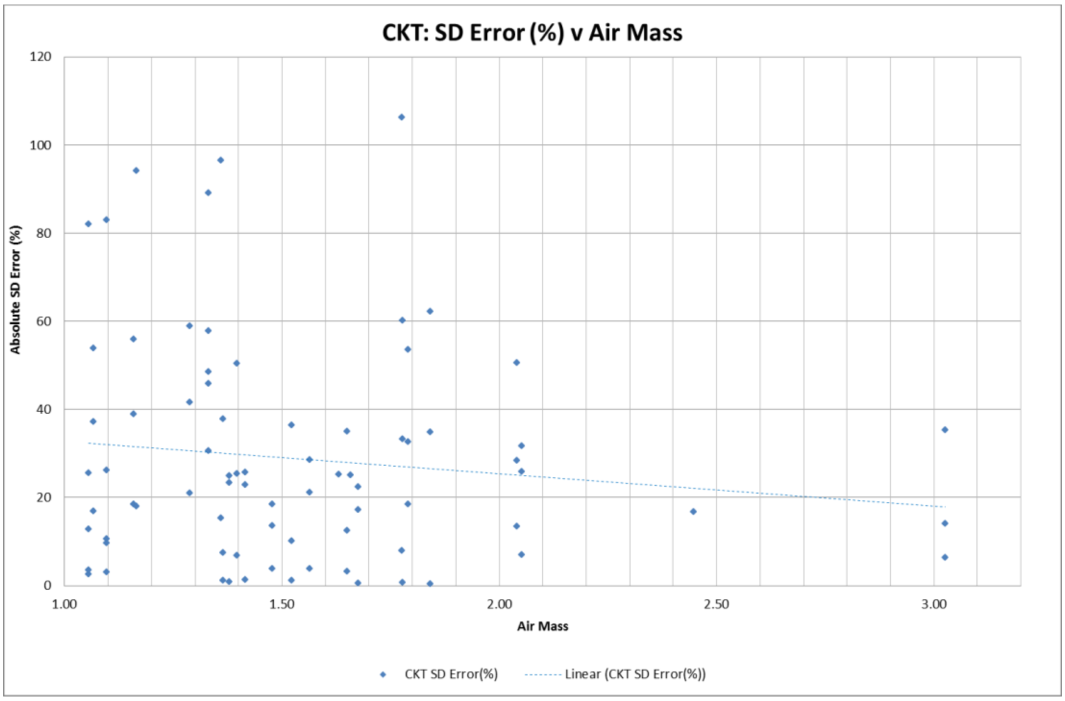


**Figure 14 CKT Telescope: Absolute SD Error (%) v Air Mass**

### 3.5.2 Non Variable Stars With Transits

The derived transit depths from the transit fitting program presented in Section 3.4.2 have been generated regardless of the duration of the observations. Figure 15 presents the derived transit depths (and their reported tolerances) and reference transit depths (from Table 5) plotted against catalogue magnitude. In most cases the reference transit depths are broadly consistent with the predicted 1SD error bars. No error bars have been assigned to the reference transit depth, however Section 3.4.2 states that the reference transit depth for WASP-10 (V=12.7) of 39.4mmag may be too high and that a more precise value would be 33±1 mmag. Inspection of Figure 15 indicates that this value is more consistent with the predicted results than the reference value of 39.4mmag.

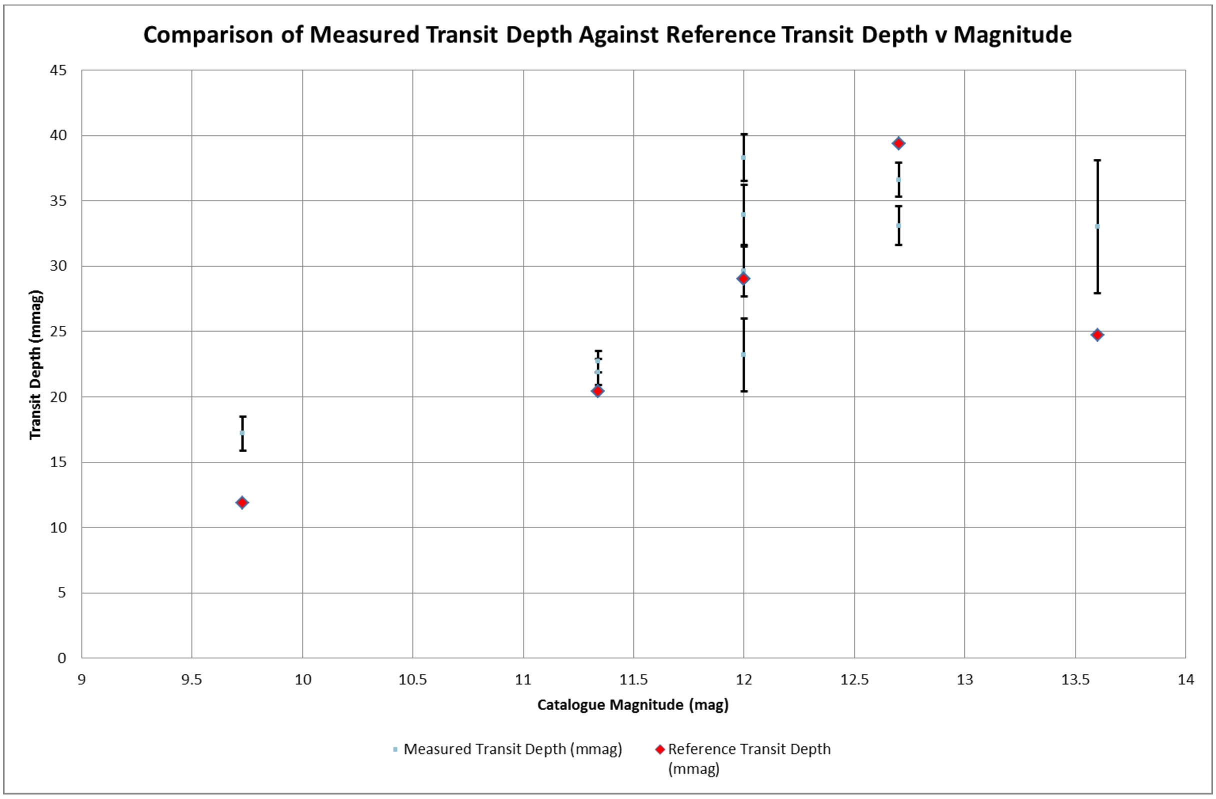


**Figure 15 Comparison of Measured Transit Depth and Reference Transit Depths v Magnitude**

The transit depth measurement for HAT-P-4 (V=11.12) of 8/9.4.2017 in Table 5 is likely to be more prone to error as inspection of Figure 68 indicates that a full transit had not been fully captured.

### 3.5.3 Eclipsing Binary Star UX UMa

The results presented in Section 3.4.3 are consistent with those obtained by Dmitrienko (Dmitrienko 1994) who conducted a large number of transit depth measurements for UX UMa (Table 3 of this reference shows that the measured transit depth values for a V filter varied between 0.68mag to 1.15mag).

The value of the SD from the light curves is much larger than the predicted SD since the observed SD from the light curve reflects the variability of the cataclysmic variable outside of the eclipse[20] with the bulk of the luminosity due to accretion (Kolb 2010). This means that the measured SD of the light curve should not be used to define precision[21].

Figure 93, despite the limitations of the observations, clearly has the displaced JHT telescope light curve largely overlapping the equivalent light curve from the RPT telescope. The match appears to improve as time advances and some of the limitations of the light curves become less pronounced. For example, the close match at approximately 1.3 hours would not be expected had the light curve

[20] The light curve reflects interactions arising from material being taken via the Roche lobe of the red giant star, falling onto the bright spot on the accretion disc and eventually migrating onto the white dwarf's surface causing novas.

[21] An alternative method to calculate the SD would be to use a check (or reference) star's light curve to define precision, but the alternative star might have a significantly different magnitude with a correspondingly different SD.

variations been solely due to measurement noise. The high degree of over-lapping of the tolerance bars[22] gives confidence that the predicted tolerances are satisfactory.

Consequently the predicted precision can be used to assist in identifying genuine physical effects in the light curve.

[22] The predicted tolerances are only believed to be indicative of the expected performance with the RPT telescope.

# 4 DISCUSSION

## 4.1 General

The observing conditions have often been compromised by the presence of cloud. However, good precision has still been achieved using differential photometry despite adverse conditions. For example, even with the cloudy conditions captured by the Bayfordbury All Sky Camera on 24/25.11.2016 (Figure 4), a good transit light curve was still captured for HAT-P-20 (see Figure 70 and Figure 83). It may have been the case that the cloud cover was reasonably uniform for all images taken during the observing period.

The light curve for WASP-10 has a close resemblance to the detailed light curves presented in Figure 5b to Sada (Sada & Ramón-Fox 2016) that had been produced at a site 989m amsl in Mexico using a 0.36m telescope with a Johnson-Cousins Ic filter. The precision of their 4 light curves was defined by the statement "Average point-to-point variation values ranged between 0.0031 and 0.0039 for these four individual light curves." Inspection of Table 4 shows that the predicted precision of the CKT telescope (for the air mass and exposure time used on WASP-10 observation of 13/14.9.2016) was approximately 4.2mmag with a measured SD of approximately 3.1mmag. Both of these figures are consistent with the observations made by Sada. Similar precision was also achieved with the check stars 1213-0608720 and 1214-0612767 that have similar magnitudes as WASP-10. In the case of the WASP-10 observation by the RPT telescope on 17/18.10.2016, the predicted precision was approximately 4.3mmag and the measured SD was approximately 3.2mmag. This means that both the CKT and RPT telescopes at Bayfordbury Observatory have achieved similar precision to that achieved by the similar telescope used by SADA.

## 4.2 Comparison of Achieved Results Compared to Predictions

The results presented in Table 2 of Section 3.4.1 show the SD derived using measured counts with the CKT telescope. These results are typically within 2mmag of the corresponding reference SD values obtained from the light curves, albeit there were some mismatches with the results from COROT-1 that may in part be due to poor observing conditions.

The more comprehensive set of results presented in Table 4 of Section 3.4.1 show the predicted SD values derived using catalogue magnitudes with the CKT telescope. The results are also typically within 2mmag of the measured values obtained from the light curves, apart from a few exceptions, and fully consistent with the errors obtained in the validation process (see Figure 26). A similar performance was not only achieved with the JHT telescope but also with the RPT telescope.

A model with the predicted precision equations was implemented in a spread sheet as part of the process to generate Table 4 of Section 3.4.1 (an example completed spread sheet for WASP-10 is provided as Table 3). This spread sheet was used to help identify which predicted exoplanet transits could be satisfactorily captured by the CKT telescope. Table 5 in Section 3.4.2 shows that the achieved observations with images correctly taken during a predicted transit (apart from the very faint inappropriate target WD 1145+017 in adverse weather conditions), captured 12 satisfactory transits with transit depths broadly consistent with the reference transit depths, even though many of the light curves did not satisfactorily capture the full transit. Furthermore, Table 5 gives transit depth tolerances (derived by transit depth equation fitting process) that are consistent with the predicted values of SD given in Table 4.

The very speculative observation of target WD 1145+017 was particularly challenging due to its low magnitude (V=17.28). However, since the quoted high depth of transit (103.5mmag) and the predicted SD (Table 4 shows predicted SD values between 17mmag and 23mmag for the achieved values of air mass) for this target suggested that the transit could be captured. However the transit was not satisfactorily captured with the observations taken on 25/26.3.2017. As already stated at the end of Section 3.4.1, WD 1145+017 was found to be an unsuitable star for precision photometry as it is a variable star. In addition, an examination of the data and observation conditions revealed that it was quite foggy that night and even using the brightest star (TYC 272-650-1) as the reference star, the light curve for the check star was unsteady as illustrated in Figure 16.

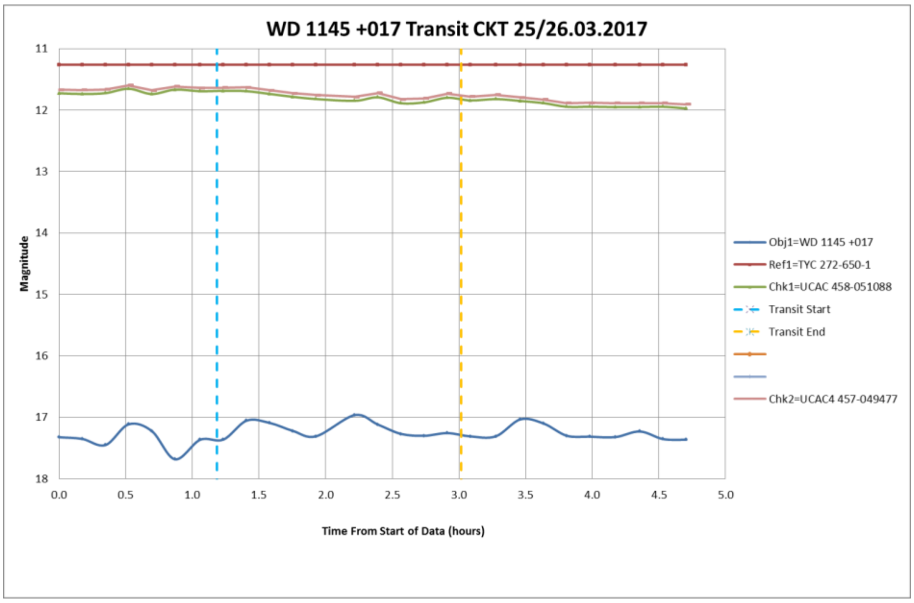


**Figure 16 Light Curves For the Transit of WD 1145+017 Taken on 25/26.3.2016 Using TYC 272-650-1 as the Reference Star**

Other factors noted that may also be relevant to other observations where poor results are obtained are:-

(a) The other non-variable stars in the image (that were identified using DS9 and the SIMBAD catalogue) were all significantly brighter than the target star. Since weather factors (such as undetectable cirrus and fog) and air mass varied quite considerably over the observing period, there was a significant risk that any stars used as a reference star/ check star could have readings exceeding the pixel well linearity limit at some stage during an observing period. The initial analysis used a reference star (TYC 272-650-1, V=11.26) that was subsequently found to be saturated in the first image. As the observations had proceeded and the air mass increased, the saturation ceased and resulted in the apparent magnitude of the check star progressively reducing, as can be observed in Figure 16. Subsequent analysis used an alternative less bright star (UCAC4 457-049477, V=11.69) as the reference star (and used in the generation of the light curve presented as Figure 46) but even this star had unacceptably high peak counts that exceeded the linearity limit, as did the check[23] star UCAC4 458-051088.

(b) The observing conditions were poor as the air mass was relatively high and varied from 1.7 to 2.4 during the observing period.

(c) As anticipated, the count for the target was low (despite having an exposure time of 600s) and the removed sky bias was relatively high compared to that of the target. For example, the first image had a recorded target count of only 6097 after subtracting the sky bias. The relatively high sky noise and irregular cross sections are illustrated in the aperture slice presented as Figure 17.

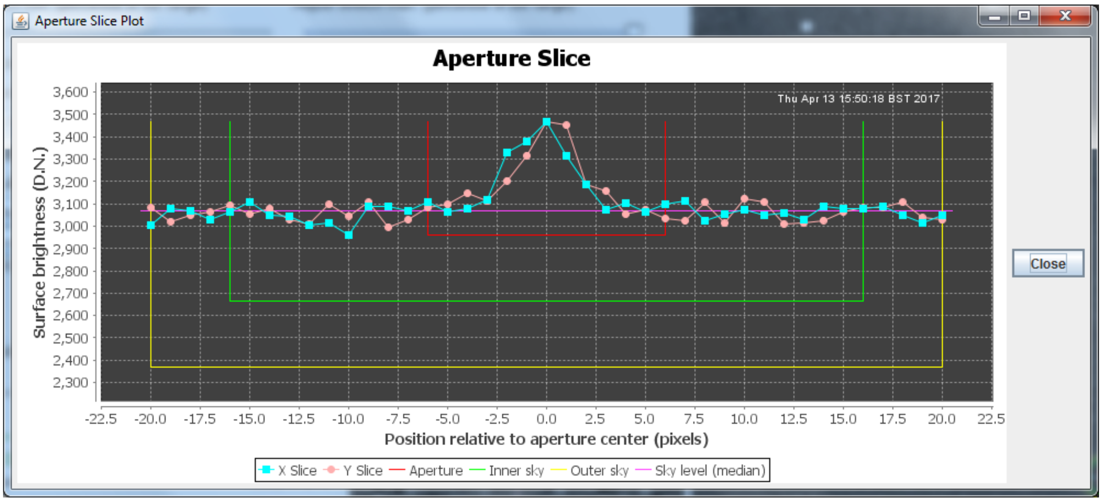


**Figure 17 Aperture Slice For WD 1145+017 in Image 39486**

(d) Apart from being difficult to identify the faint target star in an image, there is an increased risk that another faint variable star (with Poisson noise) could be present in an aperture/annulus that would have an insignificant contribution to the count with a bright star, but this may not necessarily be the case with a faint star.

### 4.3 Revision of Equations to Better Match Results

No revisions to the equations are advocated as there are no clear discrepancies in the results. The good matches obtained in this study suggest that the errors introduced by having a target and reference star of different colour was negligible with V filter.

### 4.4 Assessment of Achievements Compared to Objectives

The **first primary study aim** identified in Section 1.3 was to:-

“Create a validated model of equations that quantify the predicted photometric precision of images taken with a specific telescope, camera and filter configuration at the University of Hertfordshire’s robotically controlled telescopes located at the Bayfordbury Observatory in Hertfordshire.

This thesis provides a straightforward definitive method of deriving the predicted photometric precision for any target captured by the CKT telescope at the Bayfordbury Observatory. The analysis has furnished numerical values for a set of

---

[23] There are no other non-variable stars readily identifiable in the images taken for WD 1145+017 with a V magnitude specified in the SIMBAD catalogue. It might be possible to find alternative reference and check stars using an another star catalogue.

equations that define the precision of the CKT telescope and camera configuration whilst working in V band with 2x2 binning.

The data from a series of multiple hour observations for a wide range of target magnitudes, exposures times and values of air mass have been analysed. The achieved matches (between the predicted SD with the CKT telescope and the achieved SD from the light curves) are shown in Table 4 to be consistently good, often within 2mmag precision. A similar outcome was also achieved with the JHT telescope which nominally has an identical telescope and camera configuration. In the case of the RPT telescope, the predicted performance (using the equations tailored for the CKT telescope, even though the RPT telescope has a slightly different type of camera to the one used with the CKT telescope) was still similar to that achieved in practice.

The **second primary study aim** identified in Section 1.3 was to:-

"Demonstrate that the predicted precision can be achieved by satisfactorily capturing transits with known transit depths."

The equations defined in this thesis provide a predicted precision that is valid for any target over a large range of catalogue magnitudes and values of air mass. The predicted precision has been calculated using the catalogue magnitude of the target star, the catalogue magnitude of the reference star, the predicted range of values of air mass for an observation and the chosen value of exposure time.

Suitable forecast exo-planet transits were identified using the predicted precision calculated using these equations. In turn the achieved results were compared with the predicted precision. The results presented in Section 3.4.2 and Table 5 clearly demonstrate that multiple exo-planet transits have been successfully captured, with uncertainties in the depth of transit (defined by the equation fitting process) consistent with the predicted SDs shown in Table 4.

The **first secondary study aim** identified in Section 1.3 was to:-

"Provide a tool to calculate predicted precision so that one can quickly decide if one can reliably observe an event such as the transit of the exoplanet for star WASP-33. This tool would also enable a user to investigate the optimal value of exposure time and cadence."

The predicted precision equations were implemented in a spread sheet as part of the process to generate Table 4 of Section 3.4.1. An example of the spread sheet is provided as Table 3.

Suitable candidate exo-planet transits that could be satisfactorily captured using the CKT telescope were then identified using the predicted precision for this spread sheet.

The exposure time has been iteratively changed in this spread sheet to find an optimum value of $t_{exp}$ that gives a suitably high cadence yet still gave an acceptable predicted accuracy.

The **second secondary study aim** identified in Section 1.3 was to:-

"Establish a more reliable calculation for the recommended target exposure time for use at the Bayfordbury Observatory."

Appendix G provides a method that could be adopted at the Bayfordbury Observatory to establish a maximum value for $t_{exp}$ that keeps the peak target count from a pixel within the linearity range. The user also needs to verify that the selected value of $t_{exp}$ is not predicted to exceed the linearity limit for the reference star and for the check stars.

## 4.5 Assessment of the Applicability of Methodology to Other Equipment

No reason has been identified that would preclude using the techniques identified in this thesis for use by other observatories with similar equipment to provide predicted precision with their observations.

An alternative application of the formulation is to quantify the change in the predicted precision with a proposed new camera. Linearity plots similar to those presented as Figure 27 would establish the camera's linearity limit(s) and (assuming a similar quantum efficiency) directly translate into a scale factor on the maximum exposure time for a given target. For example, if the pixel's well depth linearity limit of the new camera was double that for the CKT camera (but still has the same effective pixel collection area as the CKT telescope's camera), then the maximum exposure time for a target would also double.

# 5 CONCLUSIONS

## 5.1 Overview

Previously there has been uncertainty in predicting what precision could be achieved from observing targets and in particular the precision when observing a variable star such as UX UMa. Indeed, there were suggestions that the telescopes at Bayfordbury Observatory would be unable to capture an exo-planet transit.

This thesis presents an extensive series of measurements and data reduction that has been conducted to derive a formulation to predict the precision of an observation by the CKT telescope operating in V band with 2x2 binning. The validity of the equations covers a range of V magnitudes from 5mag to 16.5mag, and for air masses up to 3.0.

The formulation is very straight forward and only requires knowledge of the catalogue magnitude (of both the target and reference stars), exposure time and the expected highest value of air mass in order to predict the precision, assuming acceptable observing conditions and correct equipment functionality. As a consequence an observer can iteratively predict the precision **before** an observation has been taken to:-

(a) Establish whether it is worthwhile attempting to observe a particular target in the first place.
(b) Optimise the exposure time to give the best compromise between a high cadence and the required precision.
(c) Identify any constraints on the maximum value of air mass during an observation to maintain the required predicted precision.

Alternatively, the formulation can be used to predict the achieved precision **after** an observation using the achieved values of air mass.

This formulation has been used to identify which predicted exo-planet transits would be worth observing and the optimum value of exposure time that should be used. The subsequent observations successfully captured 12 exo-planet transits with an achieved a precision consistent with the original calibration. This performance has been obtained over a wide range of weather conditions, target magnitudes and values of air mass. Consequently it is considered that the formulation has been demonstrated to be robust, often in observing conditions that were far from perfect.

A method has also been developed to calculate the maximum exposure time for a given catalogue magnitude that could be implemented on Bayfordbury Observatory. This method would provide observers with a recommended maximum observing time for any target and should help them optimise the exposure times and consequently have fewer failed observations/ potentially produce higher precision results.

This thesis has also identified a number of important considerations for precision observations. For example, it is important to ensure that the pixel well linearity limit is not exceeded by any target, reference or check star due to the variation in air mass and cloud conditions during a prolonged observation period.

An additional benefit of this work is that observations taken as part of this project have provided the database foundation for one of the main astrophysics practicals carried out by 2nd year students on the Astrophysics BSc and MPhys degree programmes. The measurement and interpretation of these images (by the students) is assessed based on physical understanding and statistical method (that has been taught in lectures). Furthermore, students have also been submitting observing jobs to capture transiting exoplanets now that it has been demonstrated that exo-planet transits can, with care, be captured using the telescopes at the Bayfordbury Observatory.

Evidence of full compliance with the study aims (Section 1.3) has been provided in Section 4.4. Consequently it is considered that all primary and secondary study aims have been fully met.

## 5.2 Applicability of Formulation to Future Observing Studies at the Bayfordbury Observatory

The techniques and formulation developed in this thesis could be used to assist in:-

(a) Optimising the exposure time/ cadence for observing predicted exo-planet transits.
(b) Identifying potential targets (such as brown dwarfs) that could be satisfactorily captured with the required precision. The equations can be used to optimise the exposure time, identify if there are certain values of air mass that would be highly undesirable – and to help identify which stars might be suitable to be used as reference stars.
(c) Conducting studies where the precision may be hard to identify, such as with the cataclysmic variable binary star UX UMa.
(d) Assisting in identifying the smallest detectable transit depth that could be detected in searches for new exo-planet transits.

## 5.3 Identification Of Further Work

The key areas where further work would be particularly useful are to:-

(a) Extend the parameterisation of the equations to cover additional telescope/ camera configurations, hardware binning options and filter options at the Bayfordbury Observatory.
(b) Use the techniques at another observatory. Dr. S. Fossey of UCL Observatory (UCLO, University College London) has expressed an interest in reviewing these techniques and comparing with current methods of photometry used at UCLO, and has requested a copy of this thesis.
(c) Explore using 1x1 binning for relatively bright targets that would potentially have a significantly reduced SD with longer exposure times (see Figure 27), but with a lower cadence. This investigation would be particularly relevant to cameras that have hardware binning that cannot fully accommodate the summing of filled individual pixel wells because of the well capacity limitation of the summing wells. This investigation might identify any saturation in individual pixels that has been disguised by the hardware binning process.
(d) Implement the derivation of an optimised exposure time calculation in the Bayfordbury Observatory software.
(e) Demonstrate that the light curves simultaneously taken of the same target using different telescopes (and potentially with different exposure times) can be successfully combined (or binned) by weighting each data point according to the predicted precision from equations tailored for each telescope. For example, if all five robotically controlled telescopes at Bayfordbury Observatory were

simultaneously observing the same exo-planet transit of a faint target, then each point on their respective light curve could be included to give a higher cadence than from one telescope alone - the corresponding predicted values of SD could then be included as the third column in the data file that is input to the transit fitting program (accessed via the web site of the Czech Astronomy Society). An extension of this process could be applied to results with significantly different telescopes and exposure times, and possibly with observations from different locations.

(f) To develop a program to provide a predicted precision on a light curve based on the predicted SD (generated by the equations), to reflect the change in air mass with an observation lasting several hours. This program could also check on whether the pixel linearity limit might be exceeded during this observation.

(g) To investigate the inclusion of a colour term to represent the error introduced by using a target and a reference star of different colours.

# 6 REFERENCES


Afanasiev V.L.M., A.V., 2005, Astronomy Letters, 31, 214

Alton K.B., 2013, Journal of the American Association of Variable Star Observers (JAAVSO), 41, 97

Arellano Ferro A., et al., 2013, Monthly Notices of the Royal Astronomical Society, 434, 1220

Baldwin J.E., Tubbs R.N., Cox G.C., Mackay C.D., Wilson R.W., Andersen M.I., 2001, Astronomy and Astrophysics, 368, L1

Balona L.A., Janes K., Upgren A.R., 1995, in: Philip A.G.D. ed., New Developments in Array Technology and Applications. p. 187

Baptista R., Horne K., Hilditch R.W., Mason K.O., Drew J.E., 1995, The Astrophysical Journal, 448, 395

Bayfordbury-Observatory, 5.9.2016. http://bayfordbury.herts.ac.uk/about/telescopes.htm,

BBC, 6.10.2017. BBC,

Bergfors C., et al., 2013, Monthly Notices of the Royal Astronomical Society, 428, 182

Bertin E., Arnouts S., 1996, Astronomy and Astrophysics Supplement Series, 117, 393

Bessell M.S., 1990, Publications of the Astronomical Society of the Pacific, 102, 1181

Bessell M.S., 2000, Publications of the Astronomical Society of the Pacific, 112, 961

Bessell M.S., 2005, Annual Review of Astronomy and Astrophysics, 43, 293

Bramich D.M., 2008, Monthly Notices of the Royal Astronomical Society, 386, L77

Brown T.M., et al., 2013, PASP, 125, 1031

Budding E., Demircan O., 2007, in: Ellis R., Huchra J., Kahn S., Rieke G., Stetson P.B. eds., Cambridge Observing Handbooks for Research Astronomers. Cambridge University Press, University Press, Cambridge, UK,

Buffington A., Booth C.H., Hudson H.S., 1991, Publications of the Astronomical Society of the Pacific, 103, 685

Carrol B.W. O.D.A., 2007, ISBN 0-321-44284-9, 1278 plus appendices

Castellano T., Laughlin G., Terry R.S., Kaufman M., Hubbert S., Schelbert G.M., Bohler D., Rhodes R., 2004, Journal of the American Association of Variable Star Observers (JAAVSO), 33, 1

Charbonneau D., Brown T.M., Latham D.W., Mayor M., 2000, The Astrophysical Journal Letters, 529, L45

Collier Cameron A., et al., 2007, Monthly Notices of the Royal Astronomical Society, 380, 1230

Conroy K.E., Prsa A., Stassun K.G., Orosz J.A., Fabrycky D.C., Welsh W.F., 2013, ArXiv e-prints. p. 512

Cooper W.A., et al., 2004, in: Norton A.J. ed., A Guide to Observational Astronomy and Planetary Science. Cambridge University Press, Cambridge, UK,

Cousins A.W.J., 1974, Monthly Notes of the Astronomical Society of South Africa, 33, 149

CyanogenImaging, 2016, http://diffractionlimited.com/product/maxim-dl/ 6.12.2016,

Czech A.S., 5.9.2016. http://var2.astro.cz/ETD/predict_detail.php?STARNAME=HAT-P-8&PLANET=b&PER=&M=,

Davenport J.R.A., West A.A., Matthiesen C.K., Schmieding M., Kobelski A., 2006, Publications of the Astronomical Society of the Pacific, 118, 1679

Davies R., Kasper M., 2012, Annual Review of Astronomy and Astrophysics, 50, 305

de Mooij E.J.W., Jayawardhana R., 2013, European Physical Journal Web of Conferences. p. 13001

de Mooij E.J.W.S., I.A.G., 2009, Astronomy and Astrophysics, 493, L35

Dmitrienko E.S., 1994, Astronomy Letters, 20, 104

Dravins D., Lindegren L., Mezey E., Young A.T., 1998, Publications of the Astronomical Society of the Pacific, 110, 610

Dravins D. L.L., Mezey M., 1997, Publications of the Astronomical Society of the Pacific, 109, 173

Ducci L.C., S.; Doroshenko, V. ; Mereghetti, S.; Sanatangelo, A.; Sasaki, M., 2016, Astronomy and Astrophysics, 538, 7

Durech J., et al., 2017,

Eibe M.T., Cuesta L., Ullán A., Pérez-Verde A., Navas J., 2011, Monthly Notices of the Royal Astronomical Society, 412, 1181
Eibe M.T., Cuesta L., Ullán A., Pérez-Verde A., Navas J., 2012, Astronomical Society of India Conference Series. p. 141
Everett M.E., Howell S.B., 2001, Publications of the Astronomical Society of the Pacific, 113, 1428
Faedi F., et al., 2013, Monthly Notices of the Royal Astronomical Society, 433, 2097
Fernández Fernández J., Chou D.-Y., Pan Y.-C., Wang L.-H., 2012, Publications of the Astronomical Society of the Pacific, 124, 507
Ferrero A., et al., 2010, Advances in Astronomy, 2010, 36
Fried D.L., 1978, Journal of the Optical Society of America (1917-1983), 68, 1651
Fukugita M., Ichikawa T., Gunn J.E., Doi M., Shimasaku K., Schneider D.P., 1996, The Astronomical Journal, 111, 1748
Gallaway M., 2016, An Introduction to Observational Astrophysics. Springer,
Gary B.L., Rappaport S., Kaye T.G., Alonso R., Hambschs F.-J., 2017, Monthly Notices of the Royal Astronomical Society, 465, 3267
Gilliland R.L., Brown T.M., 1992, Publications of the Astronomical Society of the Pacific, 104, 582
Gilliland R.L., et al., 1991, The Astronomical Journal, 101, 541
Gursoytrak H., et al., 2013, Information Bulletin on Variable Stars, 6075, 1
Guyon O., et al., 2011, in: Gajadhar S. ed., Telescopes from Afar. p. 26
Hamden E.T., et al., 2016, Journal of Astronomical Telescopes, Instruments, and Systems, 2
Hanno Rein M.-A.M., Planetaryscience, Andrew Tribick, Kenneth J Cott, Ryan Varley, Marc-Antoine, Tobias Mueller, Daveshoszowski, Allen Davis, Miguel De Val-Borro, James Gregory, Dave, Callum Rodwell, Anonymous, Darryl Hemsley, Chris Taylor 5.9.2016. www.openexoplanetcatalogue.com,
Hardy L.K., Butterley T., Dhillon V.S., Littlefair S.P., Wilson R.W., 2015, MNRAS,
Hartman J.D., Stanek K.Z., Gaudi B.S., Holman M.J., McLeod B.A., 2005, The Astronomical Journal, 130, 2241
Haswell C.A., 2010, Transiting Exoplanets. Cambridge University Press,,
Henry G.W., Marcy G.W., Butler R.P., Vogt S.S., 2000, The Astrophysical Journal Letters, 529, L41
Herrero E.M., J.C.; Ribas, I.; Naves, R., 2011, Astronomy and Astrophysics, 526, L10 (2011), 4
Holmes S., et al., 2011, PASP,
Howell S., Koehn B, Bowell,E, 1996, The Astronomical Journal, 112
Howell S.B., 2006, in: Ellis R.E. H.J. ed., Cambridge Observing Handbooks for Research Astronomers. Cambridge University Press, Cambridge, UK:,
Im M., Choi C., Kim K., 2015, Korean Astronomical Society, 48
Irwin M.J., 1985, Monthly Notices of the Royal Astronomical Society, 214, 575
Janssen A.J.E.M., van Haver S., Dirksen P., Braat J.J.M., 2006, 43
Jehin E., Manfroid J., Hutsemékers D., Gillon M., Magain P., 2011, EPSC-DPS Joint Meeting 2011. p. 1489
Jenkins F.A., White, H.E., 1957,
Johnson H.L., Morgan W.W., 1953, The Astrophysical Journal, 117, 313
Jordi C., et al., 2010, Astronomy and Astrophysics, 523, 48
Jordi K., Grebel E.K., Ammon K., 2006, Astronomy and Astrophysics, 460, 339
Joye W.A., Mandell, E., 2003, ASP Conference Series, Astronomical Data Analysis Software and Systems XII, 295, 389
Kannawadi, 2016, 18
Kjeldsen H., Frandsen S., 1992, Publications of the Astronomical Society of the Pacific, 104, 413
Kjurkchieva D.P., Marchev D.V., 1994, Information Bulletin on Variable Stars, 4122
KODAK, 1999,
Kolb U., 2010, Extreme Environment Astrophysics. Cambridge University Press, Cambridge, UK,

Koppelman M., 2010, Journal of the American Association of Variable Star Observers (JAAVSO), 38, 236
Kozhevnikov V.P., 2012, Monthly Notices of the Royal Astronomical Society, 422, 1518
Kurtz D.W.C., C.; Cunha, M.S. Cunha; et al, 2005, Monthly Notices of the Royal Astronomical Society, 358, 651
La_Silla, 5.9.2016, http://www.eso.org/public/unitedkingdom/teles-instr/lasilla/,
Laher R., 2012, http://ascl.net/1208.003 6.12.2016,
Landolt A.U., 1992, The Astronomical Journal, 104, 340
Law N.M., 2007, The Observatory, 127, 71
Law N.M., Mackay C.D., Baldwin J.E., 2006, Astronomy and Astrophysics, 446, 739
Law N.M., et al., 2009, The Astrophysical Journal, 692, 924
Licchelli D., 2007, Memorie della Societa Astronomica Italiana Supplementi, 11, 211
López-Morales M., 2006, Publications of the Astronomical Society of the Pacific, 118, 716
Mackay C., 2013, Monthly Notices of the Royal Astronomical Society, 432, 702
Maddox S.J., Efstathiou G., Sutherland W.J., 1990, Monthly Notices of the Royal Astronomical Society, 246, 433
Mahajan V.N., 1982, Journal of the Optical Society of America (1917-1983), 72, 1258
Mancini L.S., J., 2015, Haute Provence Observatory Coloquium, 12
Mandel K.A., E., 2002, The Astronomical Journal, 580, LI171
Martioli E., Jablonski F., 2007, IAU Special Session, 5, 253
MASCARA, 2017. http://mascara.strw.leidenuniv.nl/,
Moutou C., et al., 2009, Astronomy and Astrophysics, 498, L5
NASA., 21.9.2016,
Naylor T., 1998, Monthly Notices of the Royal Astronomical Society, 296, 339
Neely A.W. J.J.R., 1993, Publications of the Astronomical Society of the Pacific, 105, 1330
Pal A., 2012, Monthly Notices of the Royal Astronomical Society, 421, 13
Pecker J.-C., 1970, Spinger Astrophysics and Space Science Library, 21
Pereyra A., Zevallos M.I., Ricra J., Tello J.C., 2017, ArXiv e-prints.
Pollacco D.L., et al., 2006, Publications of the Astronomical Society of the Pacific, 118, 1407
Rameau J., et al., 2013, The Astrophysical Journal Letters, 772, L15
Ryan P., Sandler D., 1998, Publications of the Astronomical Society of the Pacific, 110, 1235
Sada P.V., Ramón-Fox F.G., 2016, Publications of the Astronomical Society of the Pacific, 128, 024402
Samolyk G., 2013, Journal of the American Association of Variable Star Observers (JAAVSO), 41, 122
SBIG, 5.9.2016. http://www.sbig.com/products/adaptive-optics/,
SBIG, 12.10.2016,
SBIG, 2003. Santa barbara California, p. 82
SBIG;, 7.10.2016, https://www.sbig.com/products/cameras/stx/stx-16803/,
Scolinic D., et al., 2014, Astrophysical Journal, 795, 23
Seal Braun P., Baruch J.E.F., 2009, Astrophysics and Space Science, 321, 177
Snellen I.A.G.K., J.; van dr Burg, R.F.J.; Driezler, S.; Greiner, J.; de Hon, M.D.J.; Husser, T.O.; Kruhler, T.; Saglia, R.P.; Vuijsje, F.N., 2008, Astronomy and Astrophysics, 497, 545
Snodgrass C., et al., 2016, MNRAS,
Southworth J., et al., 2009, Monthly Notices of the Royal Astronomical Society, 396, 1023
Southworth J., et al., 2013, Monthly Notices of the Royal Astronomical Society, 434, 1300
Soutter J.H., J.; Pepper, J.; et al, 2015, Australian Space Research Conference, 13
Steele I.A., 2004, Astron. Nachr. / AN 325, No. 6–8, 519–521 (2004) / DOI 10.1002/asna.200410271,
Strassmeier K.G., et al., 2004,
Szabo R.P., A.; Sarneczky, K.; Szabo, G.M.; Molnar, L.; Kiss, L.L.; Hanyecz, O.; Plachy, E.; Kiss. C., 2016, Astronomy and Astrophysics, 9
Thompson S.J., et al., 2016,
Tinetti G., 2014, Philosophical Transactions of the Royal Society, A372
Tomaney A.B. C.P.S., 1996, Astrophysical Journal, 112, 24

Tyson R.K., 1998,
University-of-Hertfordshire, 2017. http://observatory.herts.ac.uk/wiki,
Vanhuysse M., Cales J.-P., Technologie C., Santerne A., Moutou C., 2011, EPSC-DPS Joint Meeting 2011. p. 1456
Vidal-Madjar A.L.d.E., A.; Desert, J.M.; Ballester, G.E.; Ferlet, R.; Hebrard, G.; Mayor, M., 2002, Nature, 143
Villanueva S., Scott Gaudi B., Pogge W., Eastman D., Stassun G., Trueblood M., Trueblood P., 2017,
Wahhaj Z., et al., 2013, The Astrophysical Journal, 773, 179
Warner B.D., 2006,
Watson A.M., et al., 2016, Argelander-Institut fur Astronomie (AIfA),
Yamamoto K., et al., 2013, Publications of the Astronomical Society of Japan, 65, 90
Young A.T., Dukes R.J., Jr., Adelman C.J., 1992, in: Adelman S.J. ed., Automated Telescopes for Photometry and Imaging. p. 73
Zeilik M., Gregory S.A., 1998,
Zolotukhin I., 20.10.2016. http://exoplanet.eu/,

## ABBREVIATIONS

| Abbreviation | Definition |
|---|---|
| ADC | Analogue to Digital Conversion |
| ADU | Analogue to Digital Unit |
| amsl | Above mean sea level |
| AO | Adaptive Optics |
| APT | Automatic Precision Telescopes |
| BBC | British Broadcasting Corporation |
| CCD | Charge Coupled Device |
| CKT | Chris Kitchen Telescope |
| COATLI | Corrector de Optica Activa y de Tilts al Lımite de dIfraccion |
| CTE | Charge Transport Efficiency |
| CV | Cataclysmic Variable |
| DEMONEX | DEdicated MONitor of EXotransits and Transients |
| DIA | Difference Image Analysis |
| DS9 | SAOImage DS9 (Joye 2003) |
| ESO | European Space Observatory |
| HDR | High Dynamic Range |
| FITS | Flexible Image Transport System |
| FOV | Field Of View |
| FWHM | Full Width Half Maximum |
| JHT | Jim Hough Telescope |
| KELT | Kilodegree Extremely Little Telescope |
| LCOGT | Las Cumbres Observatory Global Telescope Network |
| LSGT | Lee Sang Gak Telescope |
| mas | Milli arc seconds |
| MASCARA | Multi-Site All Sky Camera |
| MIT | Massachusetts Institute of Technology |
| nm | Nano meter |
| NOAU | National Optical Astronomy Observatory |
| OTA | Orthogonal Transfer Array |
| Pan-STARRS | Panoramic Survey Telescope and Rapid Response System |
| PIRATE | Physics Innovations Robotic Astronomical Telescope Explorer |
| PMT | Photo Multiplier Tube |
| PSF | Point Spread Function |
| QE | Quantum Efficiency |
| REM | Rapid Eye Mount |
| RMS | Root Mean Square |
| RSS | Root of the Sum of Squares |
| RTML | Remote Telescope Markup Language |
| SBIG | Santa Barbara Instrument Group |
| SD | Standard Deviation |
| SDSS | Sloan Digital Sky Survey |
| SNR | Signal to Noise Ratio |
| SuperWASP | Super Wide Area Survey for Planets |
| TRAPPIST | TRAnsiting Planets and PlanetesImals Small Telescope |
| UBV | Ultra-violet (3500Å) Blue (4400Å) Visible (5500Å) |
| UBVRI | UBV Red (6700Å) Infrared (8000Å) |
| UCLO | University College of London Observatory |
| ugriz | u-band (3551Å) g-band (4686Å) r-band (6165Å) i-band (7481Å) z-band (8931Å) |
| WIYN | Wisconsin Indiana Yale NOAO |

# 7 ACKNOWLEDGEMENTS

Support is acknowledged from Dr M Gallaway, Dr P Lucas and Dr A Chrysostomou for the supervision and advice during the conduct of this project.

Support is also acknowledged from Mr D Campbell and Dr S Rolfe (staff at the Bayfordbury Observatory) in resolving various technical issues.

This research has made use of SAOImage DS9 (Joye 2003) (developed by Smithsonian Astrophysical Observatory), APT (Laher 2012), and Python for the analysis of data.

The Czech website (Czech 5.9.2016) has been invaluable in identifying suitable exoplanet targets and for fitting transit curves to the data.

THIS PAGE INTENTIONALLY LEFT BLANK

# Appendix A Telescopes and Cameras Available at Bayfordbury

| Telescope Name | Camera | CCD Chip | Full Well Capacity ($e^-$) | Pixel Array Size | FOV | Anti-blooming | Image Size (mm) | Pixel Size (µm) | Full Frame Download (s) |
|---|---|---|---|---|---|---|---|---|---|
| Meade =DAT | SBIG STL-1301E (see SBIG, 2003) | Kodak Enhanced KAF-1301E | 150,000 | 1280x1024 | 23.4'x15.6' | Not Standard | 20.5x16.4 | 16x16 | 3 |
| INT | Starlight Xpress SXVR-H18 (see Starlght Xpress SXVR-18 manual) | Kodak Enhanced KAF-8300M (See Truesense Imaging PS-0029) | 25,500 | 3366x2504 | 26.1'x19.6' | Yes 1000xsaturation exposure | 17.96x13.52 | 5.4x5.4 | N/A |
| CKT | SBIG STL-6303E | Kodak Enhanced KAF-6303E | 100,000 | 3060x2040 | 23.4'x15.6' | Not Standard | 27.5x18.4 | 9x9 | 14 |
| Video | None | | | | | | | | |
| New Meade =RPT | SBIG STX-16803 (see SBIG, 2003) | Kodak Enhanced KAF-16803 (See Truesense Imaging PS-0029) | 100,000 | 4096x4096 | 31.2'x31.2' | 100xsaturation exposure | 36.86x36.86 | 9x9 | 13 |
| Paramount =JHT | SBIG STL-6303E (see SBIG, 2003) | Kodak Enhanced KAF-6303E | 100,000 | 3060x2040 | 23.4'x15.6' | Not Standard | 27.5x18.4 | 9x9 | 14 |

**Table of Telescopes and the Characteristics of their Cameras at Bayfordbury**

# Appendix B Submitting Robotically Controlled Observations at Bayfordbury Observatory

An outline description of how to conduct robotic observing at the Bayfordbury Observatory is provided by their wiki (University-of-Hertfordshire 2017).

Observing plans are submitted using instructions in the Remote Telescope Markup Language (RTML). A web based RTML editor is usually used to generate observing plans. This editor readily allows the user to create observing plans that go through various checks before being added to the observing queue. The user typically supplies the following information for submitting a plan:-

(a) Telescope name.
(b) Target name (and select 'find coordinates').
(c) Filter type.
(d) Exposure time.
(e) Number of exposures.
(f) Pixel binning.
(g) Earliest time for taking exposures
(h) Latest time for taking exposures.

The RTML editor is designed as a general tool, as opposed for submitting transit observation plans. Consequently one needs to submit several plans of up to one hour duration to capture as many images as possible during the period of interest. However, the telescope might automatically refocus after each hour session that will introduce a delay and potentially a change to the size of the FWHM.

# Appendix C Location of Digital Copies of Image Data

All images reported in this thesis are available by arrangement from the web site of University of Hertfordshire Bayfordbury Observatory (University-of-Hertfordshire 2017).

# Appendix D Proprietary and Free Issue Software Packages Used

APT© (Laher 2012)

DS9© (Joye 2003)

MaximDL™© (CyanogenImaging 2016)

Microsoft EXCEL™©, Microsoft WORD™©

Python

# Appendix E ‘Union Jack’ Flat Field Results

## Results: UX UMa 60s Images

| Start Image | 15140 | 15150 | 15160 | 15338 | 15348 | 15358 |
|---|---|---|---|---|---|---|
| End Image | 15149 | 15159 | 15169 | 15347 | 15357 | 15367 |
| Diagonal 1 | 0.002761356 | 0.002295688 | -0.005168133 | 0.001867319 | -0.001496012 | -0.005296454 |
| Diagonal 2 | 5.17E-05 | 0.001123157 | -0.00139064 | -0.001143393 | -0.00132356 | -0.002968669 |
| Vertical | 0.002183792 | 0.001101702 | 0.001078084 | 0.002496692 | 0.001015809 | 0.00018662 |
| New Diagonal 1 | 0.001650509 | 0.001333412 | -0.002834888 | 0.000692487 | -0.000719668 | -0.003811388 |
| New Diagonal 2 | 9.80E-05 | 0.000544059 | -0.000958172 | -0.000303917 | -0.001054133 | -0.001853031 |
| Horizontal | 0.000672479 | 0.000619387 | -0.001992601 | 5.84E-05 | -0.001288123 | -0.002605931 |

**Table 7 Trend Line Slopes for ADU Count v Pixel Number For Various Cuts Through Image with 60s Exposure Time**

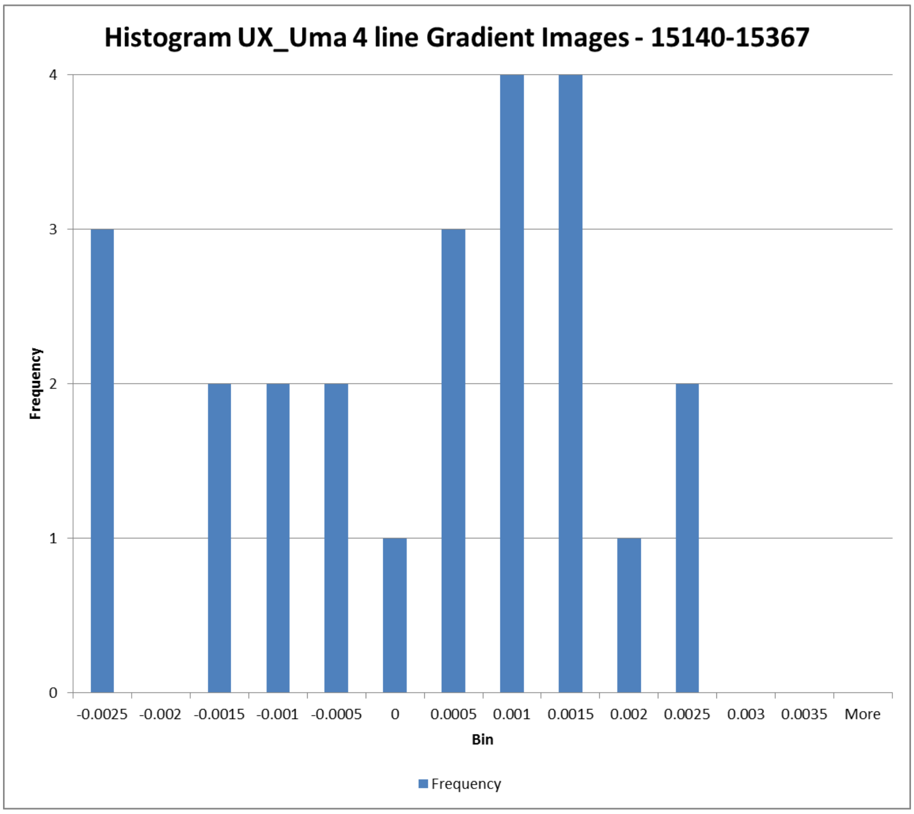


**Figure 18 Histogram of Gradients with a Sample UX UMa Images**

## Appendix E

### Results: V795 Her 60s Images

| Start Image | 14859 | 14872 | 14884 | 14897 | 14910 | 14923 | 14936 | 14949 | 14961 |
|---|---|---|---|---|---|---|---|---|---|
| End Image | 14871 | 14883 | 14896 | 14909 | 14922 | 14935 | 14947 | 14960 | 14973 |
| Diagonal 1 | 0.00144532 | 0.0019563 | 0.00151357 | 0.00143561 | 0.00170773 | 0.00182599 | 0.00267113 | 0.00218934 | -0.0002555 |
| Diagonal 2 | -0.0003839 | -0.0005412 | -0.0012142 | -0.001399 | -0.0004171 | -0.0010621 | 0.00068183 | -0.0005732 | -0.0010007 |
| Vertical | 8.17E-05 | 0.00065488 | 0.00108738 | 0.00071754 | 0.00060707 | 0.00041652 | 0.00187016 | 0.00049119 | 0.00018385 |
| New Diagonal 1 | 0.00051349 | 0.00094933 | 0.00105876 | 0.00063821 | 0.00121039 | 0.00075134 | 0.00122586 | 0.00137719 | -0.0005119 |
| New Diagonal 2 | -0.0001707 | -0.0007183 | -0.0006265 | -0.0006821 | 5.16E-05 | -0.0005602 | -7.65E-05 | -0.0003997 | -0.0004227 |
| Horizontal | -0.0001519 | 0.00049785 | 0.00062998 | 0.00013491 | -0.0003012 | 0.00050873 | 0.00026862 | 3.71E-05 | -0.0008102 |

**Table 8 Trend Line Slopes for ADU Count v Pixel Number For Various Cuts Through Image with 60s Exposure Time**

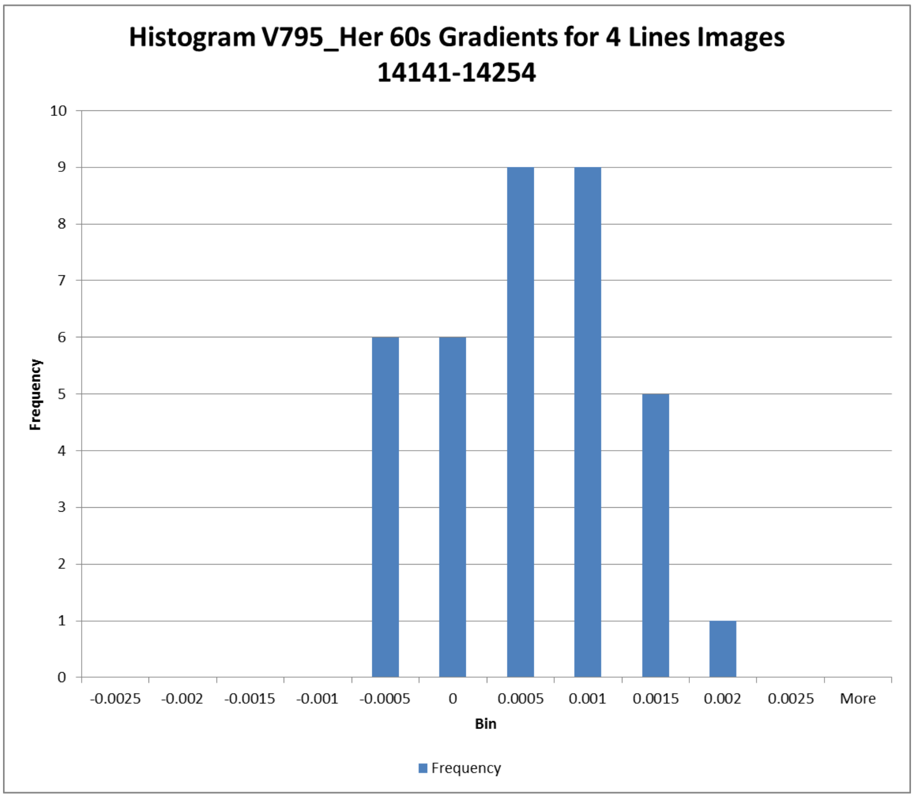


**Figure 19 Histogram of Gradients with a Sample V795-Her Images with 60s Exposure Time**

## Results: V795 Her 120s Images

| Start Image | 14141 | 14159 | 14169 | 14180 | 14190 | 14200 | 14210 | 14229 | 14245 |
|---|---|---|---|---|---|---|---|---|---|
| End Image | 14158 | 14168 | 14179 | 14189 | 14199 | 14209 | 14228 | 14243 | 14254 |
| D1 | -0.00318 | -0.0013 | -0.0021 | -0.0011 | -0.003 | -0.0015 | -0.002237 | -0.0079 | -0.0168 |
| D2 | -0.0001 | 0.00019 | 0.00085 | -0.0008 | 0.0009 | 0.00016 | 0.0020248 | -0.0011 | -0.0062 |
| Vertical | 0.000758 | 0.00252 | 0.00214 | 0.00253 | 0.00153 | 0.00218 | 0.0031064 | 0.00169 | -0.004 |
| New D 1 | -0.00226 | -0.0011 | -0.0015 | -0.0012 | -0.0016 | -0.0013 | -0.001266 | -0.0044 | -0.0111 |
| New D2 | 2.08E-05 | -0.0002 | 0.0001 | -0.0002 | 0.00069 | 0.00036 | 0.0006958 | -0.0009 | -0.0043 |
| Horizontal | -0.00152 | -0.0007 | -0.001 | -0.0005 | -0.0003 | -0.0005 | -1.81E-05 | -0.0026 | -0.0068 |

**Table 9 Trend Line Slopes for ADU Count v Pixel Number For Various Cuts Through Image with 120s Exposure Time**

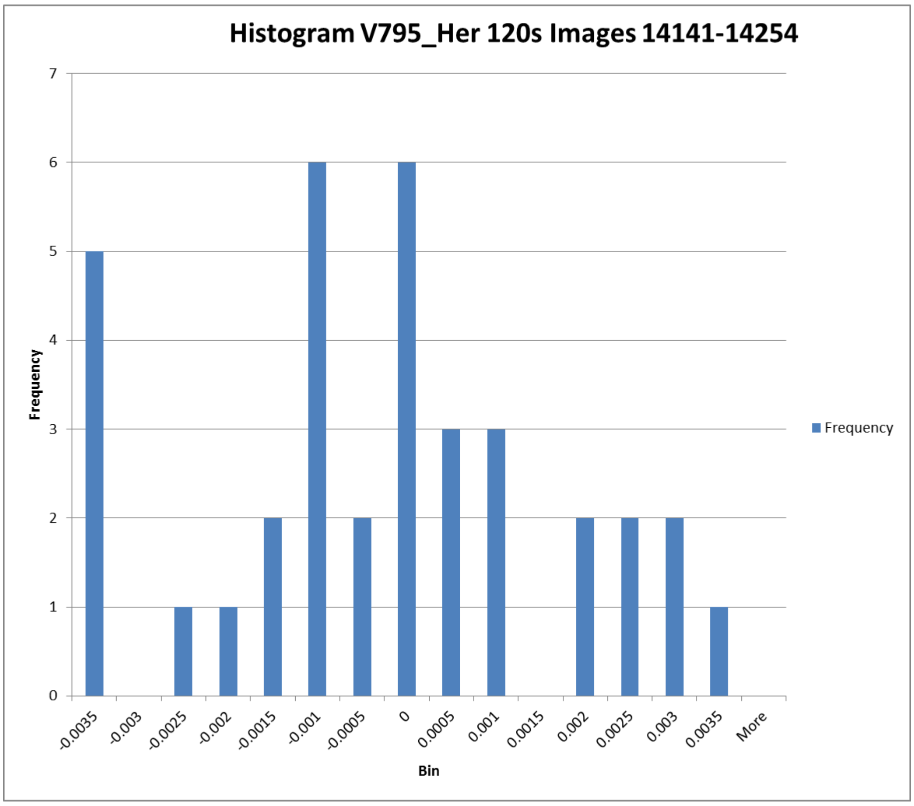


**Figure 20 Histogram of Gradients with a Sample V795-Her Images with 120s Exposure Time**

# Appendix F Derivation of Relationship Between Instrument and Catalogue Magnitudes

Section 2.2.8 generated generic equation (2.2.8.5) to convert catalogue magnitude (m) to give the instrument magnitude for a 1s exposure and an air mass of 1.0 ($\mathrm{m}'_{\mathrm{t=1s,X=1.0}}$). Section 2.2.8 also generated the associated equation (2.2.8.4) to compensate for air mass (X) and 1s of exposure to give the instrument magnitude for any value of air mass ($\mathrm{m}'_{\mathrm{t=1s,X=X}}$).

This Appendix presents the derivation of the associated parameters for the CKT telescope operating with 2x2 hardware binning and with a V filter to initially populate equation (2.2.8.4) to give equation (3.2.6.2) and to then populate equation (2.2.8.5) to give equation (3.2.6.1).

It then goes on to verify the equations by inputting the catalogue magnitude, $t_{exp}$ and X in a large sample of targets from Table 12 to back calculate the instrument magnitude to compare against the actual measurements. Finally the verified equations are then validated by using a large sample of targets (that are independent of those shown in Table 12) that explore the applicability of the equations over a wide range of catalogue magnitudes and values of air mass.

## Target Intensity ($N_{target}$) Measurements

Two sources of reference stars have been used to derive a relationship between the measured instrument magnitudes (m') with the CKT telescope/camera operating with 2x2 binning and the corresponding catalogue magnitudes (m).

The first source was from specially taken single images for four stars in the Landolt catalogue since these are standard stars with well-defined magnitudes. One image per star has been obtained with Clear, V, B, U and R filters. The reference details are presented as Table 10. The reference magnitudes were obtained using the software package DS9 and the SIMBAD catalogue. Unfortunately, SIMBAD does not provide reference magnitudes for Clear filters.

| STAR | RA | DEC | Time (s) | Tele-scope | Filter | Ref Mag | No. Runs | Image | U |
|---|---|---|---|---|---|---|---|---|---|
| SA97-284<br>BD+001237<br>GSC00117-01044<br>TYC 117-1044-1 | RA 89.604337<br>RA 05 58 25.041 | DEC 00 05 13.73<br>DEC 0.087147 | 60 | CKT | Clear | - | 1 | 7739 | 13.24 |
| | | | | | R | 10.013 | 1 | 7741 | |
| | | | | | B | 12.151 | 1 | 7743 | |
| | | | | | V | 10.787 | 1 | 8388[24] | |
| SA98-185<br>HD292574<br>GSC04800-00923 | RA 06 52 01.88<br>RA 103.007858 | DEC -00 27 21.56<br>DEC 0.455989 | 60 | CKT | Clear | - | 1 | 7855,<br>8391,<br>8735 | 10.851 |
| | | | | | R | 10.427 | 1 | 8738 | |
| | | | | | B | 10.739 | 1 | 8740 | |
| | | | | | V | 10.537 | 1 | 8753 | |
| SA98-978<br>HD292561<br>TYC4800-469-1 | RA 06 51 33.733<br>RA 102.890554 | DEC -00 11 31.56<br>DEC -0.192100 | 60 | CKT | Clear | - | 1 | 8744 | 11.277 |
| | | | | | R | 10.226 | 1 | 8747 | |
| | | | | | B | 11.183 | 1 | 8750 | |
| | | | | | V | 10.574 | 1 | 8757 | |
| SA96-36<br>TYC4736-1132-1 | RA 04 51 42.399<br>RA 72.926662 | DEC -00 10 09.39<br>DEC -0.169275 | 60 | CKT | Clear | - | 1 | 8056 | 10.954 |
| | | | | | R | 10.456 | 1 | 8057 | |
| | | | | | B | 10.836 | 1 | 8059 | |
| | | | | | V | 10.589 | 1 | 8289 | |

### Table 10 Images Produced For Four Landolt Catalogue Stars

The second source of check stars was in a much larger sample of existing images for a spread of air masses taken on different days to obtain measurements taken under a range of observing conditions.

Both sets of images have been examined using APT to obtain measurements of the flux ($N_{target}$). Only the results for a V filter have been reviewed (however a similar process would provide equivalent results with R, B and clear filters). Table 11 presents the list of stars in ascending order of magnitude that have had images processed to generate the results presented

[24] Clouds in image – gave a lower ADU count than would be expected.

in Table 12. NB a completely separate set of stars shown in Table 14 were used for the validation exercise. All stars are assumed to be non-variable as they are all categorised as stars in the SIMBAD catalogue. Some images have been used to provide results for a number of stars to maximise the use of the images. Care had to be taken to avoid stars with background galaxy stars to avoid over compensating for the sky background.

All the stars from the Landolt catalogue, as would be expected, had high values of air mass (X) and consequently the observations experienced significant atmospheric attenuation.

| STAR | V MAGNITUDE | PRIMARY STAR BEING OBSERVED |
|---|---|---|
| HR 946 | 6.038 | HIP 14748 |
| HD 16966 | 8.51 | HIP 12753 |
| BD+42 645 | 8.95 | HIP 13434 |
| BD-00 789 | 8.98 | SA96-36 (Landolt Catalogue) |
| TYC 1794-441-1 | 9.66 | HIP 14259 |
| BD+42 643 | 9.67 | HIP 13434 |
| TYC 1791-4-1 | 9.77 | HIP 14748 |
| BD+52 1722 | 9.97 | UX UMa |
| BD+50 615 | 10.08 | HIP 12753 |
| TYC 3308-1034-1 | 10.11 | HIP 12753 |
| SA98-185/ HD292574 | 10.537 | SA98-185 (Landolt Catalogue) |
| SA98-978/ HD292561 | 10.574 | SA98-978 (Landolt Catalogue) |
| SA96-36/ TYC 4736-1132-1 | 10.589 | SA96-36 (Landolt Catalogue) |
| TYC 1791-188-1 | 10.68 | HIP 14748 |
| TYC 4736-1153-1 | 10.7 | SA96-36 (Landolt Catalogue) |
| TYC 3308-476-1 | 10.73 | HIP 12753 |
| BD-00 791 | 10.9 | SA96-36 |
| TYC 4736-1196-1 | 10.9 | SA96-36 |
| TYC 4736-1027-1 | 11.2 | SA96-36 |
| TYC 4736-1080-1 | 11.3 | SA96-36 |
| TYC 3455-842-1 | 11.42 | M106 |
| TYC 4504-1564-1 | 11.44 | RORF 0014 813 |
| TYC-4504-1050-1 | 11.51 | RORF 0014 813 |
| TYC 4504-860-1 | 11.57 | RORF 0014 813 |
| TYC 3469-516-1 | 11.61 | UX UMa |
| TYC 4039-481-1 | 11.81 | PN G1266+013 |
| TYC 4383-593-1 | 12.1 | M82 |
| GPM149.442737+69.731284 | 12.3 | M82 |
| TYC 4039-650-1 | 12.33 | PN G1266+013 |
| 2MASS J12181678+1424176 | 12.6 | M99 |
| 2MASS J12181647+1419292 | 12.7 | M99 |
| 2MASS J12180786+1432113 | 12.8 | M99 |
| GPM148.725971+69.615345 | 13.2 | M82 |
| 2MASS J12190080+1428397 | 13.4 | M99 |
| 2MASS J12183329+1429325 | 13.5 | M99 |
| 2MASS J09540368+6941167 | 13.5 | M82 |
| 2MASS J12190855+1421235 | 13.5 | M99 |
| 2MASS J09545340+6939298 | 14 | M82 |
| 2MASS J12184019+1420260 | 14.3 | M99 |
| 2MASS J13365496 +5155247 | 15.287 | UX UMa |
| [HH95]UX Uma-2 | 15.46 | UX UMa |
| 2MASS J09573616+6941183 | 15.5 | M82 |

**Table 11 Stars, Catalogue Magnitudes and Image Sources**

## Appendix F

# Derivation of Parameter ϵ in Equation (2.2.8.4) to Give Equation (3.2.6.2)

Each image has been analysed using APT to generate $(\mathrm{N_{target}})_{t=t_{exp},X=X}$. This term needs to be scaled to give the count rate in 1s, as defined by equation (2.2.7.3):-

$$(N_{target})_{t=1s,X=X} = \frac{1}{t_{exp}}(N_{target})_{t=t_{exp},X=X} \qquad (2.2.7.3)$$

The corresponding measured instrumental magnitude for a 1s exposure time is consequently given by:-

$$\mathrm{m'}_{t=1s,X=X} = -2.5\log_{10}[(\mathrm{N_{target}})_{t=1s,X=X}] \qquad (2.2.8.7)$$

The relationship to compensate for air mass is defined by equation (2.2.8.1):-

$$\mathrm{m'}_{t=1s,X=X} - \mathrm{m} = \epsilon X + \zeta \qquad (2.2.8.1)$$

The extinction coefficient (ε) has been obtained from a plot of (m'-m) plotted against X: Figure 21 presents the plot produced for the reference star BD+52 1722 obtained on 30.4.2013 (with $t_{exp}$=60s, but scaled for 1s exposure).

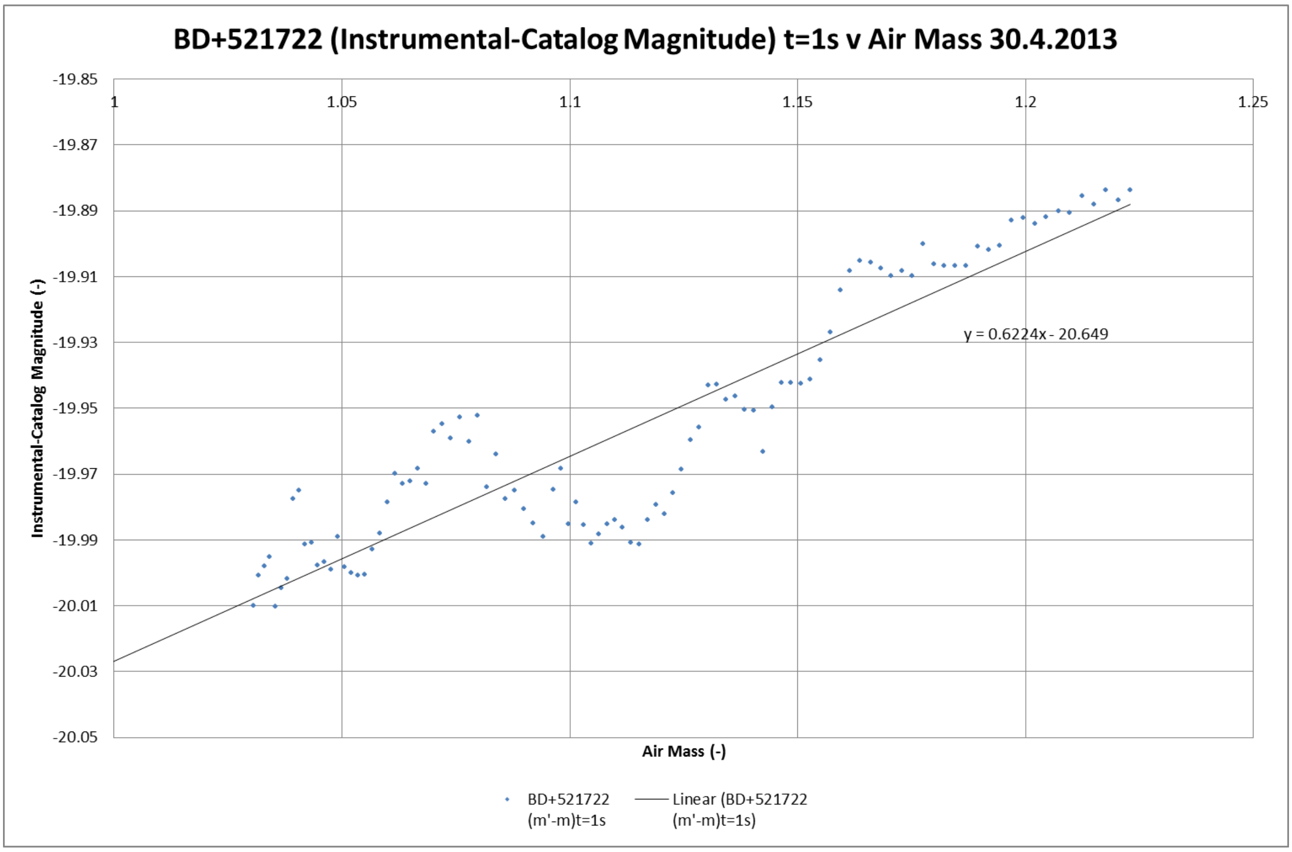


**Figure 21 (m'- m) v Air Mass for BD+52 1722 on 30.4.2013 with a V Filter**

The best fit slope shows an extinction coefficient (ε) derived by Excel of 0.6224. It is recognised that ε will change from night to night, however a typical value of 0.62 is probably the best that one can use. Consequently, substituting for ε in equation (2.2.8.4):-

$$\mathrm{m'}_{t=1s,X=1.0} = \mathrm{m'}_{t=1s,X=X} + \epsilon(1.0 - X) \qquad (2.2.8.4)$$

gives the predicted value for m' with a 1s exposure time and an air mass of X=X:-

$$[\mathrm{m'}_{t=1s,X=X}]_{predicted} = [\mathrm{m'}_{t=1s,X=1.0}]_{predicted} - 0.62(1.0 - X) \qquad (3.2.6.2)$$

Alternatively:-

$$[\mathrm{m'}_{t=1s,X=1.0}]_{predicted} = [\mathrm{m'}_{t=1s,X=X}]_{predicted} + 0.62(1.0 - X) \qquad (3.2.6.3)$$

# Derivation of Parameters for Equation (2.2.8.5) to Give Equation (3.2.6.1)

The predicted instrumentation magnitude for a star that has a catalogue magnitude of m (that is observed with an air mass of 1.0 and a 1s exposure) is defined by equation(2.2.8.5) as the best straight line fit of a plot of observed magnitude versus catalogue magnitude:-

$$[m'_{t=1s,X=1.0}]_{predicted} = gradient * m + Bias \quad (2.2.8.5)$$

Where 'gradient' and 'bias' can be extracted from a plot of $m'_{t=1s,X=1.0}$ versus m. The corresponding predicted highest count rate has also been generated for information purposes using equation (2.2.8.9).

$$[(N_{target})_{t=1s,X=1.0}]_{predicted} = 10^{-[m'_{t=1s,X=1.0}]_{predicted}/2.5} \quad (2.2.8.9)$$

Table 12 presents data obtained using APT from a wide range of images. The column headings are as follows:-

Date — is the date when the image was taken.
Image — is the image number in the Bayfordbury Observatory archive.
Star — is the chosen target within an image.
Ref Mag (m) — is the catalogue magnitude (m) for the star as indicated in Table 11.
Quality (quality /error) — is a measure of the accuracy of m as defined by the SIMBAD database. Quality has "A" for the best quality down to "E" for the worst quality. "~" is unknown quality. Error is the value of the error on the quoted magnitude.
Peak Aperture Slice Value — is the peak value in a slice through the aperture, as given by APT.
Measured Idc (no sky) — is the sky subtracted target flux count $[(N_{target})_{t=t_{exp},X=X}]$ as measured using APT.
Sky — is the sky count per pixel as measured by APT. A high value indicates poor sky conditions/ high air mass. (For information only).
$t_{exp}$ — is the image exposure time in seconds.
X — is the air mass from the Flexible Image Transport System (FITS) header of each image.
m' Inst mag $t_{exp}$=1s,X=X — is the instrument magnitude for t=1s and X=X, where $m'_{t=1s,X=X}$ is calculated from equations (2.2.7.3). and (2.2.8.7)
m' Inst mag texp =1s X=1.0 — is the instrument magnitude ($m'_{t=1s,X=X}$) normalised for air mass at X=1.0, where $m'_{t=1s,X=1.0}$ is derived using equation (3.2.6.3).
Idc $t_{exp}$ =1s X=1.0 — is the value of $(N_{target})_{t=1s,X=1.0}$ count for $m'_{t=1s,X=1.0}$ obtained using equation (2.2.8.9).

| Date | Image | Star | Ref Mag (m) | Quality (quality/ error) | | Peak Aperture Slice Value | Measured $I_{dc}$ (no sky) | Sky | $t_{exp}$ | X | m' Inst mag $t_{exp}$=1s, X=X Eq (2.2.8.7) Eq (2.2.7.3) | m' Inst mag $t_{exp}$=1s X=1.0 Eq (3.2.6.3) | Idc $t_{exp}$=1s X=1.0 Eq (2.2.8.9) |
|---|---|---|---|---|---|---|---|---|---|---|---|---|---|
| 21.12.2012 | 4447 | HR 946 | 6.038 | C~ | 0 | 45000 | 745415 | 111 | 2 | 1.11490 | -13.9284 | -14.000 | 397983 |
| 1.12.2012 | 5000 | HD16966 | 8.51 | D | 0.01 | 10000 | 213604 | 100 | 5 | 1.03547 | -11.5766 | -11.599 | 43595 |
| 22.11.2012 | 4504 | BD+42 645 | 8.95 | D | 0.05 | 4900 | 125416 | 100 | 5 | 1.07095 | -10.9985 | -11.042 | 26120 |
| 22.11.2012 | 4502 | BD+42 645 | 8.95 | D | 0.05 | 2600 | 49509 | 98 | 2 | 1.06959 | -10.9841 | -11.027 | 25758 |
| 5.3.2014 | 8289 | BD-00 789 | 8.98 | C~ | 0 | 61000 | 1212000 | 531 | 60 | 1.75809 | -10.7634 | -11.233 | 31143 |
| 22.11.2012 | 4476 | TYC 1794-441-1 | 9.66 | D | 0.03 | 2750 | 66949 | 102 | 5 | 1.11513 | -10.3169 | -10.388 | 14300 |
| 22.11.2012 | 4480 | TYC 1794-441-1 | 9.66 | D | 0.03 | 25300 | 798877 | 236 | 60 | 1.11934 | -10.3108 | -10.385 | 14254 |
| 22.11.2012 | 4504 | BD+42 643 | 9.67 | D | 0.04 | 2504 | 63608 | 101 | 5 | 1.07095 | -10.2614 | -10.305 | 13248 |
| 22.11.2012 | 4502 | BD+42 643 | 9.67 | D | 0.04 | 1260 | 25778 | 97 | 2 | 1.06959 | -10.2755 | -10.319 | 13412 |
| 21.12.2012 | 4447 | TYC 1791-4-1 | 9.77 | D | 0.04 | 1000 | 24245 | 98 | 2 | 1.11490 | -10.2090 | -10.280 | 12945 |
| 21.12.2012 | 4448 | TYC 1791-4-1 | 9.77 | D | 0.04 | 2800 | 58479 | 103 | 5 | 1.11581 | -10.1701 | -10.242 | 12495 |
| 21.12.2012 | 4453 | TYC 1791-4-1 | 9.77 | D | 0.04 | 20800 | 696095 | 246 | 60 | 1.11932 | -10.1613 | -10.235 | 12420 |
| 30.4.2013 | 10862 | BD+52 1722 | 9.97 | C~ | 0 | 16000 | 600516 | 222 | 60 | 1.03058 | -10.0009 | -10.020 | 10185 |
| 30.4.2013 | 10904 | BD+52 1722 | 9.97 | C~ | 0 | 8500 | 571014 | 251 | 60 | 1.09964 | -9.9462 | -10.008 | 10074 |
| 30.4.2013 | 10961 | BD+52 1722 | 9.97 | C~ | 0 | 15000 | 540983 | 301 | 60 | 1.22308 | -9.8876 | -10.026 | 10241 |
| 3.6.2013 | 12011 | BD+52 1722 | 9.97 | C~ | 0 | 16000 | 1422000 | 389 | 120 | 1.03533 | -10.1843 | -10.206 | 12092 |
| 4.6.2013 | 12021 | BD+52 1722 | 9.97 | C~ | 0 | 12000 | 1418000 | 335 | 120 | 1.08021 | -10.1812 | -10.231 | 12371 |
| 4.6.2013 | 12031 | BD+52 1722 | 9.97 | C~ | 0 | 12500 | 1409000 | 338 | 120 | 1.11533 | -10.1743 | -10.246 | 12541 |
| 4.6.2013 | 12041 | BD+52 1722 | 9.97 | C~ | 0 | 14200 | 1391000 | 344 | 120 | 1.15875 | -10.1604 | -10.259 | 12692 |
| 4.6.2013 | 12045 | BD+52 1722 | 9.97 | C~ | 0 | 18100 | 1385000 | 357 | 120 | 1.17818 | -10.1557 | -10.266 | 12778 |
| 4.6.2013 | 12050 | BD+52 1722 | 9.97 | C~ | 0 | 29000 | 1410000 | 343 | 120 | 1.20539 | -10.1751 | -10.302 | 13212 |
| 6.9.2013 | 15140 | BD+52 1722 | 9.97 | C~ | 0 | 11500 | 572252 | 311 | 60 | 1.52136 | -9.9486 | -10.272 | 12845 |
| 6.9.2013 | 15169 | BD+52 1722 | 9.97 | C~ | 0 | 12000 | 476837 | 273 | 60 | 1.71465 | -9.7505 | -10.194 | 11952 |
| 9.9.2013 | 15627 | BD+52 1722 | 9.97 | C~ | 0 | 33000 | 627058 | 293 | 60 | 1.52321 | -10.0479 | -10.372 | 14090 |

## Appendix F

| Date | Image | Star | Ref Mag (m) | Quality (quality/ error) | | Peak Aperture Slice Value | Measured $I_{dc}$ (no sky) | Sky | $t_{exp}$ | X | m' Inst mag $t_{exp}$=1s, X=X Eq (2.2.8.7) Eq (2.2.7.3) | m' Inst mag $t_{exp}$=1s X=1.0 Eq (3.2.6.3) | Idc $t_{exp}$=1s X=1.0 Eq (2.2.8.9) |
|---|---|---|---|---|---|---|---|---|---|---|---|---|---|
| 1.12.2012 | 5000 | BD+50 615 | 10.08 | D | 0.03 | 3500 | 56006 | 105 | 5 | 1.03547 | -10.1232 | -10.145 | 11430 |
| 1.12.2012 | 5000 | TYC 3308-1034-1 | 10.11 | D | 0.04 | 3000 | 48432 | 105 | 5 | 1.03547 | -9.9654 | -9.987 | 9885 |
| 1.4.2013 | 8753 | HD292574 | 10.537 | B | 0.001 | 19000 | 336982 | 427 | 60 | 1.93543 | -9.3736 | -9.954 | 9582 |
| 1.4.2013 | 8757 | HD292561 | 10.574 | B | 3E-04 | 23000 | 316598 | 415 | 60 | 1.93497 | -9.3059 | -9.886 | 9000 |
| 5.3.2013 | 8289 | TYC 4736-1132-1 | 10.589 | B | 5E-04 | 18000 | 283831 | 523 | 60 | 1.75809 | -9.1873 | -9.657 | 7293 |
| 21.12.2012 | 4453 | TYC 1791-188-1 | 10.68 | D | 0.08 | 12700 | 313078 | 240 | 60 | 1.11932 | -9.2938 | -9.368 | 5586 |
| 21.12.2012 | 4451 | TYC 1791-188-1 | 10.68 | D | 0.08 | 7000 | 156381 | 164 | 30 | 1.11780 | -9.2927 | -9.366 | 5575 |
| 5.3.2013 | 8289 | TYC 4736-1153-1 | 10.7 | C~ | 0 | 17500 | 273600 | 525 | 60 | 1.75809 | -9.1474 | -9.617 | 7030 |
| 1.12.2012 | 5000 | TYC 3308-476-1 | 10.73 | D | 0.06 | 1500 | 24643 | 104 | 5 | 1.03547 | -9.2318 | -9.254 | 5029 |
| 5.3.2013 | 8289 | BD-00 791 | 10.9 | C~ | 0 | 11300 | 222902 | 525 | 60 | 1.75809 | -8.9249 | -9.395 | 5728 |
| 5.3.2013 | 8289 | TYC 4736-1196-1 | 10.9 | D~ | 0 | 11000 | 188898 | 524 | 60 | 1.75809 | -8.7452 | -9.215 | 4854 |
| 5.3.2013 | 8289 | TYC 4736-1027-1 | 11.2 | C~ | 0 | 11200 | 210874 | 526 | 60 | 1.75809 | -8.8647 | -9.335 | 5419 |
| 5.3.2013 | 8289 | TYC 4736-1080-1 | 11.3 | C~ | 0 | 10500 | 188191 | 527 | 60 | 1.75809 | -8.7411 | -9.211 | 4836 |
| 7.5.2013 | 11593 | TYC 3455-842-1 | 11.42 | D | 0.11 | 27500 | 574323 | 1223 | 240 | 1.18182 | -8.4474 | -8.560 | 2655 |
| 29.10.2013 | 17489 | TYC 4504-1564-1 | 11.44 | D | 0.09 | 56000 | 905229 | 796 | 300 | 1.15492 | -8.6991 | -8.795 | 3297 |
| 29.10.2013 | 17489 | TYC 4504-1050-1 | 11.51 | D | 0.09 | 55000 | 796425 | 784 | 300 | 1.15492 | -8.5601 | -8.656 | 2900 |
| 29.10.2013 | 17489 | TYC 4504-860-1 | 11.57 | D | 0.1 | 42000 | 784715 | 793 | 300 | 1.15492 | -8.5440 | -8.640 | 2858 |
| 30.4.2013 | 10862 | TYC 3469-516-1 | 11.61 | D | 0.12 | 3600 | 167500 | 217 | 60 | 1.03058 | -8.6147 | -8.634 | 2841 |
| 30.4.2013 | 10904 | TYC 3469-516-1 | 11.61 | D | 0.12 | 2400 | 156991 | 237 | 60 | 1.09964 | -8.5443 | -8.606 | 2770 |
| 30.4.2013 | 10961 | TYC 3469-516-1 | 11.61 | D | 0.12 | 3250 | 149415 | 295 | 60 | 1.22308 | -8.4906 | -8.629 | 2829 |
| 3.6.2013 | 12011 | TYC 3469-516-1 | 11.61 | D | 0.12 | 4500 | 393518 | 383 | 120 | 1.03533 | -8.7895 | -8.811 | 3346 |
| 4.6.2013 | 12021 | TYC 3469-516-1 | 11.61 | D | 0.12 | 3600 | 391964 | 323 | 120 | 1.08021 | -8.7852 | -8.835 | 3419 |
| 4.6.2013 | 12031 | TYC 3469-516-1 | 11.61 | D | 0.12 | 3250 | 391490 | 323 | 120 | 1.11533 | -8.7838 | -8.855 | 3485 |
| 4.6.2013 | 12041 | TYC 3469-516-1 | 11.61 | D | 0.12 | 3900 | 385447 | 331 | 120 | 1.15875 | -8.7670 | -8.865 | 3517 |
| 4.6.2013 | 12045 | TYC 3469-516-1 | 11.61 | D | 0.12 | 4700 | 380352 | 337 | 120 | 1.17818 | -8.7525 | -8.863 | 3509 |
| 4.6.2013 | 12050 | TYC 3469-516-1 | 11.61 | D | 0.12 | 7600 | 384634 | 336 | 120 | 1.20539 | -8.7647 | -8.892 | 3604 |
| 6.9.2013 | 15140 | TYC 3469-516-1 | 11.61 | D | 0.12 | 3100 | 157543 | 302 | 60 | 1.52136 | -8.5481 | -8.871 | 3536 |
| 6.9.2013 | 15169 | TYC 3469-516-1 | 11.61 | D | 0.12 | 3000 | 128524 | 273 | 60 | 1.71465 | -8.3271 | -8.770 | 3222 |
| 9.9.2013 | 15627 | TYC 3469-516-1 | 11.61 | D | 0.12 | 8400 | 173615 | 287 | 60 | 1.52321 | -8.6536 | -8.978 | 3901 |
| 1.2.2012 | 2732 | TYC 4039-481-1 | 11.81 | D | 0.13 | 32000 | 552575 | 1521 | 300 | 1.40761 | -8.1632 | -8.416 | 2325 |
| 21.2.2014 | 20032 | TYC 4383-593-1 | 12.1 | D | 0.13 | 25000 | 387773 | 716 | 240 | 1.15441 | -8.0209 | -8.117 | 1765 |
| 21.2.2014 | 20032 | GPM149.442737+69.731284 | 12.3 | D~ | 0 | 14800 | 265171 | 713 | 240 | 1.15441 | -7.6083 | -7.704 | 1207 |
| 1.2.2012 | 2732 | TYC 4039-650-1 | 12.33 | D | 0.15 | 21000 | 463324 | 1518 | 300 | 1.40761 | -7.9719 | -8.225 | 1949 |
| 2.2.2013 | 2733 | TYC 4039-650-1 | 12.33 | D | 0.15 | 63000 | 1347000 | 4969 | 900 | 1.28754 | -7.9378 | -8.116 | 1764 |
| 3.2.2012 | 2734 | TYC 4039-650-1 | 12.33 | D | 0.15 | 53000 | 1338000 | 5015 | 900 | 1.06925 | -7.9305 | -7.973 | 1547 |
| 18.2.2012 | 2735 | TYC 4039-650-1 | 12.33 | D | 0.15 | 50000 | 1322000 | 2989 | 900 | 1.45902 | -7.9175 | -8.202 | 1909 |
| 19.2.2012 | 2736 | TYC 4039-650-1 | 12.33 | D | 0.15 | 27600 | 1385000 | 2799 | 900 | 1.16506 | -7.9680 | -8.070 | 1691 |
| 8.3.2012 | 2737 | TYC 4039-650-1 | 12.33 | D | 0.15 | 46000 | 1166000 | 8805 | 900 | 1.51613 | -7.7811 | -8.101 | 1740 |
| 11.3.2014 | 20656 | 2MASS J12181678+1424176 | 12.6 | D~ | 0 | 13000 | 170178 | 4101 | 240 | 1.67407 | -7.1267 | -7.545 | 1042 |
| 11.3.2014 | 20657 | 2MASS J12181678+1424176 | 12.6 | D~ | 0 | 13400 | 171815 | 4056 | 240 | 1.64722 | -7.1371 | -7.538 | 1036 |
| 11.3.2014 | 20656 | 2MASS J12181647+1419292 | 12.7 | D~ | 0 | 12000 | 161615 | 4079 | 240 | 1.67407 | -7.0707 | -7.489 | 990 |
| 11.3.2014 | 20657 | 2MASS J12181647+1419292 | 12.7 | D~ | 0 | 12200 | 162181 | 4041 | 240 | 1.64722 | -7.0745 | -7.476 | 978 |
| 11.3.2014 | 20657 | 2MASS J12180786+1432113 | 12.8 | D~ | 0 | 10300 | 151932 | 4046 | 240 | 1.64722 | -7.0036 | -7.405 | 916 |
| 21.2.2014 | 20032 | GPM148.725971+69.615345 | 13.2 | D~ | 0 | 8500 | 114016 | 716 | 240 | 1.15441 | -6.6919 | -6.788 | 519 |
| 11.3.2014 | 20656 | 2MASS J12190080+1428397 | 13.4 | D~ | 0 | 8700 | 68013 | 4177 | 240 | 1.67407 | -6.1310 | -6.549 | 416 |
| 11.3.2014 | 20657 | 2MASS J12190080+1428397 | 13.4 | D~ | 0 | 8300 | 67161 | 4126 | 240 | 1.64722 | -6.1173 | -6.519 | 405 |
| 11.3.2014 | 20656 | 2MASS J12183329+1429325 | 13.5 | D~ | 0 | 8200 | 70935 | 4146 | 240 | 1.67407 | -6.1766 | -6.595 | 434 |
| 11.3.2014 | 20657 | 2MASS J12183329+1429325 | 13.5 | D~ | 0 | 8300 | 69588 | 4097 | 240 | 1.64722 | -6.1558 | -6.557 | 420 |
| 21.2.2014 | 20032 | 2MASS J09540368+6941167 | 13.5 | D~ | 0 | 4300 | 74766 | 708 | 240 | 1.15441 | -6.2337 | -6.329 | 340 |
| 11.3.2014 | 20656 | 2MASS J12190855+1421235 | 13.5 | D~ | 0 | 7500 | 48739 | 4163 | 240 | 1.67407 | -5.7692 | -6.187 | 298 |
| 11.3.2014 | 20657 | 2MASS J12190855+1421235 | 13.5 | D~ | 0 | 7200 | 49129 | 4108 | 240 | 1.64722 | -5.7778 | -6.179 | 296 |
| 21.2.2014 | 20032 | 2MASS J09545340+6939298 | 14 | D~ | 0 | 4400 | 51535 | 712 | 240 | 1.15441 | -5.8297 | -5.925 | 235 |
| 11.3.2014 | 20656 | 2MASS J12184019+1420260 | 14.3 | D~ | 0 | 6300 | 31974 | 4136 | 240 | 1.67407 | -5.3115 | -5.729 | 196 |
| 11.3.2014 | 20657 | 2MASS J12184019+1420260 | 14.3 | D~ | 0 | 6100 | 31128 | 4079 | 240 | 1.64722 | -5.2823 | -5.684 | 188 |
| 30.4.2013 | 10862 | 2MASS J13365496+5155247 | 15.287 | D~ | 0 | 290 | 4460 | 216 | 60 | 1.03058 | -4.6780 | -4.697 | 76 |
| 30.4.2013 | 10904 | 2MASS J13365496+5155247 | 15.287 | D~ | 0 | 280 | 3900 | 235 | 60 | 1.09964 | -4.5323 | -4.594 | 69 |
| 3.6.2013 | 12011 | 2MASS J13365496+5155247 | 15.287 | D~ | 0 | 500 | 9939.7 | 384 | 120 | 1.03533 | -4.7955 | -4.817 | 85 |
| 3.6.2013 | 12021 | 2MASS J13365496+5155247 | 15.287 | D~ | 0 | 430 | 10783 | 323 | 120 | 1.08021 | -4.8839 | -4.934 | 94 |

| Date | Image | Star | Ref Mag (m) | Quality (quality/ error) | | Peak Aperture Slice Value | Measured $I_{dc}$ (no sky) | Sky | $t_{exp}$ | X | m' Inst mag $t_{exp}$=1s, X=X Eq (2.2.8.7) Eq (2.2.7.3) | m' Inst mag $t_{exp}$=1s X=1.0 Eq (3.2.6.3) | Idc $t_{exp}$=1s X=1.0 Eq (2.2.8.9) |
|---|---|---|---|---|---|---|---|---|---|---|---|---|---|
| 3.6.2013 | 12031 | 2MASS J13365496+5155247 | 15.287 | D~ | 0 | 445 | 10156 | 325 | 120 | 1.11533 | -4.8189 | -4.890 | 90 |
| 3.6.2013 | 12041 | 2MASS J13365496+5155247 | 15.287 | D~ | 0 | 460 | 10211 | 330 | 120 | 1.15875 | -4.8247 | -4.923 | 93 |
| 4.6.2013 | 12045 | 2MASS J13365496+5155247 | 15.287 | D~ | 0 | 520 | 10278 | 335 | 120 | 1.17818 | -4.8318 | -4.942 | 95 |
| 4.6.2013 | 12050 | 2MASS J13365496+5155247 | 15.287 | D~ | 0 | 620 | 10985 | 339 | 120 | 1.20539 | -4.9040 | -5.031 | 103 |
| 3.6.2013 | 12011 | [HH95]UX UMa-2 | 15.46 | D~ | 0 | 475 | 8868 | 384 | 120 | 1.03533 | -4.6716 | -4.694 | 75 |
| 3.6.2013 | 12021 | [HH95]UX UMa-2 | 15.46 | D~ | 0 | 420 | 9169.7 | 323 | 120 | 1.08021 | -4.7079 | -4.758 | 80 |
| 3.6.2013 | 12041 | [HH95]UX UMa-2 | 15.46 | D~ | 0 | 430 | 8378.2 | 330 | 120 | 1.15875 | -4.6099 | -4.708 | 76 |
| 3.6.2013 | 12031 | [HH95]UX UMa-2 | 15.46 | D~ | 0 | 430 | 8521.3 | 324 | 120 | 1.11533 | -4.6283 | -4.700 | 76 |
| 4.6.2013 | 12050 | [HH95]UX UMa-2 | 15.46 | D~ | 0 | 550 | 9358.1 | 339 | 120 | 1.20539 | -4.7300 | -4.857 | 88 |
| 21.2.2014 | 20032 | 2MASS J09573616+6941183 | 15.5 | D~ | 0 | 1900 | 20306 | 710 | 240 | 1.15441 | -4.8185 | -4.914 | 92 |

**Table 12 Derivation of ($m'_{t=1s,X=1.0}$) From Measured $I_{dc}$=$(N_{target})_{t=t_{exp},X=X}$**

Figure 22 presents the normalised measured instrument target magnitude $m'_{t=1s,X=1.0}$ plotted against catalogue magnitude (m) using the data presented in Table 12. The horizontal error bars illustrate the variation in the catalogue magnitude for each target (where known) from Table 12. The vertical error bars are the calculated SD values from the derived values of $m'_{t=1s,X=1.0}$ for each target presented in Table 12. An error bar is set to zero if the catalogue magnitude error is unknown or if only one star sample is available with the same magnitude and $t_{exp}$.

Figure 22 also presents a linear trend line with its associated equation that has been fitted by Excel. The observed slope of 1.0023 is consistent with theory (see p54, Equation (5.5) in Warner) which states that the slope is nominally 1.0. The constant term of -20.2122 is a composite term of the zero point, the extinction with an air mass of 1.0, and a colour index contribution. It was noted that the equation parameters did not significantly change as additional images were processed.

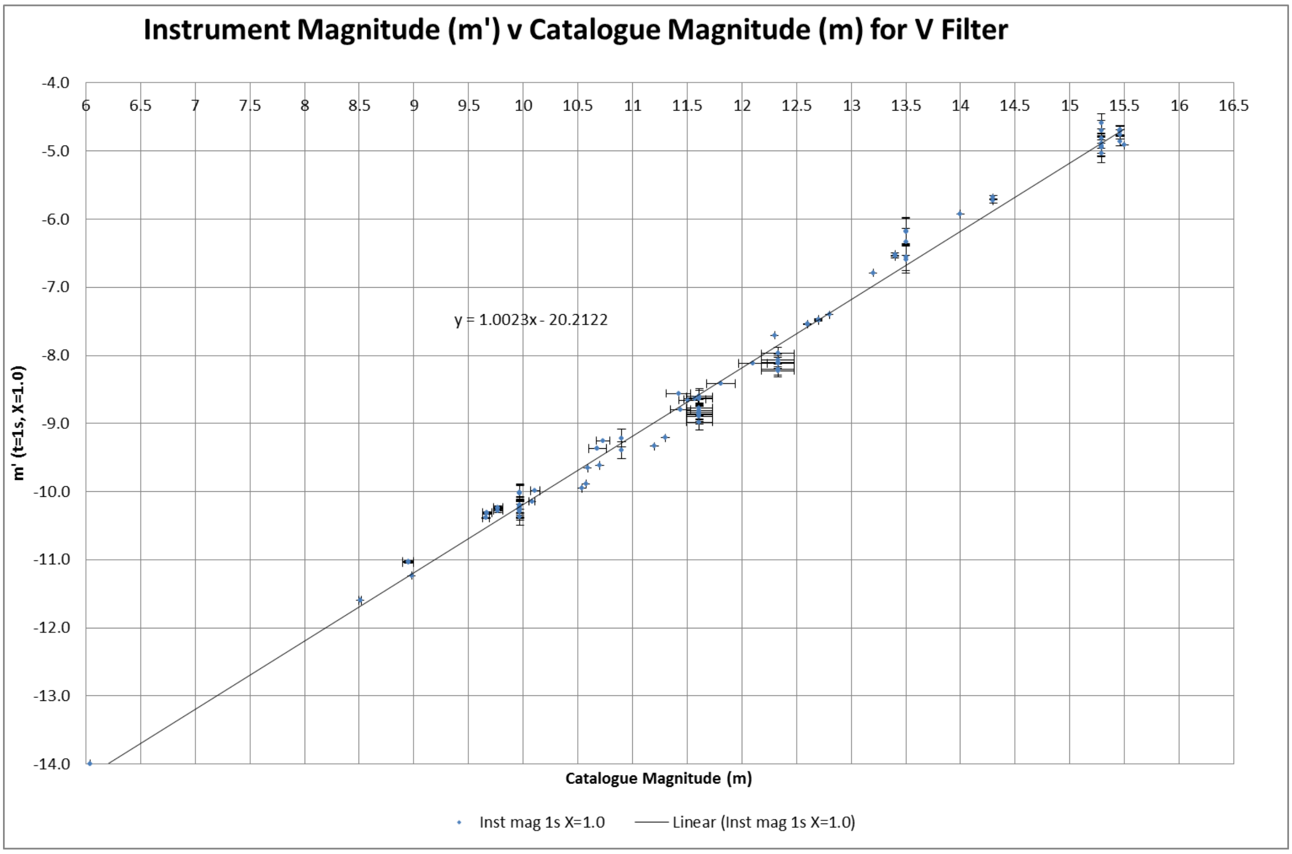


**Figure 22 Plot of Instrument Magnitude ($m'_{t=1s,X=1.0}$) Versus Catalogue Magnitude (m)**

Thus the predicted instrumentation magnitude for a star, with a catalogue magnitude of m, that is observed with an air mass of 1.0 and a 1s exposure, is defined by the best fit line shown in Figure 22. Substituting the values derived using Excel of $gradient$ and $Bias$ in equation (2.2.8.5) gives:-

$$[m'_{t=1s,X=1.0}]_{predicted} = 1.0023m - 20.2122 \quad (3.2.6.1)$$

## Appendix F

# Verification of Parameters

The verification of the formulation has been achieved by back calculating predicted values for instrument magnitude for the values of $t_{exp}$, X and m for each image. These back calculated values of instrument magnitude are ideally identical to the measured values and consequently the calculated value of the magnitude difference ($\Delta m'$) provides an estimate of the accuracy of the predictions. Verification was considered to have been achieved if there was a good match between the predicted and the actual observed results. Consequently, this section calculates the predicted instrument magnitude $[m'_{t=t_{exp},X=X}]_{predicted}$ and in turn $\Delta m'$ for each image. One benefit of this process is that these errors provide an estimate of the expected magnitude errors of any new measurement (existing or planned).

Table 13 presents the derivation of $\Delta m'$ for a sample of the measured values presented in Table 12. The derivation of $\Delta m'$ was by using the equations identified by the column headers and as summarised below:-

Values for $[m'_{t=t_{exp},X=X}]_{predicted}$ have been calculated for each image based on their respective values for m, X and $t_{exp}$ by using equation (3.2.6.1) to calculate $[m'_{t=1s,X=1.0}]_{predicted}$ and by equation (3.2.6.2) to compensate for air mass. Equations (2.2.8.8), (2.2.7.4) and (2.2.8.10) were then used to scale for exposure time:-

$$[m'_{t=1s,X=1.0}]_{predicted} = 1.0023m - 20.2122 \quad (3.2.6.1)$$

$$[m'_{t=1s,X=X}]_{predicted} = [m'_{t=1s,X=1.0}]_{predicted} - 0.62(1.0 - X) \quad (3.2.6.2)$$

$$[(N_{target})_{t=1s,X=X}]_{predicted} = 10^{-[m'_{t=1s,X=X}]_{predicted}/2.5} \quad (2.2.8.8)$$

$$[(N_{target})_{t=t_{exp},X=X}]_{predicted} = t_{exp}[(N_{target})_{t=1s,X=X}]_{predicted} \quad (2.2.7.4)$$

$$[m'_{t=t_{exp},X=X}]_{measured} = -2.5\log_{10}[(N_{target})_{t=t_{exp},X=X}]_{predicted} \quad (2.2.8.10)$$

The actual measured values of $[(N_{target})_{t=t_{exp},X=X}]_{measured}$ have been extracted from Table 12 to give $[m'_{t=t_{exp},X=X}]_{measured}$ :-

$$[m'_{t=t_{exp},X=X}]_{measured} = -2.5\log_{10}[(N_{target})_{t=t_{exp},X=X}]_{measured} \quad (2.2.8.11)$$

These predicted values of instrument magnitude have then been compared against $[m'_{t=t_{exp},X=X}]_{measured}$ to give the error ($\Delta m'$):-

$$\Delta m' = [m'_{t=t_{exp},X=X}]_{predicted} - [m'_{t=t_{exp},X=X}]_{measured} \quad (2.2.8.12)$$

Note equations (3.2.6.2) and (3.2.6.1) are only valid for a V filter with 2x2 hardware binning, and have only been proven for target magnitudes in the range 6<m<15.5.

| Date | Star | Image | Ref Mag (m) | Predicted $m'_{t=1s,X=1.0}$ Eq (3.2.6.1) | X | Predicted $m'_{t=1s,X=X}$ Eq (3.2.6.2) | Predicted $(N_{target})_{t=1s,X=X}$ Eq (2.2.8.8) | $t_{exp}$ | Predicted $(N_{target})_{t=t_{exp},X=X}$ Eq (2.2.7.4) | Predicted $m'_{t=texp,X=X}$ Eq (2.2.8.10) | Measured $(N_{target})_{t=t_{exp},X=X}$ | Measured $m'_{t=texp,X=X}$ Eq (2.2.8.11) | Δm' Eq (2.2.8.12) |
|---|---|---|---|---|---|---|---|---|---|---|---|---|---|
| 21.12.2012 | HR 946 | 4447 | 6.038 | -14.16031 | 1.114904 | -14.08907 | 432144 | 2 | 864289 | -14.8416 | 745415 | -14.6810 | -0.16065 |
| 1.12.2012 | HD16966 | 5000 | 8.51 | -11.68263 | 1.035475 | -11.66063 | 46159 | 5 | 230793 | -13.4081 | 213604 | -13.3240 | -0.08403 |
| 22.11.2012 | BD+42 645 | 4504 | 8.95 | -11.24162 | 1.070956 | -11.19762 | 30133 | 5 | 150667 | -12.9450 | 125416 | -12.7459 | -0.19916 |
| 22.11.2012 | BD+42 645 | 4502 | 8.95 | -11.24162 | 1.069593 | -11.19847 | 30157 | 2 | 60314 | -11.9510 | 49509 | -11.7367 | -0.21433 |
| 5.3.2014 | BD-00 789 | 8289 | 8.98 | -11.21155 | 1.758094 | -10.74153 | 19798 | 60 | 1187852 | -15.1869 | 1212000 | -15.2088 | 0.02185 |
| 22.11.2012 | TYC 1794-441-1 | 4476 | 9.66 | -10.52998 | 1.115133 | -10.45860 | 15256 | 5 | 76280 | -12.2060 | 66949 | -12.0644 | -0.14166 |
| 22.11.2012 | TYC 1794-441-1 | 4480 | 9.66 | -10.52998 | 1.119349 | -10.45599 | 15219 | 60 | 913157 | -14.9014 | 798877 | -14.7562 | -0.14516 |
| 22.11.2012 | BD+42 643 | 4504 | 9.67 | -10.51996 | 1.070956 | -10.47597 | 15502 | 5 | 77510 | -12.2234 | 63608 | -12.0088 | -0.21461 |
| 22.11.2012 | BD+42 643 | 4502 | 9.67 | -10.51996 | 1.069593 | -10.47681 | 15514 | 2 | 31028 | -11.2294 | 25778 | -11.0281 | -0.20126 |
| 21.12.2012 | TYC 1791-4-1 | 4447 | 9.77 | -10.41973 | 1.114904 | -10.34849 | 13785 | 2 | 27569 | -11.1011 | 24245 | -10.9616 | -0.13951 |
| 21.12.2012 | TYC 1791-4-1 | 4448 | 9.77 | -10.41973 | 1.115812 | -10.34793 | 13777 | 5 | 68887 | -12.0954 | 58479 | -11.9175 | -0.17785 |
| 21.12.2012 | TYC 1791-4-1 | 4453 | 9.77 | -10.41973 | 1.119328 | -10.34575 | 13750 | 60 | 824992 | -14.7911 | 696095 | -14.6067 | -0.18445 |
| 30.4.2013 | BD+52 1722 | 10862 | 9.97 | -10.21927 | 1.030581 | -10.20031 | 12026 | 60 | 721564 | -14.6457 | 608704 | -14.4610 | -0.18467 |
| 30.4.2013 | BD+52 1722 | 10904 | 9.97 | -10.21927 | 1.099647 | -10.15749 | 11561 | 60 | 693660 | -14.6029 | 571022 | -14.3916 | -0.21123 |
| 30.4.2013 | BD+52 1722 | 10961 | 9.97 | -10.21927 | 1.223087 | -10.08096 | 10774 | 60 | 646448 | -14.5263 | 540977 | -14.3329 | -0.19339 |
| 3.6.2013 | BD+52 1722 | 12011 | 9.97 | -10.21927 | 1.035330 | -10.19736 | 11993 | 120 | 1439219 | -15.3953 | 1422000 | -15.3822 | -0.01307 |
| 4.6.2013 | BD+52 1722 | 12021 | 9.97 | -10.21927 | 1.080219 | -10.16953 | 11690 | 120 | 1402796 | -15.3675 | 1419000 | -15.3800 | 0.01247 |
| 4.6.2013 | BD+52 1722 | 12031 | 9.97 | -10.21927 | 1.115338 | -10.14776 | 11458 | 120 | 1374944 | -15.3457 | 1409000 | -15.3723 | 0.02656 |
| 4.6.2013 | BD+52 1722 | 12041 | 9.97 | -10.21927 | 1.158752 | -10.12084 | 11177 | 120 | 1341276 | -15.3188 | 1391000 | -15.3583 | 0.03952 |
| 4.6.2013 | BD+52 1722 | 12045 | 9.97 | -10.21927 | 1.178182 | -10.10880 | 11054 | 120 | 1326477 | -15.3067 | 1367000 | -15.3394 | 0.03267 |
| 4.6.2013 | BD+52 1722 | 12050 | 9.97 | -10.21927 | 1.205397 | -10.09192 | 10884 | 120 | 1306022 | -15.2899 | 1410000 | -15.3730 | 0.08317 |
| 6.9.2013 | BD+52 1722 | 15140 | 9.97 | -10.21927 | 1.521363 | -9.89602 | 9087 | 60 | 545206 | -14.3414 | 572188 | -14.3938 | 0.05244 |
| 6.9.2013 | BD+52 1722 | 15169 | 9.97 | -10.21927 | 1.714656 | -9.77618 | 8137 | 60 | 488230 | -14.2216 | 476755 | -14.1957 | -0.02582 |
| 9.9.2013 | BD+52 1722 | 15627 | 9.97 | -10.21927 | 1.523218 | -9.89487 | 9077 | 60 | 544629 | -14.3403 | 627151 | -14.4934 | 0.15318 |
| 1.12.2012 | BD+50 615 | 5000 | 10.08 | -10.10902 | 1.035475 | -10.08702 | 10834 | 5 | 54172 | -11.8344 | 56006 | -11.8706 | 0.03614 |
| 1.12.2012 | TYC 3308-1034-1 | 5000 | 10.11 | -10.07895 | 1.035475 | -10.05695 | 10539 | 5 | 52693 | -11.8044 | 48432 | -11.7128 | -0.09155 |
| 1.4.2013 | HD292574 | 8753 | 10.537 | -9.65096 | 1.935435 | -9.07099 | 4250 | 60 | 255005 | -13.5164 | 336982 | -13.8190 | 0.30264 |
| 1.4.2013 | HD292561 | 8757 | 10.574 | -9.61388 | 1.934977 | -9.03419 | 4108 | 60 | 246507 | -13.4796 | 316598 | -13.7513 | 0.27170 |
| 5.3.2013 | TYC 4736-1132-1 | 8289 | 10.589 | -9.59885 | 1.758094 | -9.12883 | 4483 | 60 | 268956 | -13.5742 | 283831 | -13.6326 | 0.05844 |
| 21.12.2012 | TYC 1791-188-1 | 4453 | 10.68 | -9.50764 | 1.119328 | -9.43365 | 5936 | 60 | 356133 | -13.8790 | 313078 | -13.7391 | -0.13990 |
| 21.12.2012 | TYC 1791-188-1 | 4451 | 10.68 | -9.50764 | 1.117809 | -9.43459 | 5941 | 30 | 178221 | -13.1274 | 156381 | -12.9855 | -0.14194 |
| 5.3.2013 | TYC 4736-1153-1 | 8289 | 10.7 | -9.48759 | 1.758094 | -9.01757 | 4046 | 60 | 242762 | -13.4629 | 273600 | -13.5928 | 0.12984 |
| 1.12.2012 | TYC 3308-476-1 | 5000 | 10.73 | -9.45752 | 1.035475 | -9.43553 | 5946 | 5 | 29729 | -11.1830 | 24643 | -10.9792 | -0.20372 |
| 5.3.2013 | BD-00 791 | 8289 | 10.9 | -9.28713 | 1.758094 | -8.81711 | 3364 | 60 | 201835 | -13.2625 | 222902 | -13.3703 | 0.10780 |
| 5.3.2013 | TYC 4736-1196-1 | 8289 | 10.9 | -9.28713 | 1.758094 | -8.81711 | 3364 | 60 | 201835 | -13.2625 | 188898 | -13.1906 | -0.07192 |
| 5.3.2013 | TYC 4736-1027-1 | 8289 | 11.2 | -8.98644 | 1.758094 | -8.51642 | 2550 | 60 | 153010 | -12.9618 | 210874 | -13.3101 | 0.34826 |
| 5.3.2013 | TYC 4736-1080-1 | 8289 | 11.3 | -8.88621 | 1.758094 | -8.41619 | 2325 | 60 | 139517 | -12.8616 | 188191 | -13.1865 | 0.32493 |
| 7.5.2013 | TYC 3455-842-1 | 11593 | 11.42 | -8.76593 | 1.181820 | -8.65321 | 2893 | 240 | 694214 | -14.6037 | 574323 | -14.3979 | -0.20584 |
| 29.10.2013 | TYC 4504-1564-1 | 17489 | 11.44 | -8.74589 | 1.154927 | -8.64983 | 2884 | 300 | 865076 | -14.8426 | 905229 | -14.8919 | 0.04926 |
| 29.10.2013 | TYC 4504-1050-1 | 17489 | 11.51 | -8.67573 | 1.154927 | -8.57967 | 2703 | 300 | 810943 | -14.7725 | 796425 | -14.7529 | -0.01961 |
| 29.10.2013 | TYC 4504-860-1 | 17489 | 11.57 | -8.61559 | 1.154927 | -8.51953 | 2557 | 300 | 767246 | -14.7123 | 784715 | -14.7368 | 0.02444 |
| 30.4.2013 | TYC 3469-516-1 | 10862 | 11.61 | -8.57550 | 1.030581 | -8.55654 | 2646 | 60 | 158769 | -13.0019 | 167500 | -13.0600 | 0.05812 |
| 30.4.2013 | TYC 3469-516-1 | 10904 | 11.61 | -8.57550 | 1.099647 | -8.51372 | 2544 | 60 | 152629 | -12.9591 | 156991 | -12.9897 | 0.03059 |
| 30.4.2013 | TYC 3469-516-1 | 10961 | 11.61 | -8.57550 | 1.223087 | -8.43718 | 2371 | 60 | 142241 | -12.8826 | 149415 | -12.9360 | 0.05342 |
| 3.6.2013 | TYC 3469-516-1 | 12011 | 11.61 | -8.57550 | 1.035330 | -8.55359 | 2639 | 120 | 316678 | -13.7515 | 393518 | -13.9874 | 0.23587 |
| 4.6.2013 | TYC 3469-516-1 | 12021 | 11.61 | -8.57550 | 1.080219 | -8.52576 | 2572 | 120 | 308664 | -13.7237 | 391964 | -13.9831 | 0.25940 |
| 4.6.2013 | TYC 3469-516-1 | 12031 | 11.61 | -8.57550 | 1.115338 | -8.50399 | 2521 | 120 | 302535 | -13.7019 | 391490 | -13.9818 | 0.27986 |
| 4.6.2013 | TYC 3469-516-1 | 12041 | 11.61 | -8.57550 | 1.158752 | -8.47707 | 2459 | 120 | 295127 | -13.6750 | 385447 | -13.9649 | 0.28989 |
| 4.6.2013 | TYC 3469-516-1 | 12045 | 11.61 | -8.57550 | 1.178182 | -8.46502 | 2432 | 120 | 291871 | -13.6630 | 380352 | -13.9505 | 0.28749 |
| 4.6.2013 | TYC 3469-516-1 | 12050 | 11.61 | -8.57550 | 1.205397 | -8.44815 | 2395 | 120 | 287370 | -13.6461 | 384634 | -13.9626 | 0.31652 |
| 6.9.2013 | TYC 3469-516-1 | 15140 | 11.61 | -8.57550 | 1.521363 | -8.25225 | 1999 | 60 | 119964 | -12.6976 | 157543 | -12.9935 | 0.29587 |
| 6.9.2013 | TYC 3469-516-1 | 15169 | 11.61 | -8.57550 | 1.714656 | -8.13241 | 1790 | 60 | 107427 | -12.5778 | 128524 | -12.7725 | 0.19467 |
| 9.9.2013 | TYC 3469-516-1 | 15627 | 11.61 | -8.57550 | 1.523218 | -8.25110 | 1997 | 60 | 119837 | -12.6965 | 173615 | -13.0990 | 0.40249 |
| 1.2.2012 | TYC 4039-481-1 | 2732 | 11.81 | -8.37504 | 1.407619 | -8.12231 | 1774 | 300 | 532165 | -14.3151 | 552575 | -14.3560 | 0.04086 |
| 21.2.2014 | TYC 4383-593-1 | 20032 | 12.1 | -8.08437 | 1.154416 | -7.98863 | 1568 | 240 | 376413 | -13.9392 | 387773 | -13.9714 | 0.03228 |
| 21.2.2014 | GPM149.442737+69.731284 | 20032 | 12.3 | -7.88391 | 1.154416 | -7.78817 | 1304 | 240 | 312954 | -13.7387 | 265171 | -13.5588 | -0.17989 |
| 1.2.2012 | TYC 4039-650-1 | 2732 | 12.33 | -7.85384 | 1.407619 | -7.60112 | 1098 | 300 | 329282 | -13.7939 | 463324 | -14.1647 | 0.37079 |
| 2.2.2013 | TYC 4039-650-1 | 2733 | 12.33 | -7.85384 | 1.287545 | -7.67556 | 1176 | 900 | 1057957 | -15.0612 | 1347000 | -15.3234 | 0.26225 |
| 3.2.2012 | TYC 4039-650-1 | 2734 | 12.33 | -7.85384 | 1.069259 | -7.81090 | 1332 | 900 | 1198402 | -15.1965 | 1338000 | -15.3161 | 0.11963 |
| 18.2.2012 | TYC 4039-650-1 | 2735 | 12.33 | -7.85384 | 1.459021 | -7.56925 | 1066 | 900 | 959272 | -14.9549 | 1322000 | -15.3031 | 0.34822 |
| 19.2.2012 | TYC 4039-650-1 | 2736 | 12.33 | -7.85384 | 1.165068 | -7.75150 | 1261 | 900 | 1134598 | -15.1371 | 1385000 | -15.3536 | 0.21652 |
| 8.3.2012 | TYC 4039-650-1 | 2737 | 12.33 | -7.85384 | 1.516133 | -7.53384 | 1032 | 900 | 928491 | -14.9194 | 1166000 | -15.1667 | 0.24730 |
| 11.3.2014 | 2MASS J12181678+1424176 | 20656 | 12.6 | -7.58322 | 1.674077 | -7.16529 | 735 | 240 | 176331 | -13.1158 | 170178 | -13.0773 | -0.03856 |
| 11.3.2014 | 2MASS J12181678+1424176 | 20657 | 12.6 | -7.58322 | 1.647223 | -7.18194 | 746 | 240 | 179056 | -13.1325 | 171815 | -13.0877 | -0.04482 |
| 11.3.2014 | 2MASS J12181647+1419292 | 20656 | 12.7 | -7.48299 | 1.674077 | -7.06506 | 670 | 240 | 160782 | -13.0156 | 161615 | -13.0212 | 0.00561 |
| 11.3.2014 | 2MASS J12181647+1419292 | 20657 | 12.7 | -7.48299 | 1.647223 | -7.08171 | 680 | 240 | 163266 | -13.0322 | 162181 | -13.0250 | -0.00724 |
| 11.3.2014 | 2MASS J12180786+1432113 | 20657 | 12.8 | -7.38276 | 1.647223 | -6.98148 | 620 | 240 | 148869 | -12.9320 | 151932 | -12.9541 | 0.02211 |
| 21.2.2014 | GPM148.725971+69.615345 | 20032 | 13.2 | -6.98184 | 1.154416 | -6.88610 | 568 | 240 | 136349 | -12.8366 | 114016 | -12.6424 | -0.19422 |
| 11.3.2014 | 2MASS J12190080+1428397 | 20656 | 13.4 | -6.78138 | 1.674077 | -6.36345 | 351 | 240 | 84254 | -12.3140 | 68013 | -12.0815 | -0.23250 |
| 11.3.2014 | 2MASS J12190080+1428397 | 20657 | 13.4 | -6.78138 | 1.647223 | -6.38010 | 356 | 240 | 85556 | -12.3306 | 67161 | -12.0678 | -0.26284 |
| 11.3.2014 | 2MASS J12183329+1429325 | 20656 | 13.5 | -6.68115 | 1.674077 | -6.26322 | 320 | 240 | 76825 | -12.2138 | 70935 | -12.1272 | -0.08660 |
| 11.3.2014 | 2MASS J12183329+1429325 | 20657 | 13.5 | -6.68115 | 1.647223 | -6.27987 | 325 | 240 | 78012 | -12.2304 | 69588 | -12.1063 | -0.12406 |

## Appendix F

| Date | Star | Image | Ref Mag (m) | Predicted $m'_{t=1s,X=1.0}$ Eq (3.2.6.1) | X | Predicted $m'_{t=1s,X=X}$ Eq (3.2.6.2) | Predicted $(N_{target})_{t=1s,X=X}$ Eq (2.2.8.8) | $t_{exp}$ | Predicted $(N_{target})_{t=t_{exp},X=X}$ Eq (2.2.7.4) | Predicted $m'_{t=texp,X=X}$ Eq (2.2.8.10) | Measured $(N_{target})_{t=t_{exp},X=X}$ | Measured $m'_{t=texp,X=X}$ Eq (2.2.8.11) | Δm' Eq (2.2.8.12) |
|---|---|---|---|---|---|---|---|---|---|---|---|---|---|
| 21.2.2014 | 2MASS J09540368+6941167 | 20032 | 13.5 | -6.68115 | 1.154416 | -6.58541 | 431 | 240 | 103366 | -12.5359 | 74766 | -12.1843 | -0.35168 |
| 11.3.2014 | 2MASS J12190855+1421235 | 20656 | 13.5 | -6.68115 | 1.674077 | -6.26322 | 320 | 240 | 76825 | -12.2138 | 48739 | -11.7197 | -0.49406 |
| 11.3.2014 | 2MASS J12190855+1421235 | 20657 | 13.5 | -6.68115 | 1.647223 | -6.27987 | 325 | 240 | 78012 | -12.2304 | 49129 | -11.7283 | -0.50206 |
| 21.2.2014 | 2MASS J09545340+6939298 | 20032 | 14 | -6.18000 | 1.154416 | -6.08426 | 271 | 240 | 65150 | -12.0348 | 51535 | -11.7803 | -0.25453 |
| 11.3.2014 | 2MASS J12184019+1420260 | 20656 | 14.3 | -5.87931 | 1.674077 | -5.46138 | 153 | 240 | 36708 | -11.4119 | 31974 | -11.2620 | -0.14992 |
| 11.3.2014 | 2MASS J12184019+1420260 | 20657 | 14.3 | -5.87931 | 1.647223 | -5.47803 | 155 | 240 | 37276 | -11.4286 | 31128 | -11.2329 | -0.19568 |
| 30.4.2013 | 2MASS J13365496+5155247 | 10862 | 15.287 | -4.89004 | 1.030581 | -4.87108 | 89 | 60 | 5328 | -9.3165 | 4460 | -9.1233 | -0.19312 |
| 30.4.2013 | 2MASS J13365496+5155247 | 10904 | 15.287 | -4.89004 | 1.099647 | -4.82826 | 85 | 60 | 5122 | -9.2736 | 3900 | -8.9777 | -0.29598 |
| 3.6.2013 | 2MASS J13365496+5155247 | 12011 | 15.287 | -4.89004 | 1.035330 | -4.86814 | 89 | 120 | 10628 | -10.0661 | 9939.7 | -9.9934 | -0.07266 |
| 3.6.2013 | 2MASS J13365496+5155247 | 12021 | 15.287 | -4.89004 | 1.080219 | -4.84030 | 86 | 120 | 10359 | -10.0383 | 10783 | -10.0818 | 0.04359 |
| 3.6.2013 | 2MASS J13365496+5155247 | 12031 | 15.287 | -4.89004 | 1.115338 | -4.81853 | 85 | 120 | 10153 | -10.0165 | 10156 | -10.0168 | 0.00032 |
| 3.6.2013 | 2MASS J13365496+5155247 | 12041 | 15.287 | -4.89004 | 1.158752 | -4.79161 | 83 | 120 | 9904 | -9.9896 | 10211 | -10.0227 | 0.03310 |
| 4.6.2013 | 2MASS J13365496+5155247 | 12045 | 15.287 | -4.89004 | 1.178182 | -4.77957 | 82 | 120 | 9795 | -9.9775 | 10278 | -10.0298 | 0.05225 |
| 4.6.2013 | 2MASS J13365496+5155247 | 12050 | 15.287 | -4.89004 | 1.205397 | -4.76269 | 80 | 120 | 9644 | -9.9606 | 10985 | -10.1020 | 0.14135 |
| 3.6.2013 | [HH95]UX UMa-2 | 12011 | 15.46 | -4.71664 | 1.035330 | -4.69474 | 75 | 120 | 9059 | -9.8927 | 8868 | -9.8696 | -0.02313 |
| 3.6.2013 | [HH95]UX UMa-2 | 12021 | 15.46 | -4.71664 | 1.080219 | -4.66691 | 74 | 120 | 8830 | -9.8649 | 9169.7 | -9.9059 | 0.04103 |
| 3.6.2013 | [HH95]UX UMa-2 | 12041 | 15.46 | -4.71664 | 1.158752 | -4.61822 | 70 | 120 | 8442 | -9.8162 | 8378.2 | -9.8079 | -0.00829 |
| 3.6.2013 | [HH95]UX UMa-2 | 12031 | 15.46 | -4.71664 | 1.115338 | -4.64513 | 72 | 120 | 8654 | -9.8431 | 8521.3 | -9.8263 | -0.01682 |
| 4.6.2013 | [HH95]UX UMa-2 | 12050 | 15.46 | -4.71664 | 1.205397 | -4.58930 | 69 | 120 | 8221 | -9.7872 | 9358.1 | -9.9280 | 0.14072 |
| 21.2.2014 | 2MASS J09573616+6941183 | 20032 | 15.5 | -4.67655 | 1.154416 | -4.58081 | 68 | 240 | 16313 | -10.5313 | 20306 | -10.7691 | 0.23772 |

**Table 13 Verification by Comparison Between Predicted and Measured Target Counts Using Reference Images**

Figure 23 presents a plot of both measured and predicted values of $m'$ against catalogue magnitude to show the range of conditions covered. The predicted and measured instrument magnitudes are shown to be similar for a wide range of catalogue magnitudes, $t_{exp}$ and X.

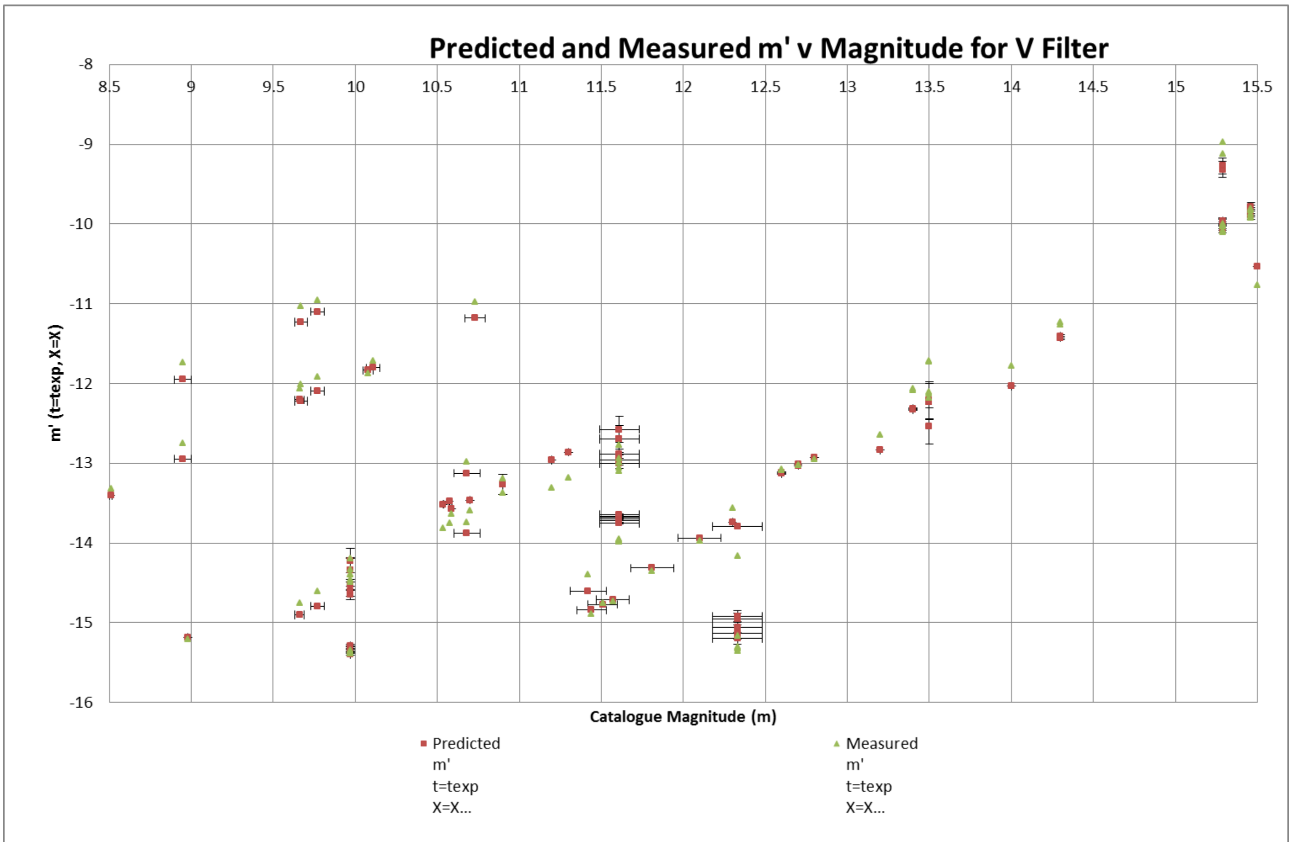


**Figure 23 Predicted and Measured ($m'_{t=t_{exp},X=X}$) V Catalogue Magnitude (m)**

Figure 24 presents a plot of $\Delta m'$ against catalogue magnitude. The distribution is fairly central about the x axis. As would be expected, there is a wider spread as the magnitude increases (ie the signal strength reduces). The average and standard deviation of the values of $\Delta m'$ presented in Table 13 and Figure 24 were calculated by Excel as 0.00045 and 0.195 respectively. These values define the expected variation[25] between the predicted and expected instrument magnitudes due to factors such as the limitations of the formulation, the variation in the sky condition, catalogue measurement errors and the precision of the differential photometry process.

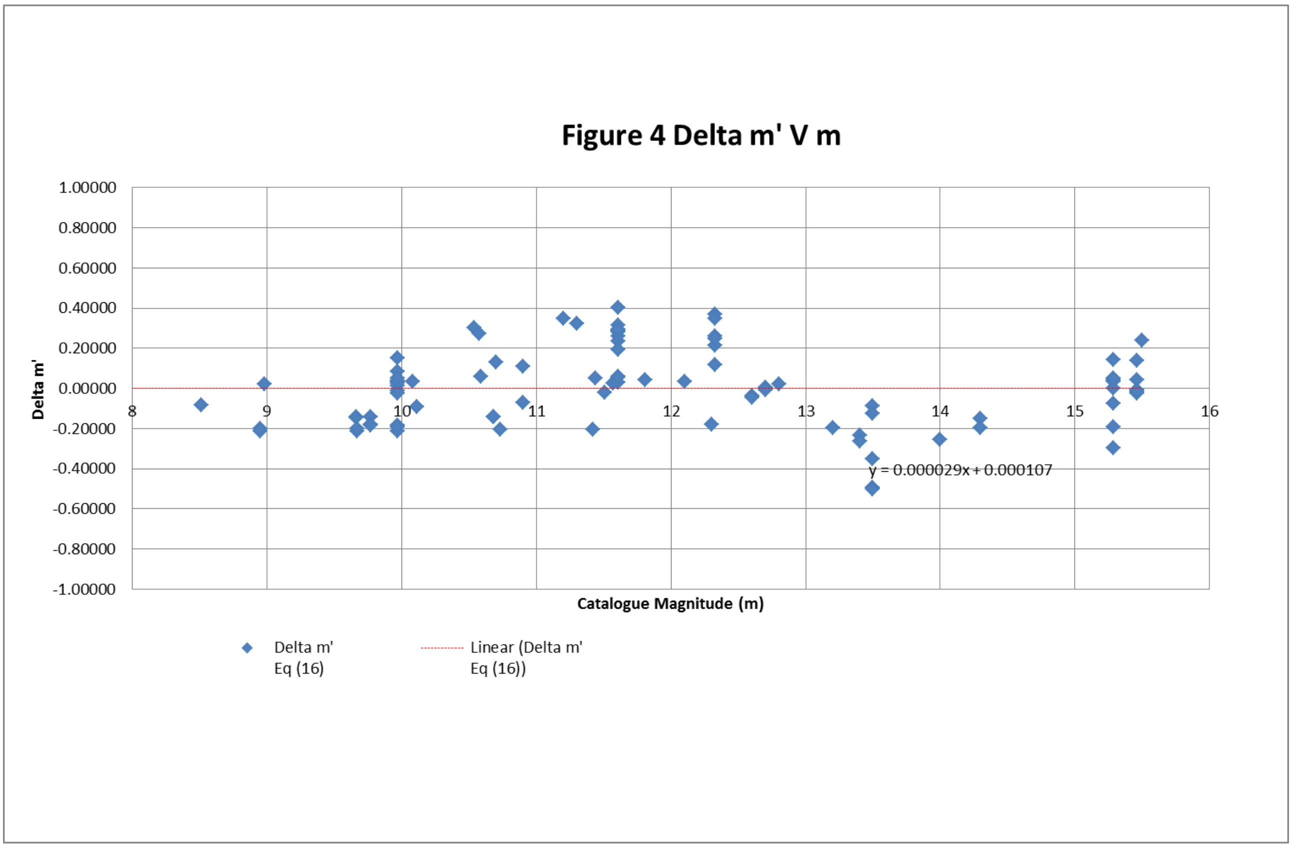


**Figure 24 Magnitude Error ($\Delta m'$) V Catalogue Magnitude (m)**

It is consequently considered that the verification exercise has demonstrated that the formulation functions correctly using catalogue magnitude m, $t_{exp}$ and X to predict values for the measured values of magnitude (m'). The standard deviation (0.20) for the term $\Delta m'$ provides an indication of the expected variation between the expected and measured results over a wide range of catalogue magnitudes, air mass and exposure time. The mean value of 0.0005 indicates that the errors are reasonably evenly spread about the X axis.

[25] A measure of the goodness of fit (for the predicted values of m' against the measured values of m') has been obtained using the $x^2$ test and Excel gave a value for P=1.0. ie the observed values are from the same data set as p>0.05.

## Appendix F

# Validation

Validation of the formulation has been achieved by a similar process employed in the verification process, but instead using different images from the Bayfordbury Observatory archive (see Appendix C) for a new range of stars that had **not** previously been used to derive the parameters for the equations. Good quality images were carefully selected to give a wide range of non-variable star magnitudes, exposure times and air masses to exercise the formulation over the expected full operational range of the APT telescope. The equations defined in Section 3.2.6 were supplied with m, $t_{exp}$ and X for each reference star in the new images to generate predicted values for the instrumental magnitude $[\mathrm{m'}_{\mathrm{t=t_{exp},X=X}}]_{\mathrm{predicted}}$ which were then compared with the measured magnitude values of $[m'_{t=t_{exp},X=X}]_{measured}$ obtained from these images using APT.

A summary of the results obtained are presented as Table 14. These results are equivalent to the results presented as Table 13 but instead with the validation data. The column entitled "star" records the names of the target stars that are all different to those used previously (see Table 12). The mean and standard deviation of $\Delta\mathrm{m'}$ for the data presented in Table 14 are 0.0687 and 0.136 respectively. The Excel $\chi^2$ test gave a p value of 1.0 confirming that the measured values are consistent with the predicted values.

| Date | Image | Star | Ref Mag (m) | Predicted $\mathrm{m'}_{t=1s,X=1.0}$ Eq (2.2.6.1) | X | Predicted $m'_{t=1s,X=X}$ Eq (2.2.6.2) | Predicted $(N_{target})_{t=1s,X=X}$ Eq (2.2.8.8) | $t_{exp}$ | Predicted $(\mathrm{N_{target}})_{t=t_{exp},X=X}$ Eq (2.2.7.4) | Predicted $m'_{t=texp,X=X}$ Eq (2.2.8.10) | Measured $(N_{target})_{t=t_{exp},X=}$ | Measured $m'_{t=texp,X=X}$ Eq (2.2.8.11) | Δm' Eq (2.2.8.12) |
|---|---|---|---|---|---|---|---|---|---|---|---|---|---|
| 20.8.2012 | 2185 | *phi Cas | 4.98 | -15.22075 | 1.21601 | -15.0868 | 1083249 | 1 | 1083249 | -15.0868 | 966235 | -14.9627 | -0.1241 |
| 20.8.2012 | 2186 | *phi Cas | 4.98 | -15.22075 | 1.24418 | -15.0694 | 1065962 | 1 | 1065962 | -15.0694 | 1062000 | -15.0653 | -0.0040 |
| 20.8.2012 | 2189 | *phi Cas | 4.98 | -15.22075 | 1.21601 | -15.0868 | 1083249 | 1 | 1083249 | -15.0868 | 966235 | -14.9627 | -0.1241 |
| 1.12.2012 | 4944 | *g Per | 5.04 | -15.16061 | 1.04760 | -15.1311 | 1128333 | 0.1 | 112833 | -12.6311 | 125350 | -12.7453 | 0.1142 |
| 1.12.2012 | 4945 | *g Per | 5.04 | -15.16061 | 1.04721 | -15.1313 | 1128587 | 0.5 | 564293 | -14.3788 | 549702 | -14.3503 | -0.0284 |
| 26.7.2012 | 1961 | HR 9013 | 5.048 | -15.15259 | 1.34526 | -14.9385 | 944955 | 1 | 944955 | -14.9385 | 909156 | -14.8966 | -0.0419 |
| 26.7.2012 | 1962 | HR 9013 | 5.048 | -15.15259 | 1.24028 | -15.0036 | 1003336 | 1 | 1003336 | -15.0036 | 912530 | -14.9006 | -0.1030 |
| 1.12.2012 | 5074 | *24 Tau | 6.28 | -13.91776 | 1.18097 | -13.8056 | 332829 | 1 | 332829 | -13.8056 | 322118 | -13.7700 | -0.0355 |
| 1.12.2012 | 5075 | HD 23463 | 7.569 | -12.62579 | 1.17982 | -12.5143 | 101326 | 5 | 506629 | -14.2617 | 436010 | -14.0987 | -0.1630 |
| 5.11.2012 | 4005 | HD 14827 | 7.63 | -12.56465 | 1.31231 | -12.3710 | 88799 | 2 | 177598 | -13.1236 | 191863 | -13.2075 | 0.0839 |
| 1.12.2012 | 5074 | HD 23479 | 7.96 | -12.23389 | 1.18097 | -12.1217 | 70579 | 1 | 70579 | -12.1217 | 70075 | -12.1139 | -0.0078 |
| 1.12.2012 | 5075 | HD 23479 | 7.96 | -12.23389 | 1.17982 | -12.1224 | 70625 | 5 | 353127 | -13.8698 | 345915 | -13.8474 | -0.0224 |
| 1.11.2012 | 4941 | HD 15397 | 7.99 | -12.20382 | 1.05302 | -12.1709 | 73855 | 2 | 147710 | -12.9235 | 135335 | -12.8285 | -0.0950 |
| 1.12.2012 | 4971 | HD 15397 | 7.99 | -12.20382 | 1.05181 | -12.1717 | 73906 | 2 | 147812 | -12.9243 | 136542 | -12.8382 | -0.0861 |
| 1.12.2012 | 4972 | HD 15397 | 7.99 | -12.20382 | 1.05181 | -12.1717 | 73906 | 5 | 369530 | -13.9191 | 343663 | -13.8403 | -0.0788 |
| 9.10.2013 | 16976 | HD 163128 | 8.6 | -11.59242 | 1.33074 | -11.3874 | 35888 | 30 | 1076631 | -15.0802 | 1278000 | -15.2663 | 0.1862 |
| 9.10.2013 | 16978 | HD 163128 | 8.6 | -11.59242 | 1.33558 | -11.3844 | 35789 | 30 | 1073656 | -15.0772 | 1275000 | -15.2638 | 0.1866 |
| 9.10.2013 | 16985 | HD 163128 | 8.6 | -11.59242 | 1.36074 | -11.3688 | 35278 | 30 | 1058340 | -15.0616 | 1283000 | -15.2706 | 0.2090 |
| 1.4.2013 | 8842 | HD38978 | 8.61 | -11.58240 | 1.60750 | -11.2057 | 30360 | 4 | 121439 | -12.7109 | 129477 | -12.7805 | 0.0696 |
| 1.4.2013 | 8839 | HD38978 | 8.61 | -11.58240 | 1.60076 | -11.2099 | 30477 | 1 | 30477 | -11.2099 | 31807 | -11.2563 | 0.0464 |
| 21.11.2012 | 4380 | HD 15325 | 8.63 | -11.56235 | 1.00516 | -11.5592 | 42040 | 5 | 210199 | -13.3066 | 197454 | -13.2387 | -0.0679 |
| 6.2.2013 | 7293 | HD31001 | 8.65 | -11.54231 | 1.42475 | -11.2790 | 32478 | 15 | 487165 | -14.2192 | 554841 | -14.3604 | 0.1412 |
| 6.2.2013 | 7292 | HD31001 | 8.65 | -11.54231 | 1.42054 | -11.2816 | 32556 | 1 | 32556 | -11.2816 | 37379 | -11.4316 | 0.1500 |
| 1.4.2013 | 8842 | HD39136 | 8.77 | -11.42203 | 1.60750 | -11.0454 | 26191 | 4 | 104764 | -12.5505 | 111764 | -12.6208 | 0.0702 |
| 1.4.2013 | 8839 | HD39136 | 8.77 | -11.42203 | 1.60076 | -11.0496 | 26292 | 1 | 26292 | -11.0496 | 27455 | -11.0966 | 0.0470 |
| 9.10.2013 | 16976 | BD+37 2968 | 8.86 | -11.33182 | 1.33074 | -11.1268 | 28230 | 30 | 846891 | -14.8196 | 1007000 | -15.0076 | 0.1880 |
| 9.10.2013 | 16978 | BD+37 2968 | 8.86 | -11.33182 | 1.33558 | -11.1238 | 28152 | 30 | 844551 | -14.8166 | 1001000 | -15.0011 | 0.1845 |
| 9.10.2013 | 16985 | BD+37 2968 | 8.86 | -11.33182 | 1.36074 | -11.1082 | 27750 | 30 | 832504 | -14.8010 | 1007000 | -15.0076 | 0.2066 |
| 5.3.2013 | 8289 | BD-00 789 | 8.98 | -11.21155 | 1.75809 | -10.7415 | 19798 | 60 | 1187852 | -15.1869 | 1212000 | -15.2088 | 0.0219 |
| 2.12.2012 | 5246 | HD113562 | 9.28 | -10.91086 | 1.27515 | -10.7403 | 19775 | 10 | 197745 | -13.2403 | 194799 | -13.2240 | -0.0163 |
| 1.12.2012 | 4944 | HD 232582 | 9.28 | -10.91086 | 1.04760 | -10.8813 | 22518 | 0.1 | 2252 | -8.3813 | 2629.2 | -8.5496 | 0.1682 |
| 1.12.2012 | 4945 | HD 232582 | 9.28 | -10.91086 | 1.04721 | -10.8816 | 22523 | 0.5 | 11262 | -10.1290 | 10828 | -10.0864 | -0.0426 |
| 1.12.2012 | 4925 | BD +57 249 | 9.96 | -10.22929 | 1.03076 | -10.2102 | 12136 | 1 | 12136 | -10.2102 | 12100 | -10.2070 | -0.0033 |
| 20.8.2012 | 2185 | BD +57 249 | 9.96 | -10.22929 | 1.21601 | -10.0954 | 10918 | 1 | 10918 | -10.0954 | 10142 | -10.0153 | -0.0801 |
| 20.8.2012 | 2186 | BD +57 249 | 9.96 | -10.22929 | 1.24418 | -10.0779 | 10744 | 1 | 10744 | -10.0779 | 13209 | -10.3022 | 0.2243 |
| 20.8.2012 | 2189 | BD +57 249 | 9.96 | -10.22929 | 1.21601 | -10.0954 | 10918 | 1 | 10918 | -10.0954 | 10142 | -10.0153 | -0.0801 |
| 20.8.2012 | 2187 | BD +57 249 | 9.96 | -10.22929 | 1.21193 | -10.0979 | 10944 | 2 | 21887 | -10.8505 | 20892 | -10.8000 | -0.0505 |
| 26.7.2012 | 1961 | TYC 4479-720-1 | 10.23 | -9.95867 | 1.34526 | -9.7446 | 7904 | 1 | 7904 | -9.7446 | 7090.8 | -9.6267 | -0.1179 |
| 26.7.2012 | 1962 | TYC 4479-720-1 | 10.23 | -9.95867 | 1.24028 | -9.8097 | 8392 | 1 | 8392 | -9.8097 | 6676.1 | -9.5613 | -0.2484 |
| 12.7.2013 | 13427 | HD 345448 | 10.29 | -9.89853 | 1.15206 | -9.8043 | 8350 | 300 | 2505091 | -15.9971 | 2306000 | -15.9071 | -0.0899 |
| 6.2.2013 | 7293 | HD283949 | 10.33 | -9.85844 | 1.42475 | -9.5951 | 6887 | 15 | 103307 | -12.5353 | 99587 | -12.4955 | -0.0398 |
| 6.2.2013 | 7292 | HD283949 | 10.33 | -9.85844 | 1.42054 | -9.5977 | 6904 | 1 | 6904 | -9.5977 | 6575 | -9.5447 | -0.0530 |
| 12.7.2013 | 13427 | HD 345450 | 10.34 | -9.84842 | 1.15206 | -9.7541 | 7974 | 300 | 2392090 | -15.9469 | 2414000 | -15.9568 | 0.0099 |
| 1.12.2012 | 4971 | TYC 3299-970-1 | 10.34 | -9.84842 | 1.05181 | -9.8163 | 8443 | 2 | 16887 | -10.5689 | 16998 | -10.5760 | 0.0071 |
| 1.12.2012 | 4972 | TYC 3299-970-1 | 10.34 | -9.84842 | 1.05181 | -9.8163 | 8443 | 5 | 42217 | -11.5637 | 43260 | -11.5902 | 0.0265 |
| 21.11.2012 | 4380 | TYC 3695-1932-1 | 10.52 | -9.66800 | 1.00516 | -9.6648 | 7344 | 5 | 36719 | -11.4122 | 33727 | -11.3199 | -0.0923 |
| 2.12.2012 | 5246 | BD+28 2177 | 10.71 | -9.47757 | 1.27515 | -9.3070 | 5282 | 10 | 52819 | -11.8070 | 53372 | -11.8183 | 0.0113 |
| 12.7.2013 | 13427 | HD 345451 | 10.75 | -9.43748 | 1.15206 | -9.3432 | 5461 | 300 | 1638326 | -15.5360 | 1851000 | -15.6685 | 0.1325 |
| 8.3.2012 | 2207 | TYC 2667-338-1 | 10.8 | -9.38736 | 1.34249 | -9.1750 | 4677 | 300 | 1403230 | -15.3678 | 1199000 | -15.1970 | -0.1708 |
| 8.3.2012 | 2208 | TYC 2667-338-1 | 10.8 | -9.38736 | 1.32336 | -9.1869 | 4729 | 300 | 1418640 | -15.3797 | 1216000 | -15.2123 | -0.1673 |
| 26.7.2012 | 1961 | TYC 4479-781-1 | 10.8 | -9.38736 | 1.34526 | -9.1733 | 4670 | 1 | 4670 | -9.1733 | 5357.8 | -9.3225 | 0.1492 |
| 26.7.2012 | 1962 | TYC 4479-781-1 | 10.8 | -9.38736 | 1.24028 | -9.2384 | 4959 | 1 | 4959 | -9.2384 | 5320.1 | -9.3148 | 0.0764 |
| 26.7.2012 | 1961 | TYC 4479-1038-1 | 10.85 | -9.33725 | 1.34526 | -9.1232 | 4459 | 1 | 4459 | -9.1232 | 4427.5 | -9.1154 | -0.0078 |
| 26.7.2012 | 1962 | TYC 4479-1038-1 | 10.85 | -9.33725 | 1.24028 | -9.1883 | 4735 | 1 | 4735 | -9.1883 | 4717.2 | -9.1842 | -0.0041 |
| 10.11.2012 | 4166 | HD282625 | 10.95 | -9.23702 | 1.55546 | -8.8926 | 3606 | 30 | 108187 | -12.5854 | 150660 | -12.9450 | 0.3596 |
| 11.11.2012 | 4189 | HD282625 | 10.95 | -9.23702 | 1.11478 | -9.1659 | 4638 | 30 | 139143 | -12.8587 | 162394 | -13.0264 | 0.1678 |
| 1.1.2013 | 6545 | HD282625 | 10.95 | -9.23702 | 1.11566 | -9.1653 | 4636 | 30 | 139073 | -12.8581 | 166994 | -13.0568 | 0.1986 |
| 4.2.2013 | 7117 | HD282625 | 10.95 | -9.23702 | 1.12156 | -9.1616 | 4620 | 30 | 138605 | -12.8545 | 143218 | -12.8900 | 0.0355 |

| Date | Image | Star | Ref Mag (m) | Predicted $m'_{t=1s,X=1.0}$ Eq (2.2.6.1) | X | Predicted $m'_{t=1s,X=X}$ Eq (2.2.6.2) | Predicted $(N_{target})_{t=1s,X=X}$ Eq (2.2.8.8) | $t_{exp}$ | Predicted $(N_{target})_{t=t_{exp},X=X}$ Eq (2.2.7.4) | Predicted $m'_{t=texp,X=X}$ Eq (2.2.8.10) | Measured $(N_{target})_{t=t_{exp},X=}$ | Measured $m'_{t=texp,X=X}$ Eq (2.2.8.11) | Δm' Eq (2.2.8.12) |
|---|---|---|---|---|---|---|---|---|---|---|---|---|---|
| 3.3.2013 | 8161 | HD282625 | 10.95 | -9.23702 | 1.10995 | -9.1688 | 4651 | 30 | 139527 | -12.8616 | 131788 | -12.7997 | -0.0620 |
| 3.3.2013 | 8174 | HD282625 | 10.95 | -9.23702 | 1.34943 | -9.0204 | 4056 | 30 | 121694 | -12.7132 | 123153 | -12.7261 | 0.0129 |
| 1.4.2013 | 8959 | BD+30 2443 | 10.99 | -9.19692 | 1.11357 | -9.1265 | 4473 | 60 | 268383 | -13.5719 | 241437 | -13.4570 | -0.1149 |
| 1.4.2013 | 8842 | TYC 2409-1268-1 | 11 | -9.18690 | 1.60750 | -8.8102 | 3343 | 4 | 13371 | -10.3154 | 14284 | -10.3871 | 0.0717 |
| 1.4.2013 | 8839 | TYC 2409-1268-1 | 11 | -9.18690 | 1.60076 | -8.8144 | 3356 | 1 | 3356 | -8.8144 | 3626.3 | -8.8987 | 0.0842 |
| 8.3.2012 | 2207 | TYC 2667-746-1 | 11 | -9.18690 | 1.34249 | -8.9746 | 3889 | 300 | 1166661 | -15.1674 | 1265000 | -15.2552 | 0.0879 |
| 8.3.2012 | 2208 | TYC 2667-746-1 | 11 | -9.18690 | 1.32336 | -8.9864 | 3932 | 300 | 1179473 | -15.1792 | 1265000 | -15.2552 | 0.0760 |
| 5.8.2013 | 14141 | TYC 2595-1498-1 | 11.03 | -9.15683 | 1.07799 | -9.1085 | 4399 | 120 | 527926 | -14.3064 | 609241 | -14.4620 | 0.1555 |
| 7.9.2013 | 15370 | TYC 2595-1498-1 | 11.03 | -9.15683 | 1.25739 | -8.9972 | 3971 | 60 | 238259 | -13.4426 | 283359 | -13.6308 | 0.1882 |
| 7.9.2013 | 15400 | TYC 2595-1498-1 | 11.03 | -9.15683 | 1.39947 | -8.9092 | 3662 | 60 | 219693 | -13.3545 | 265149 | -13.5587 | 0.2042 |
| 9.9.2013 | 15657 | TYC 2595-1498-1 | 11.03 | -9.15683 | 1.22104 | -9.0198 | 4054 | 60 | 243258 | -13.4652 | 269162 | -13.5750 | 0.1099 |
| 6.2.2013 | 7293 | HD283951 | 11.06 | -9.12676 | 1.42475 | -8.8634 | 3510 | 15 | 52657 | -11.8036 | 58841 | -11.9242 | 0.1206 |
| 6.2.2013 | 7292 | HD283951 | 11.06 | -9.12676 | 1.42054 | -8.8660 | 3519 | 1 | 3519 | -8.8660 | 3795.7 | -8.9482 | 0.0822 |
| 5.8.2013 | 14141 | TYC 2595-666-1 | 11.07 | -9.11674 | 1.07799 | -9.0684 | 4240 | 120 | 508787 | -14.2663 | 558128 | -14.3668 | 0.1005 |
| 5.8.2013 | 14141 | TYC 2595-725-1 | 11.07 | -9.11674 | 1.07799 | -9.0684 | 4240 | 120 | 508787 | -14.2663 | 671062 | -14.5669 | 0.3006 |
| 7.9.2013 | 15370 | TYC 2595-666-1 | 11.07 | -9.11674 | 1.25739 | -8.9572 | 3827 | 60 | 229622 | -13.4025 | 257303 | -13.5261 | 0.1236 |
| 7.9.2013 | 15370 | TYC 2595-725-1 | 11.07 | -9.11674 | 1.25739 | -8.9572 | 3827 | 60 | 229622 | -13.4025 | 310085 | -13.7287 | 0.3262 |
| 7.9.2013 | 15400 | TYC 2595-666-1 | 11.07 | -9.11674 | 1.39947 | -8.8691 | 3529 | 60 | 211729 | -13.3144 | 240385 | -13.4523 | 0.1378 |
| 7.9.2013 | 15400 | TYC 2595-725-1 | 11.07 | -9.11674 | 1.39947 | -8.8691 | 3529 | 60 | 211729 | -13.3144 | 287253 | -13.6457 | 0.3312 |
| 9.9.2013 | 15657 | TYC 2595-666-1 | 11.07 | -9.11674 | 1.22104 | -8.9797 | 3907 | 60 | 234439 | -13.4251 | 246993 | -13.4817 | 0.0566 |
| 9.9.2013 | 15657 | TYC 2595-725-1 | 11.07 | -9.11674 | 1.22104 | -8.9797 | 3907 | 60 | 234439 | -13.4251 | 296748 | -13.6810 | 0.2559 |
| 1.4.2013 | 8842 | HD248227 | 11.09 | -9.09669 | 1.60750 | -8.7200 | 3076 | 4 | 12305 | -10.2252 | 13682 | -10.3404 | 0.1152 |
| 1.4.2013 | 8839 | HD248227 | 11.09 | -9.09669 | 1.60076 | -8.7242 | 3088 | 1 | 3088 | -8.7242 | 3299.6 | -8.7962 | 0.0719 |
| 8.3.2012 | 2207 | TYC 2667-853-1 | 11.16 | -9.02653 | 1.34249 | -8.8142 | 3355 | 300 | 1006463 | -15.0070 | 1139000 | -15.1413 | 0.1343 |
| 8.3.2012 | 2208 | TYC 2667-853-1 | 11.16 | -9.02653 | 1.32336 | -8.8260 | 3392 | 300 | 1017515 | -15.0189 | 1117000 | -15.1201 | 0.1013 |
| 5.8.2013 | 14141 | TYC 2595-575-1 | 11.2 | -8.98644 | 1.07799 | -8.9381 | 3760 | 120 | 451249 | -14.1360 | 545391 | -14.3418 | 0.2057 |
| 7.9.2013 | 15370 | TYC 2595-575-1 | 11.2 | -8.98644 | 1.25739 | -8.8269 | 3394 | 60 | 203654 | -13.2722 | 253295 | -13.5091 | 0.2368 |
| 7.9.2013 | 15400 | TYC 2595-575-1 | 11.2 | -8.98644 | 1.39947 | -8.7388 | 3130 | 60 | 187785 | -13.1841 | 235507 | -13.4300 | 0.2459 |
| 9.9.2013 | 15657 | TYC 2595-575-1 | 11.2 | -8.98644 | 1.22104 | -8.8494 | 3465 | 60 | 207927 | -13.2948 | 241228 | -13.4561 | 0.1613 |
| 19.4.2012 | 20977 | TYC 878-573-1 | 11.27 | -8.91628 | 1.41353 | -8.6599 | 2910 | 120 | 349250 | -13.8578 | 362592 | -13.8985 | 0.0407 |
| 19.4.2012 | 20978 | TYC 878-573-1 | 11.27 | -8.91628 | 1.40810 | -8.6633 | 2919 | 120 | 350335 | -13.8612 | 366381 | -13.9098 | 0.0486 |
| 19.4.2012 | 20979 | TYC 878-573-1 | 11.27 | -8.91628 | 1.40283 | -8.6665 | 2928 | 120 | 351391 | -13.8645 | 373635 | -13.9311 | 0.0666 |
| 19.4.2012 | 20980 | TYC 878-573-1 | 11.27 | -8.91628 | 1.39771 | -8.6697 | 2937 | 120 | 352420 | -13.8677 | 368254 | -13.9154 | 0.0477 |
| 19.4.2012 | 20981 | TYC 878-573-1 | 11.27 | -8.91628 | 1.39286 | -8.6727 | 2945 | 120 | 353398 | -13.8707 | 373425 | -13.9305 | 0.0598 |
| 1.4.2013 | 8959 | TYC 2005-989-1 | 11.28 | -8.90626 | 1.11357 | -8.8358 | 3422 | 60 | 205347 | -13.2812 | 173471 | -13.0981 | -0.1832 |
| 8.3.2012 | 2207 | TYC 2667-858-1 | 11.33 | -8.85614 | 1.34249 | -8.6438 | 2868 | 300 | 860283 | -14.8366 | 962769 | -14.9588 | 0.1222 |
| 8.3.2012 | 2208 | TYC 2667-858-1 | 11.33 | -8.85614 | 1.32336 | -8.6557 | 2899 | 300 | 869730 | -14.8485 | 939746 | -14.9325 | 0.0841 |
| 19.7.2013 | 13561 | TYC 3063-2354-1 | 11.36 | -8.82607 | 1.28954 | -8.6466 | 2875 | 300 | 862470 | -14.8394 | 1104000 | -15.1074 | 0.2681 |
| 19.7.2013 | 13565 | TYC 3063-2354-1 | 11.36 | -8.82607 | 1.30644 | -8.6361 | 2847 | 300 | 854185 | -14.8289 | 1103000 | -15.1064 | 0.2776 |
| 8.3.2012 | 2218 | TYC 2667-69-1 | 11.38 | -8.80603 | 1.32655 | -8.6036 | 2763 | 300 | 828988 | -14.7964 | 962185 | -14.9581 | 0.1618 |
| 8.3.2012 | 2207 | TYC 2667-698-1 | 11.4 | -8.78598 | 1.34249 | -8.5736 | 2688 | 300 | 806449 | -14.7664 | 928209 | -14.9191 | 0.1527 |
| 8.3.2012 | 2208 | TYC 2667-698-1 | 11.4 | -8.78598 | 1.32336 | -8.5855 | 2718 | 300 | 815305 | -14.7783 | 907397 | -14.8945 | 0.1162 |
| 19.4.2012 | 4543 | 2mass j13072064+2731144 | 11.41 | -8.77596 | 1.38000 | -8.5404 | 2607 | 5 | 13035 | -10.2878 | 12209 | -10.2167 | -0.0711 |
| 8.3.2012 | 2218 | TYC 2667-835-1 | 11.45 | -8.73587 | 1.32655 | -8.5334 | 2590 | 300 | 777113 | -14.7262 | 1002000 | -15.0022 | 0.2760 |
| 8.3.2012 | 2218 | TYC 2667-825-1 | 11.48 | -8.70580 | 1.32655 | -8.5033 | 2520 | 300 | 755886 | -14.6961 | 711716 | -14.6308 | -0.0654 |
| 19.7.2013 | 13561 | TYC 3063-50-1 | 11.5 | -8.68575 | 1.28954 | -8.5062 | 2526 | 300 | 757906 | -14.6990 | 969103 | -14.9659 | 0.2669 |
| 19.7.2013 | 13565 | TYC 3063-50-1 | 11.5 | -8.68575 | 1.30644 | -8.4958 | 2502 | 300 | 750625 | -14.6886 | 974736 | -14.9722 | 0.2837 |
| 8.3.2012 | 2207 | TYC 2667-819-1 | 11.5 | -8.68575 | 1.34249 | -8.4734 | 2451 | 300 | 735334 | -14.6662 | 736372 | -14.6677 | 0.0015 |
| 8.3.2012 | 2208 | TYC 2667-819-1 | 11.5 | -8.68575 | 1.32336 | -8.4853 | 2478 | 300 | 743410 | -14.6781 | 719496 | -14.6426 | -0.0355 |
| 5.8.2013 | 14141 | TYC 2595-1515-1 | 11.51 | -8.67573 | 1.07799 | -8.6274 | 2825 | 120 | 338946 | -13.8253 | 323090 | -13.7733 | -0.0520 |
| 7.9.2013 | 15370 | TYC 2595-1515-1 | 11.51 | -8.67573 | 1.25739 | -8.5161 | 2550 | 60 | 152971 | -12.9615 | 148351 | -12.9282 | -0.0333 |
| 7.9.2013 | 15400 | TYC 2595-1515-1 | 11.51 | -8.67573 | 1.39947 | -8.4281 | 2351 | 60 | 141050 | -12.8734 | 139653 | -12.8626 | -0.0108 |
| 9.9.2013 | 15657 | TYC 2595-1515-1 | 11.51 | -8.67573 | 1.22104 | -8.5387 | 2603 | 60 | 156180 | -12.9841 | 142697 | -12.8860 | -0.0980 |
| 8.3.2012 | 2218 | TYC 2667-878-1 | 11.51 | -8.67573 | 1.32655 | -8.4733 | 2451 | 300 | 735239 | -14.6661 | 724281 | -14.6498 | -0.0163 |
| 1.4.2013 | 8842 | TYC 2410-948-1 | 11.54 | -8.64566 | 1.60750 | -8.2690 | 2030 | 4 | 8122 | -9.7742 | 8712.2 | -9.8503 | 0.0762 |
| 1.4.2013 | 8839 | TYC 2410-948-1 | 11.54 | -8.64566 | 1.60076 | -8.2732 | 2038 | 1 | 2038 | -8.2732 | 2135 | -8.3235 | 0.0503 |
| 23.11.2012 | 4582 | TYC 1994-2237-1 | 11.56 | -8.62561 | 1.36644 | -8.3984 | 2288 | 60 | 137252 | -12.8438 | 155736 | -12.9810 | 0.1372 |
| 23.11.2012 | 4581 | TYC 1994-2237-1 | 11.56 | -8.62561 | 1.37361 | -8.3940 | 2278 | 30 | 68346 | -12.0868 | 78181 | -12.2328 | 0.1460 |
| 23.11.2012 | 4580 | TYC 1994-2237-1 | 11.56 | -8.62561 | 1.37924 | -8.3905 | 2271 | 10 | 22709 | -10.8905 | 25971 | -11.0362 | 0.1457 |
| 23.11.2012 | 4578 | TYC 1994-2237-1 | 11.56 | -8.62561 | 1.38380 | -8.3877 | 2265 | 5 | 11325 | -10.1351 | 12931 | -10.2791 | 0.1440 |
| 23.11.2012 | 4576 | TYC 1994-2237-1 | 11.56 | -8.62561 | 1.38796 | -8.3851 | 2260 | 2 | 4519 | -9.1377 | 4946.2 | -9.2357 | 0.0980 |
| 11.12.2012 | 6036 | TYC 1994-2237-1 | 11.56 | -8.62561 | 1.53623 | -8.2931 | 2076 | 30 | 62285 | -11.9860 | 65364 | -12.0383 | 0.0524 |
| 11.12.2012 | 6035 | TYC 1994-2237-1 | 11.56 | -8.62561 | 1.54268 | -8.2891 | 2069 | 10 | 20685 | -10.7891 | 22143 | -10.8631 | 0.0739 |
| 19.4.2012 | 4543 | TYC 1995-2195-1 | 11.64 | -8.54543 | 1.38000 | -8.3098 | 2108 | 5 | 10541 | -10.0573 | 13513 | -10.3269 | 0.2696 |
| 8.3.2012 | 2207 | TYC 2667-49-1 | 11.68 | -8.50534 | 1.34249 | -8.2930 | 2076 | 300 | 622758 | -14.4858 | 895317 | -14.8799 | 0.3941 |
| 8.3.2012 | 2208 | TYC 2667-49-1 | 11.68 | -8.50534 | 1.32336 | -8.3049 | 2099 | 300 | 629597 | -14.4977 | 876511 | -14.8569 | 0.3592 |
| 10.11.2012 | 4166 | HD282626 | 11.7 | -8.48529 | 1.55546 | -8.1409 | 1805 | 30 | 54136 | -11.8337 | 75537 | -12.1954 | 0.3617 |
| 11.11.2012 | 4189 | HD282626 | 11.7 | -8.48529 | 1.11478 | -8.4141 | 2321 | 30 | 69626 | -12.1069 | 77544 | -12.2239 | 0.1169 |
| 1.1.2013 | 6545 | HD282626 | 11.7 | -8.48529 | 1.11566 | -8.4136 | 2320 | 30 | 69591 | -12.1064 | 83354 | -12.3023 | 0.1959 |
| 4.2.2013 | 7117 | HD282626 | 11.7 | -8.48529 | 1.12156 | -8.4099 | 2312 | 30 | 69357 | -12.1027 | 77981 | -12.2300 | 0.1272 |
| 3.3.2013 | 8161 | HD282626 | 11.7 | -8.48529 | 1.10995 | -8.4171 | 2327 | 30 | 69818 | -12.1099 | 71369 | -12.1338 | 0.0239 |
| 3.3.2013 | 8174 | HD282626 | 11.7 | -8.48529 | 1.34943 | -8.2686 | 2030 | 30 | 60894 | -11.9614 | 66474 | -12.0566 | 0.0952 |
| 5.8.2013 | 14141 | TYC 2595-733-1 | 11.72 | -8.46524 | 1.07799 | -8.4169 | 2327 | 120 | 279214 | -13.6148 | 226440 | -13.3874 | -0.2275 |
| 7.9.2013 | 15370 | TYC 2595-733-1 | 11.72 | -8.46524 | 1.25739 | -8.3057 | 2100 | 60 | 126013 | -12.7510 | 106259 | -12.5659 | -0.1851 |
| 9.10.2013 | 16976 | TYC 3089-995-1 | 11.72 | -8.46524 | 1.33074 | -8.2602 | 2014 | 30 | 60422 | -11.9530 | 65836 | -12.0462 | 0.0932 |
| 9.10.2013 | 16976 | TYC 3089-1111-1 | 11.72 | -8.46524 | 1.33074 | -8.2602 | 2014 | 30 | 60422 | -11.9530 | 68509 | -12.0894 | 0.1364 |
| 9.10.2013 | 16978 | TYC 3089-995-1 | 11.72 | -8.46524 | 1.33558 | -8.2572 | 2009 | 30 | 60255 | -11.9500 | 65159 | -12.0349 | 0.0849 |
| 9.10.2013 | 16978 | TYC 3089-1111-1 | 11.72 | -8.46524 | 1.33558 | -8.2572 | 2009 | 30 | 60255 | -11.9500 | 68212 | -12.0847 | 0.1347 |
| 9.10.2013 | 16985 | TYC 3089-995-1 | 11.72 | -8.46524 | 1.36074 | -8.2416 | 1980 | 30 | 59396 | -11.9344 | 65871 | -12.0467 | 0.1123 |

# Appendix F

| Date | Image | Star | Ref Mag (m) | Predicted $m'_{t=1s,X=1.0}$ Eq (2.2.6.1) | X | Predicted $m'_{t=1s,X=X}$ Eq (2.2.6.2) | Predicted $(N_{target})_{t=1s,X=X}$ Eq (2.2.8.8) | $t_{exp}$ | Predicted $(N_{target})_{t=t_{exp},X=X}$ Eq (2.2.7.4) | Predicted $m'_{t=texp,X=X}$ Eq (2.2.8.10) | Measured $(N_{target})_{t=t_{exp},X=}$ | Measured $m'_{t=texp,X=X}$ Eq (2.2.8.11) | Δm' Eq (2.2.8.12) |
|---|---|---|---|---|---|---|---|---|---|---|---|---|---|
| 9.10.2013 | 16985 | TYC 3089-1111-1 | 11.72 | -8.46524 | 1.36074 | -8.2416 | 1980 | 30 | 59396 | -11.9344 | 68801 | -12.0940 | 0.1596 |
| 8.3.2012 | 2218 | TYC 2667-628-1 | 11.74 | -8.44520 | 1.32655 | -8.2427 | 1982 | 300 | 594589 | -14.4355 | 801185 | -14.7593 | 0.3238 |
| 8.3.2012 | 2207 | TYC 2667-872-1 | 11.75 | -8.43518 | 1.34249 | -8.2228 | 1946 | 300 | 583788 | -14.4156 | 691705 | -14.5998 | 0.1842 |
| 8.3.2012 | 2208 | TYC 2667-872-1 | 11.75 | -8.43518 | 1.32336 | -8.2347 | 1967 | 300 | 590199 | -14.4275 | 675974 | -14.5748 | 0.1473 |
| 8.3.2012 | 2207 | TYC 2667-920-1 | 11.81 | -8.37504 | 1.34249 | -8.1627 | 1841 | 300 | 552331 | -14.3555 | 514031 | -14.2775 | -0.0780 |
| 8.3.2012 | 2208 | TYC 2667-920-1 | 11.81 | -8.37504 | 1.32336 | -8.1746 | 1861 | 300 | 558397 | -14.3674 | 502741 | -14.2534 | -0.1140 |
| 1.4.2013 | 8842 | TYC 2410-1184-1 | 11.89 | -8.29485 | 1.60750 | -7.9182 | 1470 | 4 | 5880 | -9.4234 | 6464.6 | -9.5264 | 0.1030 |
| 1.4.2013 | 8839 | TYC 2410-1184-1 | 11.89 | -8.29485 | 1.60076 | -7.9224 | 1476 | 1 | 1476 | -7.9224 | 1797.8 | -8.1369 | 0.2145 |
| 9.10.2013 | 16976 | TYC 3089-885-1 | 11.92 | -8.26478 | 1.33074 | -8.0597 | 1675 | 30 | 50236 | -11.7525 | 56141 | -11.8732 | 0.1207 |
| 9.10.2013 | 16978 | TYC 3089-885-1 | 11.92 | -8.26478 | 1.33558 | -8.0567 | 1670 | 30 | 50097 | -11.7495 | 56730 | -11.8845 | 0.1350 |
| 9.10.2013 | 16985 | TYC 3089-885-1 | 11.92 | -8.26478 | 1.36074 | -8.0411 | 1646 | 30 | 49382 | -11.7339 | 56640 | -11.8828 | 0.1489 |
| 8.3.2012 | 2207 | TYC 2667-140-1 | 11.98 | -8.20465 | 1.34249 | -7.9923 | 1574 | 300 | 472110 | -14.1851 | 681893 | -14.5843 | 0.3992 |
| 8.3.2012 | 2208 | TYC 2667-140-1 | 11.98 | -8.20465 | 1.32336 | -8.0042 | 1591 | 300 | 477295 | -14.1970 | 663812 | -14.5551 | 0.3581 |
| 12.7.2013 | 13427 | TYC 2141-1734-1 | 12 | -8.18460 | 1.15206 | -8.0903 | 1722 | 300 | 516714 | -14.2831 | 679048 | -14.5798 | 0.2966 |
| 10.11.2012 | 4166 | TYC 2387-447-1 | 12.01 | -8.17458 | 1.55546 | -7.8302 | 1355 | 30 | 40663 | -11.5230 | 49304 | -11.7322 | 0.2092 |
| 11.11.2012 | 4189 | TYC 2387-447-1 | 12.01 | -8.17458 | 1.11478 | -8.1034 | 1743 | 30 | 52298 | -11.7962 | 52467 | -11.7997 | 0.0035 |
| 1.1.2013 | 6545 | TYC 2387-447-1 | 12.01 | -8.17458 | 1.11566 | -8.1029 | 1742 | 30 | 52272 | -11.7957 | 55075 | -11.8524 | 0.0567 |
| 4.2.2013 | 7117 | TYC 2387-447-1 | 12.01 | -8.17458 | 1.12156 | -8.0992 | 1737 | 30 | 52096 | -11.7920 | 51521 | -11.7800 | -0.0121 |
| 3.3.2013 | 8161 | TYC 2387-447-1 | 12.01 | -8.17458 | 1.10995 | -8.1064 | 1748 | 30 | 52443 | -11.7992 | 48268 | -11.7091 | -0.0901 |
| 3.3.2013 | 8174 | TYC 2387-447-1 | 12.01 | -8.17458 | 1.34943 | -7.9579 | 1525 | 30 | 45740 | -11.6507 | 47523 | -11.6923 | 0.0415 |
| 8.3.2012 | 2207 | TYC 2667-849-1 | 12.02 | -8.16455 | 1.34249 | -7.9522 | 1517 | 300 | 454995 | -14.1450 | 549893 | -14.3507 | 0.2057 |
| 8.3.2012 | 2208 | TYC 2667-849-1 | 12.02 | -8.16455 | 1.32336 | -7.9641 | 1533 | 300 | 459991 | -14.1569 | 535414 | -14.3217 | 0.1649 |
| 23.11.2012 | 4582 | TYC 1994-201-1 | 12.09 | -8.09439 | 1.36644 | -7.8672 | 1402 | 60 | 84145 | -12.3126 | 93520 | -12.4273 | 0.1147 |
| 23.11.2012 | 4581 | TYC 1994-201-1 | 12.09 | -8.09439 | 1.37361 | -7.8628 | 1397 | 30 | 41901 | -11.5556 | 46794 | -11.6755 | 0.1199 |
| 23.11.2012 | 4580 | TYC 1994-201-1 | 12.09 | -8.09439 | 1.37924 | -7.8593 | 1392 | 10 | 13922 | -10.3593 | 15419 | -10.4701 | 0.1109 |
| 23.11.2012 | 4578 | TYC 1994-201-1 | 12.09 | -8.09439 | 1.38380 | -7.8564 | 1389 | 5 | 6943 | -9.6039 | 7616.4 | -9.7044 | 0.1005 |
| 23.11.2012 | 4576 | TYC 1994-201-1 | 12.09 | -8.09439 | 1.38796 | -7.8539 | 1385 | 2 | 2771 | -8.6064 | 3030.3 | -8.7037 | 0.0973 |
| 11.12.2012 | 6036 | TYC 1994-201-1 | 12.09 | -8.09439 | 1.53623 | -7.7619 | 1273 | 30 | 38185 | -11.4547 | 39139 | -11.4815 | 0.0268 |
| 11.12.2012 | 6035 | TYC 1994-201-1 | 12.09 | -8.09439 | 1.54268 | -7.7579 | 1268 | 10 | 12682 | -10.2579 | 13325 | -10.3117 | 0.0537 |
| 9.10.2013 | 16976 | TYC 3089-703-1 | 12.09 | -8.09439 | 1.33074 | -7.8893 | 1431 | 30 | 42939 | -11.5821 | 47505 | -11.6918 | 0.1097 |
| 9.10.2013 | 16978 | TYC 3089-703-1 | 12.09 | -8.09439 | 1.33558 | -7.8863 | 1427 | 30 | 42821 | -11.5791 | 47859 | -11.6999 | 0.1208 |
| 9.10.2013 | 16985 | TYC 3089-703-1 | 12.09 | -8.09439 | 1.36074 | -7.8707 | 1407 | 30 | 42210 | -11.5635 | 47501 | -11.6918 | 0.1282 |
| 9.10.2013 | 16976 | NAME TrES-3 Parent Star | 12.402 | -7.78168 | 1.33074 | -7.5766 | 1073 | 30 | 32194 | -11.2694 | 39794 | -11.4995 | 0.2301 |
| 9.10.2013 | 16978 | NAME TrES-3 Parent Star | 12.402 | -7.78168 | 1.33558 | -7.5736 | 1070 | 30 | 32105 | -11.2664 | 39625 | -11.4949 | 0.2285 |
| 9.10.2013 | 16985 | NAME TrES-3 Parent Star | 12.402 | -7.78168 | 1.36074 | -7.5580 | 1055 | 30 | 31647 | -11.2508 | 39691 | -11.4967 | 0.2459 |
| 8.3.2012 | 2207 | TYC 2667-919-1 | 12.43 | -7.75361 | 1.34249 | -7.5413 | 1039 | 300 | 311623 | -13.7341 | 350393 | -13.8614 | 0.1273 |
| 8.3.2012 | 2208 | TYC 2667-919-1 | 12.43 | -7.75361 | 1.32336 | -7.5531 | 1050 | 300 | 315045 | -13.7459 | 342169 | -13.8356 | 0.0897 |
| 1.4.2013 | 8842 | TYC 2410-1405-1 | 12.62 | -7.56317 | 1.60750 | -7.1865 | 749 | 4 | 2997 | -8.6917 | 2664 | -8.5638 | -0.1278 |
| 9.11.2013 | 17997 | 2MASS J02195438+5702037 | 13.67 | -6.51076 | 1.12396 | -6.4339 | 375 | 600 | 224757 | -13.3793 | 201067 | -13.2584 | -0.1209 |
| 9.11.2013 | 17993 | 2MASS J02195438+5702037 | 13.67 | -6.51076 | 1.11025 | -6.4424 | 378 | 600 | 226523 | -13.3878 | 200510 | -13.2553 | -0.1324 |
| 5.8.2013 | 14141 | [HH95] V795 Her-2 | 13.767 | -6.41354 | 1.07799 | -6.3652 | 352 | 120 | 42194 | -11.5631 | 47076 | -11.6820 | 0.1189 |
| 7.9.2013 | 15370 | [HH95] V795 Her-2 | 13.767 | -6.41354 | 1.25739 | -6.2540 | 317 | 60 | 19043 | -10.6993 | 21724 | -10.8423 | 0.1430 |
| 9.11.2013 | 17997 | 2MASS J02200834+5707122 | 13.791 | -6.38948 | 1.12396 | -6.3126 | 335 | 600 | 201002 | -13.2580 | 184117 | -13.1627 | -0.0953 |
| 9.11.2013 | 17993 | 2MASS J02200834+5707122 | 13.791 | -6.38948 | 1.11025 | -6.3211 | 338 | 600 | 202582 | -13.2665 | 183379 | -13.1584 | -0.1081 |
| 5.8.2013 | 14141 | [PBS2006] V795 Her S3 | 14.047 | -6.13289 | 1.07799 | -6.0845 | 272 | 120 | 32583 | -11.2825 | 36462 | -11.4046 | 0.1221 |
| 7.9.2013 | 15370 | [PBS2006] V795 Her S3 | 14.047 | -6.13289 | 1.25739 | -5.9733 | 245 | 60 | 14705 | -10.4187 | 17277 | -10.5937 | 0.1750 |
| 5.8.2013 | 14141 | [HH95] V795 Her-3 | 14.431 | -5.74801 | 1.07799 | -5.6997 | 190 | 120 | 22858 | -10.8976 | 24525 | -10.9740 | 0.0764 |
| 7.9.2013 | 15370 | [HH95] V795 Her-3 | 14.431 | -5.74801 | 1.25739 | -5.5884 | 172 | 60 | 10316 | -10.0338 | 11339 | -10.1364 | 0.1026 |
| 5.8.2013 | 14141 | [PBS2006] V795 Her S1 | 14.565 | -5.61370 | 1.07799 | -5.5653 | 168 | 120 | 20199 | -10.7633 | 22906 | -10.8999 | 0.1366 |
| 7.9.2013 | 15370 | [PBS2006] V795 Her S1 | 14.565 | -5.61370 | 1.25739 | -5.4541 | 152 | 60 | 9116 | -9.8995 | 10503 | -10.0533 | 0.1538 |
| 9.11.2013 | 17997 | 2MASS J02184176+5702179 | 14.66 | -5.51848 | 1.12396 | -5.4416 | 150 | 600 | 90116 | -12.3870 | 76635 | -12.2111 | -0.1759 |
| 9.11.2013 | 17993 | 2MASS J02184176+5702179 | 14.66 | -5.51848 | 1.11025 | -5.4501 | 151 | 600 | 90824 | -12.3955 | 77613 | -12.2248 | -0.1707 |
| 5.8.2013 | 14141 | [PBS2006] V795 Her S4 | 14.688 | -5.49042 | 1.07799 | -5.4421 | 150 | 120 | 18030 | -10.6400 | 20576 | -10.7834 | 0.1434 |
| 7.9.2013 | 15370 | [PBS2006] V795 Her S4 | 14.688 | -5.49042 | 1.25739 | -5.3308 | 136 | 60 | 8137 | -9.7762 | 9991 | -9.9990 | 0.2228 |
| 9.11.2013 | 17997 | 2MASS J02175117+5713299 | 14.81 | -5.36814 | 1.12396 | -5.2913 | 131 | 600 | 78463 | -12.2367 | 68482 | -12.0889 | -0.1477 |
| 9.11.2013 | 17993 | 2MASS J02175117+5713299 | 14.81 | -5.36814 | 1.11025 | -5.2998 | 132 | 600 | 79079 | -12.2452 | 69585 | -12.1063 | -0.1389 |
| 5.8.2013 | 14141 | [PBS2006] V795 Her S2 | 14.865 | -5.31301 | 1.07799 | -5.2647 | 128 | 120 | 15312 | -10.4626 | 17656 | -10.6172 | 0.1546 |
| 7.9.2013 | 15370 | [PBS2006] V795 Her S2 | 14.865 | -5.31301 | 1.25739 | -5.1534 | 115 | 60 | 6911 | -9.5988 | 8372.5 | -9.8071 | 0.2083 |
| 9.11.2013 | 17997 | 2MASS J02201860+5712331 | 14.96 | -5.21779 | 1.12396 | -5.1409 | 114 | 600 | 68316 | -12.0863 | 61108 | -11.9652 | -0.1211 |
| 9.11.2013 | 17997 | 2MASS J02174011+5704271 | 14.96 | -5.21779 | 1.12396 | -5.1409 | 114 | 600 | 68316 | -12.0863 | 57730 | -11.9035 | -0.1828 |
| 9.11.2013 | 17993 | 2MASS J02201860+5712331 | 14.96 | -5.21779 | 1.11025 | -5.1494 | 115 | 600 | 68853 | -12.0948 | 60726 | -11.9584 | -0.1364 |
| 9.11.2013 | 17993 | 2MASS J02174011+5704271 | 14.96 | -5.21779 | 1.11025 | -5.1494 | 115 | 600 | 68853 | -12.0948 | 57856 | -11.9059 | -0.1889 |
| 9.11.2013 | 17997 | 2MASS J02202166+5707215 | 15.09 | -5.08749 | 1.12396 | -5.0106 | 101 | 600 | 60591 | -11.9560 | 54230 | -11.8356 | -0.1204 |
| 9.11.2013 | 17993 | 2MASS J02202166+5707215 | 15.09 | -5.08749 | 1.110253 | -5.0191 | 102 | 600 | 61067 | -11.96451421 | 54860 | -11.84813951 | -0.1164 |
| 9.11.2013 | 17997 | 2MASS J02202146+5711276 | 15.1 | -5.07747 | 1.123962 | -5.0006 | 100 | 600 | 60034 | -11.94599167 | 51728 | -11.78431422 | -0.1617 |
| 9.11.2013 | 17993 | 2MASS J02202146+5711276 | 15.1 | -5.07747 | 1.110253 | -5.0091 | 101 | 600 | 60506 | -11.95449121 | 52180 | -11.79376019 | -0.1607 |
| 5.8.2013 | 14141 | [HH95] V795 Her-9 | 15.495 | -4.68156 | 1.077987 | -4.6332 | 71 | 120 | 8560 | -9.8312 | 9192 | -9.9085 | 0.0774 |
| 7.9.2013 | 15370 | [HH95] V795 Her-9 | 15.495 | -4.68156 | 1.257393 | -4.5220 | 64 | 60 | 3863 | -8.9674 | 4002.3 | -9.0058 | 0.0384 |
| 5.8.2013 | 14141 | [HH95] V795 Her-18 | 15.918 | -4.25759 | 1.077987 | -4.2092 | 48 | 120 | 5793 | -9.4072 | 6052 | -9.4547 | 0.0476 |
| 7.9.2013 | 15370 | [HH95] V795 Her-18 | 15.918 | -4.25759 | 1.257393 | -4.0980 | 44 | 60 | 2614 | -8.5434 | 3001.3 | -8.6933 | 0.1499 |
| 9.11.2013 | 17997 | 2MASS J02175277+5701507 | 15.96 | -4.21549 | 1.123962 | -4.1386 | 45 | 600 | 27140 | -11.08401367 | 23631 | -10.93370525 | -0.1503 |
| 5.8.2013 | 14141 | [HH95] V795 Her-13 | 16.155 | -4.02004 | 1.077987 | -3.9717 | 39 | 120 | 4654 | -9.1696 | 5049 | -9.2580 | 0.0884 |
| 7.9.2013 | 15370 | [HH95] V795 Her-13 | 16.155 | -4.02004 | 1.257393 | -3.8605 | 35 | 60 | 2101 | -8.3058 | 2273 | -8.3915 | 0.0857 |
| 8.3.2012 | 2218 | UCAC3 253-168549 | 16.5 | -3.67425 | 1.326545 | -3.4718 | 24 | 300 | 7342 | -9.664594912 | 7761.4 | -9.724850166 | 0.0603 |

**Table 14 Validation by Comparison Of Predicted and Measured Target Magnitudes**

Figure 25 presents a plot of $[m'_{t=t_{exp},X=X}]_{predicted}$ and $[m'_{t=t_{exp},X=X}]_{measured}$ versus catalogue magnitude to show the range of conditions covered. This plot shows that the predicted and measured instrument magnitudes are similar for a wide range of catalogue magnitudes. Figure 25 also illustrates a good coverage of data points over a wide range of m from magnitude 5 to magnitude 16.5.

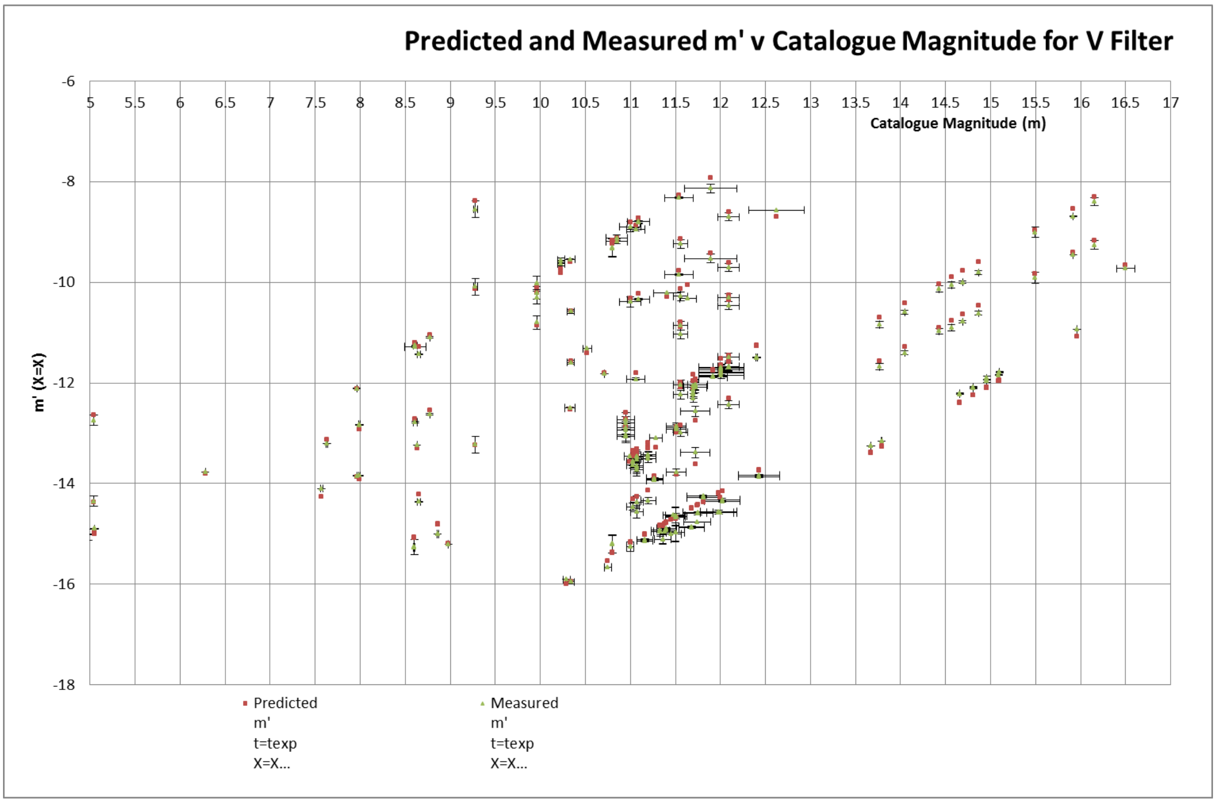


**Figure 25 Predicted and Measured ($m'_{t=t_{exp},X=X}$) V Catalogue Magnitude (m)**

Figure 26 presents a plot of $\Delta m'$ against catalogue magnitude. The distribution is shown to be fairly central about the x axis. As would be expected, there is a wider spread in $\Delta m'$ as the magnitude increases (ie the signal strength reduces).

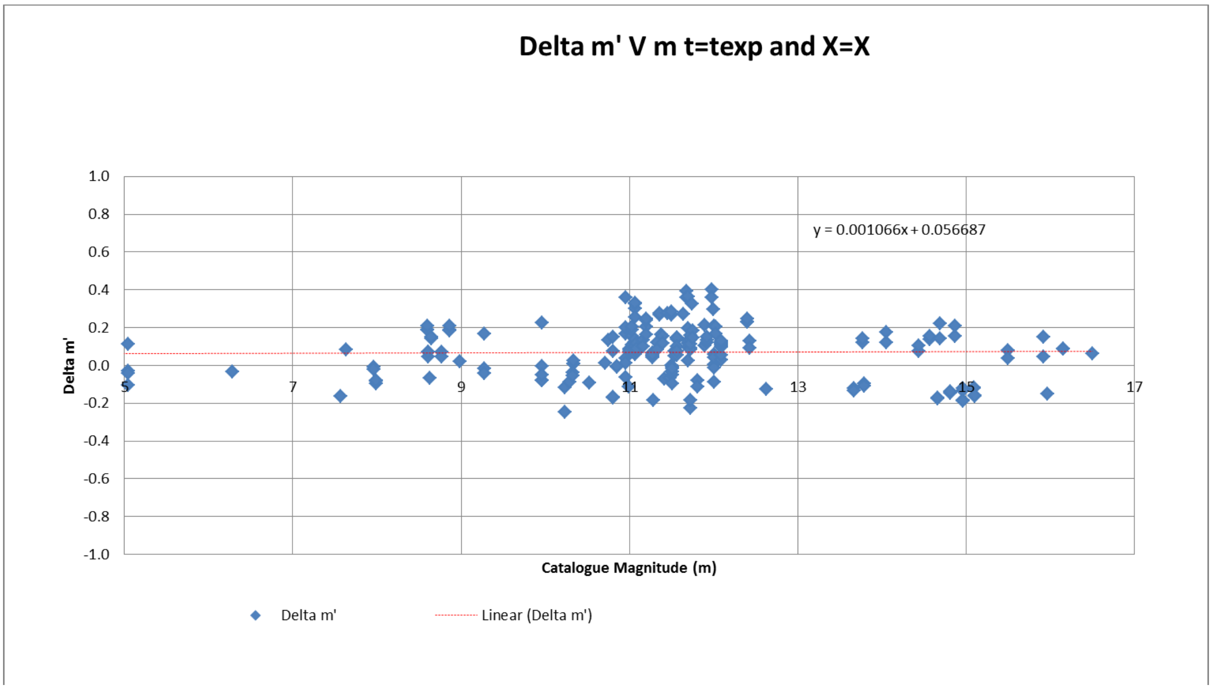


**Figure 26 Magnitude Error ($\Delta m'$) V Catalogue Magnitude (m)**

The validation exercise with a completely new set of targets had an standard deviation of 0.0687 that is significantly lower than the value of 0.20 obtained with the verification exercise. It is consequently considered that the formulation is considered to have been validated.

# Appendix G Recommended Formulation to be Used at Bayfordbury for Calculating a Maximum Exposure Time for any Given Target

The peak individual pixel count should not exceed the pixel's linearity. A series of flat field measurements with the CKT telescope were taken to identify the limit(s) by taking measurements with different exposure times and binning options[26]. The results are presented as Figure 27.

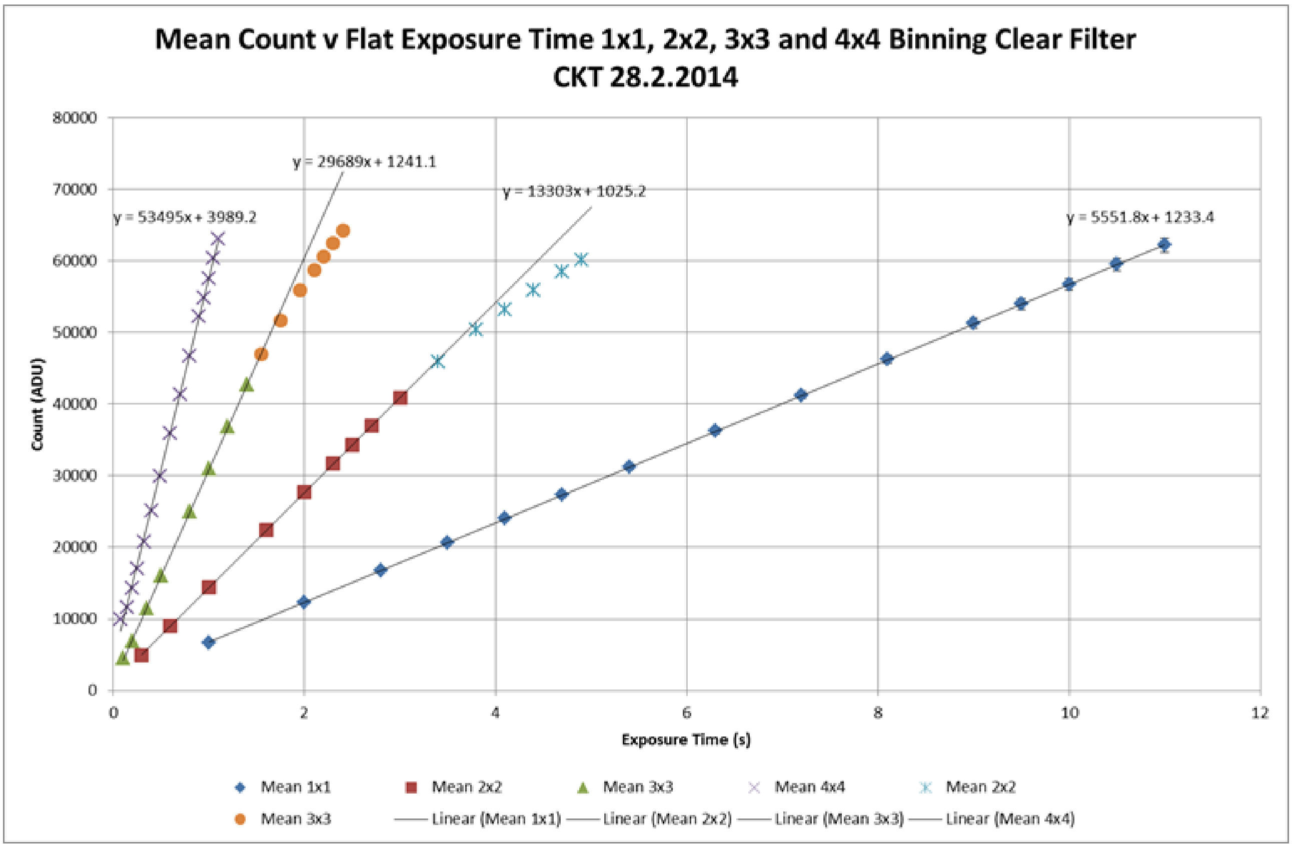


**Figure 27 Plot of Count Versus Exposure Time with Different Binning Options**

This plot clearly shows that the linearity is held with 2x2 binning until the ADU count reaches approximately 40,000. If a value for FWHM is defined then (assuming a bivariate normal distribution) the total count in the target aperture can be derived for a peak pixel count of 40,000.

A sample value of total count has been input into a spread sheet with bivariate normal equations and fixed values of FWHM. By iteratively inputting different values of $t_{exp}$, a maximum value of $t_{exp}$ was identified that could be used before the measurements lose linearity.

[26] In general the linear relationship of ADU count with light level will start to become non-linear before the saturation level is reached. However, the limiting value with different binning options is also influenced by factors that might not be immediately obvious. In particular, the hardware binning limit is approximately only twice the pixel limit (the vertical CCD capacity is 100,000 - 120,000 electrons whereas the summing floating diffusion charge capacity is only 220,000 to 240,000 electrons KODAK, 1999, consequently 2x2 hardware binning is limited by the floating diffusion charge limit.

# Appendix H Light Curves of Non-Transiting Targets

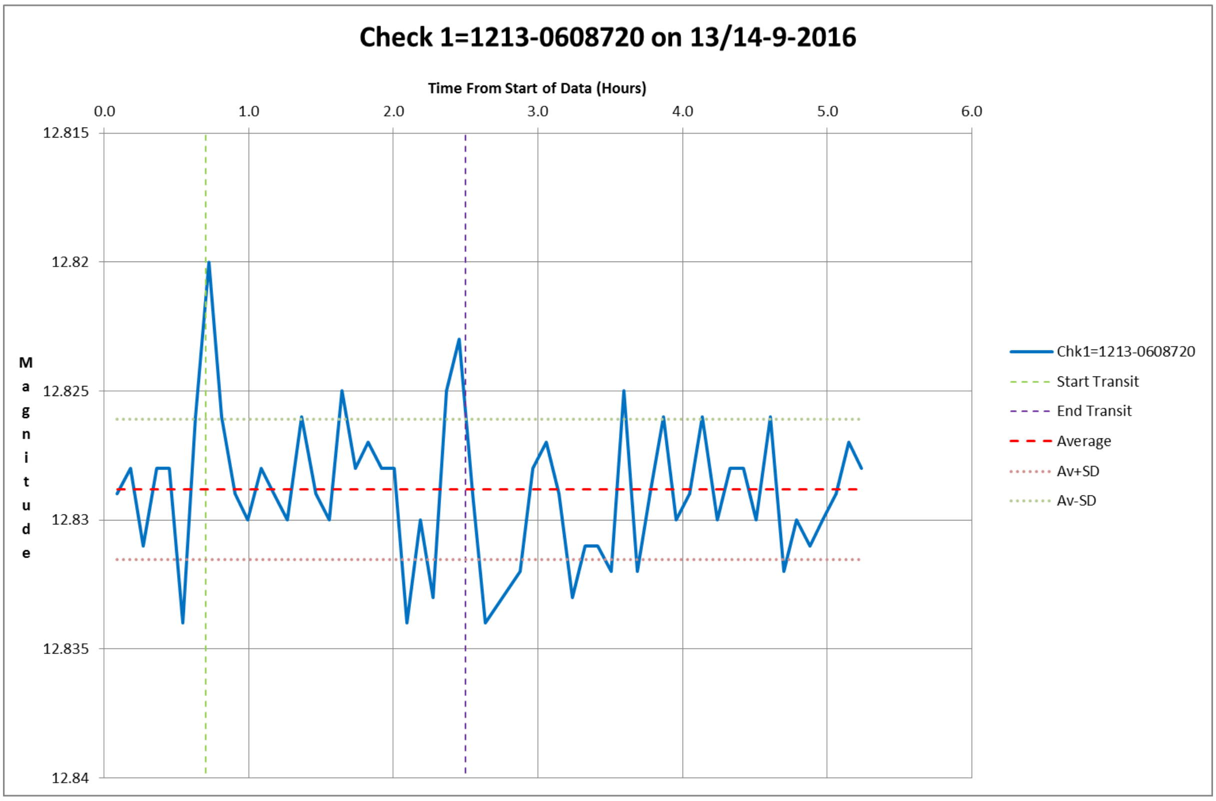


**Figure 28 WASP-10 Check Star 1213-0608720 of 13/14-9-2016 by CKT Telescope**

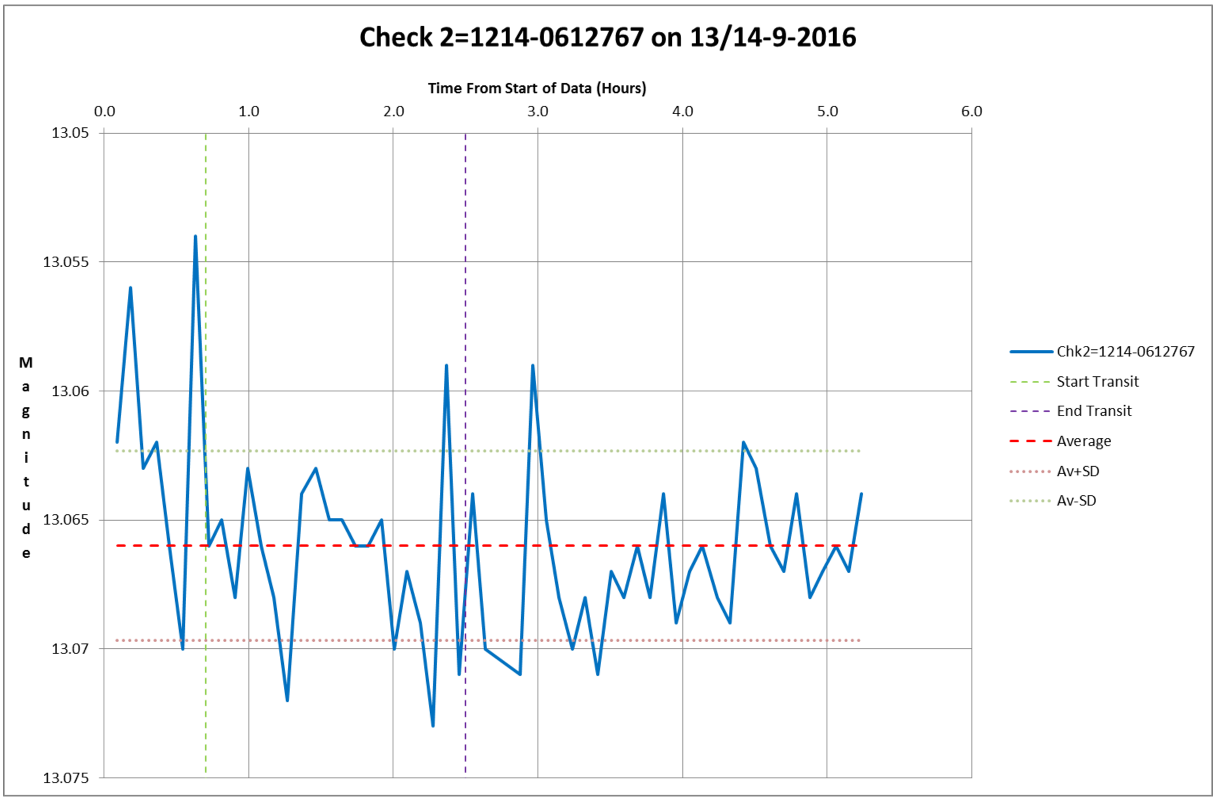


**Figure 29 WASP-10 Check Star 1214-0612767 of 13/14-9-2016 by CKT Telescope**

## Appendix H

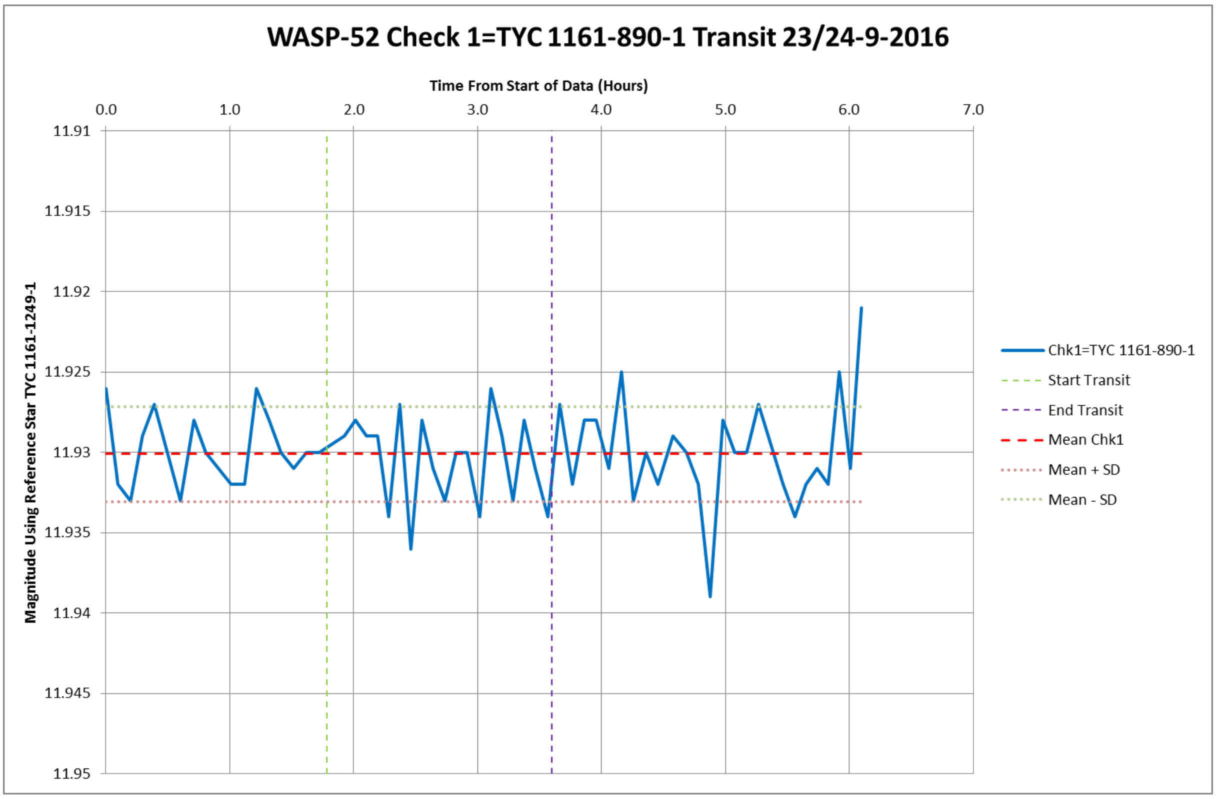


**Figure 30 WASP-52 Check Star TYC 1161-890-1 of 23/24-9-2016 by CKT Telescope**

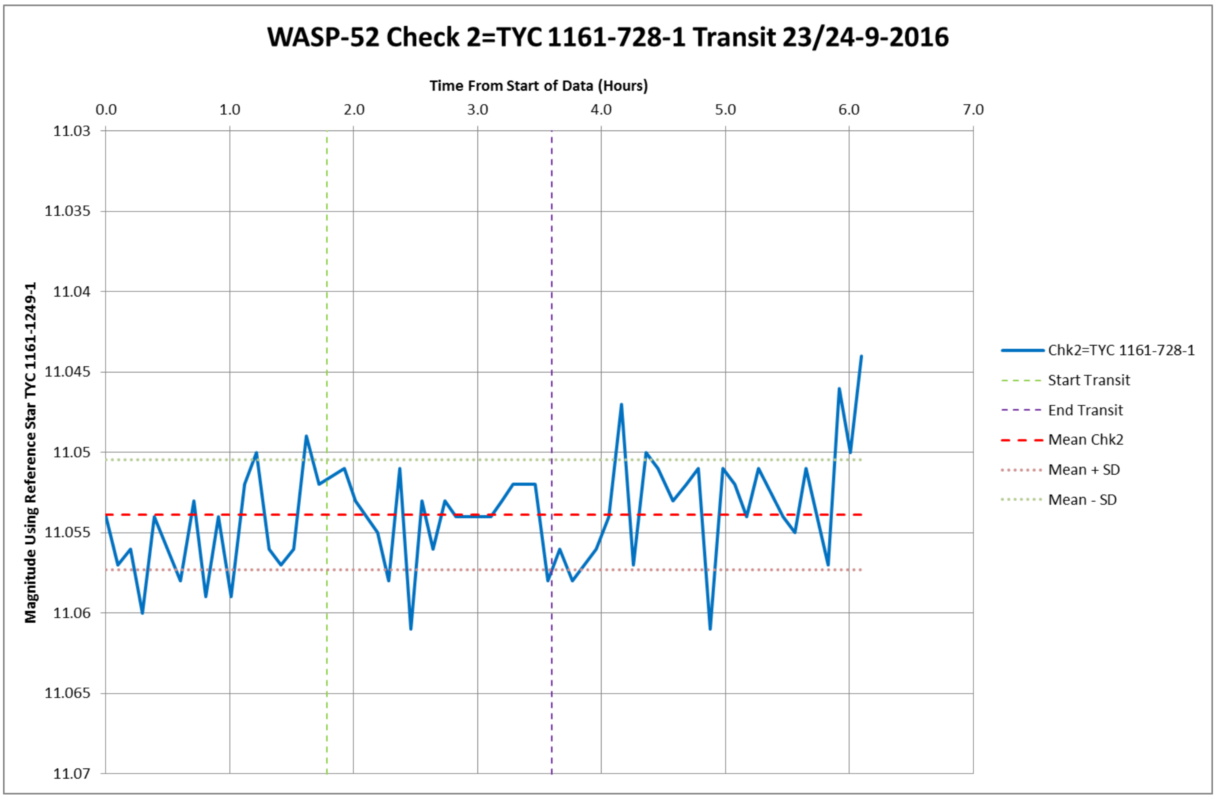


**Figure 31 WASP-52 Check Star TYC 1161-728-1 of 23/24-9-2016 by CKT Telescope**

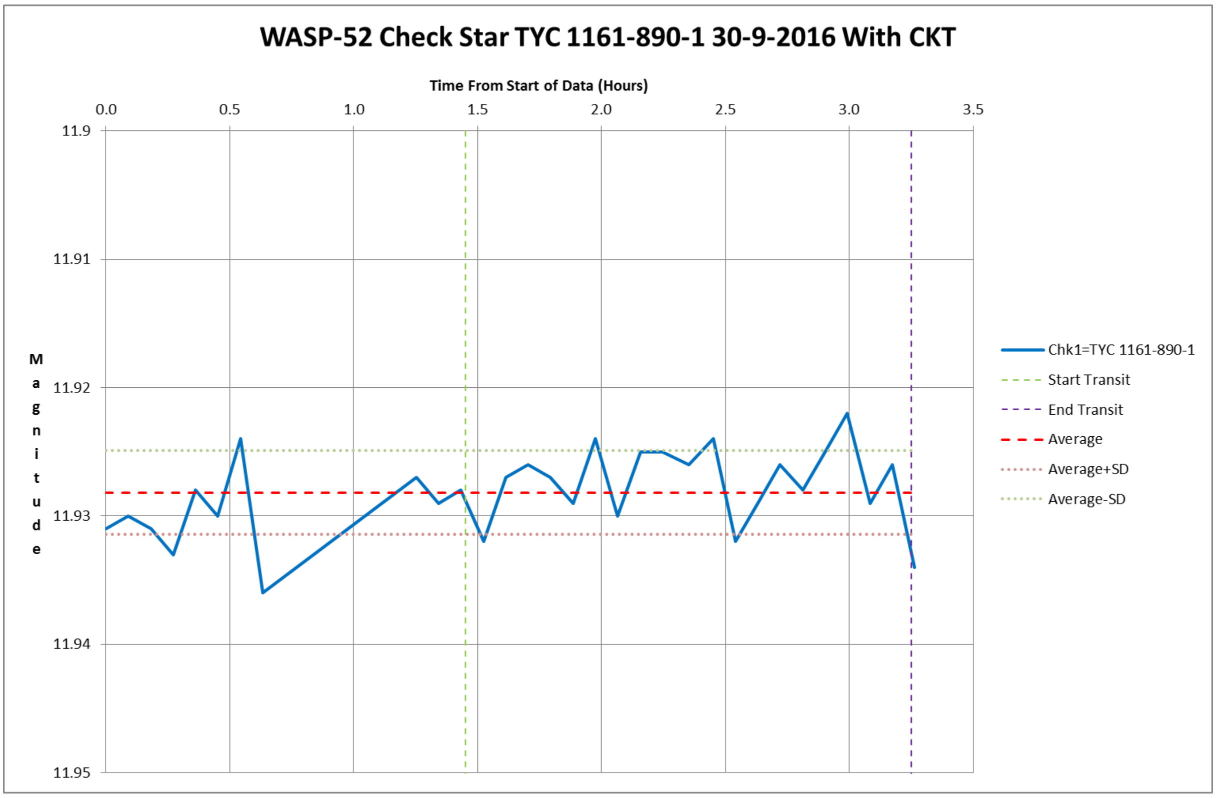


**Figure 32 WASP-52 Check Star TYC 1161-890-1 of 30-9-2016 by CKT Telescope**

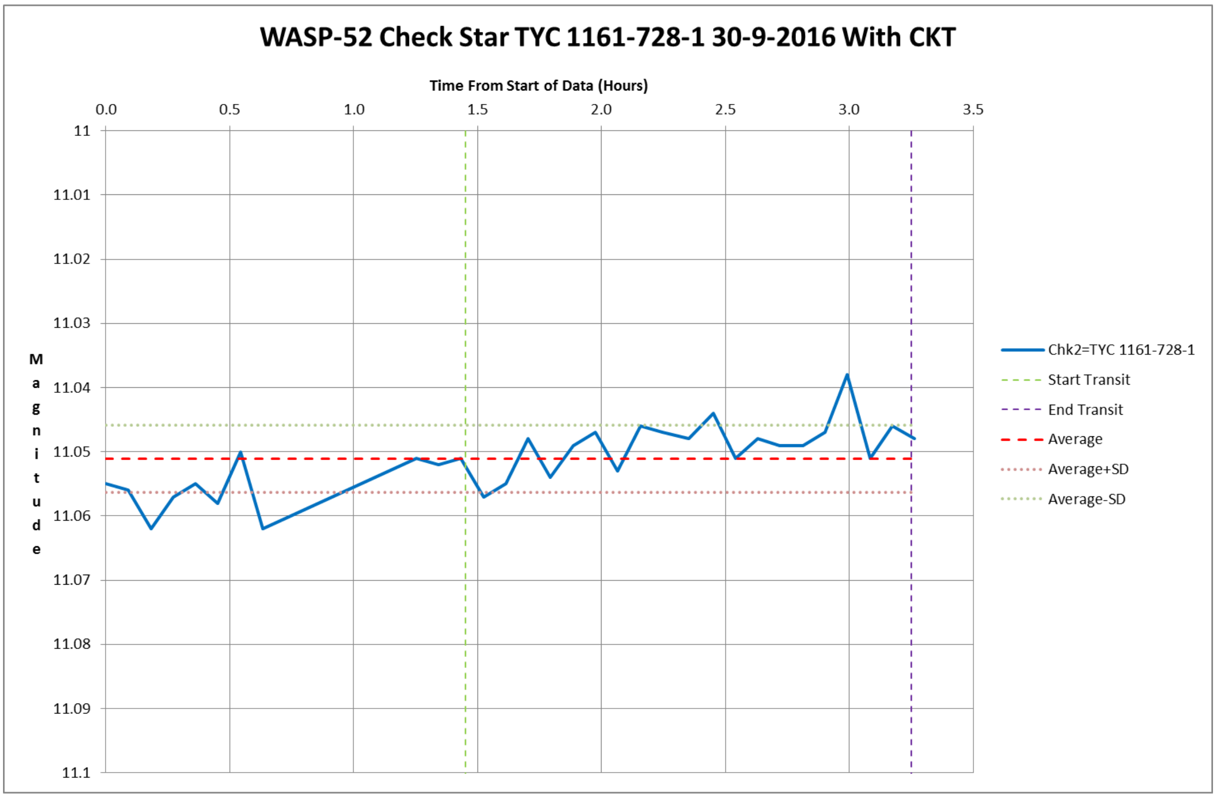


**Figure 33 WASP-52 Check Star TYC 1161-728-1 of 30-9-2016 by CKT Telescope**

## Appendix H

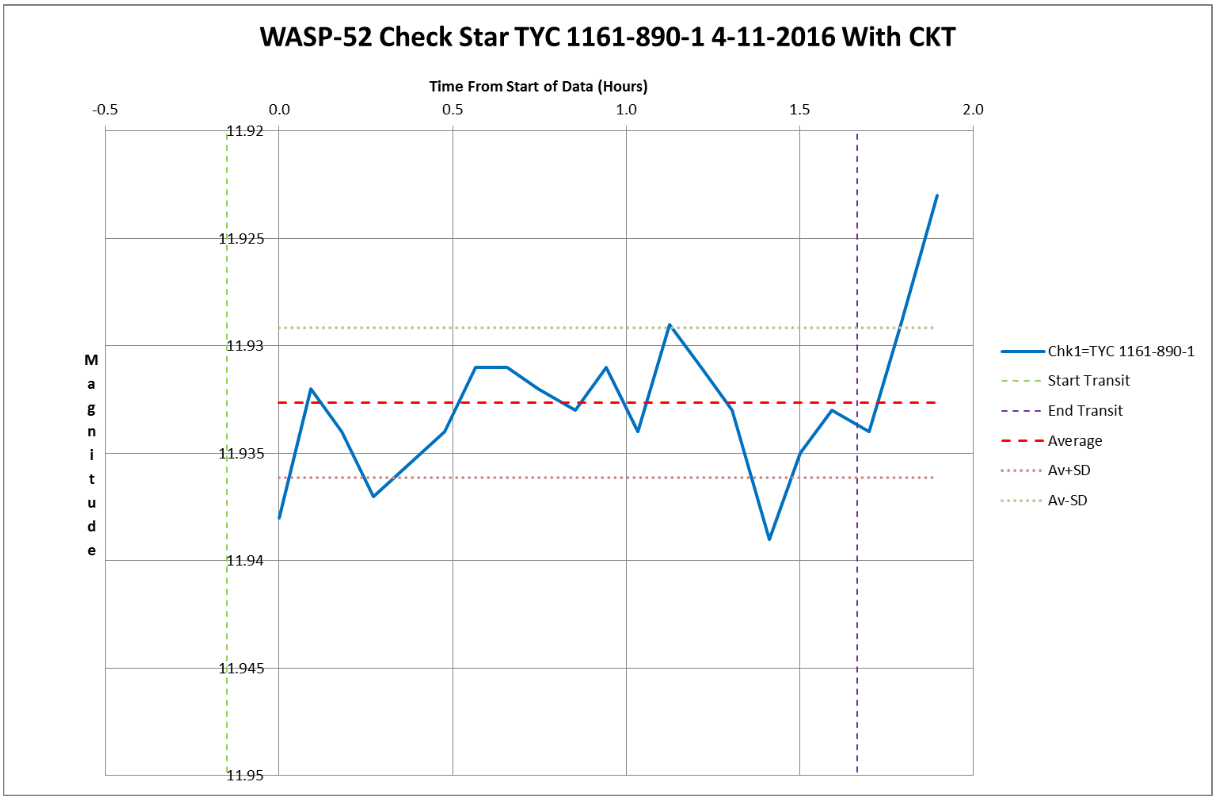


**Figure 34 WASP-52 Check Star TYC 1161-890-1 of 4-11-2016 by CKT Telescope**

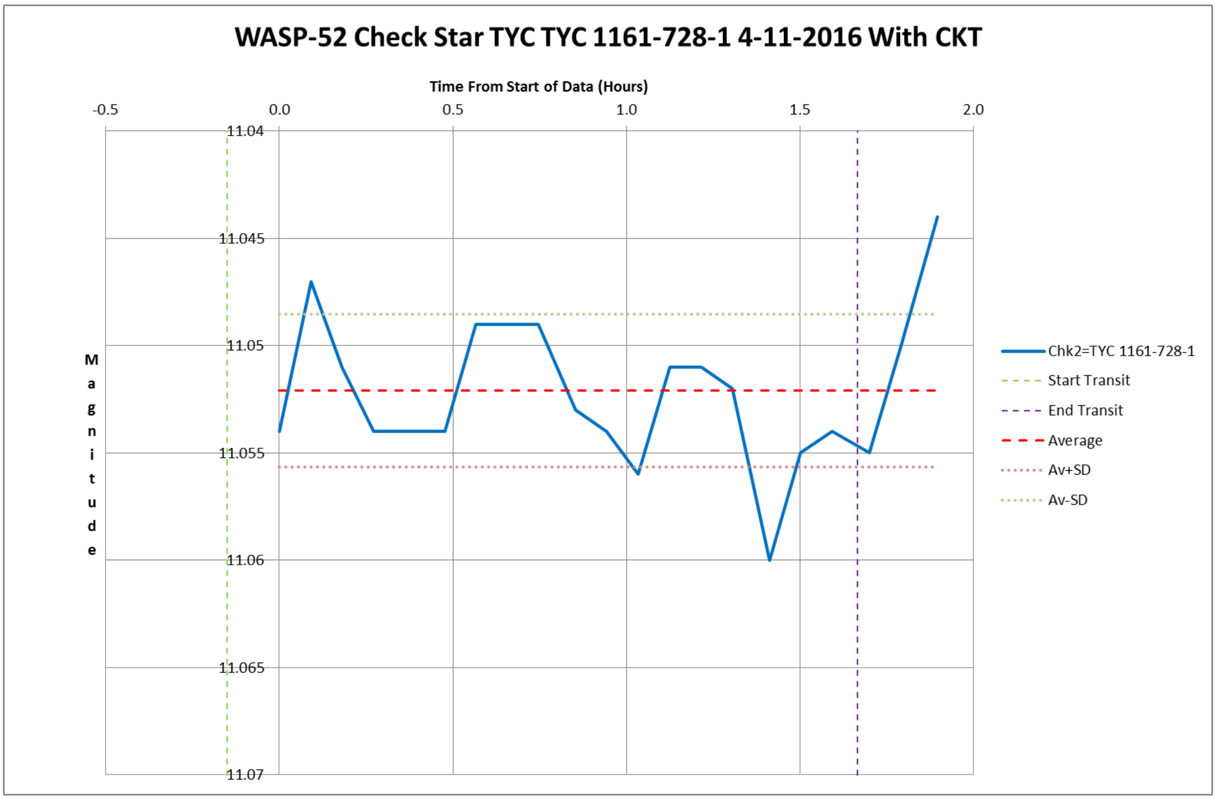


**Figure 35 WASP-52 Check Star TYC 1161-728-1 of 4-11-2016 by CKT Telescope**

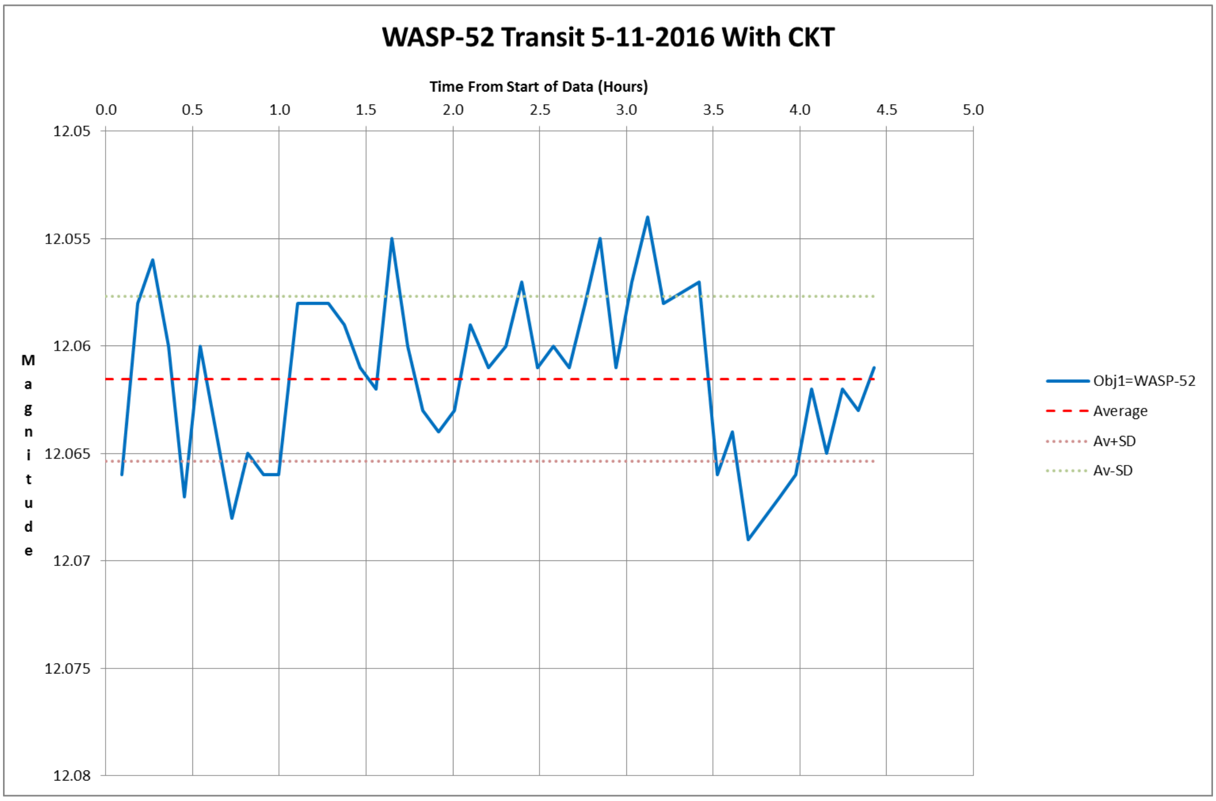


**Figure 36 WASP-52 Light Curve of 5-11-2016 by CKT Telescope**

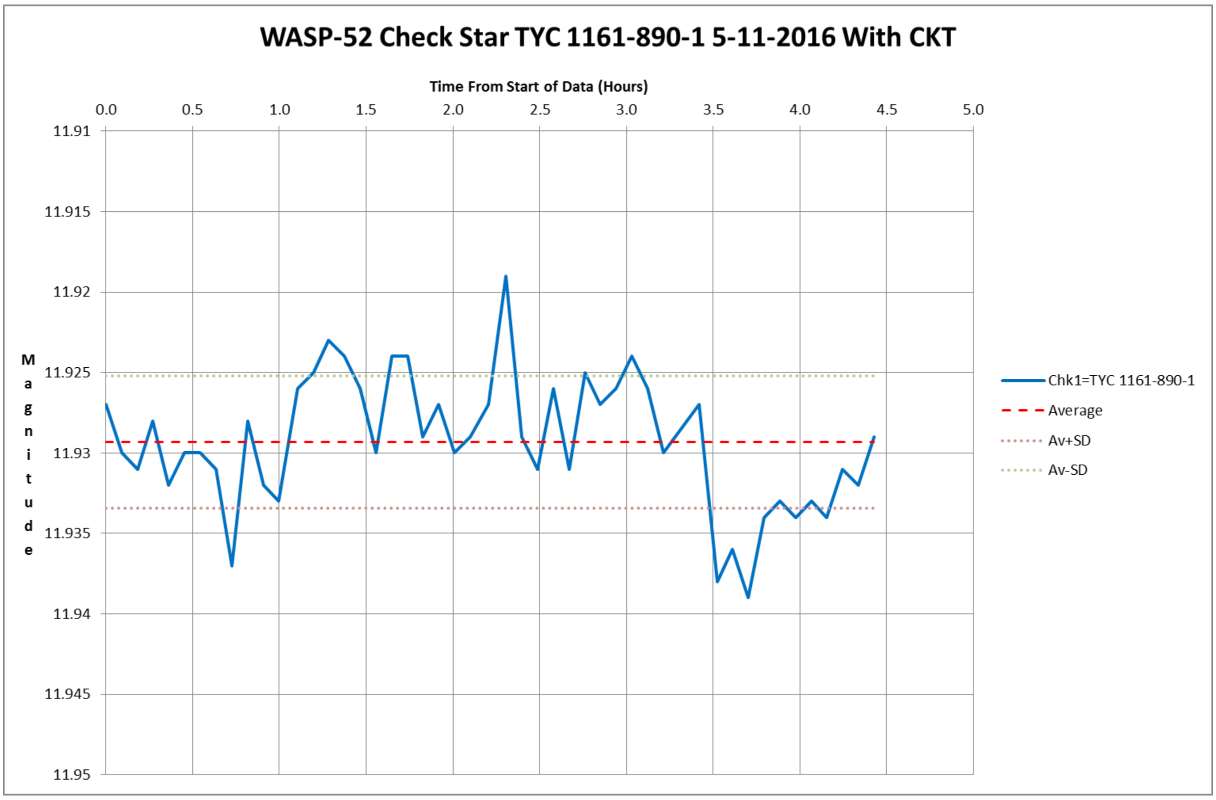


**Figure 37 WASP-52 Check Star TYC 1161-890-1 of 5-11-2016 by CKT Telescope**

## Appendix H

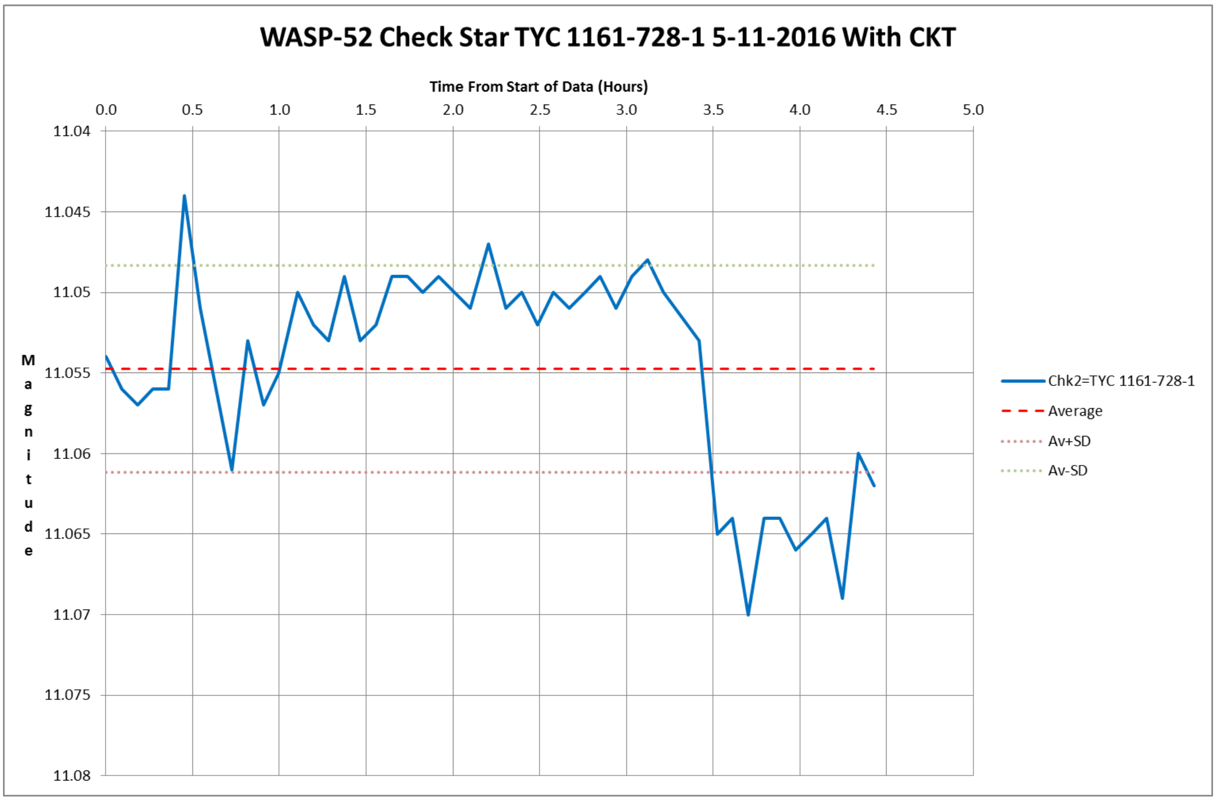


**Figure 38 WASP-52 Check Star TYC 1161-728-1 of 5-11-2016 by CKT Telescope**

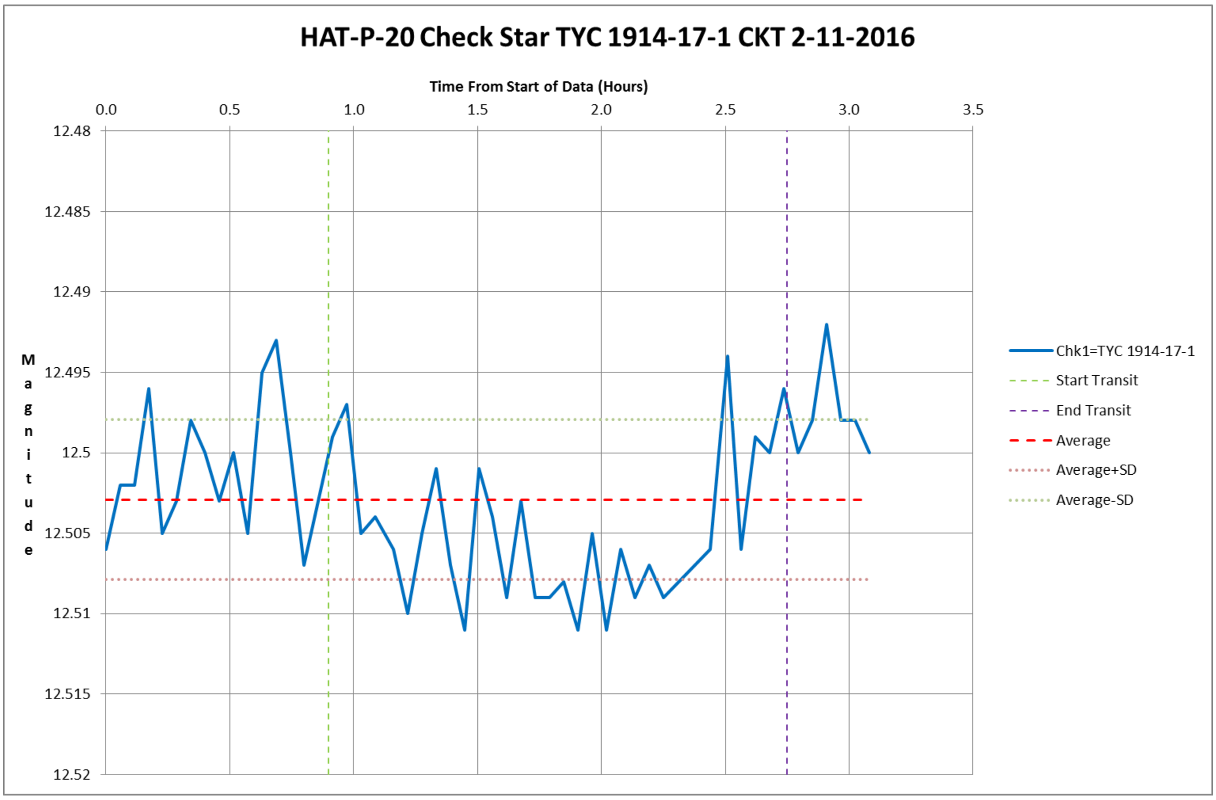


**Figure 39 HAT-P-20 Check Star TYC 1914-17-1 of 2-11-2016 by CKT Telescope**

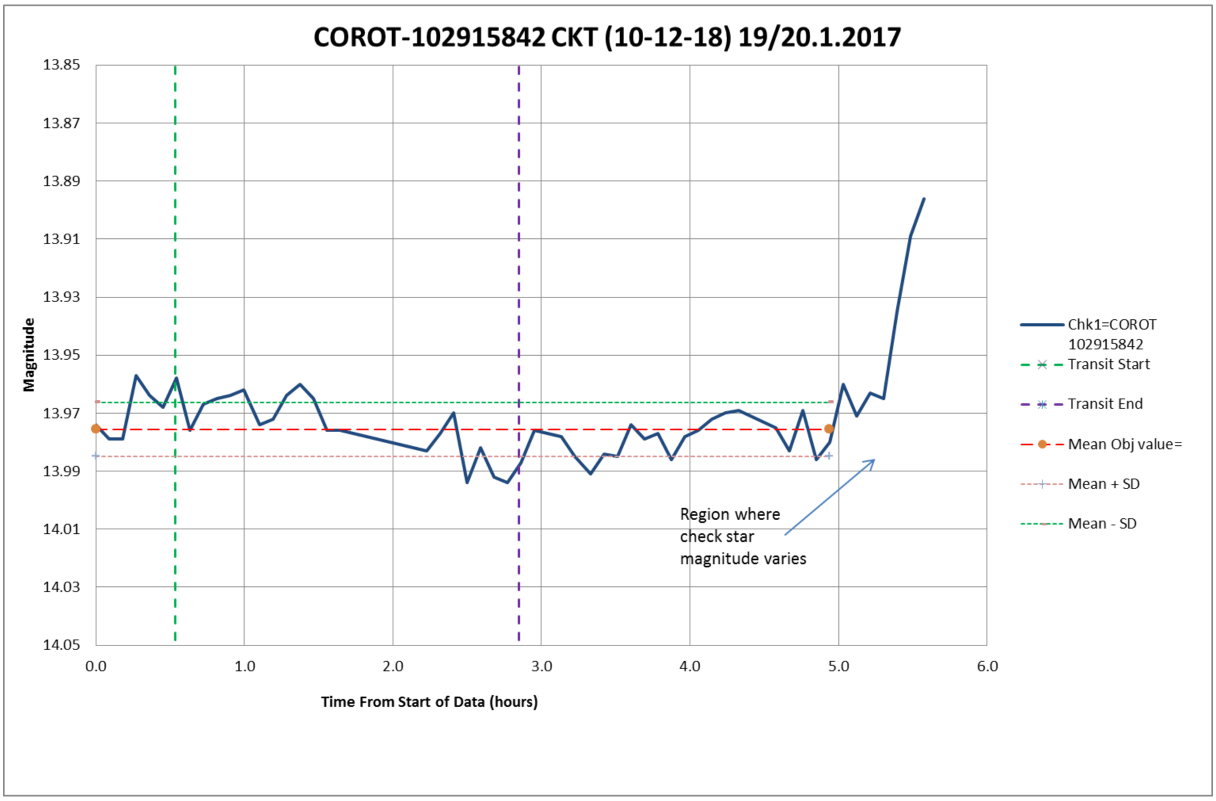


**Figure 40 COROT-1 Check Star COROT-102915842 of 19/20-1-2017 by CKT Telescope**

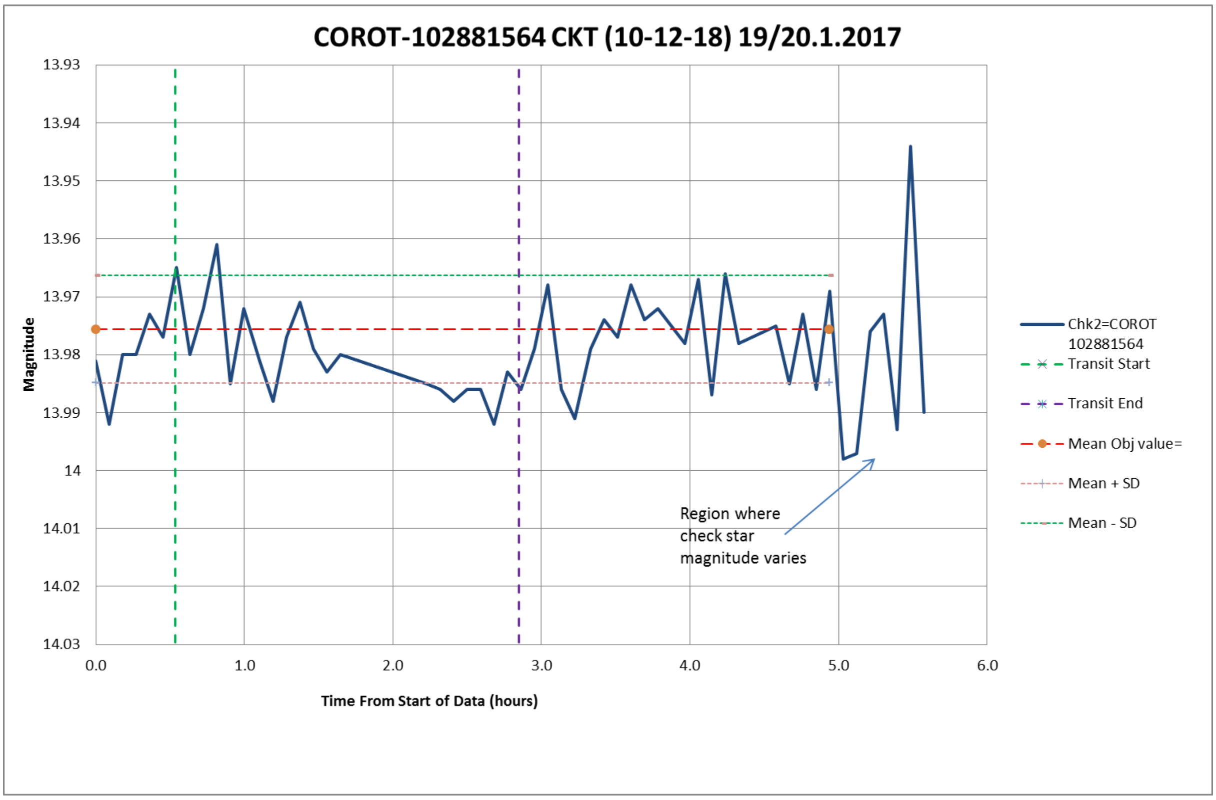


**Figure 41 COROT-1 Check Star COROT-102881564 of 19/20-1-2017 by CKT Telescope**

## Appendix H

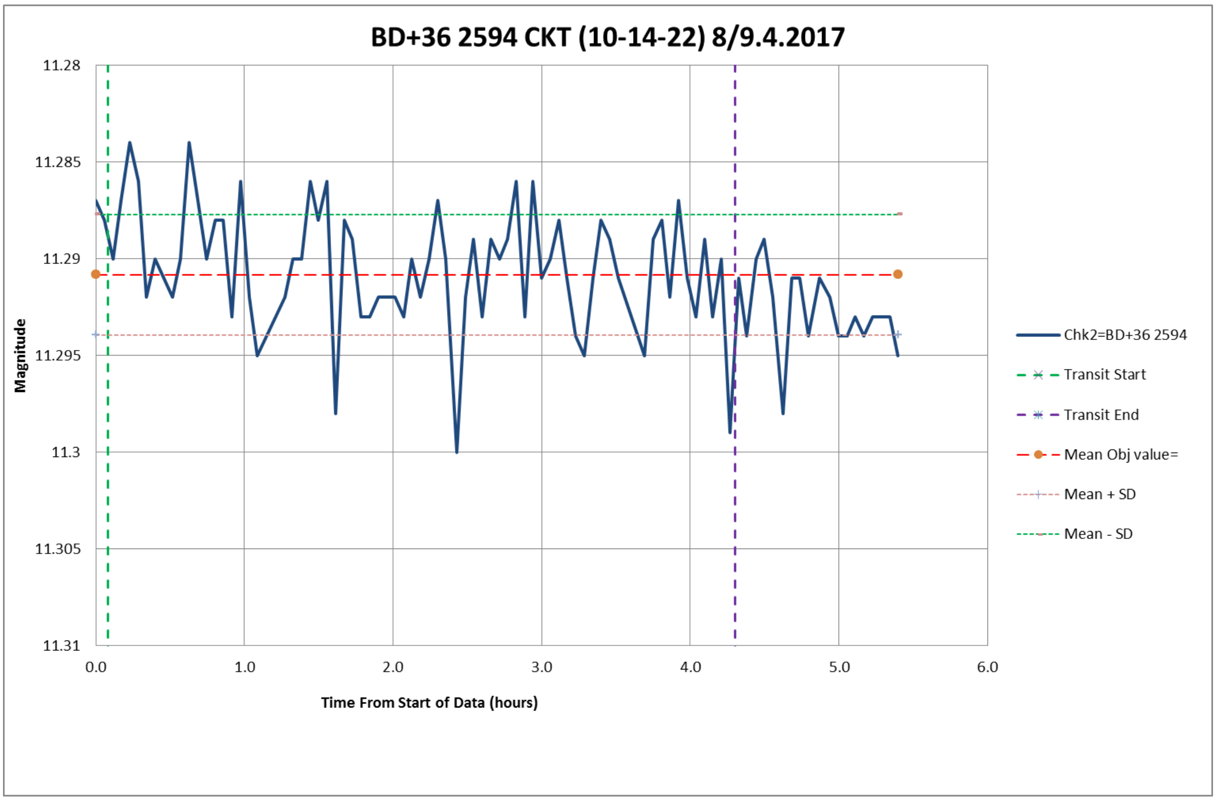


**Figure 42 HAT-P-4 Check Star BD+36 2594 of 8/9-4-2017 by CKT Telescope**

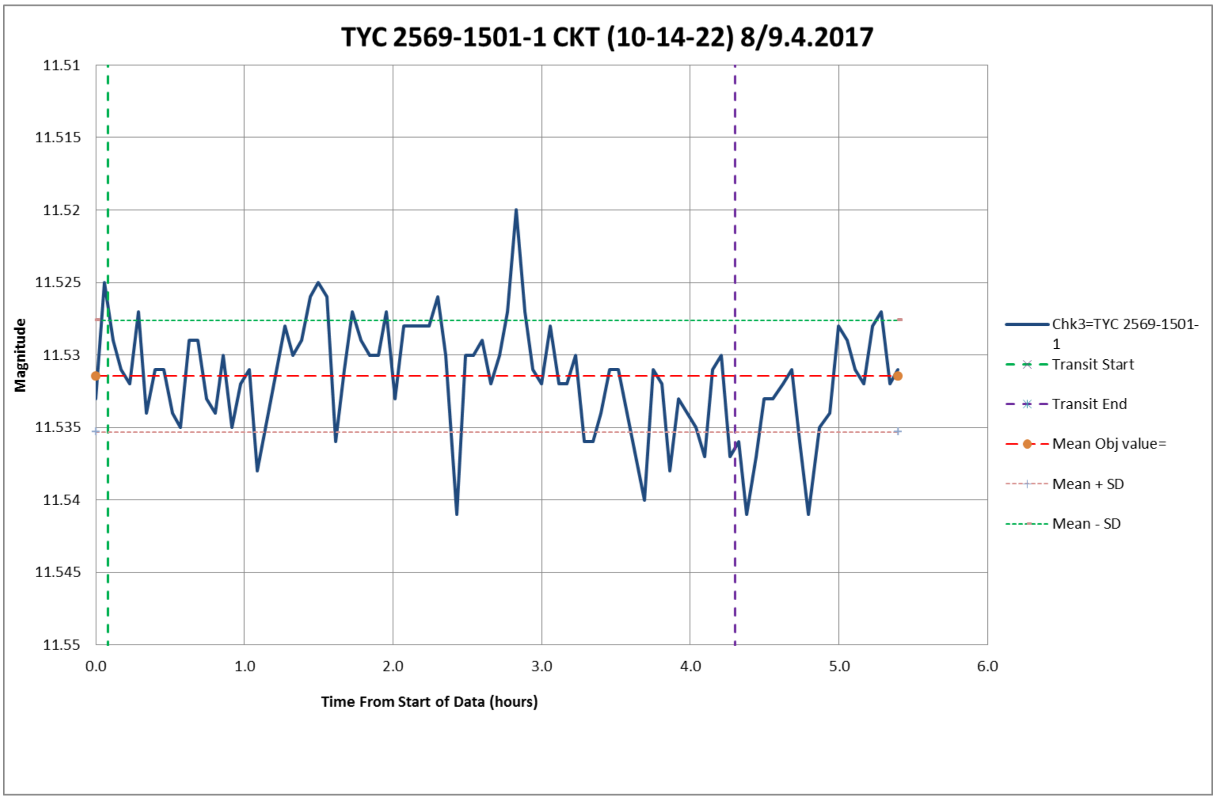


**Figure 43 HAT-P-4 Check Star TYC 2569-1501-1 of 8/9-4-2017 by CKT Telescope**

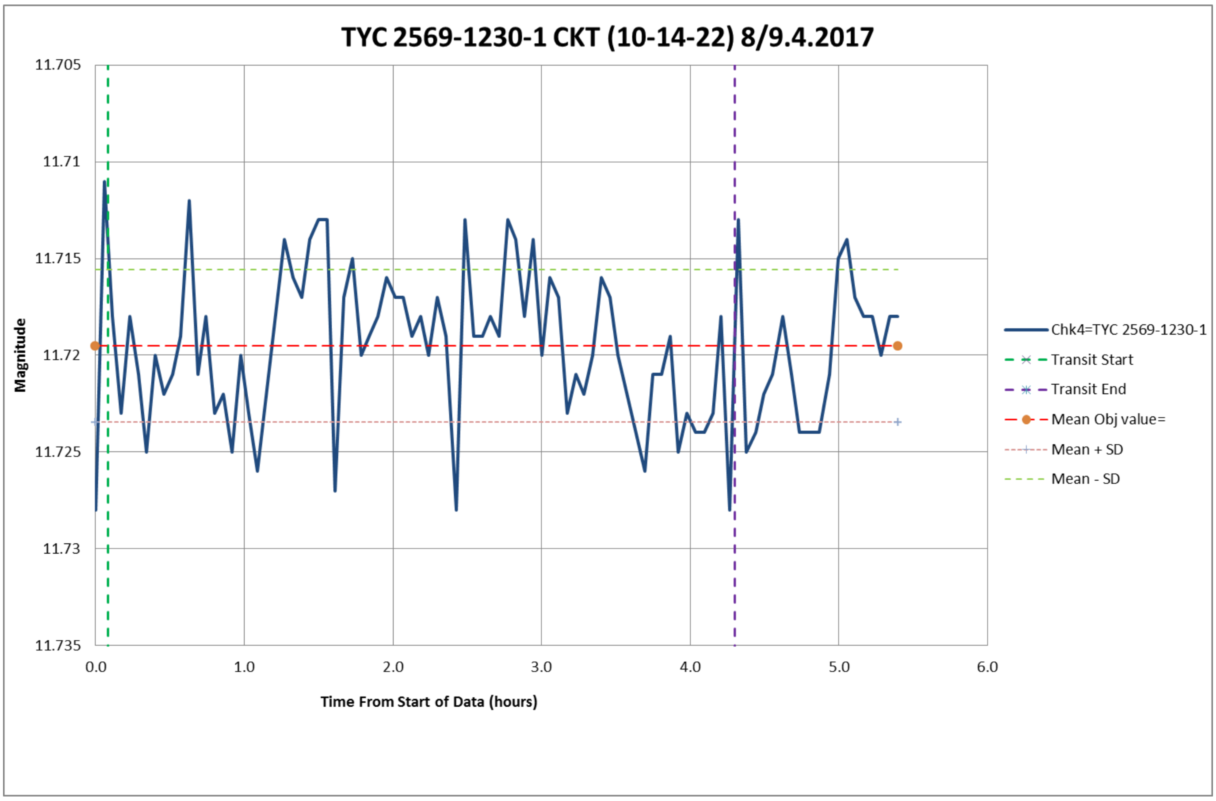


**Figure 44 HAT-P-4 Check Star TYC 2569-1230-1 of 8/9-4-2017 by CKT Telescope**

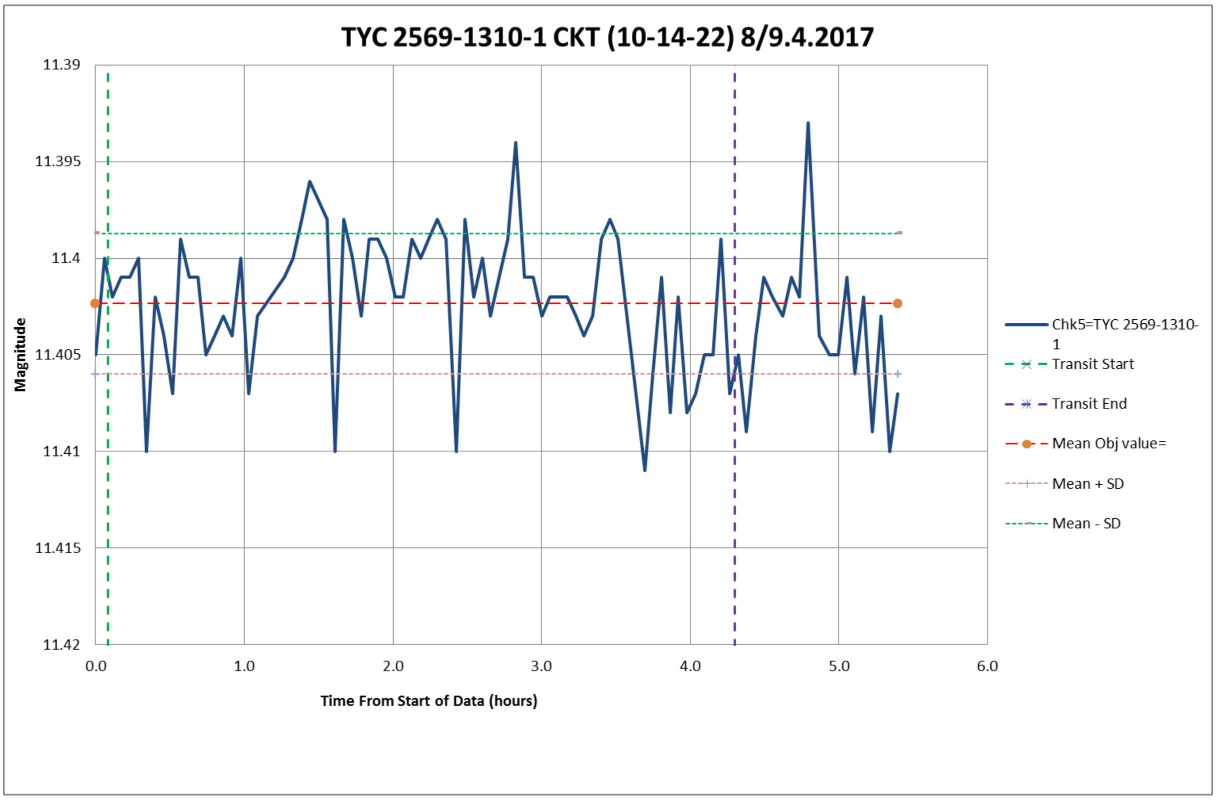


**Figure 45 HAT-P-4 Check Star TYC 2569-1310-1 of 8/9-4-2017 by CKT Telescope**

## Appendix H

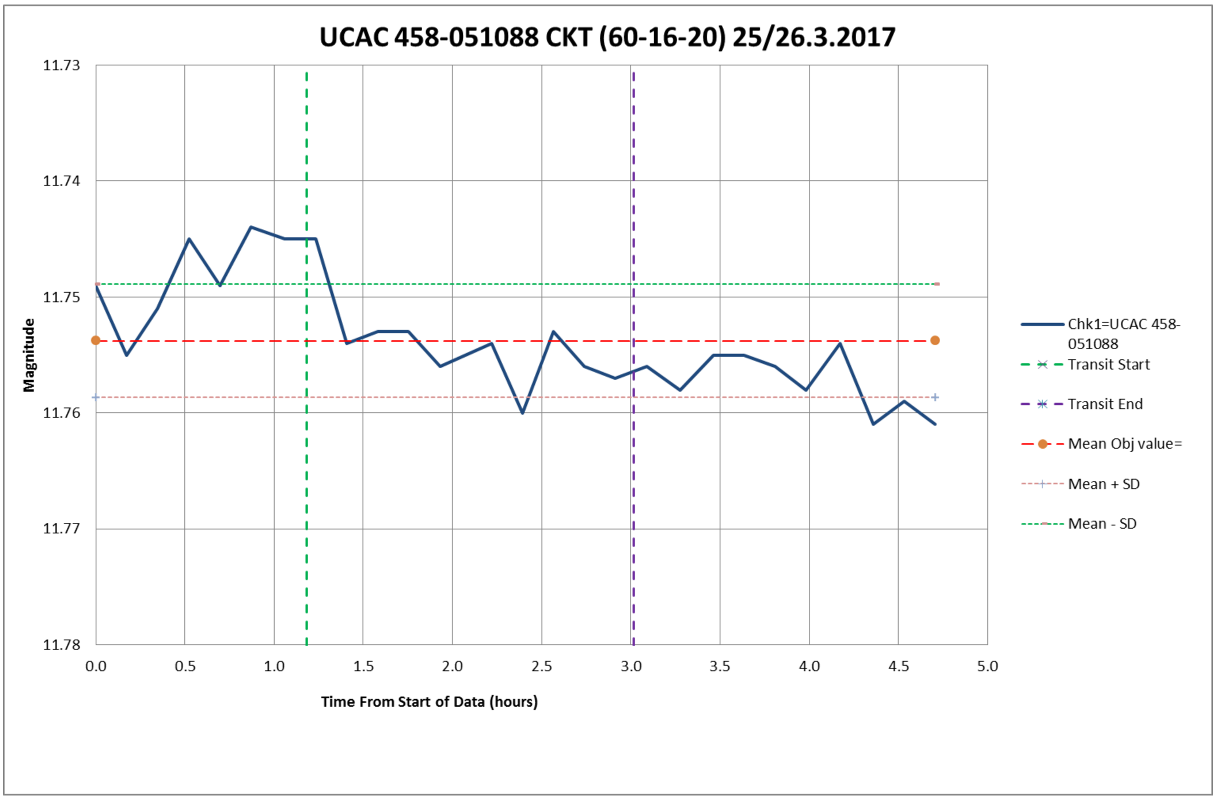


**Figure 46 WD 1145+017 Check Star UCAC4 458-051088 of 25/26-3-2017 by CKT Telescope**

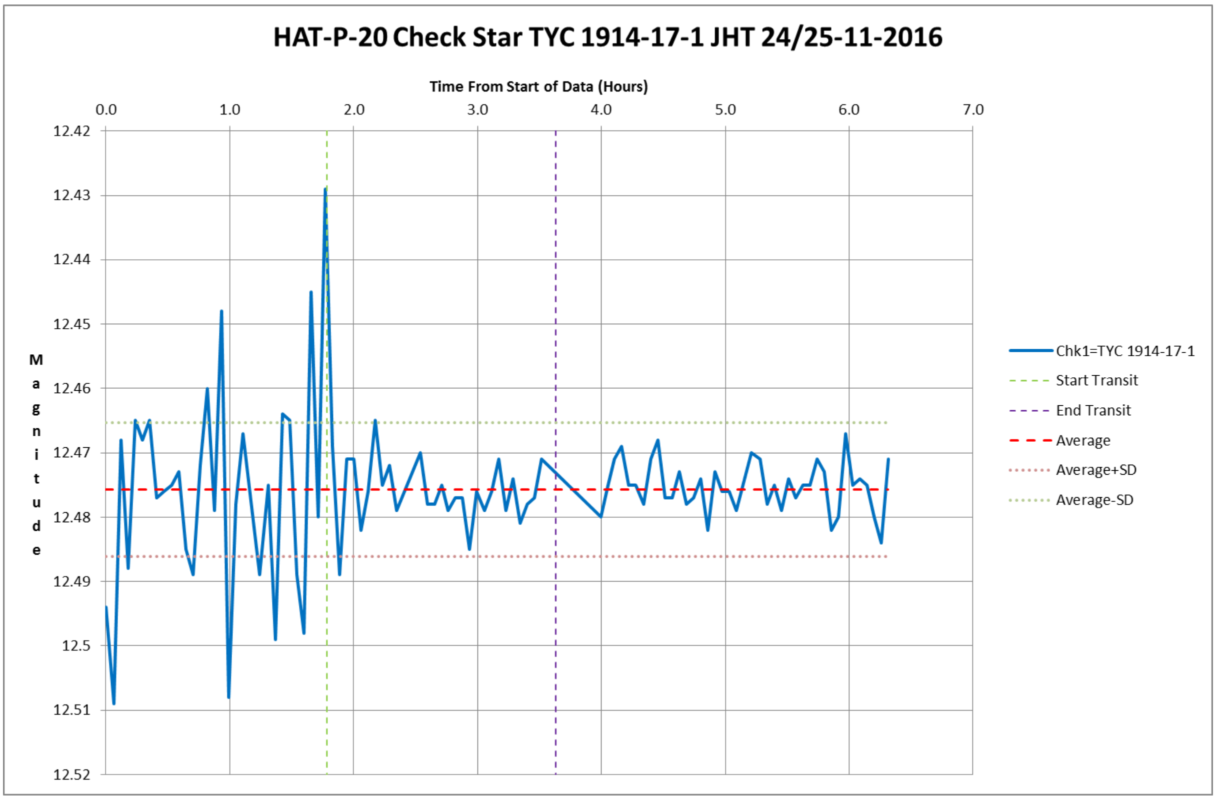


**Figure 47 HAT-P-20 Check Star TYC 1914-17-1 of 24/25-11-2016 by JHT Telescope**

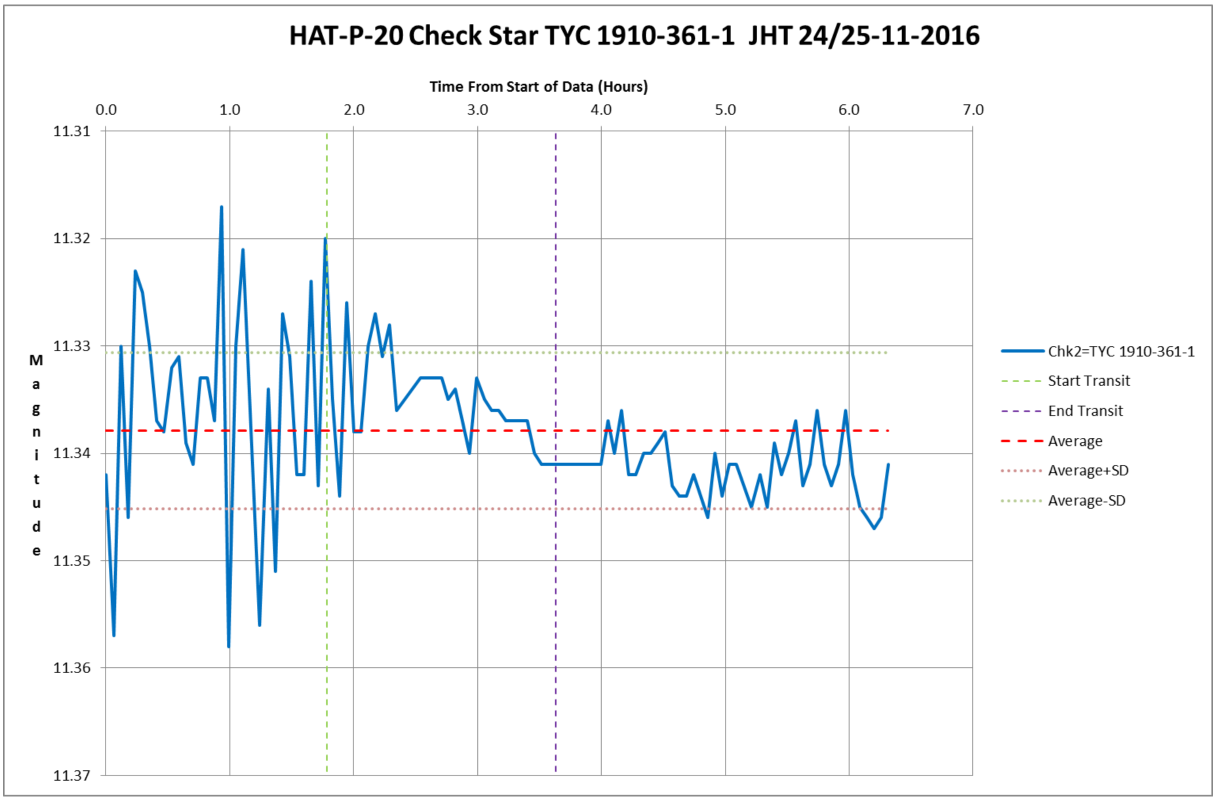


**Figure 48 HAT-P-20 Check Star TYC 1910-361-1 of 24/25-11-2016 by JHT Telescope**

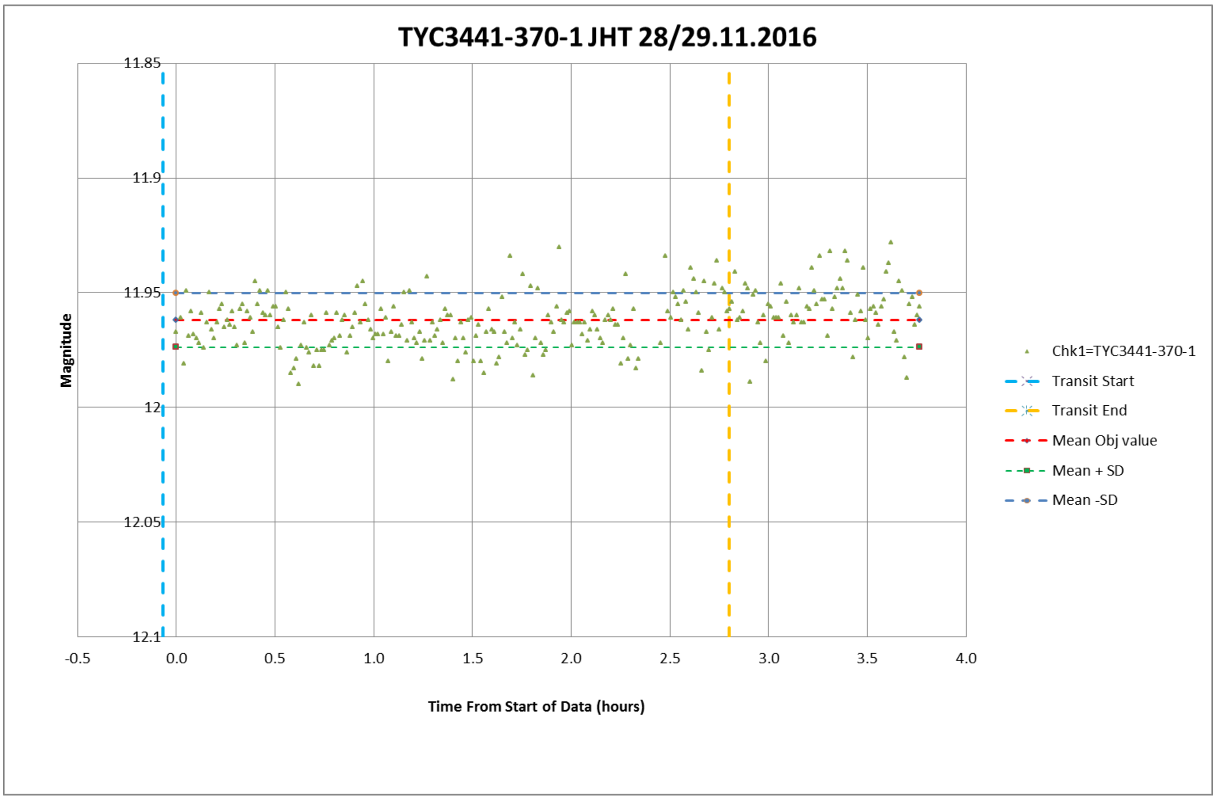


**Figure 49 HAT-P-22 Check Star TYC3441-370-1 of 28/29-11-2016 by JHT Telescope**

## Appendix H

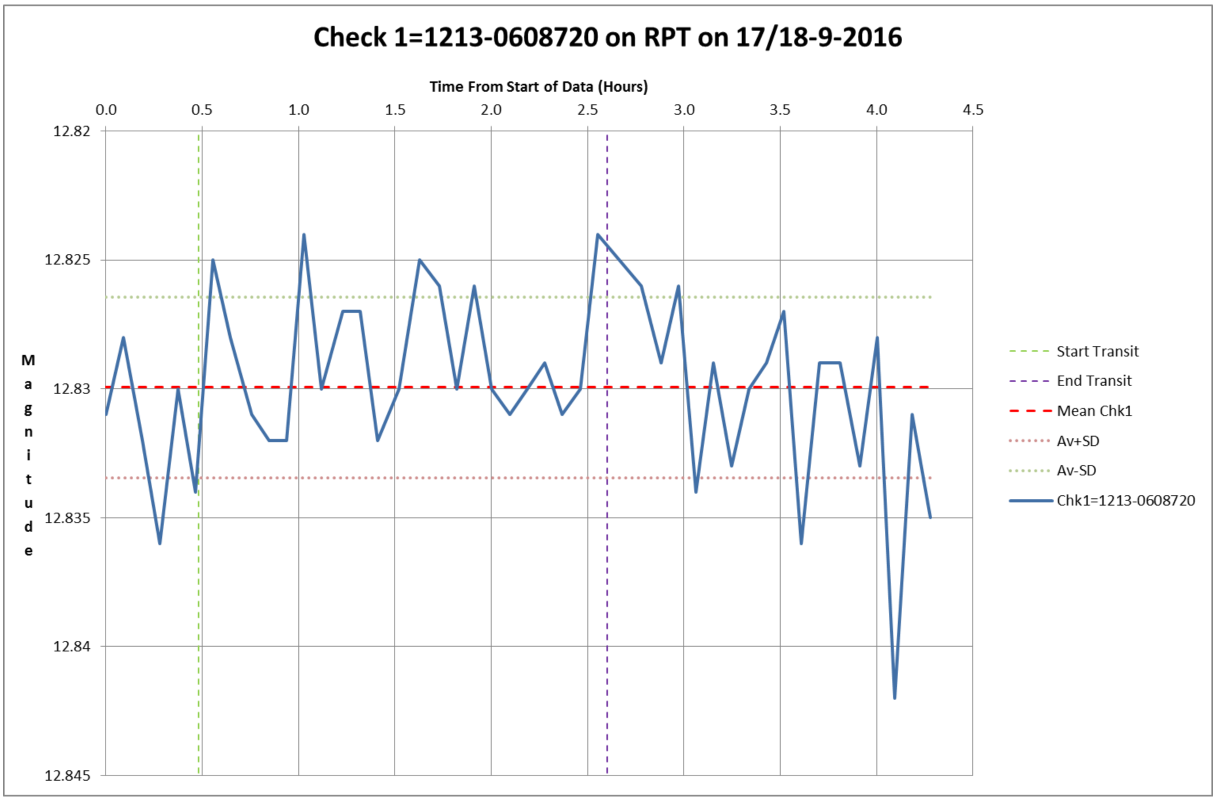


**Figure 50 WASP-10 Check Star 1213-0608720 of 17/18-10-2016 by RPT Telescope**

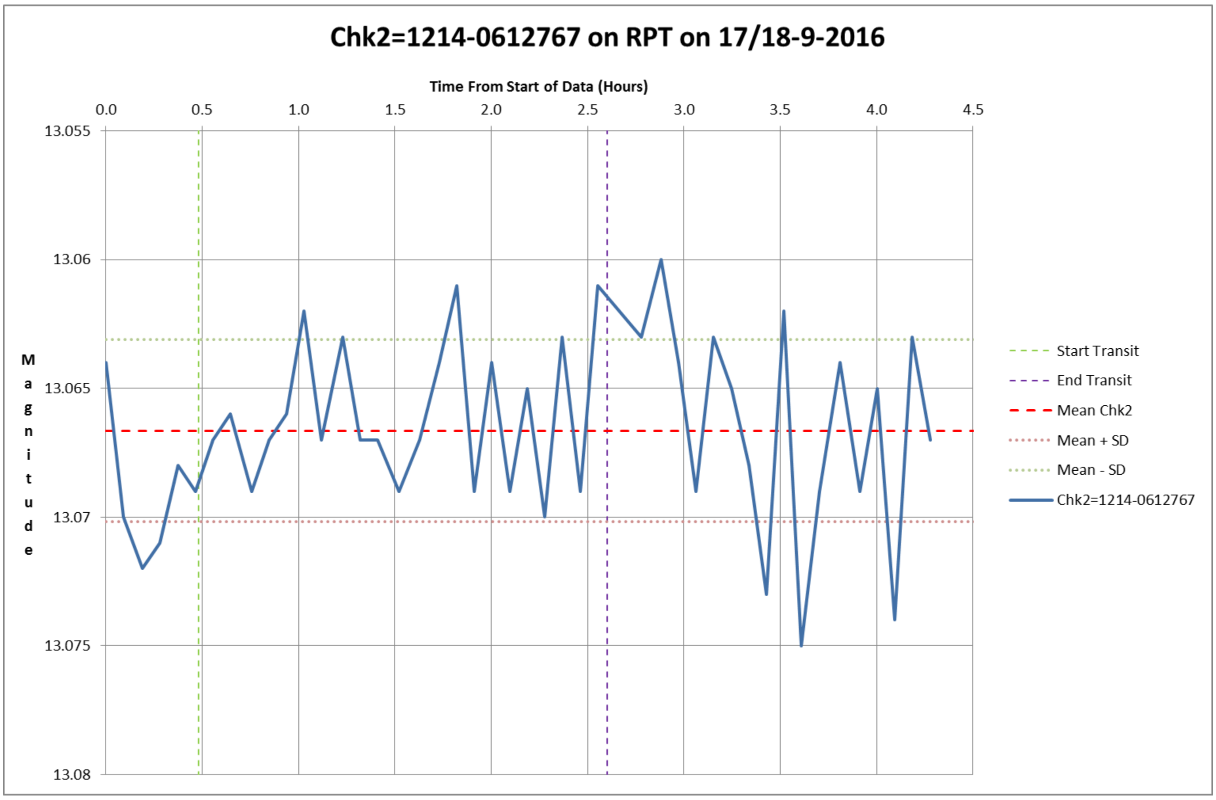


**Figure 51 WASP-10 Check Star 1214-0612767of 17/18-10-2016 by RPT Telescope**

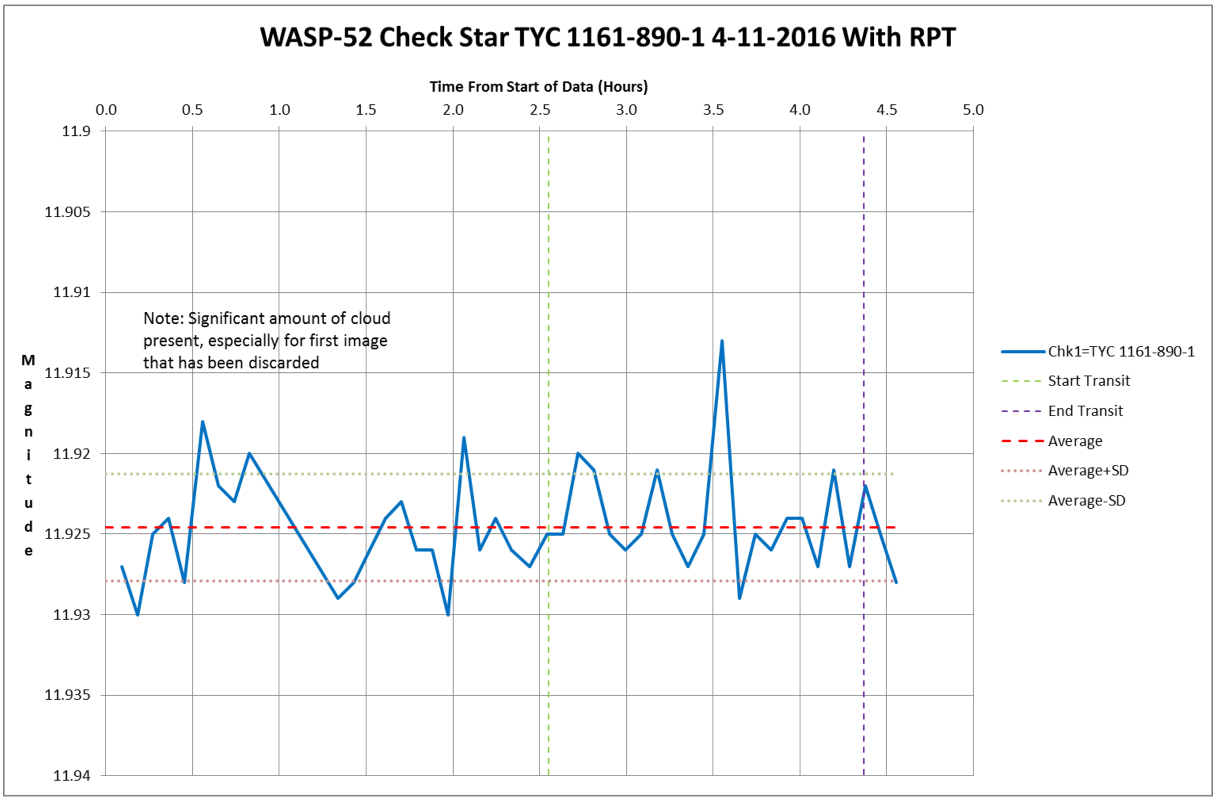


Figure 52 WASP-52 Check Star TYC 1161-890-1 of 4-11-2016 by RPT Telescope

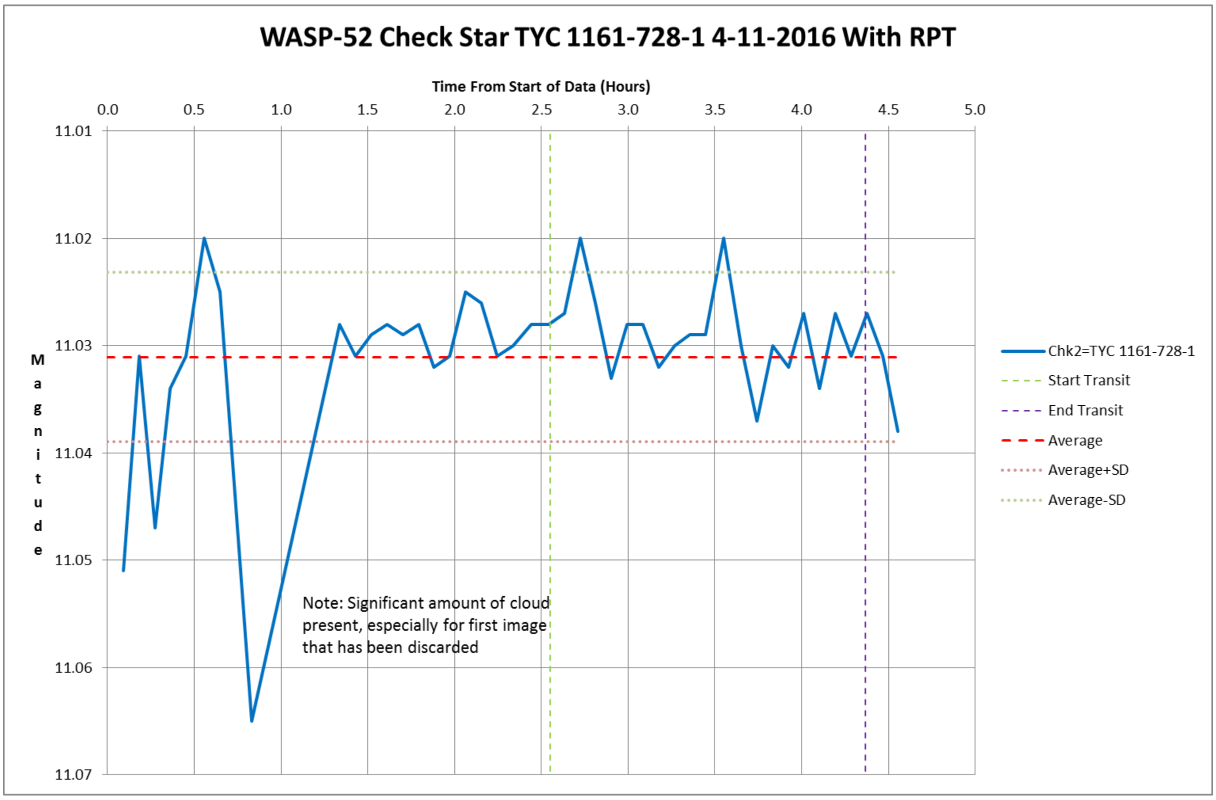


Figure 53 WASP-52 Check Star TYC 1161-728-1 of 4-11-2016 by RPT Telescope

## Appendix H

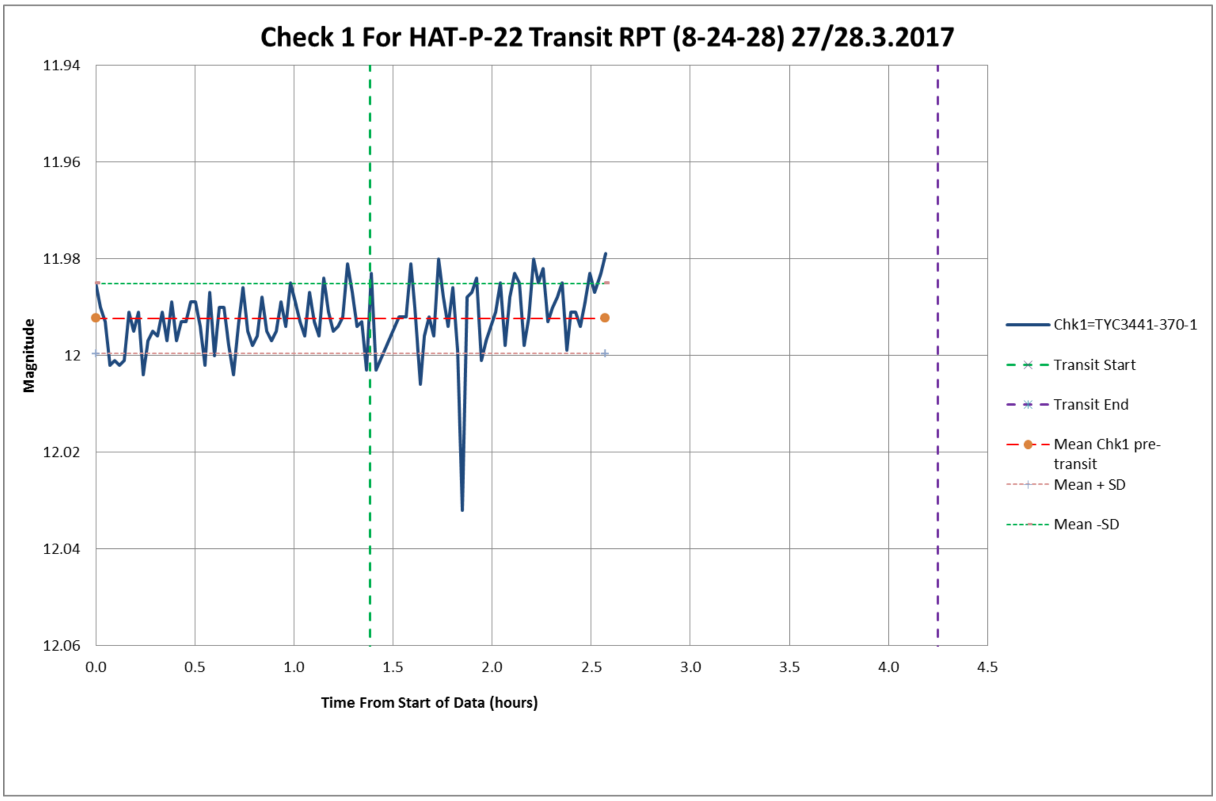


**Figure 54 HAT-P-22 Check Star TYC3441-370-1 of 27/28-3-2017 by RPT Telescope**

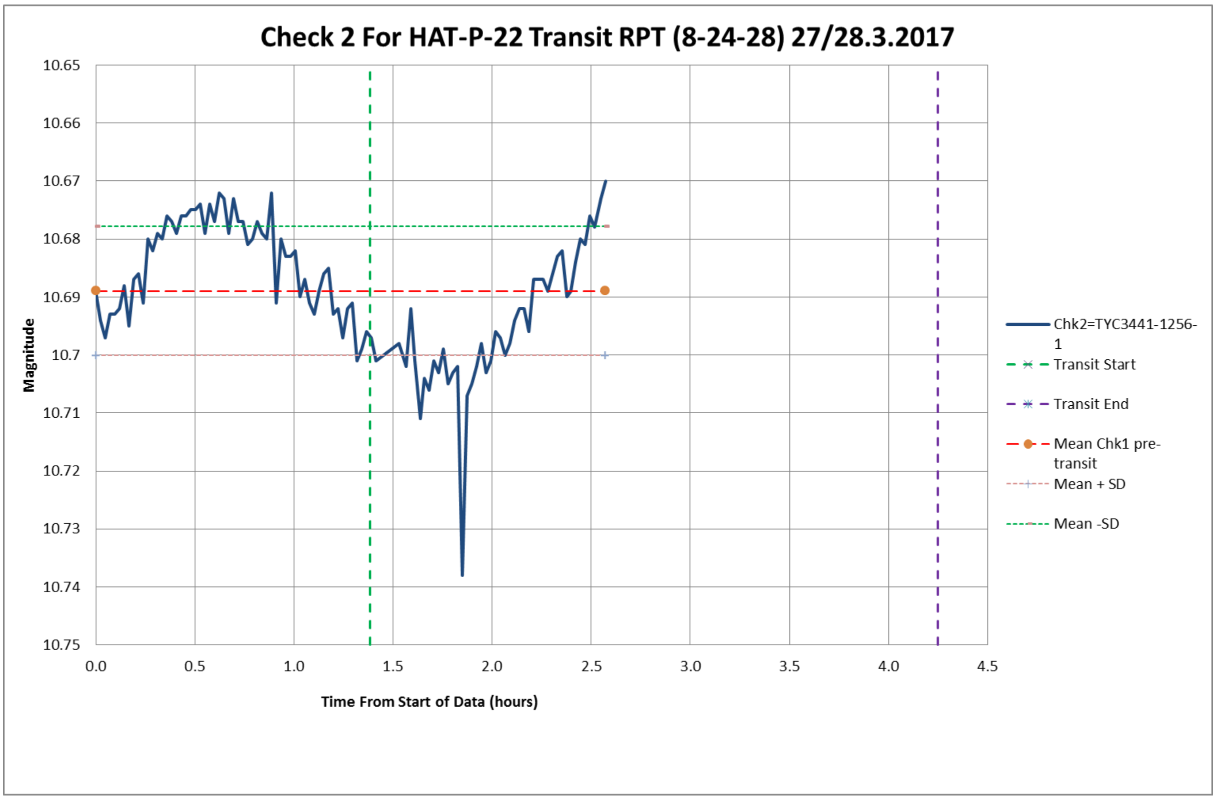


**Figure 55 HAT-P-22 Check Star TYC3441-1256-1 of 27/28-3-2017 by RPT Telescope**

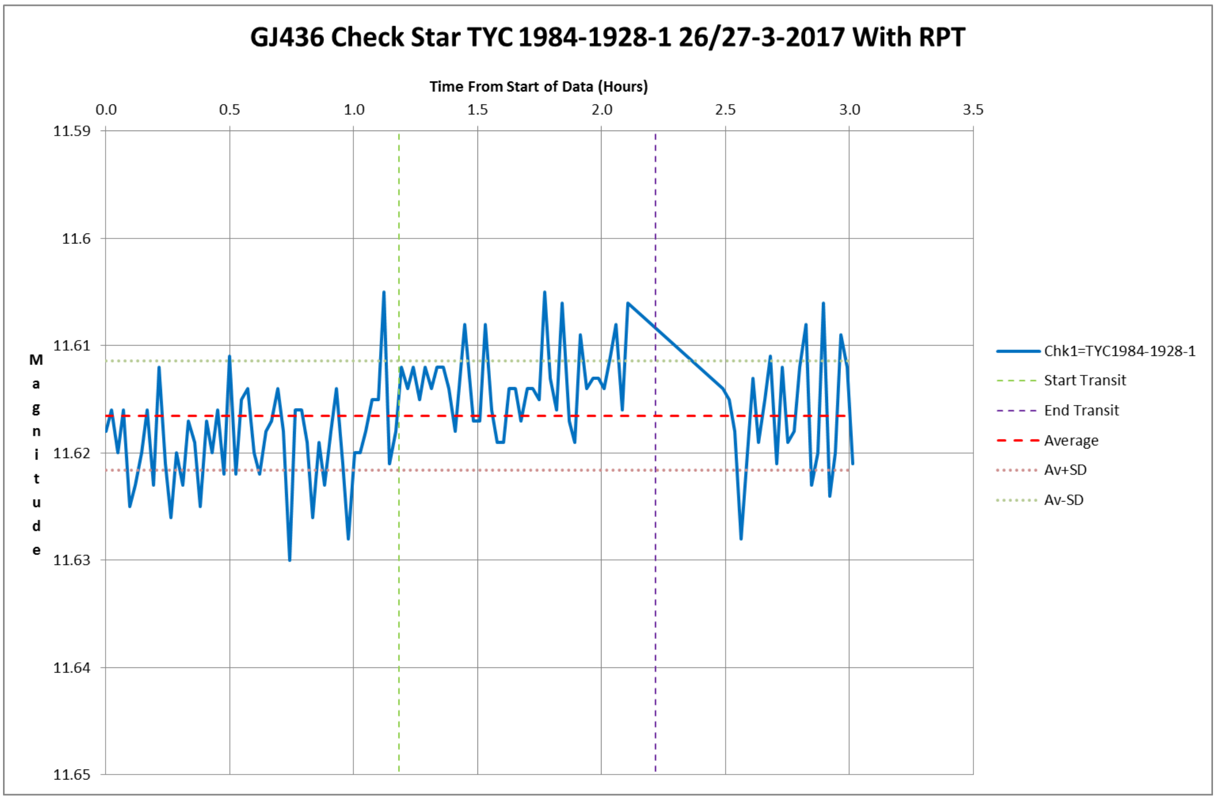


Figure 56 GJ 436 Check Star TYC 1984-1928-1 of 26/27-3-2017 by RPT Telescope

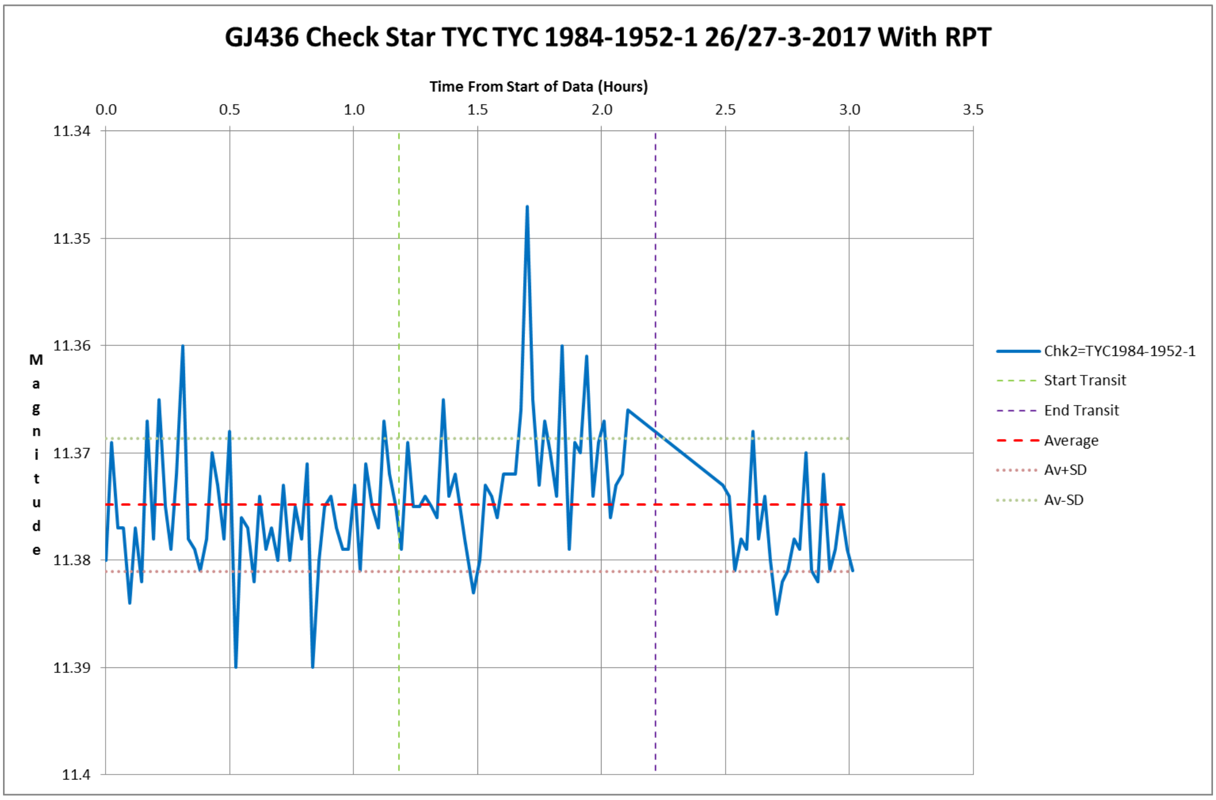


Figure 57 GJ 436 Check Star TYC 1984-1952-1 of 26/27-3-2017 by RPT Telescope

## Appendix H

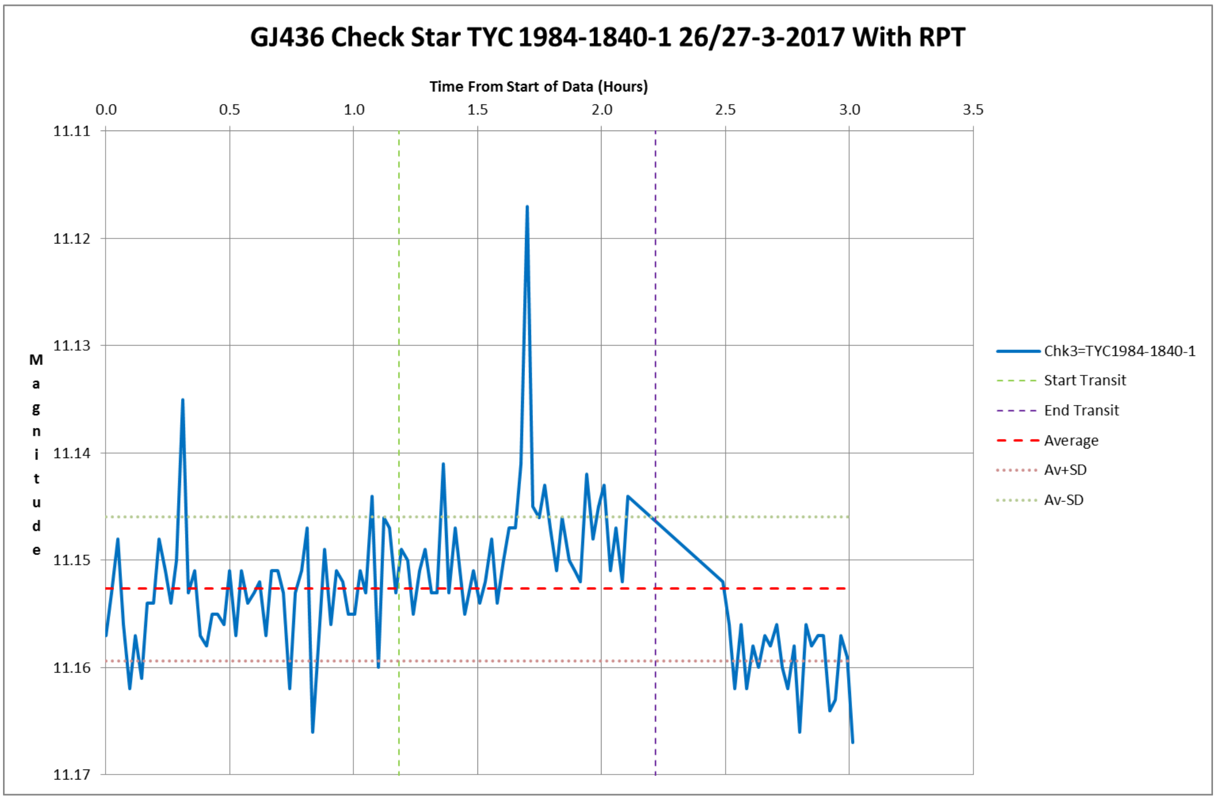


**Figure 58 GJ 436 Check Star TYC 1984-1840-1 of 26/27-3-2017 by RPT Telescope**

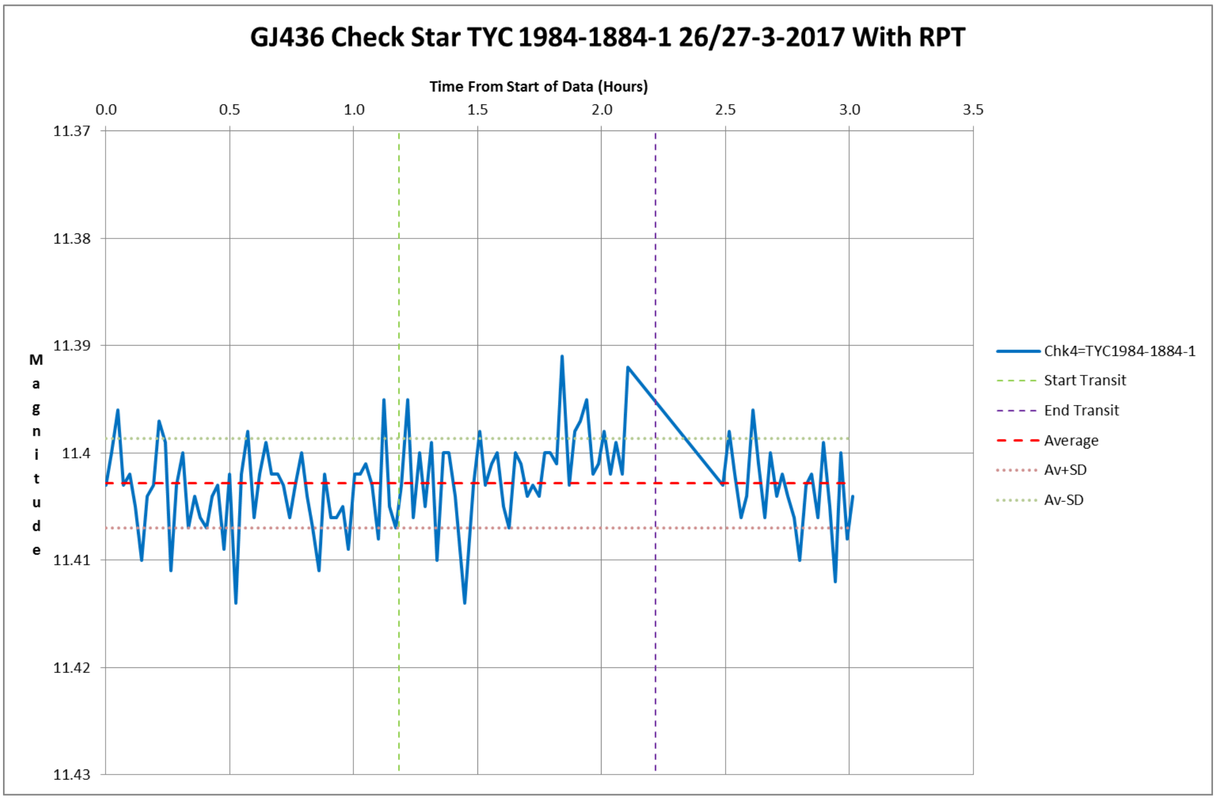


**Figure 59 GJ 436 Check Star TYC 1984-1840-1 of 26/27-3-2017 by RPT Telescope**

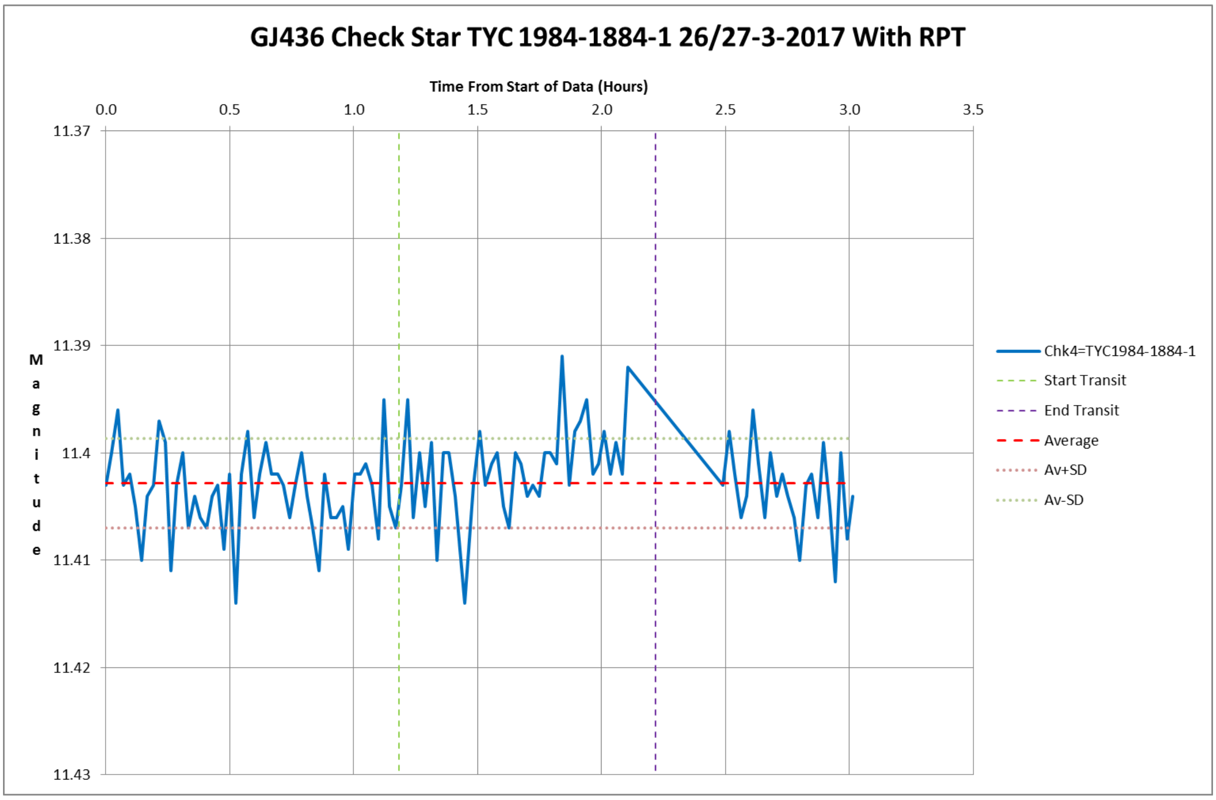


Figure 60 GJ 436 Check Star TYC 1984-1884-1 of 26/27-3-2017 by RPT Telescope

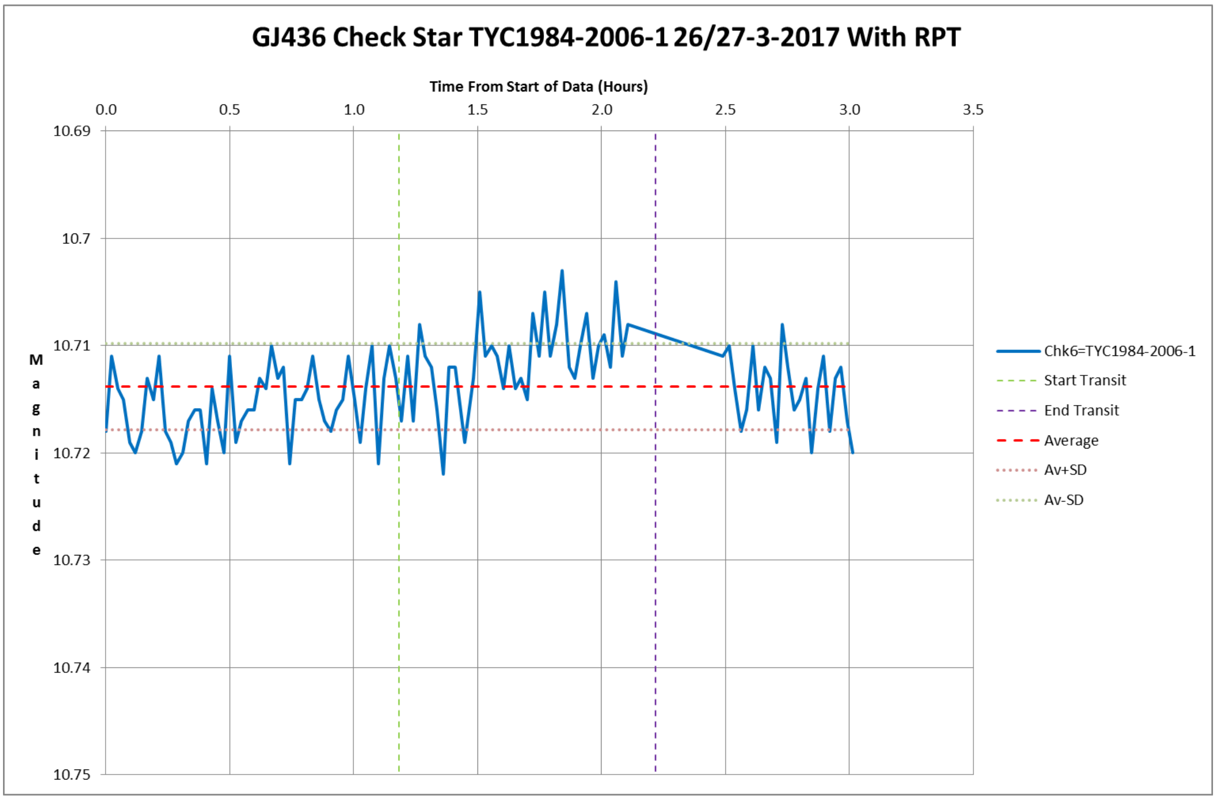


Figure 61 GJ 436 Check Star TYC 1984-2008-1 of 26/27-3-2017 by RPT Telescope

# Appendix I Light Curves with Transits of Exo-Planets

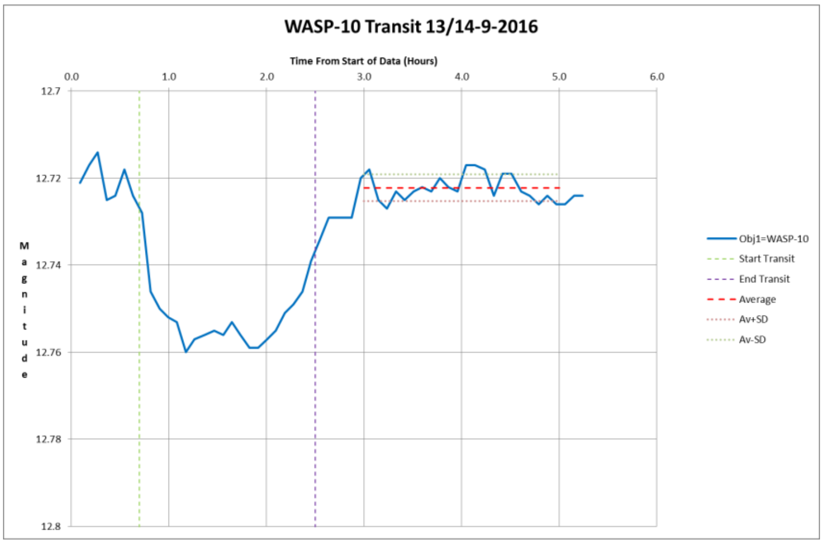


**Figure 62 WASP-10 Transit of 13/14-9-2016 by CKT Telescope**

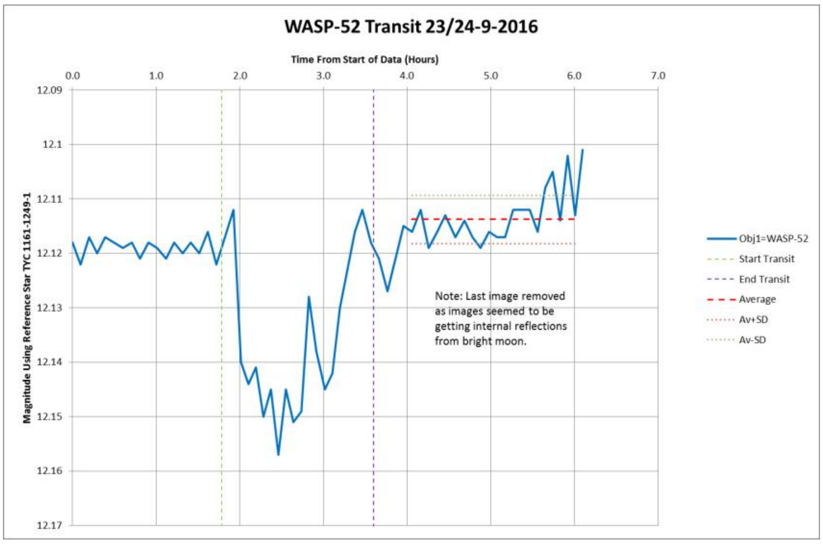


**Figure 63 WASP-52 Transit of 23/24-9-2016 by CKT Telescope**

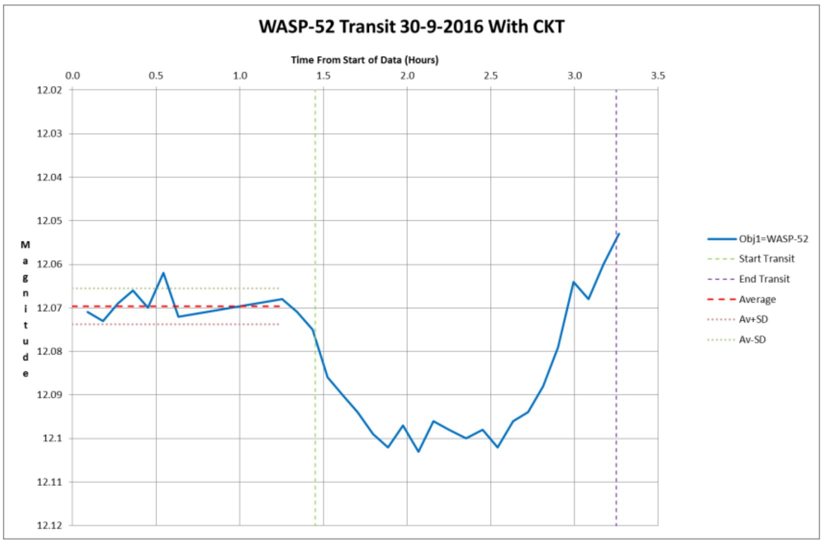


**Figure 64 WASP-52 Transit of 30-9-2016 by CKT Telescope**

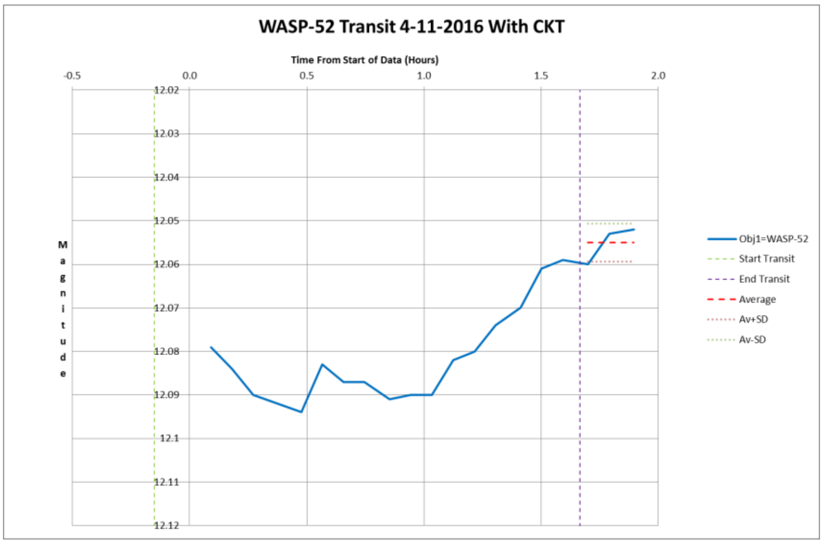


**Figure 65 WASP-52 Partial Transit of 4-11-2016 by CKT Telescope**

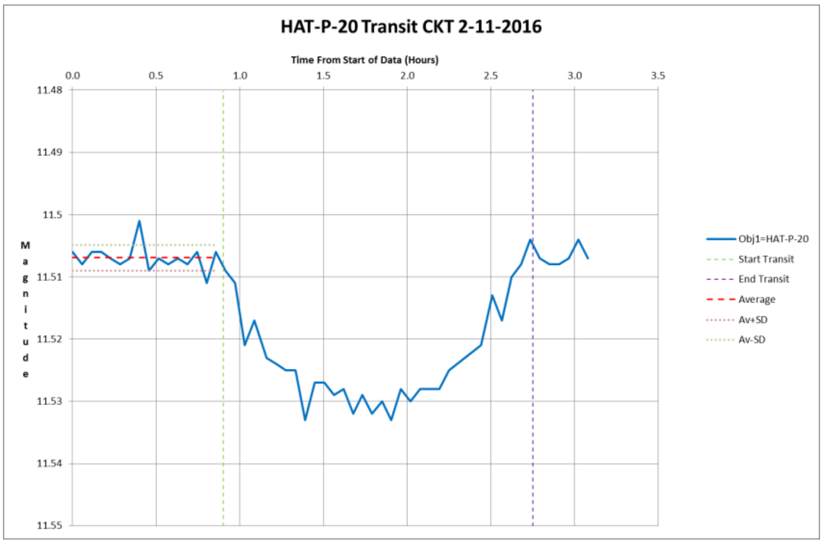


**Figure 66 HAT-P-20 Transit of 2-11-2016 by CKT Telescope**

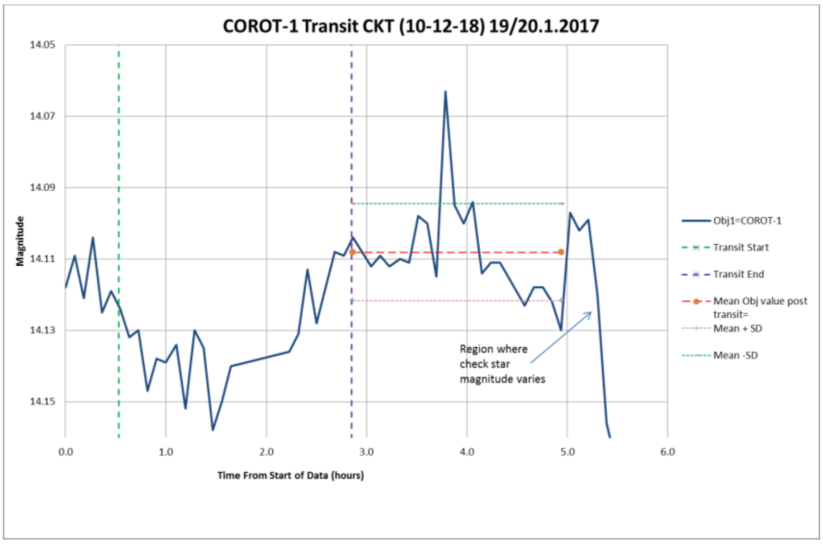


**Figure 67 COROT-1 Transit of 19/20-1-2017 by CKT Telescope**

## Appendix I

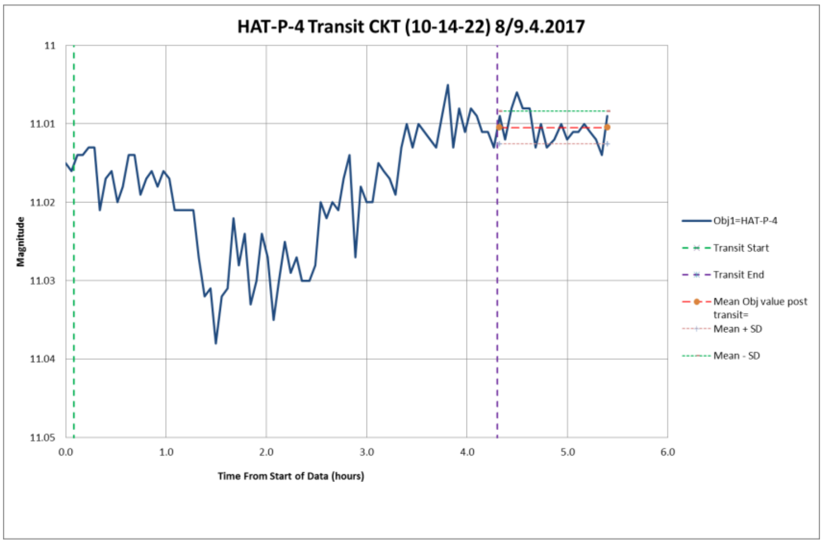


**Figure 68 HAT-P-4 Transit of 8/9-4-2017 by CKT Telescope**

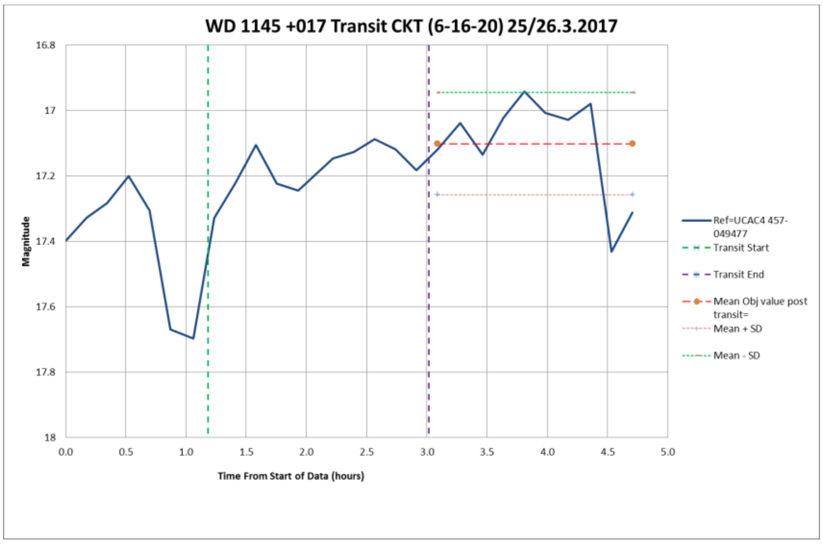


**Figure 69 WD 1145+017 Transit of 25/26-3-2017 by CKT Telescope**

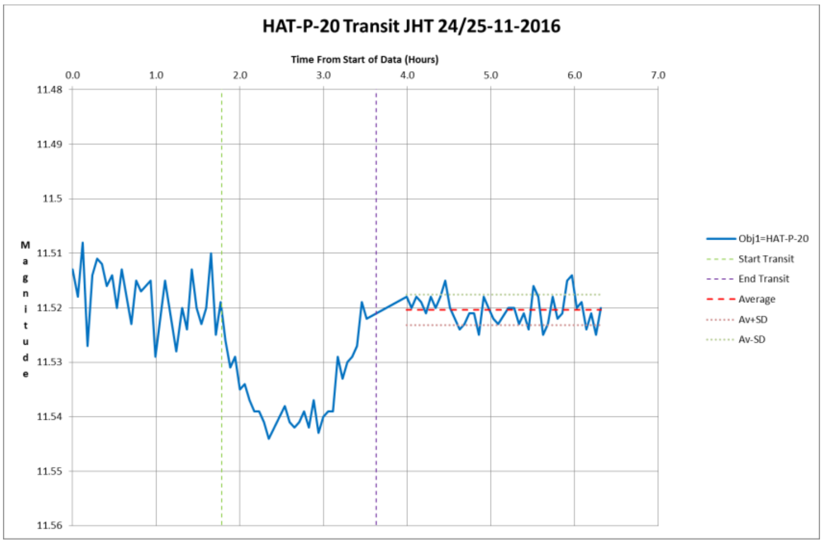


**Figure 70 HAT-P-20 Transit of 24/25-11-2016 by JHT Telescope**

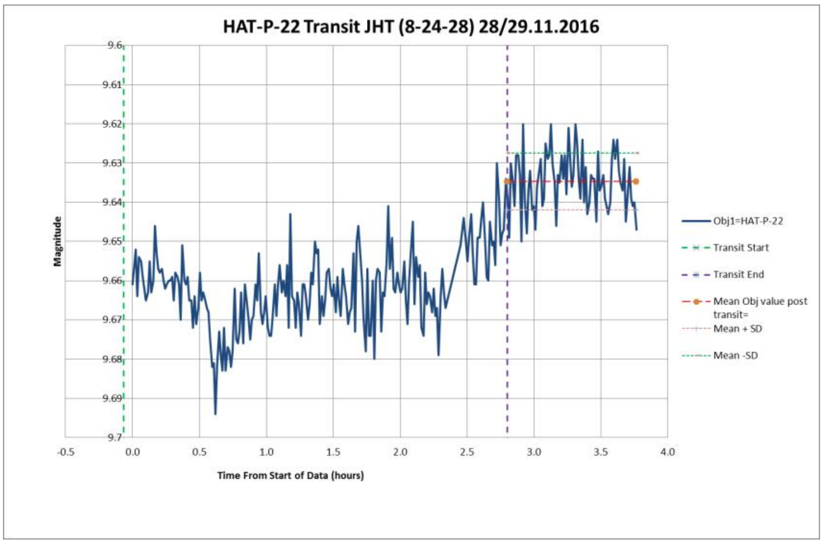


**Figure 71 HAT-P-22 Transit of 28/29-11-2016 by JHT Telescope**

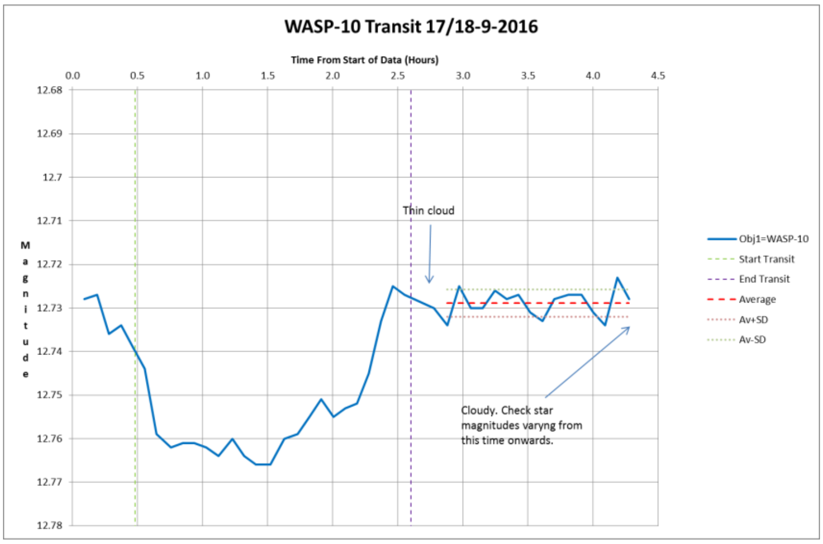


**Figure 72 WASP-10 Transit of 17/18-10-2016 by RPT Telescope**

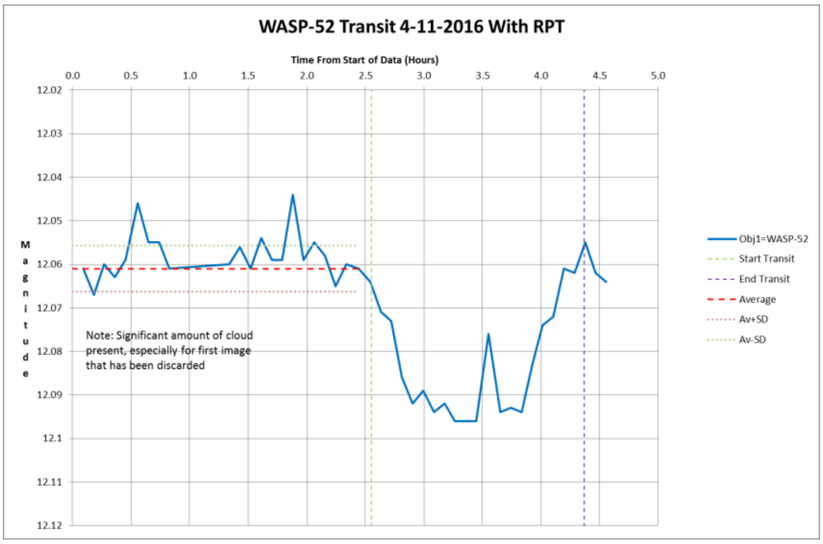


**Figure 73 WASP-52 Transit of 4-11-2016 by RPT Telescope**

## Appendix I

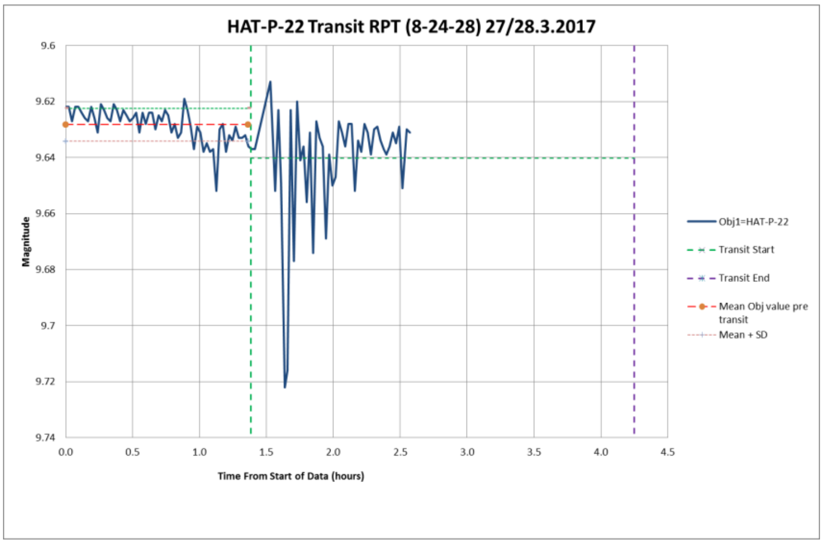


**Figure 74 HAT-P-22 Incomplete Transit of 27/28-3-2017 by RPT Telescope**

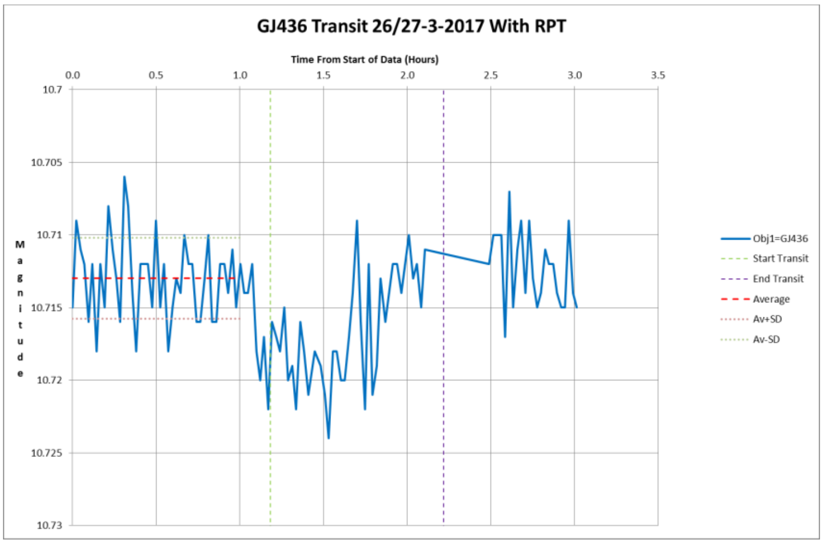


**Figure 75 GJ 436 Transit of 26/27-3-2017 by RPT Telescope**

# Appendix J Equation Fitted Exo-Planet Light Curves

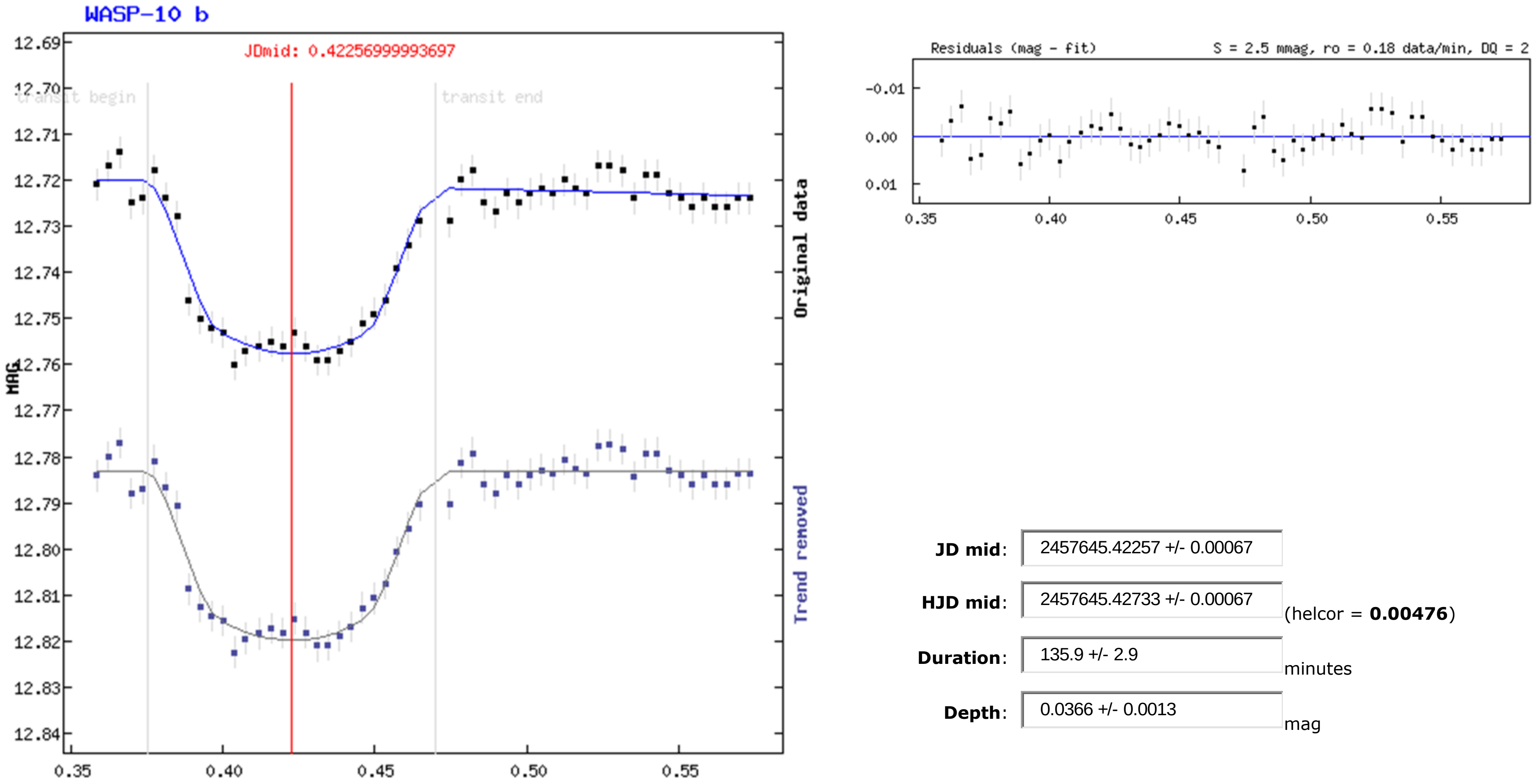


Figure 76 WASP-10 Transit of 13/14-10-2016 With CKT Telescope and Equation Fitting

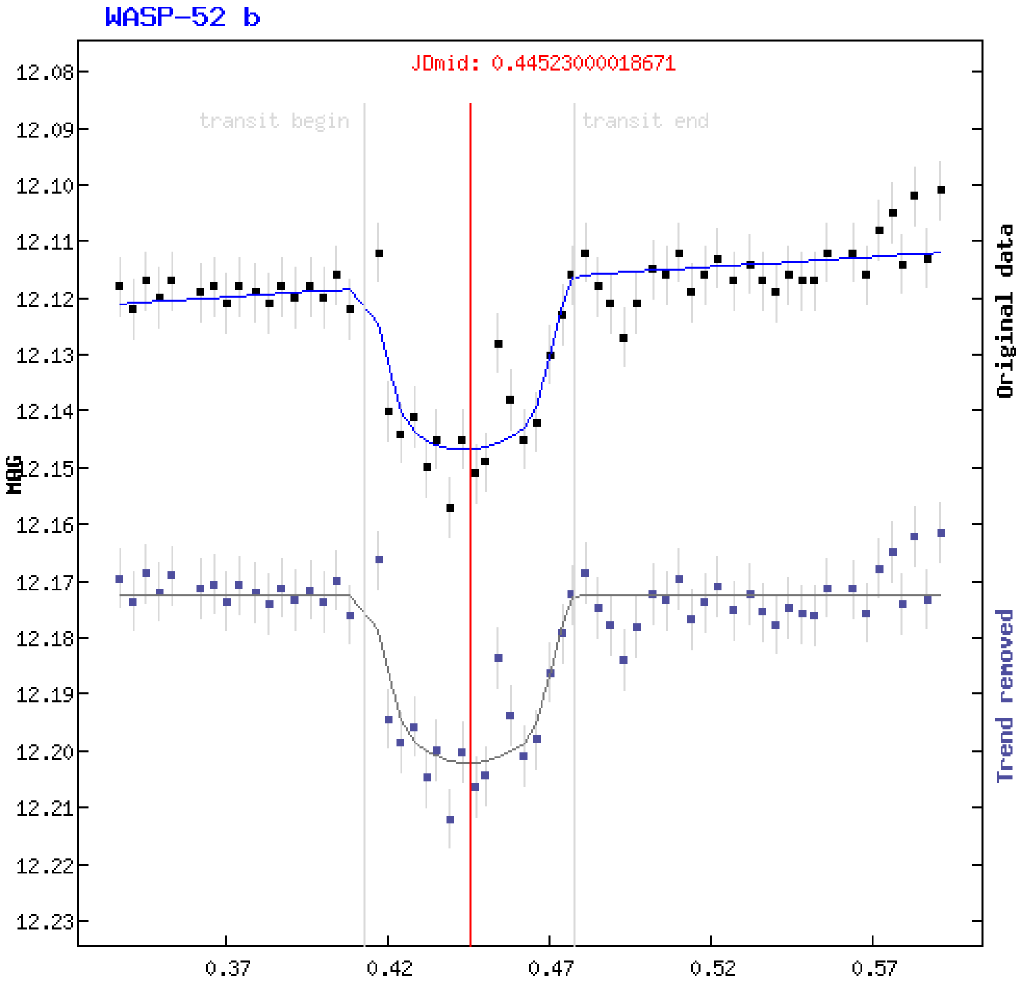


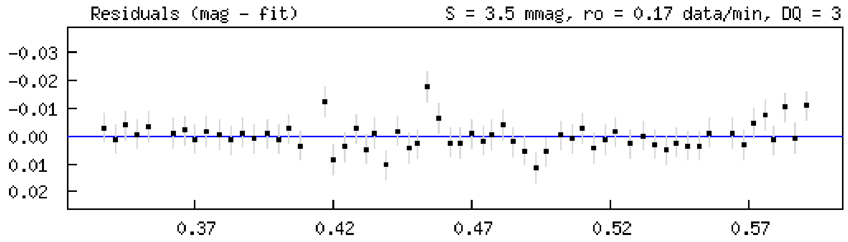


**JD mid**: 2457655.44523 +/- 0.00098

**HJD mid**: 2457655.45082 +/- 0.00098 (helcor = **0.00559**)

**Duration**: 93.2 +/- 4.0 minutes

**Depth**: 0.0296 +/- 0.0019 mag

**Figure 77 WASP-52 Transit of 23/24-9-2016 With CKT Telescope and Equation Fitting**

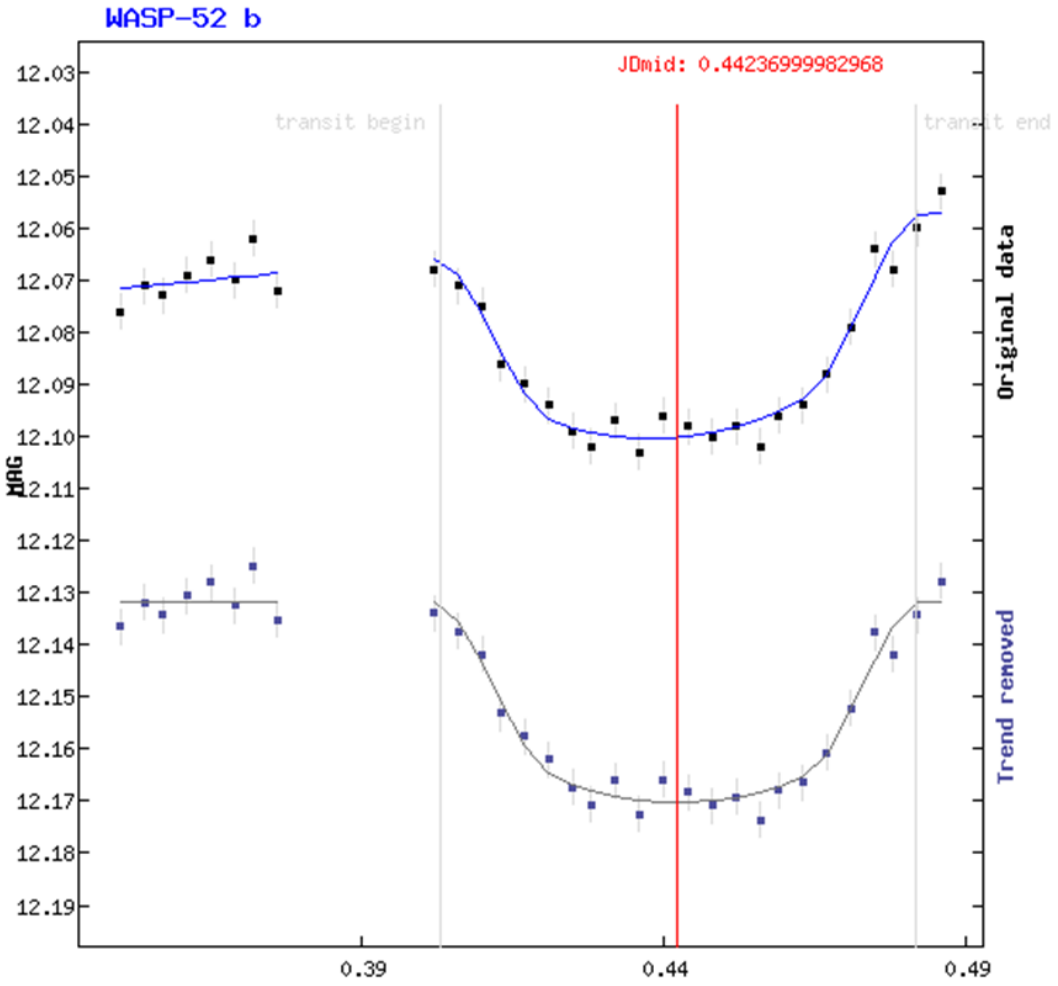


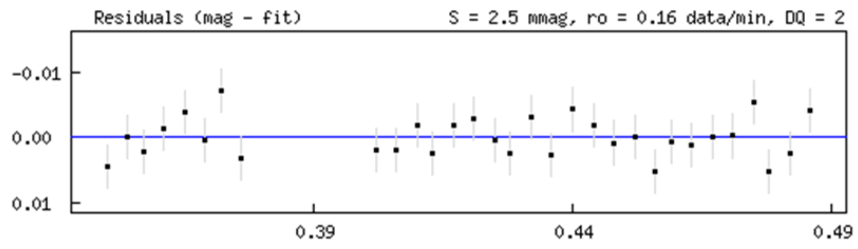


**JD mid**: 2457662.44237 +/- 0.00064

**HJD mid**: 2457662.44781 +/- 0.00064 (helcor = **0.00544**)

**Duration**: 113.6 +/- 2.7 minutes

**Depth**: 0.0383 +/- 0.0018 mag

**Figure 78 WASP-52 Transit of 30-9-2016 With CKT Telescope and Equation Fitting**

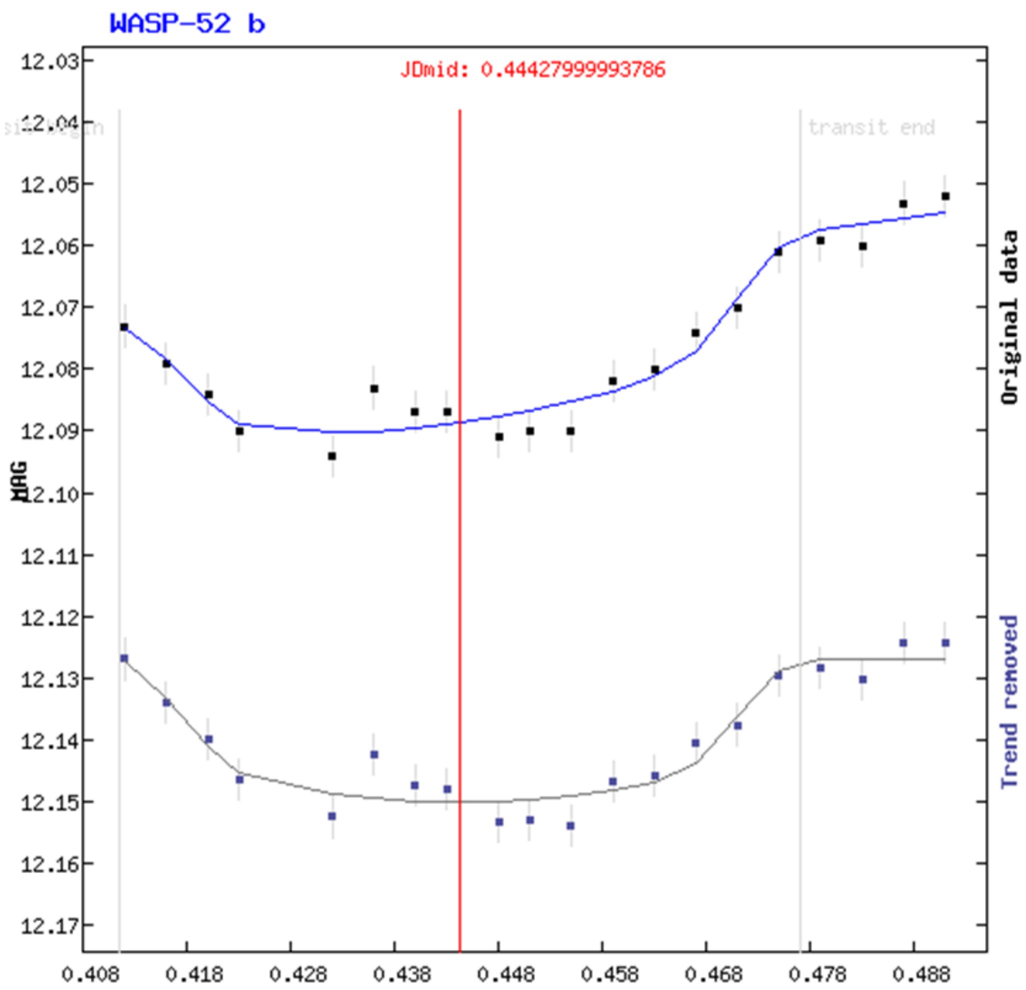


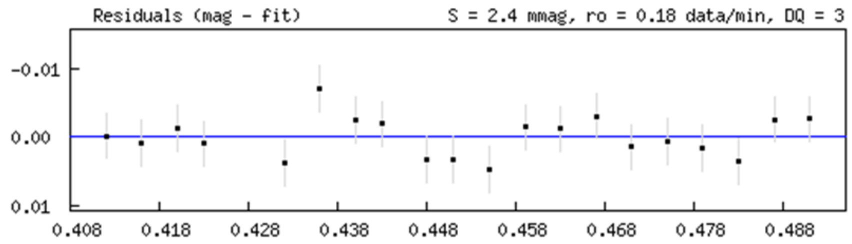


**JD mid**: 2457697.44428 +/- 0.00135

**HJD mid**: 2457697.44785 +/- 0.00135 (helcor = **0.00357**)

**Duration**: 94.4 +/- 4.7 minutes

**Depth**: 0.0232 +/- 0.0028 mag

**Figure 79 WASP-52 Transit of 4-11-2016 With CKT Telescope and Equation Fitting**

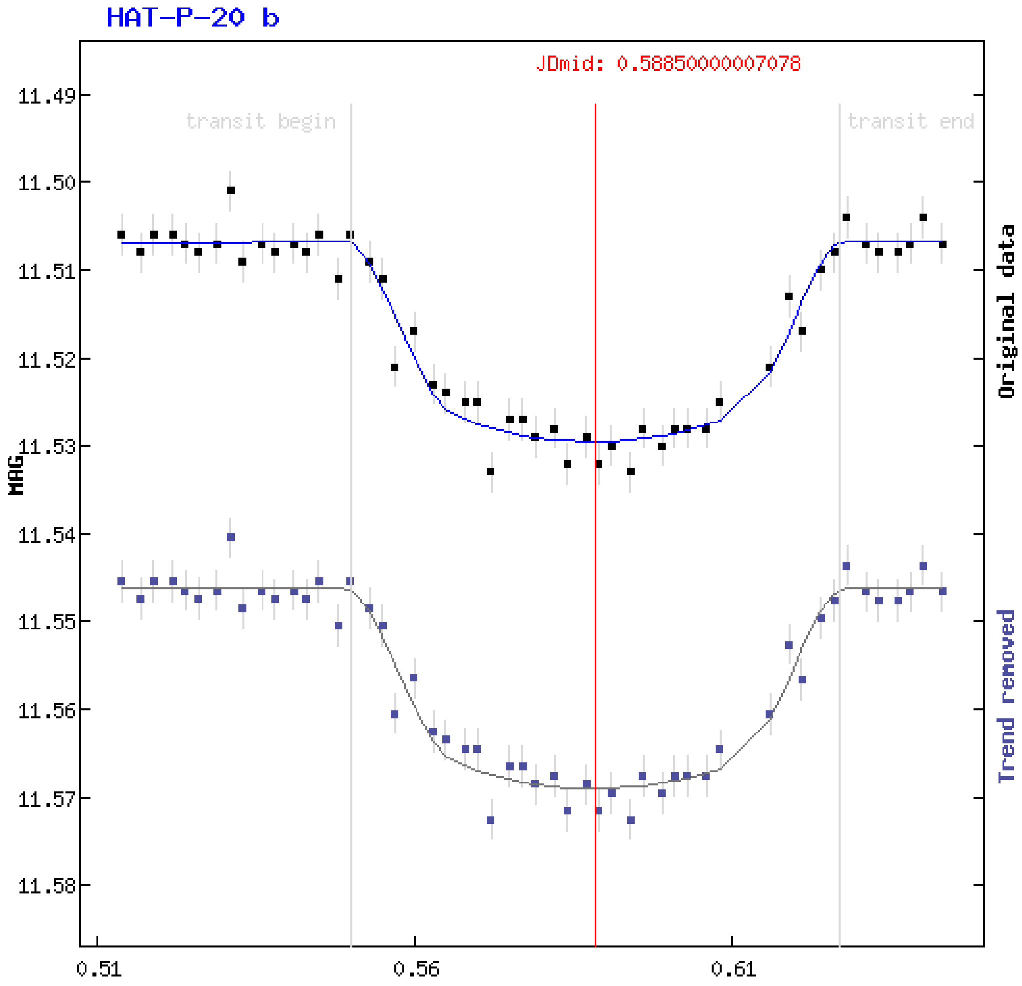


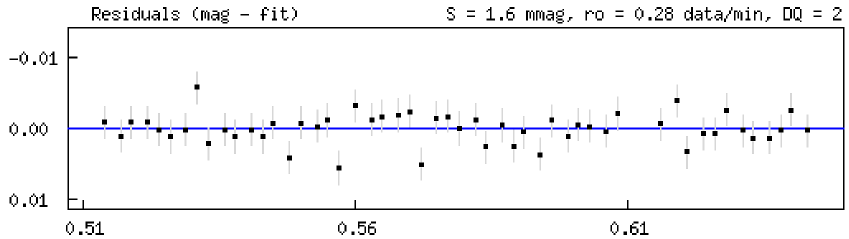


| | | |
|---|---|---|
| **JD mid**: | 2457694.58850 +/- 0.00055 | |
| **HJD mid**: | 2457694.59049 +/- 0.00055 | (helcor = **0.00199**) |
| **Duration**: | 110.9 +/- 2.1 | minutes |
| **Depth**: | 0.0227 +/- 0.0008 | mag |

**Figure 80 HAT-P-20 Transit of 2-11-2016 Taken Using CKT Telescope and Equation Fitting**

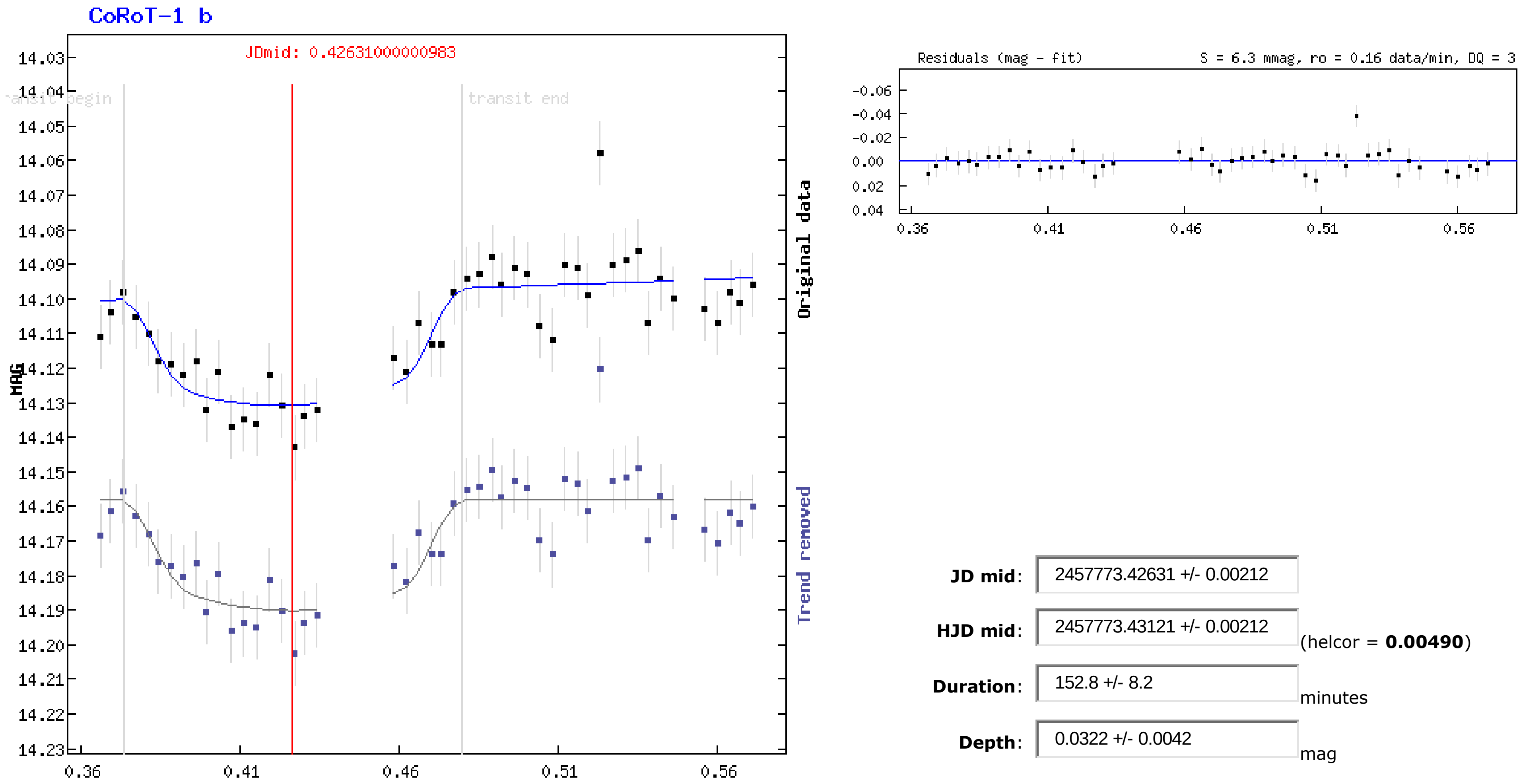


**Figure 81 COROT-1 Transit of 19/20-1-2017 Taken Using CKT Telescope and Equation Fitting**

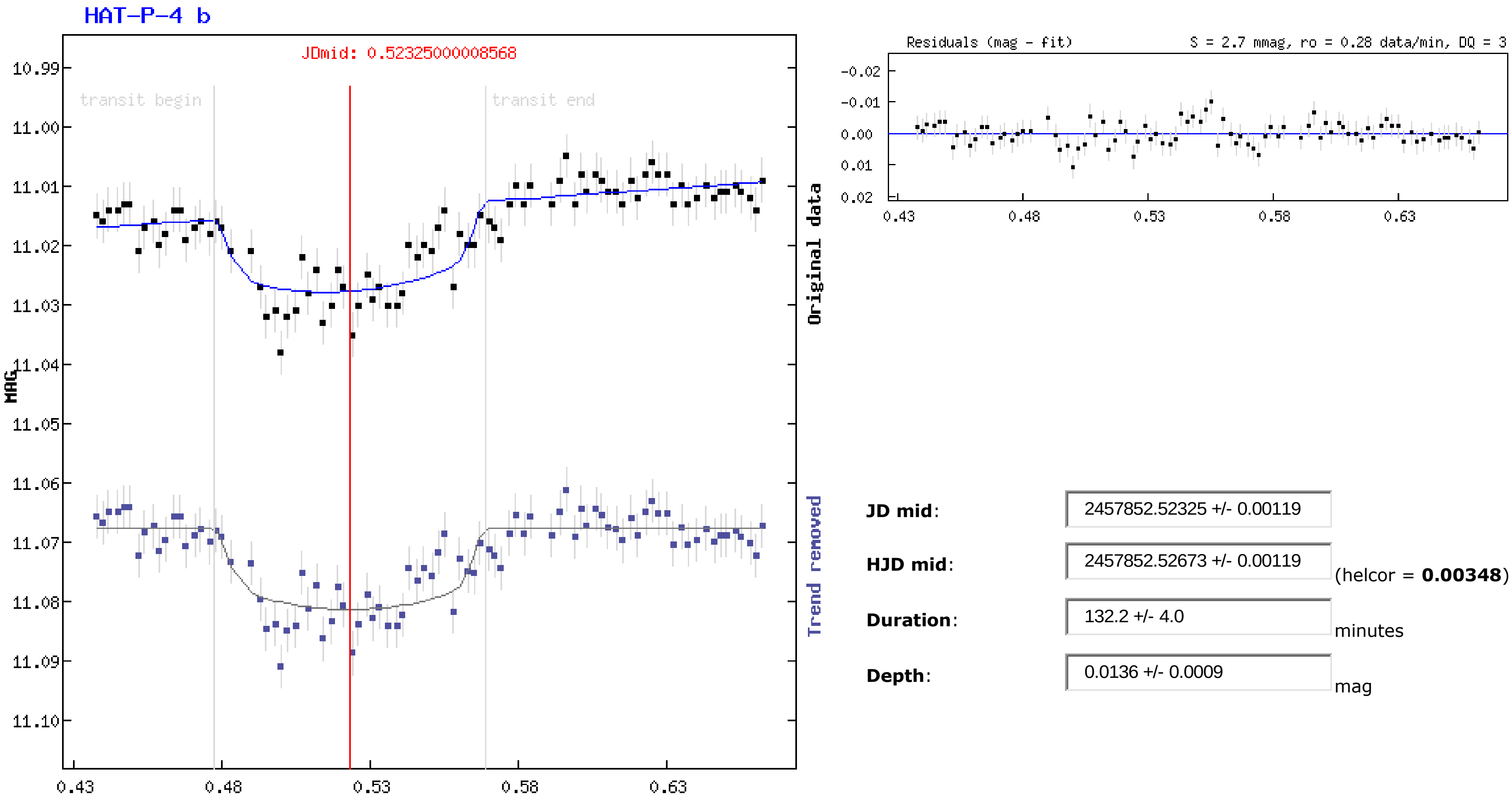


**Figure 82 HAT-P-4 Transit of 8/9-4-2017 Taken Using CKT Telescope and Equation Fitting**

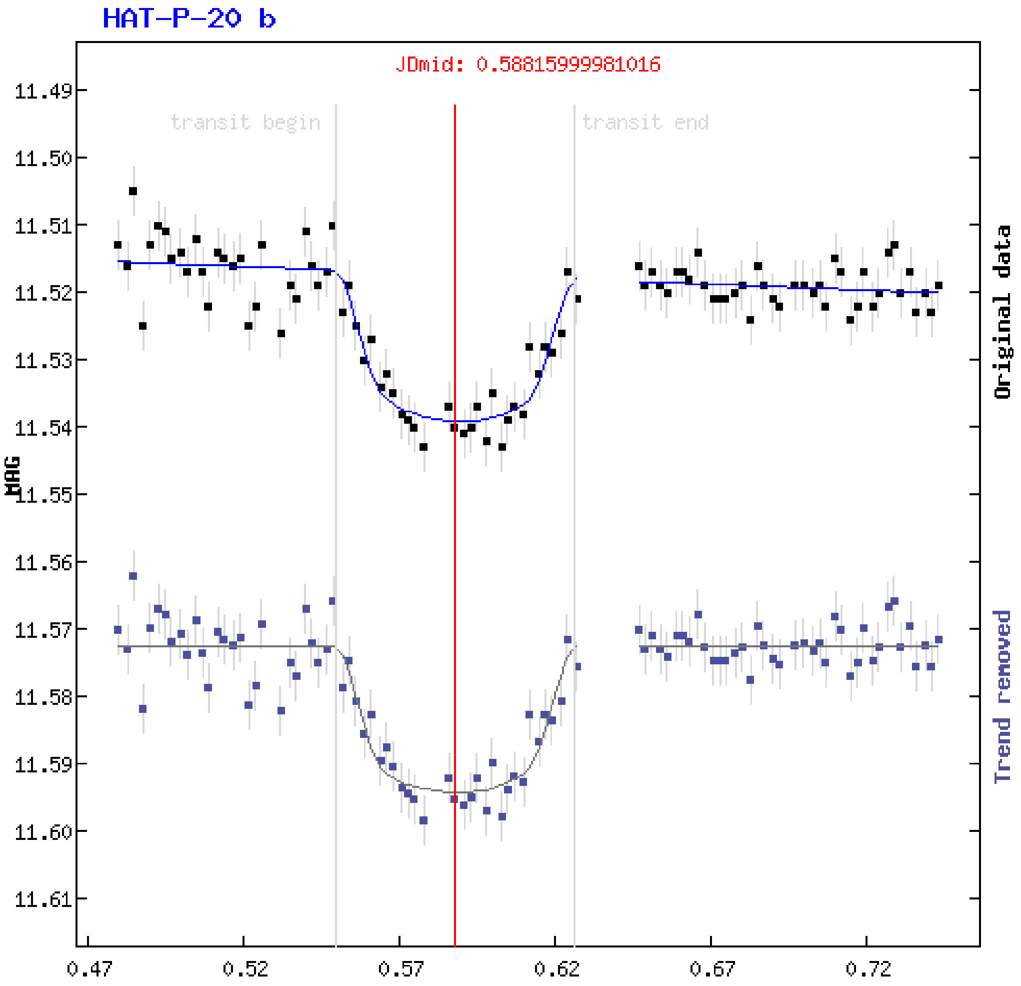


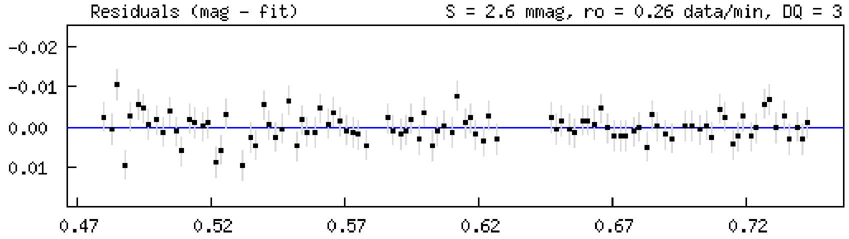


**JD mid**: 2457717.58816 +/- 0.00079

**HJD mid**: 2457717.59208 +/- 0.00079 (helcor = **0.00392**)

**Duration**: 110.3 +/- 3.1 minutes

**Depth**: 0.0219 +/- 0.0010 mag

**Figure 83 HAT-P-20 Transit of 24/25-11-2016 Taken Using JHT Telescope and Equation Fitting**

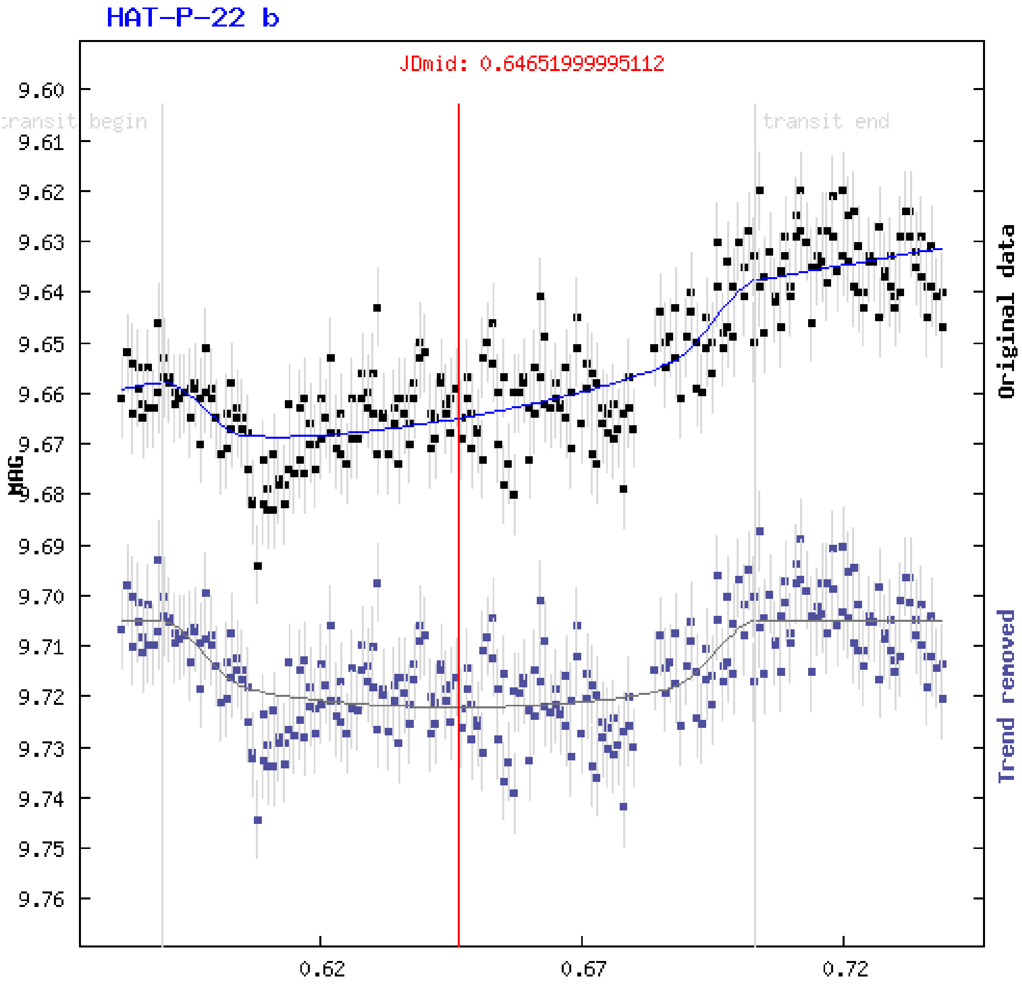


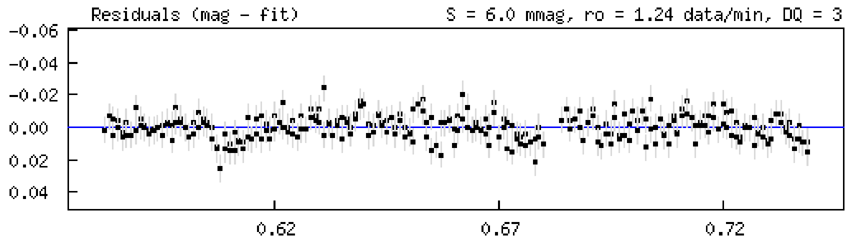


**JD mid**: 2457721.64652 +/- 0.00139

**HJD mid**: 2457721.64813 +/- 0.00139 (helcor = **0.00161**)

**Duration**: 163.0 +/- 4.6 minutes

**Depth**: 0.0172 +/- 0.0013 mag

**Figure 84 HAT-P-22 Partial Transit of 28/29-11-2016 Taken Using JHT Telescope and Equation Fitting**

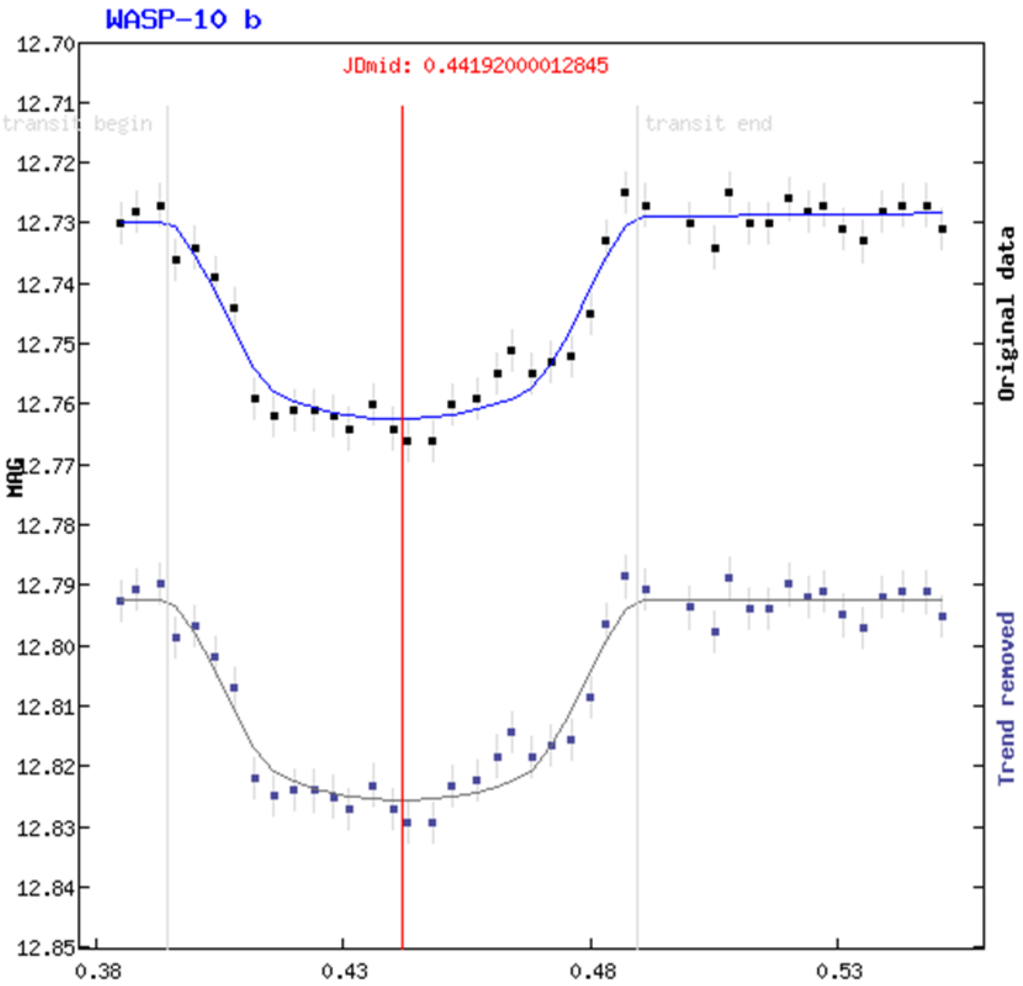


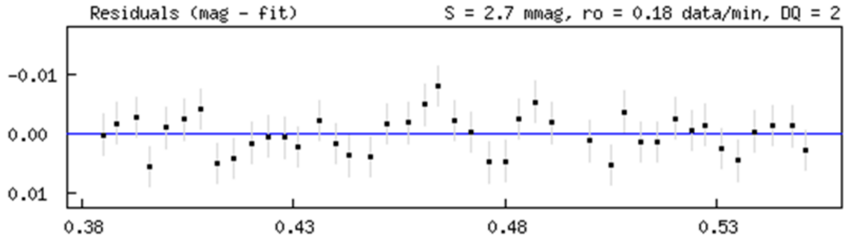


| | | |
|---|---|---|
| **JD mid**: | 2457679.44192 +/- 0.00084 | |
| **HJD mid**: | 2457679.44642 +/- 0.00084 | (helcor = **0.00450**) |
| **Duration**: | 136.5 +/- 3.5 | minutes |
| **Depth**: | 0.0331 +/- 0.0015 | mag |

**Figure 85 WASP-10 Transit of 17/18-10-2016 With RPT Telescope and Equation Fitting**

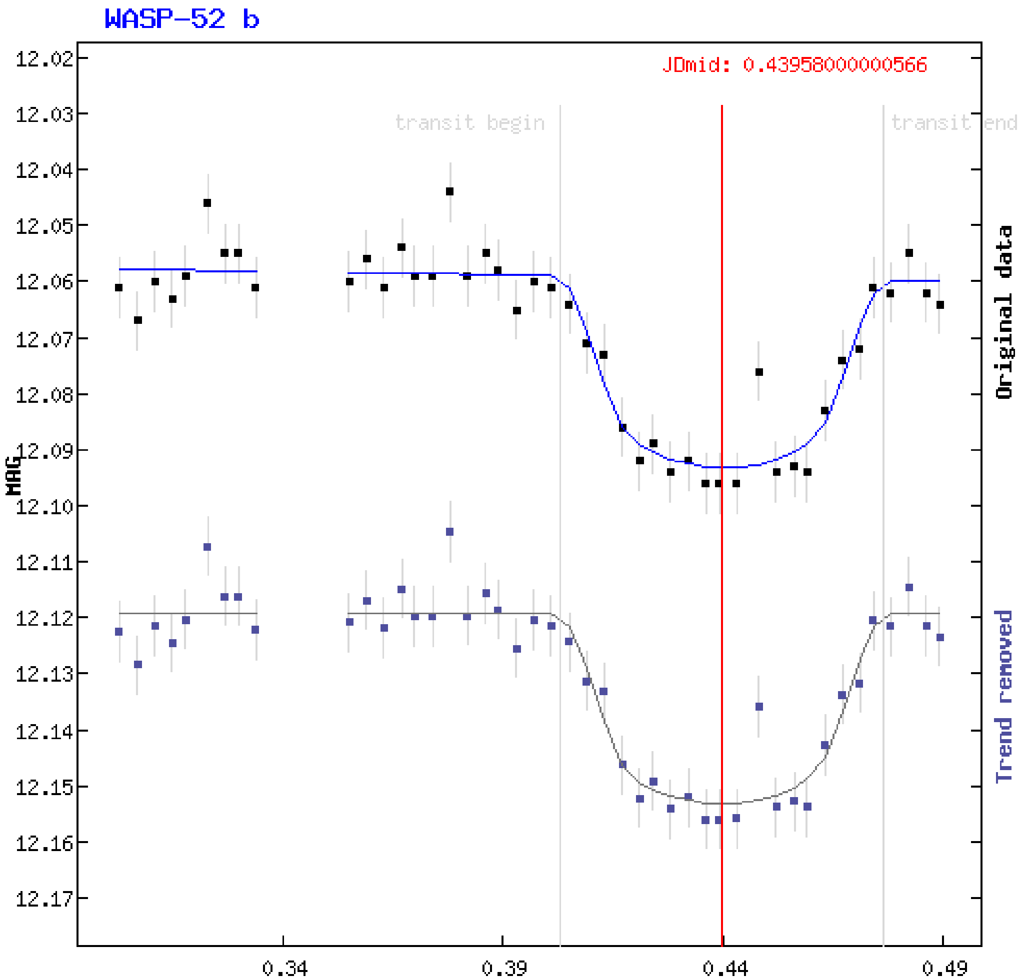


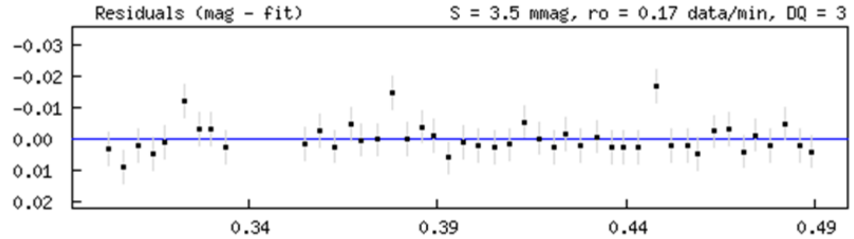


**JD mid**: 2457697.43958 +/- 0.00098

**HJD mid**: 2457697.44315 +/- 0.00098 (helcor = **0.00357**)

**Duration**: 106.0 +/- 4.1 minutes

**Depth**: 0.0339 +/- 0.0023 mag

**Figure 86 WASP-52 Transit of 4-11-2016 With RPT Telescope and Equation Fitting**

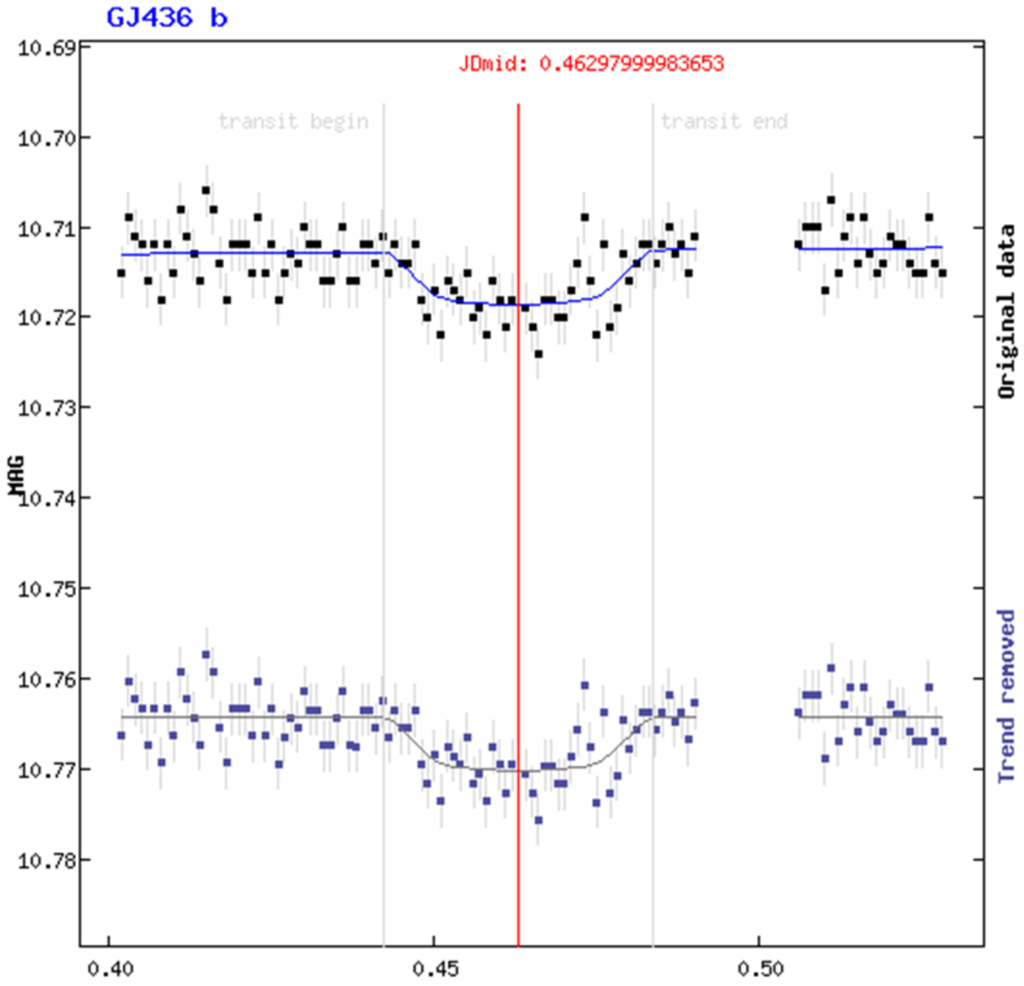


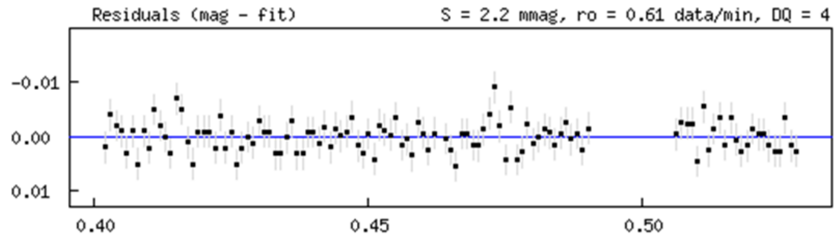


| | | |
|---|---|---|
| **JD mid**: | 2457839.46298 +/- 0.00110 | |
| **HJD mid**: | 2457839.46792 +/- 0.00110 | (helcor = **0.00494**) |
| **Duration**: | 59.6 +/- 4.4 | minutes |
| **Depth**: | 0.0059 +/- 0.0007 | mag |

**Figure 87 GJ 436 Transit of 26/27-3-2017 Taken Using RPT Telescope and Equation Fitting**

# Appendix K  Eclipsing Binary Transit Light Curves

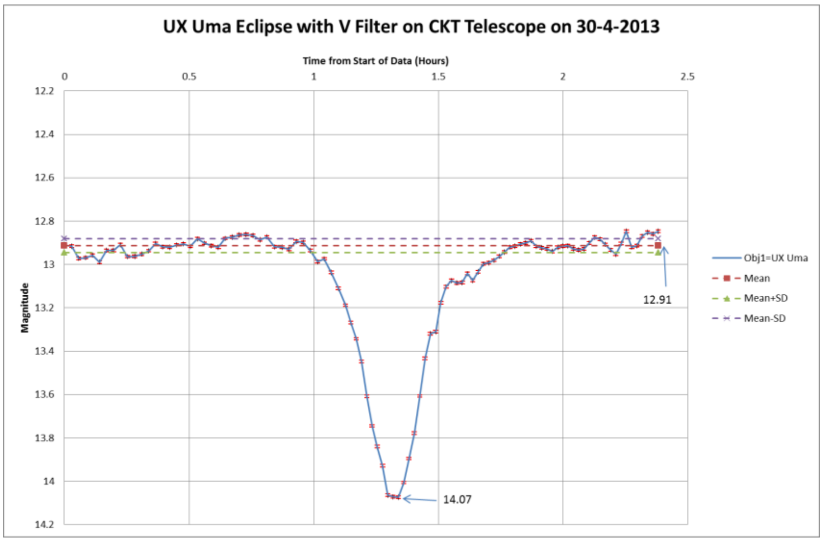


**Figure 88 UX UMa Eclipse with V Filter on CKT Telescope on 30-4-2013**

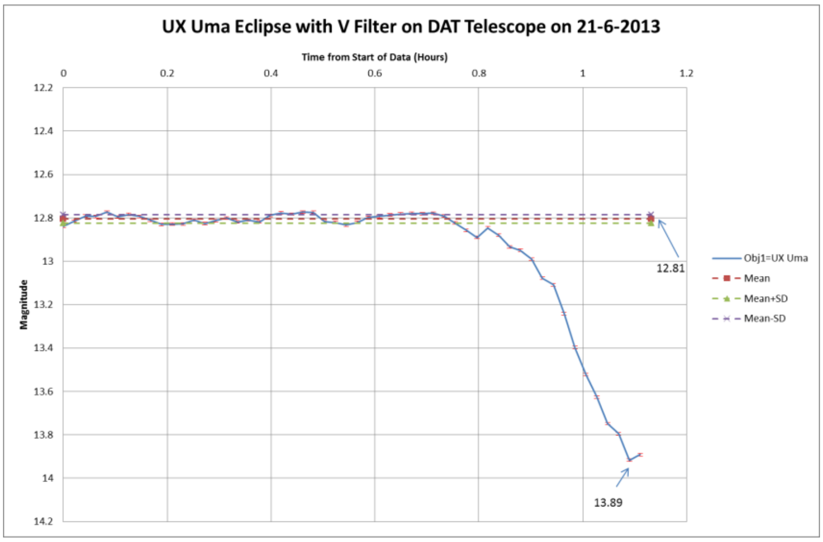


**Figure 89 UX UMa Eclipse with V Filter on DAT Telescope on 21-6-2013**

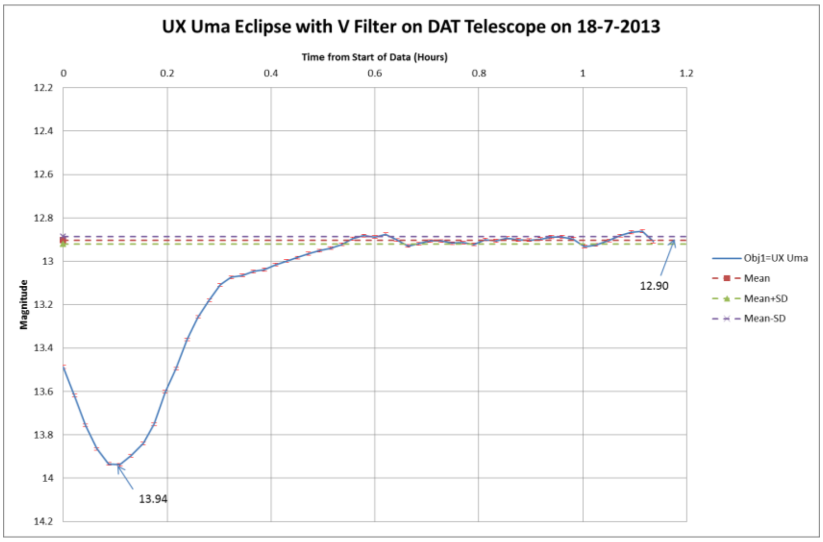


**Figure 90 UX UMa Eclipse with V Filter on DAT Telescope on 18-7-2013**

## Appendix K

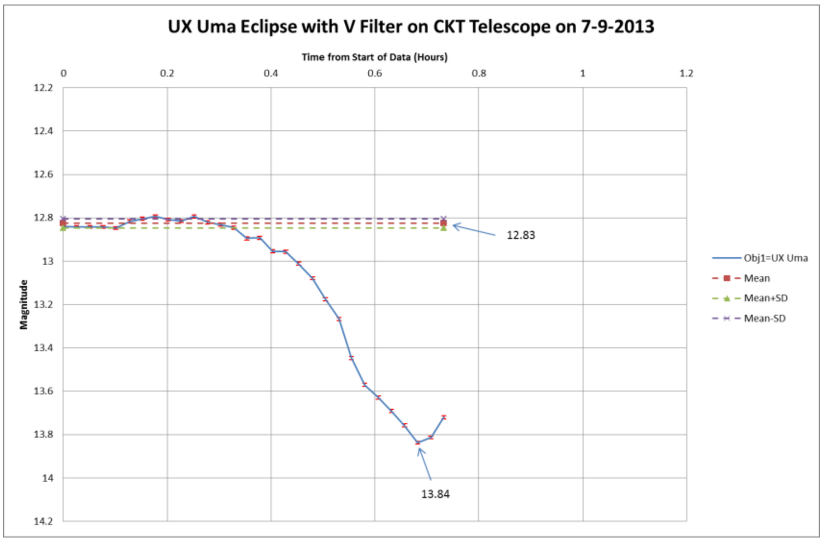


**Figure 91 UX UMa Eclipse with V Filter on CKT Telescope on 7-9-2013**

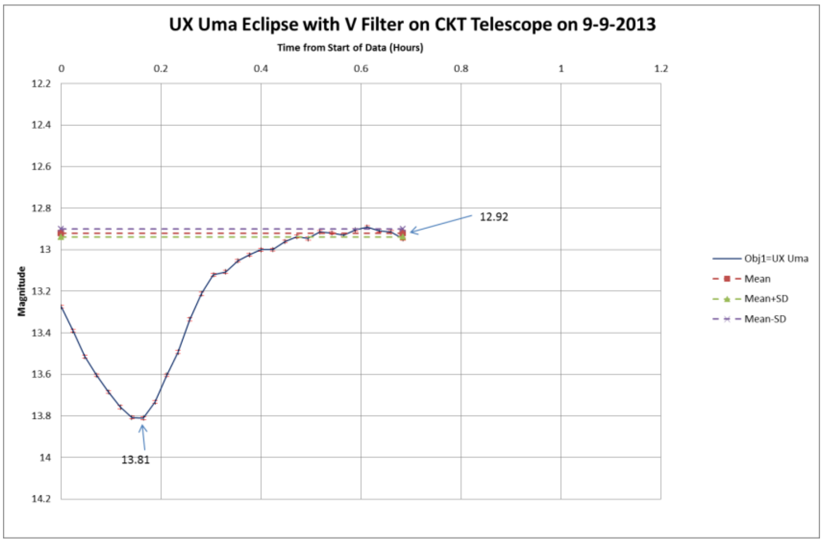


**Figure 92 UX UMa Eclipse with V Filter on CKT Telescope on 9-9-2013**

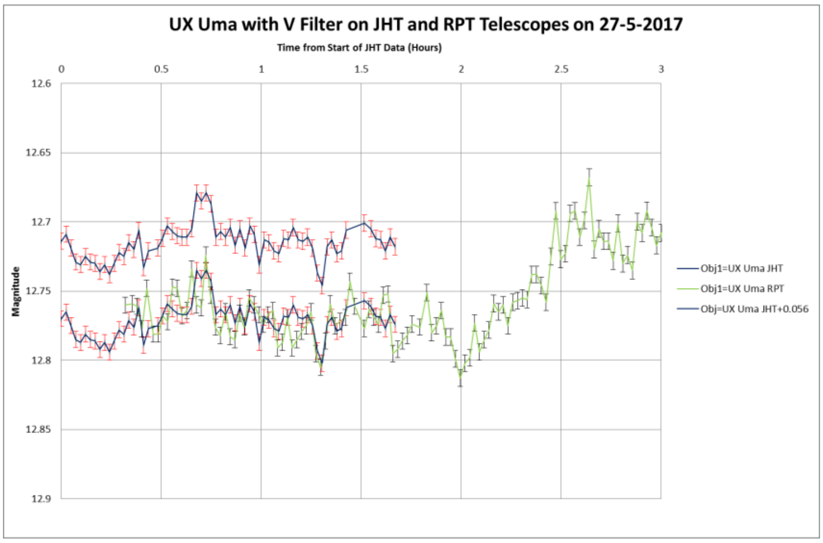


**Figure 93 UX UMa with V Filter on JHT and RPT Telescopes on 27-5-2017**